

**REMODELING OF THE SECRETORY PATHWAY AND
CELL POLARITY MACHINERY IN DIVIDING AND
ENVIRONMENTALLY STRESSED
SCHIZOSACCHAROMYCES POMBE CELLS**

ALEKSANDAR VJESTICA

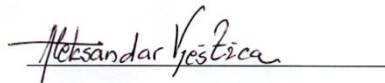
**A THESIS SUBMITTED
FOR THE DEGREE OF DOCTOR OF PHILOSOPHY**

**TEMASEK LIFE SCIENCES LABORATORY
NATIONAL UNIVERSITY OF SINGAPORE
2013**

DECLARATION

I hereby declare that this thesis is my original work and it has been written by me in its entirety. I have duly acknowledged all the sources of information which have been used in the thesis.

This thesis has also not been submitted for any degree in any university previously.

A handwritten signature in black ink, reading "Aleksandar Vjestica", is written over a horizontal line.

Aleksandar Vjestica

January 14th, 2013

Acknowledgements

It is after having placed the full stop on this manuscript that I cannot but take a moment and reflect on the people who have so wholeheartedly helped in my graduate studies. Their efforts have enabled preparation of this manuscript and acknowledging them must precede the contents of this thesis.

I thank Snezhana Oliferenko, my mentor. It is her unfaltering devotion to developing students into independent scientific minds that impresses me. It must have taken near-infinite determination on her behalf to provide continuous support and encouragement in the face of my own failings, and I am grateful for that. Her advice was invaluable to the work presented here but it is her insight into what elegant and beautiful work evolution has crafted that I appreciate most, for it provides a lasting motivation.

My colleague and collaborator Dan Zhang (张丹) deserves a special mention for it was in the midst of our discussions that my scientific opinions could take novel perspective. I cannot but thank her for the strict criticism but even more so for the kind words of support. Though reaching the collaborative scientific goal has been gratifying it is the friendship we have developed that I cherish most.

The advice received from Dr. Greenfield Sluder has been most instructive in developing my research ethics and integrity. I highly appreciate the suggestions and criticism of Dr. Gregory Jedd and would also like to thank Dr. Cynthia He, Dr. Thirumaran Thanabalu and Dr. Mohan Balasubramanian for their time and effort in guiding my research. Furthermore, I am grateful to Dr. Jianhua Liu and Dr. Kathleen Gould for providing the setting for the execution of some experiments. The attachment students Xin-Zi Tang and Daniel Huang, who had far exceeded the goals set in their training programs, were a delight to work with and directly contributed to obtaining results presented here. My graduate work also received a valuable input from collaborations with Yuen Chyao Ling and Dr. Maria Makarova. Training received from Liangmeng Wee and Liling Zheng was essential to execution of experiments presented. I am thankful to Candice Yam and other members of the Oliferenko group for daily aid and discussions. The work presented here was funded by the Temasek Life Sciences Laboratory and the Singapore Millennium Foundation.

Friendships of old and new have served as my emotional pillar throughout years spent in the graduate program. I am thankful for the support of my dear *Komuna*, *SFamily*, *KSNgM_{INC}*, *PMS*, *Molekuli*, *CrazyHouse*, *T2Le[®]s*, *G&Co.*, *sOs* and *IBISS*.

It is my family to whom I am grateful beyond words for their unconditional love and encouragement to pursue scientific research. I owe the deepest gratitude to my sister Nada Vjestica, my grandfather Nenad Majstorovic, my mother Dobrinka Vjestica and my father Jovan Vjestica.

Table of contents

Title page	i
Declaration page	ii
Acknowledgements	iii
Table of contents	iv
Summary	vii
List of tables.....	x
List of figures.....	xi
List of publications	xiii
CHAPTER I - Introduction.....	1
1.1. Specification of growth and division sites	3
1.1.1. Cell tip specification in <i>S. pombe</i>	3
1.1.2. The Cdc42-GTPase module.....	9
1.1.3. Division site positioning	16
1.2. Actin cytoskeleton	19
1.2.1 Interphase actin cytoskeleton in fission yeast.....	20
1.2.2 The actomyosin ring	26
1.2.3. Temporal regulation of actin cytoskeleton in fission yeast	32
1.3. Secretory pathway.....	36
1.3.1. Endoplasmic reticulum	36
1.3.2. Golgi apparatus	41
1.3.3. Exocyst.....	48
1.4. Objectives	52
CHAPTER II - Materials and methods.....	54
2.1. Drugs and staining reagents	54
2.2. Growth media and conditions	54
2.3. <i>S. pombe</i> strains	55
2.4. Construction of <i>S. pombe</i> strains	55
2.4.1. <i>S. pombe</i> transformation	55
2.4.2. Recombinant DNA technology and heterologous gene sequences	56
2.4.3 Genetic crosses.....	57
2.4.4. Targeted mutagenesis of the <i>cdc15</i> genomic locus.....	57
2.5. Gene expression analysis	58
2.5.1. Microarray analysis.....	58

2.5.2. Quantitative PCR	58
2.6. Fluorescence Activated Cell Sorting (FACS).....	59
2.7. Protein biochemistry techniques	60
2.7.1. Preparation of cell lysates and co-immunoprecipitation.....	60
2.7.2. Trichloroacetic acid (TCA) precipitation	60
2.7.3. SDS-PAGE, Western blotting and antibodies	61
2.8. Microscopy techniques	61
2.8.1. Epifluorescence and DIC microscopy	61
2.8.2. Scanning confocal microscopy	61
2.8.3. Spinning-disk confocal microscopy.....	62
2.9. Image processing and analysis.....	63
2.9.1. 3D-rendered and projection images	63
2.9.2. Analysis of the spatial distribution of the early secretory pathway compartments and Golgi maturation dynamics	63
2.9.3. New-end growth analysis.....	65
2.9.4. Analysis of fluorescence intensity profiles	65
CHAPTER III - Results	67
3.1. Characterization of the Secretory Pathway in Fission Yeast.....	67
3.1.1. The fission yeast tER is a distinct ER subcompartment present as numerous stable entities.....	67
3.1.2. The fission yeast Golgi apparatus is organized as stacks of cisternae and the dynamics of Golgi maturation in fission yeast are in accordance with the cisternal progression model	72
3.1.3. Early secretory pathway compartments accumulate at the division site	77
3.2. Mechanisms of Spatial and Temporal Regulation of the Secretory Pathway in Fission Yeast.....	82
3.2.1. Actomyosin ring assembly is required for secretory machinery recruitment to the division site.....	82
3.2.2. Maintenance of a polarized state of the early secretory pathway compartments requires an intact actin cytoskeleton	86
3.2.3. The recruitment of the early secretory compartments to the actomyosin ring and the septation site is not under direct regulation of cell cycle	90
3.2.4. The Septation Initiation Network is required for maintenance but not for the initial recruitment of the early secretory pathway compartments at the division site.....	92
3.2.5. The EFC domain protein Cdc15 is required for tER recruitment to the division site	96

3.2.6. Overexpression of Cdc15 is sufficient to promote relocalization of the tER to the cell equator in interphase cells	102
3.2.7. Cdc15 is required for the tER polarization to the post-metaphase actomyosin rings.	104
3.2.8. tER and ER tubules polarization to the division site have distinct molecular requirements	110
3.2.9. Polarization of the tER to the division site does not depend on net centripetal movement of pre-existing COPII positive membranes using type-V myosins.	114
3.2.10. Type-V myosin along actin cables recruits ER to the cell tips in interphase <i>S. pombe</i> cells.	118
3.3. Remodeling of Cell Polarity Under Heat-stress in Fission Yeast Cells..	120
3.3.1. Heat-stress induces transient loss of polarized growth succeeded by monopolar growth pattern in cells adapting to elevated temperature.	120
3.3.2. Cortical association of Cdc42 GEFs and GAP is modulated by temperature	128
3.3.3. Cdc42 activation at the lateral cell cortex upon heat-stress is mediated by Cdc42-GEFs and counteracted by the Cdc42-GAP	134
3.3.4. Heat-stress associated transcription is essential to polarize growth at elevated temperature and sufficient to induce monopolar growth pattern	138
3.3.5. Cells with impaired Hsp70•Hsp40 complex Mas5•Ssa2 have elevated levels of heat-stress associated transcription.	142
3.3.6. Ssa2•Mas5 complex regulates nucleo-cytoplasmic shuttling of the Hsp90 chaperone Swo1 and its target protein Hsf1	152
3.3.7. Cells lacking the Mas5•Ssa2 complex exhibit an intermittent, monopolar growth pattern.....	156
CHAPTER IV - Discussion	164
4.1. Organization of the early secretory pathway compartments in fission yeast	164
4.2. Polarization of the secretory pathway to the division site	166
4.3. Remodeling of cell polarity in response to ambient temperature	171
4.4. Conclusions and perspectives	178
Bibliography	183
Appendix I – List of strains	A1
Appendix II – List of quantitative PCR primers.....	A7
Appendix III - Publications.....	

Summary

Cellular polarity underlies multiple aspects of life including morphogenesis, differentiation and proliferation. The fission yeast *Schizosaccharomyces pombe* (*S. pombe*) are highly polarized, rod-shaped cells that grow exclusively at cell tips and divide by placing a medial septum. Newly born daughter cell initiates monopolar growth at the cell tip inherited from the mother but then transition to bipolar growth during the G₂ phase of the cell cycle.

Upon reaching sufficient cell size *S. pombe* cells enter mitosis and assemble an equatorial, actomyosin-based division ring that is thought to provide physical force for the plasma membrane invagination. Membrane trafficking through the secretory pathway is essential to allow closure, septum deposition and cell separation. However, organization of the early secretory compartments, such as the Golgi apparatus and the endoplasmic reticulum (ER), remain poorly understood. Here I surveyed dynamics of fluorophore tagged proteins that served as markers for various compartments of the secretory pathway. I demonstrated that Golgi apparatus in fission yeast is organized primarily as adjacent stacks of few proteomically distinct cisternae that can arise *de novo*. My data provide evidence that individual cisternae undergo identity change concordant with the cisternal progression model of Golgi maturation. Furthermore I find that the ER sheets, ER tubules and transitional ER are distinct ER subdomains and that their spatial distribution during cell division is under differential regulation. I also find that recruitment of the ER to the cell tips in interphase cells requires type-V myosin based transport along actin cables.

Targeting of secretory vesicles and exocytosis to the division site has been previously reported but the extent of polarization of the upstream secretion apparatus was previously unknown. I found that the secretion machinery exhibited a marked

polarization to the division site. Specifically, an actomyosin ring dependent enrichment was observed for the ER tubules, the tER and Golgi cisternae but not for the ER sheets. While the tubular ER accumulation to the division site relied on the anilin-like protein Mid1, the tER polarization required function of the EFC-domain protein Cdc15. Equatorial recruitment of both ER tubules and tER were independent of type-V myosins. Thus, fission yeast polarizes its secretory machinery to the cell division site by utilizing molecular cues provided by the actomyosin ring. I propose that the polarization of the secretory compartments might fulfill the need for massive vesicle trafficking events occurring at the division site

Sensing ecological parameters and orchestrating an adaptive response allows organisms to thrive in a changing habitat. Temperature fluctuations are one of the most common environmental stresses. Free-living microorganisms, such as yeast, maintain regular patterns of growth over a range of ambient temperatures. Here I investigated dynamics of key polarity regulators during mild heat-stress and subsequent adaptation to elevated temperature. Upon mild heat-stress, the tip specification by the multiprotein polarisome complex did not appear impaired. However activity of the Rho-family GTPase Cdc42 was no longer confined to the cortical domains specified by the polarisome and instead was observed spreading throughout the cell cortex. The transient redistribution of the active Cdc42 was accompanied by relocalization of its effectors regulating cellular growth. I found that the Cdc42-guanine-nucleotide-exchange-factor (Cdc42-GEF) Gef1 was required for expanding the active Cdc42 domain while the Cdc42-GTPase-activating-protein (Cdc42-GAP) Rga4 functioned to counteract the Cdc42 activity at the lateral cell cortex under these conditions. I also observe that the cortical levels of Cdc42-GAP and Cdc42-GEFs change according to environmental temperature.

Surprisingly, *S. pombe* cells recovering from heat-stress or overexpressing the heat-shock transcriptional factor Hsf1 grow in a monopolar fashion. Thus the heat-stress response and the Hsf1 mediated transcription modulate the growth pattern in fission yeast cells. To corroborate these findings, I employed a genetic screen and identified Mas5•Ssa2 chaperone complex as a negative regulator of heat-stress associated transcription. I show that Mas5 and Ssa2 regulate the Hsf1 nucleo-cytoplasmic shuttling during heat-stress, possibly through direct interaction with its repressor, the Hsp90 protein Swo1. Even though polarisome function appeared intact, *mas5Δ* cells were unable to efficiently maintain the cortical Cdc42 activity and exhibited an intermittent, monopolar tip extension pattern. Furthermore, the cortical levels of Cdc42 regulators were decreased in cells lacking Mas5. Based on these results I propose that the Hsf1 mediated transcription modulates the Cdc42 GTPase module to efficiently maintain polarized growth at different temperatures.

List of tables

Table 3.3.5. Overview of putative Hsp70-binding chaperones in fission yeast	147
---	-----

List of figures

Figure 3.1.1. Characterization of the tER in fission yeast.	70
Figure 3.1.2. Characterization of the Golgi complex in <i>S. pombe</i>	74
Figure 3.1.3.1. Spatial distribution of the early secretory pathway throughout the cell cycle.	79
Figure 3.1.3.2. Accumulation of the early secretory pathway compartments at the site of division is statistically significant.	80
Figure 3.1.3.3. Spatial distribution of the ER sheets and tubules throughout the cell cycle.	81
Figure 3.2.1. Actomyosin ring assembly is required for secretory pathway recruitment to the division site.	84
Figure 3.2.2. Maintenance of the secretory pathway polarization to the site of cell division requires an intact actin cytoskeleton.	88
Figure 3.2.3. The recruitment of the early secretory compartments to the actomyosin ring and the septation site is not under direct regulation of cell cycle.	91
Figure 3.2.4.1. The Septation Initiation Network is required for maintenance but not for the initial recruitment of the early secretory pathway compartments at the division site.	94
Figure 3.2.4.2. The Septation Initiation Network is required for maintenance but not for the initial recruitment of the early secretory pathway compartments at the division site.	95
Figure 3.2.5. The EFC domain protein Cdc15 was required for the recruitment of the tER to the division site.	100
Figure 3.2.6. Overexpression of Cdc15 is sufficient to induce medial tER accumulation in interphase.	103
Figure 3.2.7. Characterization of the <i>cdc15-22</i> mutants	108
Figure 3.2.8. The dynamics of the tubular ER and the tER are distinct differentially regulated processes	112
Figure 3.2.9. Polarization of the tER to the division site does not depend on net centripetal movement of pre-existing COPII positive membranes using type-V myosins.	116
Figure 3.2.10. Type-V myosin along actin cables recruits ER to the cell tips in interphase <i>S. pombe</i> cells.	119
Figure 3.3.1.1. Heat-stress induces transient longitudinal growth arrest succeeded by monopolar growth.	125

Figure 3.3.1.2. Heat-stress leads to a transient loss of cell polarity succeeded by monopolar growth.....	126
Figure 3.3.2.1. Heat-stress leads to a transient loss of cell polarity succeeded by monopolar growth.....	131
Figure 3.3.2.2. Recruitment of the Cdc42 regulators to the cell cortex is regulated by temperature.	132
Figure 3.3.3. Cdc42 activity at the lateral cell cortex upon heat-stress is enabled by cdc42-GEFs and counteracted by the cdc42-GAP.....	137
Figure 3.3.4. Heat-stress associated transcription regulates growth pattern in fission yeast	140
Figure 3.3.5.1. Cells with impaired function of the Ssa2•Mas5 complex have elevated levels of heat-stress associated transcription.	148
Figure 3.3.5.2. Cells lacking a DnaJ chaperone Mas5 have elevated levels of heat-stress associated transcription.	150
Figure 3.3.6. Ssa2•Mas5 complex regulates nuclear shuttling of Hsf1 and Swo1....	155
Figure 3.3.7.1. Cells with impaired Ssa2•Mas5 complex have decreased cortical Cdc42 activity and exhibit monopolar intermittent growth pattern.....	160
Figure 3.3.7.2. Cells lacking DnaJ chaperone Mas5 exhibit monopolar intermittent growth in G ₂ phase of the cell cycle.	162

List of publications

Zhang, D., *Vjestica, A., and Oliferenko, S. (2012). Plasma Membrane Tethering of the Cortical ER Necessitates Its Finely Reticulated Architecture. *Current Biology* : CB 22, 2048–2052. ***First co-author publication**

Zhang, D., Vjestica, A., and Oliferenko, S. (2010). The cortical ER network limits the permissive zone for actomyosin ring assembly. *Current Biology* : CB 20, 1029–1034.

Ling, Y.C., *Vjestica, A., and Oliferenko, S. (2009). Nucleocytoplasmic shuttling of the TACC protein Mia1p/Alp7p is required for remodeling of microtubule arrays during the cell cycle. *PloS One* 4, e6255. ***First co-author publication**

Vjestica, A., Tang, X.-Z., and Oliferenko, S. (2008). The actomyosin ring recruits early secretory compartments to the division site in fission yeast. *Molecular Biology of the Cell* 19, 1125–1138.

Vjestica, A., and Oliferenko, S. (2012). Nuclear geometry: mitotic nucleus flares out when arrested. *Current Biology* : CB 22, R489–91. **Review article**

CHAPTER I - Introduction

The processes of differentiation, proliferation and morphogenesis are tightly linked to mechanisms regulating cell polarity in a wide range of species (reviewed by Macara and Mili, 2008; Dettmer and Friml, 2011; Royer and Lu, 2011; Sabherwal and Papalopulu, 2012). In the prokaryotic *Bacillus subtilis* spore formation upon nutrient starvation involves an asymmetric cell division where only the smaller forespore will differentiate into a spore (reviewed by Higgins and Dworkin, 2012). During *Drosophila* neuroblast development, the cell fate determinants Numb, Pros and Bra are positioned specifically to the basal cell cortex and upon unequal division inherited solely by the smaller daughter cell that proceeds to differentiate while the larger daughter retains neuroblast stem cell identity (reviewed by De Craene et al., 2006; Voeltz et al., 2006). Deregulated signaling in Crumbs, Par or Scribble complexes regulating mammalian cell polarity have all been implicated in cancer progression (reviewed by Royer and Lu, 2011; Ellenbroek et al., 2012).

Instead of relying on cell type- and species-specific machineries, the immense diversity in cellular morphologies of unicellular and multicellular eukaryotes evolved through subtle adaptations of the core machineries carrying out signaling, cytoskeletal remodeling and targeted secretion (reviewed by Nelson, 2003a). Concordantly, many of the known molecules involved in cell polarity are conserved across species (reviewed by Cotteret and Chernoff, 2002; Nelson, 2003b; Field et al., 2011; Wickstead and Gull, 2011; Eliáš and Klimeš, 2012).

The polarity modules exhibit a high degree of hierarchy. Localized signaling, for example at the incipient bud in budding yeast or between

segregating chromosomes in mammalian cells, is propagated to orient the filamentous actin (Park et al., 1997; Kang et al., 2001; Yüce et al., 2005). Localized signaling and actin cytoskeleton then orient secretion and promote targeted delivery of membranes and proteins involved in cell adhesion, growth, cell division, etc. (Boyd et al., 2004; Pruyne et al., 2004; Estravís et al., 2011). More recent work also suggests that feedback mechanisms, such as reinforcement of actin nucleation by targeted secretion, also operate between the polarity modules (Wedlich-Soldner, 2003). While feedback systems confer robustness (Howell et al., 2012), mechanisms orchestrating polarity also possess a degree of plasticity that allows cells to readily adjust in response to both intrinsic and extrinsic signals. In such a manner, epithelial-to-mesenchymal transition allows animal embryogenesis while reorientation of growth in yeast promotes mating with non-sister cells (Iden and Collard, 2008; Bendezú and Martin, 2012).

The fission yeast *Schizosaccharomyces pombe* (*S. pombe*) is an attractive model organism because of its fully sequenced and annotated genome (Wood et al., 2002), a fairly large cell size convenient for cytological studies and the ease of molecular manipulations and genetic analyses. Though a seemingly simple rod-shaped cell, fission yeast is in fact a highly polarized eukaryotic cell that undergoes three major morphological transitions during the vegetative cell cycle. Newly born cells initiate apical growth in a monopolar fashion and elongate only from the so-called old-end that existed prior to the last round of septation. When cells achieve sufficient size during the G₂ phase of the cell cycle, they transition to bipolar growth in a process termed New-End-Take-Off (NETO) (Mitchison and Nurse, 1985). Finally,

when a cell reaches the size optimal for cell division, tip elongation ceases and mitosis occurs followed by cytokinesis at the cell equator (Mitchison and Nurse, 1985).

The following sections provide an overview of 1) signaling mechanisms positioning the actin cytoskeleton, 2) regulators of actin dynamics and 3) the secretory apparatus. Focus is placed on the current understanding of these modules in *S. pombe* and briefly touches upon other model systems.

1.1. Specification of growth and division sites

1.1.1. Cell tip specification in *S. pombe*

Genetic screens for aberrantly shaped *S. pombe* mutants identified genes regulating cell morphology and provided foundations for the ongoing work on understanding the underlying molecular mechanisms (Verde et al., 1995; Brunner and Nurse, 2000). Analysis of a bent- and T-shaped mutant led to identification of cell tip localized kelch-repeat protein Tea1 as a key regulator of NETO and cell morphology (Verde et al., 1995; Mata and Nurse, 1997). Tea1 is also observed on microtubules, concentrating at their (+)-ends, and application of the microtubule-destabilizing drug tiabendazol (TBZ) impairs Tea1 cell tip localization (Mata and Nurse, 1997). Tea1 physically interacts and is responsible for the microtubule and cell tip recruitment of another polarity factor, the SH3 domain protein Tea4 (Martin et al., 2005; Tatebe et al., 2005). A screen for genes whose overexpression induces aberrant morphologies isolated a microtubule dynamics regulator CLIP170-family protein Tip1 that exhibits a similar localization pattern to Tea1

(Brunner and Nurse, 2000). *tip1* Δ cells fail to localize Tea1 to the cell tips and phenocopy morphological defects of *tea1* Δ cells (Brunner and Nurse, 2000). The Tip1 functions in localizing Tea1 and regulating microtubules are separable and depend on the N-terminal and the C-terminal segment of the protein respectively (Brunner and Nurse, 2000). Interestingly, CLIP-170 has been proposed to mediate the communication between actin cytoskeleton and microtubules at the leading edge of migrating mammalian cells (reviewed by Rodriguez et al., 2003; Siegrist and Doe, 2007).

Efficient recruitment of Tip1 to microtubules and its localization to the cell tips are dependent on the EB1-family protein Mal3 which binds Tip1 both *in vitro* and *in vivo* (Busch and Brunner, 2004). Mal3 also promotes microtubule recruitment and motor activity of the kinesin Tea2 (Browning et al., 2003; Busch and Brunner, 2004; Busch et al., 2004; Browning and Hackney, 2005). Cells lacking Tea2 have bent and T-shaped morphology and are unable to localize Tea1 to the cell tips (Browning et al., 2000). Furthermore, Tea2 co-immunoprecipitates with both Mal3 and Tip1 suggesting that the three proteins are present in the so-called +TIP complex (Busch et al., 2004). Fluorescently tagged Tea2 and Tip1 are readily observed as microtubule-associated punctae undergoing both slow and rapid directional movements (Busch et al., 2004). Whereas the slow Tip1 punctae movements correlate with the speed of microtubule growth, the rapid Tip1 movements are absent in Tea2 rigor mutant cells (Busch et al., 2004). These findings have led to a model where Mal3 promotes Tip1 and Tea2 microtubule binding. Increase in motor activity of Tea2 then promotes rapid Tip1 transport towards microtubule (+) ends where Mal3 serves to dock the +TIP complex.

Remarkably, Mal3, Tip1 and Tip2 based microtubule-(+)-end tracking system can be reconstituted *in vitro* (Bieling et al., 2007). Thus microtubule-(+)-end growth simultaneously promotes efficient transport of the +TIP complex and the associated Tea1 to the cell tips (Thadani et al., 2011, reviewed by Martin, 2009). Even though Tea1 interacts with Tip1, additional mechanisms must recruit Tea1 to microtubules since this association persists in *tip1Δ* cells (Brunner and Nurse, 2000).

Anchoring of Tea1 at the cell cortex requires the prenylated factor Mod5 (Snaith and Sawin, 2003). Cells lacking Mod5, or carrying a mutation in its prenylation motif, exhibit decreased localization of Tea1 to the cell tips and defects similar to those of *tea1Δ* cells (Snaith and Sawin, 2003). Interestingly, in *tea1Δ* cells Mod5 is no longer restricted to the cell tips and spreads across the entire plasma membrane suggesting a feedback mechanism focusing both proteins to cell tips (Snaith and Sawin, 2003). FRAP analysis showing that Mod5 dynamics at the cell tip are more rapid than those of Tea1 discards a simple anchoring mechanism based solely on the reported Mod5-Tea1 direct interaction (Snaith et al., 2005; Bicho et al., 2010). A recent model proposes that Mod5 acts as a catalyst for formation of the Tea1 polymeric network at the cell tips (Bicho et al., 2010). This hypothesis is supported by the observation that mutants in the putative Tea1 trimerization motif are defective in anchoring even though they interact with Mod5 (Bicho et al., 2010). However, *in vitro* studies of the proposed Tea1 clustering, potentially involving additional factors, will be required to support this model. Auxiliary mechanisms anchoring Tea1 to the growing and the non-growing cell tip have

been proposed to rely on Tea4 and a Tea1-related protein Tea3 respectively (Martin et al., 2005; Snaith et al., 2005; Tatebe et al., 2005).

More recently a second mechanism linking microtubules to cell polarity has been reported. When physically constrained in a microfluidics chamber *S. pombe* cells recruit the growth machinery to ectopic sites at the lateral cell cortex (Terenna et al., 2008; Minc et al., 2009). Application of microtubule depolymerizing drug carbendazim prevents initiation of these ectopic growth sites (Minc et al., 2009). Interestingly the lateral recruitment in physically constrained cells occurs independently of Tip1, Tea1 and Tea4 and instead requires Mal3 and the translation initiation factor Moe1 that physically interact with each other (Chen et al., 1999; Minc et al., 2009). Remarkably, defects in localizing growth machinery to the cell tips in a number of morphological mutants are reversed by physically constraining cell shape (Terenna et al., 2008). These results suggest presence of a feedback between machinery regulating polarized growth and the cell shape (Terenna et al., 2008).

While microtubules function to transport the +TIP complex and the associated Tea1, these regulators of cell polarity in return provide a guidance mechanism to orient microtubule bundles along the long cell axis (Brunner and Nurse, 2000). In fission yeast, interphase microtubules are organized into several bundles each containing one primary, long microtubule and several shorter microtubules (reviewed by Piel and Tran, 2009). The more stable (-)-ends of the bundles attach to the nuclear envelope while the dynamic (+) ends explore the cell interior. When (+)-ends encounter the lateral cell cortex, continued microtubule polymerization and bundle rigidity provide forces that

allow bundle sliding along the cell cortex, orienting it along the long cell axis. However, when a microtubule (+)-end reaches the cell tip it undergoes a catastrophe and the bundle rapidly shrinks (Brunner and Nurse, 2000; Busch and Brunner, 2004). Mal3, Tip1 and Tea2 mutants all exhibit short microtubules that undergo frequent catastrophes before they reach the cell tips (Brunner and Nurse, 2000; Busch and Brunner, 2004; Busch et al., 2004). High affinity binding of Mal3 calponin-homology domain has been suggested to bridge and stabilize microtubule protofilaments and thus suppresses catastrophe (Kumar and Wittmann, 2012; Maurer et al., 2012). In cells lacking Tip1, Mal3 is efficiently recruited to microtubules but dissociates from the (+)-ends as they contact the cell cortex suggesting that Tip1 functions to stabilize Mal3 at these locations (Busch and Brunner, 2004). Tea2 focusing of Tip1 to the microtubule (+)-ends is also likely to play a role (Busch et al., 2004). Importantly, cells lacking Tea1 exhibit long microtubule bundles that rarely depolymerize as they reach a cell tip and instead curve around it (Mata and Nurse, 1997). Furthermore, Tea1 is required to accumulate Tip1 and Tea2 to the cell tips (Brunner and Nurse, 2000; Behrens and Nurse, 2002; Browning et al., 2003). These data are concordant with a model where Tea1 recruitment to the cell tips is functionally linked to unloading of the +TIP complex from the microtubule (+)-ends and their subsequent catastrophe (Behrens and Nurse, 2002).

Mutations in multiple genes encoding regulators of core microtubule dynamics, such as γ -tubulin-ring-complex proteins Mto1 and Mto2 or acidic-coiled-coil protein Mia1/Alp7, also lead to aberrant cell morphology (Venkatram et al., 2004; Samejima et al., 2005; Zheng et al., 2006). However,

microtubules are not essential for maintenance of overall cell polarity in interphase *S. pombe* cells (Sawin and Snaith, 2004). Furthermore, the spherical fission yeast protoplasts that have the cell wall enzymatically removed are able to restore polarized growth in presence of carbendazim (Kelly and Nurse, 2011).

The Tea proteins are proposed to promote localization of other polarity factors to the cell tips through direct protein-protein interactions. Tea1 can be isolated from cell lysates in large complexes termed the polarisome (Feierbach, 2004). These 45S and 70S complexes do not contain Tip1 that appears to interact with Tea1 within smaller 12S and 20S particles (Feierbach, 2004). The interphase actin cable nucleator, the formin For3 and its binding partner Bud6 are also recruited to the polarisome, possibly through direct interactions between For3 and Tea4 (Feierbach, 2004; Martin et al., 2005). However, cells lacking Tea4 still recruit For3 to the growing cell tip suggesting additional mechanisms function to localize For3 (Martin et al., 2005). Both *tea4* Δ and *for3* Δ cells display NETO defects, but a fusion protein between Tea1 and For3 efficiently recruits For3 to both cell tips and promotes bipolar growth in *tea4* Δ cells (Martin et al., 2005). Furthermore, *tea4* Δ cells fail to recruit the Dual-Specificity-Tyrosine-Phosphorylation-Regulated-Kinase (DYRK) Pom1 to the cell cortex (Tatebe et al., 2005). *pom1* Δ cells are also NETO deficient (Bähler and Pringle, 1998; Tatebe et al., 2005). The Pom1 dependent phosphorylation of the Cdc42-GT Pase-Activating-Protein (Cdc42-GAP) Rga4 has been proposed to exclude Rga4 from the cell tips and allow activation of the Rho-family GTPase Cdc42 at the new-cell-end during NETO (Tatebe et al., 2008). Concordantly, double *rga4* Δ *pom1* Δ mutants

localize active Cdc42 to both cell tips while its activity is restricted to one cell tip in *pom1* mutants (Tatebe et al., 2008). Thus, the polarisome functions in several pathways including recruitment of the formin For3 to trigger the polarized assembly of actin cables and regulation of the Rho-family GTPase Cdc42. Molecular evidence of Tea1 phosphorylation by the Cdc42 effector Orb2/Shk1 suggest existence of feedback mechanisms operating in between these polarity modules (Kim et al., 2003).

The relevance of the +TIP complex in regulating cell polarity is particularly obvious as cells recover from stress. The frequency of ectopic growth sites in *tea1* Δ or *tea4* Δ cells is drastically increased upon osmotic and heat-stress (Mata and Nurse, 1997; Tatebe et al., 2005). Tea4 co-precipitates with the stress-response Mitogen-Activated-Protein-Kinase-Kinase-Kinase (MAPKKK) Win1 and the lack of MAPK Sty1 exacerbates morphological defects of *tea1* Δ cells (Tatebe et al., 2005). A mild heat-stress leads to bent and branched morphology of *sty1* Δ cells suggesting involvement of MAPK signaling in regulating cell polarity (Tatebe et al., 2005). Interestingly, point mutations in Tea4 that abolish binding to the Protein-Phosphatase-1 (PP1) subunit Dis2 also cause defects in cells recovering from osmotic stress (Alvarez-Tabares et al., 2007). The Tea4 mediated recruitment of Dis2 to the cell tips has been proposed to promote Pom1 dephosphorylation and plasma membrane association (Hachet et al., 2011).

1.1.2. The Cdc42-GTPase module

The Rho-family GTPase Cdc42 is best recognized for its highly conserved role in regulating polymerization and subcellular distribution of

actin filaments. Through cytoskeletal regulation and via other mechanisms, Cdc42 has well established roles in a number of cellular processes including morphogenesis, cell migration, cell adhesion, secretion and cytokinesis (reviewed by Etienne-Manneville, 2004; Iden and Collard, 2008). In fission yeast Cdc42 activity is constrained to the sites of growth and division (Tatebe et al., 2008). Null *cdc42* mutants arrest growth as small, round, dense cells while increased levels of Cdc42 activity lead to formation of large, misshapen cells (Miller and Johnson, 1994).

The Rho-family GTPases are molecular switches that attain distinct conformations when GDP- or GTP-bound. In the GTP-bound state Cdc42 Switch-I and Switch-II domains mediate interactions with multiple Cdc42 effector proteins (Mott et al., 1999). The apparent flexibility of the Switch-I region, that is restrained by effector binding, has been suggested to allow recruitment of multiple partners (Feltham et al., 1997; Mott et al., 1999; Spoerner et al., 2001; Phillips et al., 2008). Many effectors employ their Cdc42/Rac-Interactive-Binding (CRIB) motif to bind the active Cdc42 (Burbelo et al., 1995). Membrane association and activity of Cdc42 also require its C-terminal prenyl group (Ziman et al., 1991). The extraction of Cdc42 from the membranes is performed by the guanine-nucleotide-dissociation-inhibitors (GDIs) that are proposed to preferentially bind the GDP-bound form (Johnson et al., 2009). Furthermore, GDIs inhibit GDP dissociation from Cdc42 thus acting as negative regulators of its activity (reviewed by DerMardirossian and Bokoch, 2005).

The guanine nucleotide binding state of Cdc42 is regulated by the Guanine-Nucleotide-Exchange-Factors (GEFs) and the GTPase-Activating-

Proteins (GAPs) (Rossman et al., 2005; Sinha and Yang, 2008). The fission yeast genome encodes two Cdc42-GEFs, Scd1 and Gef1, that both localize to the growing cell ends but appear to play somewhat distinct roles in regulating cell polarity (Chang et al., 1994; Coll et al., 2003). While deletion of both *S. pombe* GEFs is lethal, cells lacking Scd1 have a rounded morphology and *gef1* Δ cells delay NETO and exhibit a slightly decreased diameter (Chang et al., 1994; Coll et al., 2003). The scaffolding protein Scd2 has two Src-Homology-3 (SH3) domains at its N-terminus, a central Phox-Homology (PX) domain and a C-terminal Phox-and-Bem1 (PB1) domain all of which have been implicated in mediating protein-protein interactions (Wheatley and Rittinger, 2005). Cells lacking Scd2 display an increased diameter and the effects of *scd2* Δ and *scd1* Δ are not additive consistent with the role of Scd2 in promoting Cdc42 interaction with its GEF (Chang et al., 1994). Based on studies of the Scd2 budding yeast homologue Bem1, the PB1 domain of Scd2 is presumed to bind the Cdc42-GEF (Peterson et al., 1994; Bose, 2000). The pull-down experiments suggest that Cdc42 is bound by the SH3-containing N-terminus of Scd2 (Endo et al., 2003). Similarly, budding yeast Bem1 binding to the Cdc42-GEF Cdc24 relies on an SH3 domain and its flanking region (Yamaguchi et al., 2007). In a yeast two-hybrid assay, the interaction between Scd1 and Cdc42 requires presence of Scd2 (Endo et al., 2003). SH3 domains of both Scd2 and Bem1 have been shown to bind a class of Cdc42 effectors, the p21-Activated-Protein-Kinases (PAKs) (Chang et al., 1999; Bose, 2000). Interestingly, the role of Bem1 in symmetry breaking has recently been shown to rely on its function in bridging a PAK kinase to the Cdc42-GEF (Kozubowski et al., 2008).

The low intrinsic GTPase activity of Cdc42 is greatly enhanced by GAP binding. Crystal structures of Rho-GTPase•GAP complexes locked in distinct conformational states by nucleotide analogs suggest that GAP binding to GTP-Rho induces a conformational change where the arginine finger of the GAP is positioned directly into the nucleotide binding pocket of Rho (Rittinger et al., 1997). The Arg85 of the GAP then stabilizes the Gln65 of the Rho allowing it to form a hydrogen bond and position a molecule of water for subsequent GTP hydrolysis (Rittinger et al., 1997). The sole identified fission yeast Cdc42-GAP Rga4 localizes to the cell cortex but is excluded from the growing cell tips (Das et al., 2007). Overexpression of Rga4 decreases levels of GTP-bound Cdc42 consistent with its role as a negative Cdc42 regulator (Tatebe et al., 2008). Cells lacking Rga4 have increased cell diameter, possibly due to decreased Cdc42 inactivation at the lateral cell cortex (Das et al., 2007; Tatebe et al., 2008).

Spatial distribution of the active Cdc42 is regulated both by upstream regulators and by intrinsic mechanisms operating within Cdc42-GTPase module. In *S. pombe*, Scd1 has been suggested to mediate signaling from the polarisome to the Cdc42, possibly through its interaction with Moe1 (Chen et al., 1999; Minc et al., 2009). However, the *scd1*Δ cells are capable of polarizing the growth machinery due to existence of additional pathways linking the polarisome and Cdc42 (Kelly and Nurse, 2011). Cdc42 regulation by the tip specification machinery might also involve Rga4, which is restricted to the lateral cell cortex by the Pom1 kinase (Tatebe et al., 2008). Tea4 has also been shown to directly recruit For3 (Martin et al., 2005), a formin essential for assembly of interphase actin cables that could participate in the

Cdc42 feedback mechanisms (Wedlich-Soldner, 2003; Wedlich-Soldner et al., 2004).

In budding yeast the daughter cells inherit spatially confined cortical landmark proteins that localize activity of the Ras-like GTPase Rsr1 (reviewed by Chant, 1999; Howell and Lew, 2012). The active Rsr1 can interact with the Cdc24 and the GDP-bound Cdc42 to promote localized Cdc42 activity required for bud formation (Zheng et al., 1995; Kozminski et al., 2003). During cytokinesis in fission yeast, efficient recruitment of Cdc42 to the division site requires the Bin-Amphiphysin-Rvs (BAR) domain protein Hob3 which physically interacts with both Cdc42 and Gef1 (Coll et al., 2007). *hob3Δ* cells are slow to constrict the actomyosin ring and display a cell separation defect (Coll et al., 2007). In turn, Hob3 recruitment to the site of division requires the intact actomyosin ring and the Extended-Fer/CIP4-Homology (EFC) domain protein Cdc15 (Coll et al., 2007); EFC proteins contain the Fer/CIP4-Homology-BAR (F-BAR) domain weakly homologous to the BAR domain.

Feedback loops appear to be a crucial feature in initiation and maintenance of polarized Cdc42 activity (reviewed by Johnson et al., 2011). When the constitutively active Cdc42^{Q61L} is expressed in budding yeast cells arrested in G₁, it organizes into one or two polar caps suggestive of a feedback mechanism concentrating active Cdc42 at the plasma membrane (Wedlich-Soldner, 2003). Application of actin depolymerizing drug latrunculin A (LatA) prevents both Cdc42^{Q61L} cap formation and maintenance (Wedlich-Soldner, 2003). Furthermore, mutations impairing the type-V myosin Myo2 or secretion were found to prevent Cdc42^{Q61L} polar cap formation (Wedlich-

Soldner, 2003). Based on this evidence it was proposed that Cdc42 polarization involves a positive feedback mechanism where active Cdc42 promotes actin cable formation and the type-V myosin mediated delivery of secretory vesicles to the plasma membrane to reinforce the Cdc42 activity (Wedlich-Soldner, 2003; Johnson et al., 2011). Concordantly, the Cdc42^{Q61L} was found to co-fractionate with the secretory vesicle marker Sec4 (Johnson et al., 2011). However, the mechanisms that would explain wild-type Cdc42 recruitment to the secretory vesicles still remain elusive. An alternative model was developed from studies on *S. cerevisiae* cells that lack the instructional signals from Rsr1 and polarize Cdc42 to single random cortical spot (Irazoqui et al., 2003). Breaking of symmetry required for the bud formation in *rsr1Δ* cells depends on the scaffold protein Bem1 (Irazoqui et al., 2003). Bridging the Cdc42 effector PAK kinase and GEF Cdc24 is the essential role of Bem1 in *rsr1Δ* cells since artificial chimera linking PAK and GEF was found to bypass the Bem1 requirement (Kozubowski et al., 2008). Thus positive reinforcement of active Cdc42 was proposed to rely on its effector PAK interacting with Bem1 to promote recruitment of the Cdc42-GEF (Kozubowski et al., 2008). Mathematical simulations of the two described positive feedback systems have relied on a limited parameter range thus leaving physiological relevance of each mechanism under debate (Johnson et al., 2011).

Recent high-end imaging techniques have uncovered rapid oscillations in Cdc42 activity in both budding and fission yeast (Das et al., 2012; Howell et al., 2012). The *rsr1Δ S. cerevisiae* cells in initial stages of symmetry breaking form multiple foci of Cdc42 activity that compete until one activity

center “wins” suggesting a competition mechanism operating between them (Howell et al., 2012). Interestingly, the initial clusters show oscillatory levels of GTP-bound Cdc42 (Howell et al., 2012). In case of *S. pombe*, time-lapse imaging revealed oscillations in the Cdc42 activity at a single cell tip (Das et al., 2012). In case of bipolar cells, the oscillations in active Cdc42 between two cell tips had opposite phase implying a competitive mechanism (Das et al., 2012). The theoretical models developed to describe this phenomena postulate negative feedback as an integral element of Cdc42 regulation (Das et al., 2012; Howell et al., 2012). Though molecular mechanisms of negative feedback remain elusive, both Cdc42-directed GAP and the endocytic internalization of Cdc42 could play a role (Ozbudak et al., 2005; Marco et al., 2007). Furthermore, *S. pombe* PAK kinase Orb2/Pak1/Shk1 has been suggested to participate in the negative feedback and limit the maximum level of Cdc42 at a single cell tip (Das et al., 2012).

The interlocked feedbacks are proposed to provide robustness to the Cdc42-GTPase module based polarity mechanisms (Howell et al., 2012). However, spatial regulation of Cdc42 also displays a degree of plasticity that allows morphological transitions. During invasive filament formation, *S. pombe* cells grow only at one cell tip to which active Cdc42 is localized (Dodgson et al., 2010). In response to a pheromone, fission yeast cells in G₁ stage of the cell cycle orient active Cdc42 zones and growth towards their mating partners (Segall, 1993; Bendezú and Martin, 2012). Remarkably, in the early stage of this process active Cdc42, Scd1 and Scd2 colocalize to dynamic zones that are observed probing the entire cell cortex (Bendezú and Martin, 2012). At this stage, the growth is impeded due to a block in exocytosis of cell

wall remodeling enzymes Bgs1 and Bgs4 (Bendezú and Martin, 2012). The mechanisms operating between the pheromone signaling and active Cdc42 in fission yeast remain unclear. In case of migrating myeloid cells, chemoattractants activate the G-protein-coupled receptors and promote dissociation between its α and $\beta\gamma$ subunits (Murphy, 1994). The $G_{\beta\gamma}$ then directly recruits PAK1 and the coupled Cdc42 activator α -PIX to promote localized activation of Cdc42 responsible for actin cytoskeletal dynamics associated with lamellipodium formation (Li et al., 2003).

1.1.3. Division site positioning

Cell division is the final event in the cell cycle that results in physical separation of two daughter cells. Positioning the cleavage plane is of major importance for the morphology of individual cells as well as tissue architecture in both plants and animals (reviewed by Gillies and Cabernard, 2011; Rasmussen et al., 2011).

Upon anaphase distinct signals originating from the microtubules of the central spindle and spindle asters position the division plane in animal cells (Bringmann and Hyman, 2005; Werner et al., 2007). The dynamic subpopulation of astral microtubules appears to negatively regulate cortical accumulation of the myosin II in *C. elegans* thus restricting the cleavage furrow away from the spindle asters (Werner et al., 2007). The central spindle and potentially stable astral microtubules have been proposed to promote the cleavage plane positioning by activating the small GTPase RhoA, a key regulator of actomyosin ring dynamics (Bement et al., 2005). The RhoA activator GEF ECT2 binds to the RhoA GAP CYK-4 which is also interacting

with the kinesin motor MKLP1 to form the centralspindlin complex accumulated at the central spindle (Yüce et al., 2005; Nishimura and Yonemura, 2006; Pavicic-Kaltenbrunner et al., 2007; Hutterer et al., 2009; Su et al., 2011). How these spindle localized RhoA regulators reach the cellular cortex remains unclear. The mechanisms involved could involve diffusion, transport along microtubules or actin cables (Hu et al., 2008a; Vale et al., 2009; von Dassow et al., 2009).

During the G₂ stage of the cell cycle, cortical microtubule arrays of plant somatic cells organize a cortical band of cytoskeletal filaments termed the preprophase band that marks the future division plane (reviewed by Van Damme, 2009). The preprophase band also has a role in the formation and initial orientation of the mitotic spindle (Yoneda et al., 2005; Ambrose and Cyr, 2008). Interestingly, the preprophase band is disassembled in prometaphase and the future division plane can be visualized as the so-called actin depleted zone, a region of low actin cytoskeleton abundance flanked by actin rich regions termed “twin peaks” (Cleary and Gunning, 1992). A prominent role for such actin organization in positioning the division site has been suggested by findings that transient depolymerization of actin during prophase or metaphase disrupts the cell plate orientation while likewise treatment during cytokinesis has almost no effect (Hoshino et al., 2003). More recently, identification of adenomatous-polyposis-coli-related-protein TAN and RanGAP1 in maize and *Arabidopsis* suggested a mechanism how preprophase band positional signals are maintained until cytokinesis is completed (Cleary and Smith, 1998; Walker et al., 2007; Xu et al., 2008). TAN is recruited to the division site at prophase by a microtubule dependent

mechanism where it persists until completion of cytokinesis in a microtubule independent manner (Walker et al., 2007).

Similarly to higher plants, yeast cells specify their division plane prior to mitosis (reviewed by Oliferenko et al., 2009). In fission yeast, the role of microtubules in division site placement is indirect and mediated by its function in positioning the nucleus (Tolic-Nørrelykke et al., 2005). Displacement of the nucleus from the cell middle in interphase or early mitosis leads to placement of the division plane away from the cell equator and to the cortical region overlaying the displaced nucleus (Daga and Chang, 2005; Tolic-Nørrelykke et al., 2005). Interestingly, nuclear displacement by centrifugation in plant cells has been reported to cause formation of the preprophase band in the region of the displaced nucleus (Murata and Wada, 1991).

Identified in a screen for fission yeast cells defective in division site placement, the anillin-like protein Mid1 has been suggested to signal the nuclear position to the overlying cortex (Chang et al., 1996; Paoletti and Chang, 2000; Almonacid et al., 2009). During interphase Mid1 shuttles between the nucleus and the overlying cortical band of nodes where it is anchored by the Synapses-of-Aphids-Defective (SAD) family kinase Cdr2 (Almonacid et al., 2009). As cells enter mitosis Polo-family kinase Plo1 phosphorylates Mid1 to promote its nuclear export and recruitment to the cortical nodes in a Cdr2 independent manner (Bähler et al., 1998; Almonacid et al., 2009). Multiple Nuclear-Export-Sequences (NES) and Nuclear-Localization-Signal (NLS) have been identified to contribute to the nucleocytoplasmic shuttling of Mid1 (Paoletti and Chang, 2000; Almonacid et al., 2009). Deletion of both NESes abolishes nuclear export of Mid1 and impairs

its function in positioning the division plane whereas Mid1 nuclear localization mutants misplace the septum in *cdr2Δ* cells (Paoletti and Chang, 2000; Almonacid et al., 2009). During cell division the cortical Mid1 recruits several actomyosin ring components including the type-II myosin heavy chain Myo2 thus instructing the position of the division site (Wu et al., 2003; Motegi et al., 2004).

Interestingly, cells lacking ER tubulating proteins localize Mid1 to a very wide cortical region suggesting that reticulation of the ER network allows Mid1 to access the inner surface of the plasma membrane (Zhang et al., 2010, 2012). Since the cortical band of Mid1 and Cdr2 nodes also expands laterally in Pom1 kinase mutants, it appears that inhibitory signals from the cell tips also participate in positioning the division site (Celton-Morizur et al., 2006; Moseley et al., 2009). Furthermore, tip localized polarity determinants Tea1, Tea3 and Pom1 function to prevent septum formation at the cell poles in a Mid1 independent manner (Huang et al., 2007).

1.2. Actin cytoskeleton

The combination of bioinformatics, structural data and cell biological approaches have to date given a glimpse of cytoskeletal proteins diversity in the domains of *Bacteria*, *Archea* and *Eukarya* (reviewed by Wickstead and Gull, 2011). Evolutionary conservation of the large number of cytoskeletal regulators between distant eukaryotic lineages implies a remarkable build up in the cytoskeleton complexity preceding the last eukaryotic common ancestor (reviewed by Rivero and Cvrcková, 2000; Cavalier-Smith, 2006). This ancestral cell appears to have evolved not only actin and myosin, but an

extensive set of modules remodeling the microfilament system (Rivero and Cvrcková, 2000). During subsequent eukaryotic diversification this basic “toolbox” of actin cytoskeleton was employed to build diverse actin structures essential to cell division, contractility, motility and intracellular transport (Wickstead and Gull, 2011). However, the basic mechanisms of actin cytoskeleton dynamics and regulation appear conserved and the research in yeast has been of great value to their understanding.

Distantly related to the Hsp70 chaperones, actin is an ATPase that exists as the monomeric G-actin that can polymerizes into F-actin filaments consisting of two protofilaments wound into a right-handed helix. At sufficiently high concentrations ATP-actin monomers in solution oligomerize to form the nucleus of the actin filament. Subsequent dynamics of the actin polymer, referred to as “treadmiling”, include addition of ATP-actin at the so-called “barbed” end of the filament while the loss of ADP-actin occurs from the opposite, “pointed” end. In an *in vivo* context, the nucleation, nucleotide exchange and both polymerization and depolymerization of actin are regulated by a number of accessory proteins (Alberts et al., 2007).

The following sections focus on actin cytoskeleton organization and dynamics in fission yeast cells and offer a brief overview of microfilament dynamics in other model systems.

1.2.1 Interphase actin cytoskeleton in fission yeast

In interphase fission yeast actin cytoskeleton forms morphologically distinct actin patches, polarizing towards the growing cell tips, and actin

cables extending from the cell tips towards the cell interior (Marks et al., 1986)

Formation of actin patches requires activation of the highly conserved Arp2/3 complex to stimulate nucleation of approximately 150 short actin filaments organized into a branched network in *S. pombe* (Berro et al., 2010; Sirotkin et al., 2010). Proteins that crosslink and bundle actin filaments, such as fimbrin Fim1, transgelin Stg1 and drebrin App1, localize to actin patches and might function to strengthen the actin network (Nakano et al., 2005; Sirotkin et al., 2010; Skau and Kovar, 2010).

The mechanisms regulating the Arp2/3 complex tightly link actin patches to the sites of endocytosis. In fact, endocytic internalization in yeast requires formation actin patches (Chvatchko et al., 1986; Kübler and Riezman, 1993; Munn et al., 1995). Recruitment of clathrin and multiple scaffold and adaptor proteins to the plasma membrane precedes actin patch assembly (Sirotkin et al., 2010, reviewed by Moseley and Goode, 2006). Subsequent recruitment of the Wiskott-Aldrich-Syndrome-Protein (WASP) Wsp1 is presumably the key step in activation of the Arp2/3 complex with additional regulation provided by the type-I myosin Myo1 and endocytic adaptor protein Pan1 (Lee et al., 2000; Sirotkin et al., 2005, 2010). Additional mechanisms of Arp2/3 complex regulation might link actin patches to the sites of polarized growth possibly through phosphorylation of type-I myosins by PAK kinases or formin mediated WASP recruitment to the cell cortex in budding yeast (Wu et al., 1997; Lechler et al., 2001). Furthermore, Rho-GTPases have been implicated in relieving inhibition of WASPs in higher eukaryotes though these mechanisms remain controversial in yeast (Kurisu and Takenawa, 2009).

Unlike budding yeast, the fission yeast cells lacking interphase actin cables are viable but exhibit defects in cell polarity and NETO (Pruyne et al., 1998; Feierbach and Chang, 2001). The electron microscopy studies suggest that fission yeast interphase actin cables consist of overlapping, parallel actin filaments with their barbed ends oriented towards the cell cortex (Kamasaki et al., 2005). The formins are a highly conserved family of actin nucleators proposed to simultaneously initiate actin polymerization and to bind barbed ends of actin filaments (reviewed by Faix and Grosse, 2006). In such a manner they are expected to promote formation of long linear chains of actin polymers.

In fission yeast, nucleation of actin cables in interphase is dependent on the formin For3 (Feierbach and Chang, 2001). For3 is activated and resides at the cell tips of *S. pombe* cells for only several seconds before moving inwards, presumably by retrograde flow of the actin filaments in the cable (Martin and Chang, 2006). The For3 activation appears to rely on several overlapping mechanisms. G-actin binding protein profilin has been shown to bind the proline rich sequences of several formins and is likely to contribute to For3 function since fission yeast cells carrying the *cdc3-113* temperature sensitive profilin allele lack interphase actin cables (Romero et al., 2004; Kovar et al., 2006; Martin and Chang, 2006). For3 co-immunoprecipitates with polarisome component Tea4 and strikingly, Tea4 overexpression induces ectopic actin cable nucleation in a For3 dependent manner (Martin et al., 2005). Furthermore, a polarisome component Bud6 also binds For3 and is required for the tip localization of the For3 C-terminus but not its N-terminus (Martin et al., 2007). Bud6 also appears to regulate For3 actin nucleating

activity since mutations that partially relieve For3 autoinhibition have been shown to rescue the weak actin cables and NETO defects of *bud6Δ* cells (Martin et al., 2007). Autoinhibition through intramolecular binding of the N-terminal Diaphanous-Inhibitory-Domain (DID) to the C-terminal Diaphanous-Autoregulatory-Domain (DAD) is an important regulatory mechanism of the Diaphanous related formins (Watanabe et al., 1997; Li and Higgs, 2003; Lammers et al., 2005). Even though For3 lacks a conventional DAD domain, an inhibitory intramolecular interaction between the N- and the C- terminal halves of the protein has been implicated in its regulation (Martin et al., 2007). Binding of Rho-GTPases to the GTPase-Binding-Domain (GBD) of Diaphanous related formins alleviates the autoinhibition and Cdc42 has been proposed to exert similar action in regulating For3 activity (Watanabe et al., 1997; Alberts, 2001; Martin et al., 2007).

Polarized growth and delivery of secretory vesicles to the growth sites is reliant on type-V myosin transport along actin cables in budding yeast cells and in fission yeast cells with compromised exocyst function (Pruyne et al., 1998; Bendezú and Martin, 2011). Accordingly, *myo52Δ* cells are misshapen and display an abnormal accumulation of secretory vesicles throughout the cytoplasm in electron micrographs (Motegi et al., 2001; Win et al., 2001). The Myo52 fused to a fluorescent protein can be observed undergoing long-distance, directional movement and accumulating at the sites of growth and division (Motegi et al., 2001; Win et al., 2001). The second type-V myosin encoded by the fission yeast genome Myo51 does not appear to play a prominent role in vegetative growth (Doyle et al., 2009). The type-V myosins utilize their globular tail domain to bind distinct, organelle specific receptors.

In fission yeast extensive studies on type-V myosin receptors are lacking but the *S. cerevisiae* exocyst subunit Sec15 and Rab-family GTPases Ypt31, Ypt32 and Sec4 mediate its recruitment to secretory vesicles, Ypt11 and Rab2 are likely linkers to the late Golgi compartments and Vac17•Vac8 complex is the vacuole specific receptor (Jin et al., 2011 and reviewed by Hammer and Sellers, 2012). However, the molecular details of how type-V myosins mediate inheritance of the cortical ER in budding yeast remain to be explored (Estrada et al., 2003). The actomyosin dependent mechanism for the peripheral ER transport have also been reported in higher eukaryotes including plants and Purkinje neurons (Ueda et al., 2010; Wagner et al., 2011). It has been recently proposed that Myo52 may also functions in regulating the actin cable dynamics and organization (Presti et al., 2012).

Distinct eukaryotic lineages appear to utilize the microtubule and actin cytoskeleton to a varying degree for organelle transport (reviewed by Vale, 2003). As described above, in both budding and fission yeast the actin cables serve as the primary tracks for the vectorial transport of the endomembrane system (Pruyne et al., 2004). Remarkably, rerouting the actin-based transport to microtubules by fusing the motor domain of kinesin Tea2 to the cargo-binding region of Myo52 rescues the multiple defects of cells lacking interphase actin cables (Lo Presti and Martin, 2011).

The mechanisms regulating polarized actin cytoskeleton exhibit a high degree of plasticity. Yeast cells readily orient actin filaments towards their mating partners (Bendezú and Martin, 2012). Furthermore, it has been recently shown in budding yeast that the protein kinase C Pkc1 functions to enable relocalization of the growth machinery including F-actin to the site of cell

injury (Kono et al., 2012). The heat-stressed *S. cerevisiae* cells redistribute the bud localized β -glucan synthase and the F-actin throughout the entire cell cortex in an actin cytoskeleton dependent manner (Delley and Hall, 1999). In budding yeast, heat-stress has been proposed to activate the cell wall integrity pathway and promote nucleotide exchange of the Rho-family GTPase Rho1, which in turn initiates F-actin redistribution (Philip and Levin, 2001). Interestingly, repolarization of actin to the cell bud as cells adapt to elevated temperature has been suggested to depend on a negative feedback mechanism where Pkc1 activates MAPK cascade to inhibit the Rho1-GEF Rom2 (Guo et al., 2009). In *S. pombe* several types of stress, including heat and osmolytes, also activate MAP kinases and cause F-actin to redistribute throughout the cell cortex (Shiozaki et al., 1998; Bao, 2001; Kanai et al., 2005; Petersen and Hagan, 2005; Ma et al., 2006; Robertson and Hagan, 2008; Garcia et al., 2009). Interestingly, fission yeast MAPK partially regulate the actin cytoskeleton through the Polo-kinase Plo1 (Petersen and Hagan, 2005). Upon stress or in cells with constitutive MAPK signaling Plo1 is phosphorylated at the Ser402 (Petersen and Hagan, 2005). Cells carrying Ser402Ala mutation in Plo1 are deficient in restoring polarized actin distribution after some stress conditions (Petersen and Hagan, 2005). Actin cytoskeleton remodeling might also be required for initiation of bipolar growth since brief LatA treatment can promote NETO in the monopolar, G₁ arrested cells (Rupes et al., 1999). Accordingly, cells with stabilized actin cytoskeleton due to deletion of serine/threonine protein kinase Ssp1 are monopolar (Rupes et al., 1999). Interestingly, osmotic-stress promotes bipolar growth of the NETO-defective *ssp1* Δ cells possibly through perturbations of actin cytoskeleton (Rupes et al.,

1999). Early studies on actin cytoskeleton suggest that its remodeling during stress is in fact evolutionarily conserved (Welch and Suhan, 1985; Hirono et al., 1987). However, the dynamics and roles of actin regulators during environmental stress and adaptation remain poorly understood.

1.2.2 The actomyosin ring

Fidelity of cell division is essential to prevent polyploidy that contributes to cancer development (Fujiwara et al., 2005; Rosario et al., 2010; Lind et al., 2011; reviewed by Sagona and Stenmark, 2010). With a notable exception of plant cells and some protists, most eukaryotes including fungi, nematodes, insects and vertebrates, execute cell division through action of an actomyosin based contractile ring (reviewed by Hales et al., 1999). In animal cells the initial recruitment of actin filaments and type II myosin to the cell cortex is independent of each other but both require RhoA activity (Dean et al., 2005; Werner et al., 2007; Zhou and Wang, 2008; Vale et al., 2009; Uehara et al., 2010). In some organisms and specific cell types additional mechanisms of actin and myosin II delivery to the cell equator *via* cortical flow have been described (Murthy and Wadsworth, 2005; Yumura et al., 2008). The active RhoA on one hand stimulates the formins to nucleate linear actin polymers while CYK-4 has been proposed to diminish branched filament formation at the cleavage furrow by preventing activation of Arp2/3 complex (Castrillon and Wasserman, 1994; Watanabe et al., 1997; Canman et al., 2008). On the other hand, RhoA stimulates ROCK kinase to activate type II myosin by direct phosphorylation and through inactivation of myosin-II phosphatase (Kimura et al., 1996). The RhoA appears to also be directly

involved in recruiting anilin to the cleavage furrow in human cells (Piekny and Glotzer, 2008). Anilin has been proposed to function as a scaffolding protein that links RhoA, actin and myosin through direct interactions (Piekny and Glotzer, 2008). Furthermore, it physically interacts and organizes septins at the division site (Kinoshita et al., 2002; Maddox et al., 2007). Anilin-depleted cells initiate furrowing but either fail or undergo defective cytokinesis (Echard et al., 2004; Straight et al., 2005; Maddox et al., 2007). Molecular mechanisms recruiting and roles of additional proteins localized to the cleavage furrow, such as alpha-actinin, and filamin have been described to various extents (Mukhina et al., 2007; Mondal et al., 2010) (reviewed by Glotzer, 2005). The temporal control of cytokinesis in higher eukaryotes is comprised of several overlapping processes (reviewed by Barr and Gruneberg, 2007). The drop of Cdk1/cyclin B1 associated with anaphase onset regulates initiation of cytokinesis and drugs inhibiting Cdk1 kinase activity cause premature cytokinesis (Wheatley et al., 1997; Niiya et al., 2005). In contrast, Aurora and Polo family kinases promote cytokinesis possibly through phosphorylating RhoA regulators ECT2 and CYK-4 (Minoshima et al., 2003; Burkard et al., 2007; Petronczki et al., 2007).

S. pombe has been an invaluable model system for identifying highly conserved cytokinetic components and exploring their roles in actomyosin ring dynamics (for a comparative review see Balasubramanian et al., 2004). The initial accumulation and assembly of the type-II myosin heavy and light chains Myo2 and Cdc4 to the division site is F-actin dependent but their maintenance after ring assembly is not (Naqvi et al., 1999). The electron microscopy suggest that the early anaphase ring is predominantly comprised

from two semicircular bundles of actomyosin filaments with opposite orientation (Kamasaki et al., 2007). Such organization is in line with the “leading cable” model where the ring assembly is initiated at a single point at the cell cortex from which actomyosin filaments extend within a zone defined by Mid1 to circumscribe the cell equator (Chang et al., 1997; Arai and Mabuchi, 2002). The essential mitotic formin Cdc12, specifically required to nucleate actin cables during cytokinesis, has been reported to localize to a single cortical spot before ring formation (Chang et al., 1997). Furthermore, Myo2 and its regulatory light chain Rlc1 have also been observed as a single dot at the medial cortex prior to ring assembly (Wong et al., 2002).

The alternative “search and capture” model of actomyosin ring assembly proposes an elegant explanation how Mid1 positions the cytokinetic machinery. Upon nuclear exit in early mitosis, Mid1 organizes a narrow band of cortical nodes and recruits ring components that on one hand nucleate actin, and on the other hand capture actin filaments nucleated from other nodes. Such a broad network of interconnected nodes would then coalesce into a single ring by the pull of type-II myosin that is also recruited to the Mid1 nodes (Bähler et al., 1998; Vavylonis et al., 2008; Laporte et al., 2011). Key components of the cytokinetic machinery reported to localize to the Mid1 nodes include the IQGAP protein Rng2, EFC domain protein Cdc15 and myosin-II heavy, light and regulatory chains Myo2, Cdc4 and Rlc1 and the formin Cdc12 (Wu et al., 2003; Laporte et al., 2011). Highly resolved spatio-temporal imaging coupled with genetic epistasis analysis and co-immunoprecipitation experiments have suggested that a complex system of physical interactions allows sequential recruitment of ring components to

Mid1 nodes. Mid1, Rng2 and Cdc4 interact *in vivo* (D'souza et al., 2001; Laporte et al., 2011; Padmanabhan et al., 2011) and the efficient recruitment of Myo2 to the Mid1 nodes requires both Rng2 and Cdc4 (Laporte et al., 2011). The recruitment of the EFC protein Cdc15 to Mid1 nodes is somewhat controversial and might be mediated by interactions with both Mid1 and Rng2 (Roberts-Galbraith et al., 2010; Laporte et al., 2011). Cdc12 fails to efficiently localize to Mid1 nodes in cells lacking Cdc15, Rng2 or Cdc4 and has been reported to physically interact with Cdc15 (Carnahan and Gould, 2003; Laporte et al., 2011). However, the reported co-immunoprecipitation results might reflect interactions in later stages of ring formation rather than in Mid1 nodes. Resolving this issue will require *in vitro* analysis of interactions between ring components much like those showing that Mid1 directly binds Rng2 (Padmanabhan et al., 2011). Furthermore, how the force is generated during Mid1 nodes compaction versus ring constriction will need to be resolved. In that respect it might be interesting to explore the role of Myo2 regulator, a UCS-domain protein Rng3 (Wong et al., 2000; Lord and Pollard, 2004).

The two mechanisms of ring assembly are not mutually exclusive and both might be employed to a various degree under different conditions. Ring components do not assemble into cortical nodes in cells lacking Mid1 and instead organize several filaments that compact into mislocated and misshapen contractile rings (Bähler et al., 1998; Motegi et al., 2004) . However, when septum deposition is impaired *mid1Δ* cells are capable of correcting the ring morphology and forming septa perpendicular to the long cell axis (Huang et al., 2008).

As cells exit mitosis, a signaling cascade termed Septation-Initiation-Network triggers the actomyosin ring constriction (reviewed by Krapp and Simanis, 2008). Concomitantly with ring constriction, membrane material is inserted at the division site and the septum is synthesized (Jochová et al., 1991). The molecular linkage between the actomyosin ring and the plasma membrane is not well understood. The essential EFC domain protein Cdc15 has been suggested to coordinate actomyosin ring constriction with membrane dynamics. The founding member of the Pombe-Cdc15-Homology (PCH) family of proteins, Cdc15 contains an N-terminal F-BAR domain, weakly homologous to canonical BARs, and a C-terminal SH3 domain. The F-BAR domain has been shown to bind liposomes containing phosphatidylserine, PI(4,5)P2 and PI(3,4,5)P3 (Itoh et al., 2005; Tsujita et al., 2006). Furthermore F-BAR domains can promote membrane curvature (Itoh et al., 2005; Tsujita et al., 2006). In crystal structures human FBP17 and CIP4 F-BAR domain dimers assume a slightly curved, banana-like shape where the concave surface binds to membranes (Shimada et al., 2007). The dimers may polymerize in an end-to-end fashion and assemble helical lattice stabilized by lateral interactions between dimers (Shimada et al., 2007; Frost et al., 2008). The N-terminus of Cdc15 has been shown to also directly engage with Cdc12 and Myo1 *in vitro* and *in vivo* (Carnahan and Gould, 2003).

Cdc15 localizes to the actin patches in interphase but is recruited to the actomyosin ring early in mitosis (Fankhauser et al., 1995; Carnahan and Gould, 2003; Arasada and Pollard, 2011). Its essential function in stabilizing contractile rings is exhibited only upon SIN signaling activation (Wachtler et al., 2006). At restrictive temperatures, cells carrying the conditional *cdc15*

alleles are capable of forming transient actomyosin rings early in mitosis (Fankhauser et al., 1995; Chang et al., 1996; Balasubramanian et al., 1998). In *cdc15* deficient cells experimentally arrested at metaphase the actomyosin rings are maintained (Wachtler et al., 2006). However, it appears that Cdc15 together with Mid1 supports contractile ring stability also at metaphase since the rings are disassembled in metaphase arrested cells when function of both proteins is impaired (Wachtler et al., 2006). In Cdc15 mutants lacking the SH3 domain, actomyosin ring constriction is wobbly and occurs at decreased rates suggesting that SH3 domain functions in stabilizing the contractile ring, possibly by recruiting the C2 domain protein Fic1 and the paxillin homolog Pxl1 (Roberts-Galbraith et al., 2009).

Cdc15 undergoes extensive phosphorylation at 30-50 distinct sites in a cell cycle dependent manner with the hypophosphorylated form dominant in dividing and hyperphosphorylated in interphase cells (Fankhauser et al., 1995; Roberts-Galbraith et al., 2010). Cdc12 preferentially interacts with dephosphorylated Cdc15 isoform that attains a “stretched” filament-like conformation in electron micrographs, as compared to the globular appearance of the hyperphosphorylated Cdc15 (Roberts-Galbraith et al., 2010). Conversion of endogenous Cdc15 phosphorylatable residues to alanine causes precocious relocalization of the mutant Cdc15 and several other contractile ring components including Cdc12 to the cell equator (Roberts-Galbraith et al., 2010). However, these mutants do not exhibit equatorial F-actin in interphase, a phenotype associated with overexpression of wild-type Cdc15 (Fankhauser et al., 1995; Roberts-Galbraith et al., 2010). It has been reported that Clp1

phosphatase promotes mitotic dephosphorylation of Cdc15 and regulates its mobility at the contractile ring (Wachtler et al., 2006; Clifford et al., 2008).

Centripetal septum deposition and ring constriction seem to be tightly linked since 1,3- β -glucan-synthase Cps1 loss-of-function mutants that can not form the septum are also incapable of ring constriction (Liu et al., 2000). Brefeldin A treatment, which inhibits the anterograde ER to Golgi trafficking, prevents Cps1 delivery to the division site and phenocopies the mutant Cps1 phenotype. As septum biogenesis proceeds, actin reorganizes to clusters of patches on both sides of the septum (Marks and Hyams, 1985) . Secondary septa are then formed on either side of the primary one that is eventually dissolved resulting in cell separation (Humbel et al., 2001).

1.2.3. Temporal regulation of actin cytoskeleton in fission yeast

Interphase *S. pombe* cells polarize actin cables and patches towards the cell tips. As cells enter mitosis however, the F-actin is lost from the cell poles and an equatorial actomyosin ring forms. An emerging view is that such spatio-temporal distribution of actin cytoskeleton is regulated by two interconnected signaling pathways termed Septation-Initiation-Network (SIN) and Morphogenesis-Related-NDR-Kinase-Network (MOR) (Ray et al., 2010).

A common feature of identified MOR mutants in fission yeast is the loss of polarized actin distribution in interphase cells (Kanai et al., 2005). The identified components of the pathway include the *Drosophila*-Furry-like protein Mor2, human-mo25-family protein Pmo25, the germinal center (GC) kinase Nak1, the nuclear Dbf2-related (NDR) kinase Orb6 and its activator Mob2 (Snell and Nurse, 1994; Verde et al., 1998; Hirata, 2002; Hou et al.,

2003; Kanai et al., 2005; Leonhard and Nurse, 2005). Even though I lack comprehensive understanding of how MOR signaling orchestrates polarized growth, its individual components have been implicated in regulating distinct aspects of cell polarity (reviewed by Maerz and Seiler, 2010). Nak1 has been reported to regulate the localization and to physically engage the amphiphysin homolog Hob1 and Wiskott-Aldrich-syndrome-protein Wsp1 and in that manner is suggested to control the Arp2/3 complex mediated polymerization of actin patches (Huang et al., 2005). Furthermore, cells require Orb6 kinase activity to restrict the active Cdc42 and Gef1 to the cell tips (Das et al., 2009). Concordantly, Orb6 and Cdc42-GAP Rga4 interact in a yeast-two-hybrid assay and Orb6•Mob2 complex can phosphorylate the Cdc42-GEF Gef1 *in vitro* (Das et al., 2007, 2009). Studies on homologous pathways in budding yeast and *Neurospora* suggest that MOR might also regulate the secretory pathway and gene expression (Nelson et al., 2003; Kurischko et al., 2008).

Actomyosin ring constriction and successful execution of cytokinesis in fission yeast requires activation of the SIN signaling pathway (reviewed by Krapp and Simanis, 2008). Mutations inactivating SIN signaling lead to defects in actomyosin ring maturation, constriction and septation thus causing formation of elongated, multinucleate cells that eventually lyse (Fankhauser and Simanis, 1994; Schmidt et al., 1997; Sparks et al., 1999; Chang and Gould, 2000; Guertin et al., 2000). The NDR kinase Sid2 and its regulatory subunit Mob1 are the only component of the SIN pathway reported to localize to the actomyosin ring but their targets relevant to ring contractility remain elusive (Sparks et al., 1999; Salimova et al., 2000). Interestingly, all identified components of the SIN signaling at least at some point in the cell cycle

localize to the spindle pole bodies (SPB), the yeast analogue of centrosomes (reviewed by Krapp et al., 2004b). Based on dependencies for recruitment to the SPB, the Sid2 has been proposed to be activated by Sid1 kinase and its regulatory subunit Cdc14, which are in turn positively regulated by Cdc7 kinase (Guertin et al., 2000). However, the biochemical support for this model is presently lacking. The kinase activity of Cdc7 does not oscillate throughout the cell cycle but its localization to the SPB is mitosis specific and depends on the nucleotide state of the Ras-family GTPase Spg1 (Sohrmann et al., 1998; Li et al., 2000a). Spg1 localizes to the SPB throughout the cell cycle but its activity is repressed in interphase by the GAP activity of the Cdc16•Byr4 complex (Schmidt et al., 1997; Furge et al., 1998, 1999; Li et al., 2000a). Recruitment of Spg1 and downstream SIN components to the SPB depends on the scaffolding proteins Cdc11, Sid4 and Ppc89 (Krapp et al., 2001; Morrell et al., 2004; Rosenberg et al., 2006). The coordination between the cell cycle and the SIN signaling is likely provided by the Polo kinase Plo1 and ubiquitin ligase Dma1. When *plo1* transcription is shut-off cells fail to septate and artificial activation of SIN in *plo1* mutant cells allows for septum formation (Ohkura et al., 1995; Tanaka et al., 2001). Furthermore, Plo1 binds Sid4 and has been implicated in phosphorylating fission yeast Cdc11 and the Byr4 homologue in budding yeast (Hu et al., 2001; Krapp et al., 2004a; Morrell et al., 2004). Ubiquitination of Sid4 by Dma1 has been proposed to antagonize Plo1 binding and to prolong Byr4 recruitment to the SPB thus effectively inhibiting SIN activation (Guertin et al., 2002; Johnson and Gould, 2011). Cells lacking Dma1 fail to inhibit cytokinesis upon spindle assembly checkpoint activation indicating that Dma1 might link SIN to the cell cycle

(Murone and Simanis, 1996; Guertin et al., 2002). Furthermore, Sid2 phosphorylation of Cdc11 has been recently proposed to increase SIN signaling robustness through establishing a positive feedback (Feoktistova et al., 2012).

Mutations inactivating Cdc16 and Byr4 lead to hyperactivation of SIN signaling and formation of the ectopic actomyosin rings which constrict to form septa in interphase cells (Fankhauser et al., 1993; Song et al., 1996). Surprisingly, SIN hyperactivation causes cell elongation to cease, prevents G2/M progression and disrupts interphase polarity of actin cytoskeleton (Fankhauser et al., 1993; Ray et al., 2010). The mechanistic details of SIN regulation of interphase polarity remain unclear but appear to be mediated by the MOR signaling (Kanai et al., 2005; Ray et al., 2010). SIN signaling kinases Cdc7 and Sid1, but not Sid2, contribute to upregulation of the Nak1 kinase activity in early interphase (Kanai et al., 2005). However, constitutive SIN signaling throughout interphase inhibits activity of the NDR kinase Orb6 (Ray et al., 2010). Even though MOR signaling does not interfere with the SIN activity directly, it does antagonize precocious actomyosin ring assembly in mutants with elevated SIN activity (Ray et al., 2010).

Even though signaling pathways homologous to SIN and MOR do not exist in metazoans, analogous regulatory Hippo/Lats and Ndr1/2 networks focused around the evolutionarily conserved NDR kinases appear also involved in cytokinesis/mitotic exit and polarity/morphogenesis (Guo et al., 2007; ten Klooster et al., 2009; Zwaenepoel et al., 2012).

1.3. Secretory pathway

An elaborate endomembrane system is a landmark property of eukaryotic cells. Whereas mitochondria and chloroplasts have likely arose through endosymbiosis most other organelles appear to have evolved autogenously, from structures intrinsic to the predecessors of the first eukaryotic common ancestor (Martin, 1999). The seminal work of George Palade, Randy Schekman and Jim Rothman on protein secretion led to postulation of the vesicular transport hypothesis, reiteration of which has served to explain the basic principles of trafficking between autogenously derived organelles of endo- and exocytic pathways. Conceptually, the cargo of the donor subcellular compartments is selectively recruited to the budding vesicles during their formation through a regulated assembly of protein coats. The fully formed vesicles subsequently reach specific acceptor compartments to which they fuse. Research efforts based on this framework have since provided insight into structural, mechanistic and regulatory aspects of each step in the secretory pathway some of which are discussed in subsequent sections. Comparative genomics suggest that these mechanisms are highly conserved and suggest that the last common eukaryotic ancestor exhibited a great degree of endomembrane complexity (Field and Dacks, 2009).

1.3.1. Endoplasmic reticulum

The ER is a highly dynamic membranous system undergoing branching, sliding and fusion of individual elements connected by three-way junctions to organize an intricate network of morphologically distinct compartments termed cisternae and tubules (Lee and Chen, 1988). While the

flattened membranous stacks of the ER cisternae are frequently populated by the ER associated ribosomes, the high curvature ER tubules mostly lack them, suggesting a link between morphology and function of the ER subdomains (Shibata et al., 2010; Pendin et al., 2011). Concordantly, the ER of the highly active secretory cells such as activated B lymphocytes have extensive rough ER organized into cisternae while the muscle cell ER is present largely as a network of smooth tubules (Shohat et al., 1973; Ogata and Yamasaki, 1997). In yeast, the ER is comprised of largely sheet-like nuclear envelope, a peripheral network of tubules and sheets underlying the plasma membrane and elements connecting the two (Johnson et al., 1973; West et al., 2011).

Both membrane lipid composition and several specific protein families have been implicated in shaping the ER morphology (reviewed by Phillips et al., 2009; Pendin et al., 2011). The “wedge”-shaped transmembrane topology of reticulons and DP/Yop1 family proteins has been proposed to introduce positive curvature to membranes (Hu et al., 2008b). Their ability to form homo- and hetero-oligomers is likely crucial to provide scaffolding for the ER tubules (Hu et al., 2008b). Surprisingly, attractive interactions between the curvature-inducing proteins adsorbed at a membrane may arise solely as a consequence of membrane curvature they induce (Reynwar et al., 2007). The dynamin-like GTPase Sey1, homologous to mammalian atlastin, localizes at the three way junctions and helps structure the polygonal network of ER tubules possibly by driving their fusion (Hu et al., 2009). Lunapark family protein Lnp1 also localizes to the three-way junctions and functions to antagonize Sey1 but the underlying mechanism is poorly understood (Chen et al., 2012). Another evolutionarily conserved protein, Tts1 has also been

implicated to contribute in shaping ER tubules but the structural basis of its function remain to be determined (Zhang et al., 2010). Interestingly, the reticulons and DP/Yop1 proteins might also function to stabilize the high curvature at periphery of the ER cisternae (Shibata et al., 2010). The coiled-coil protein Climp-63 has been suggested as an physical intraluminal spacer of sheets in mammalian cells (Shibata et al., 2010). Overexpression of Climp-63 leads to proliferation of the ER sheets whereas its depletion does not abolish the ER sheets and instead causes a reduction in the luminal width (Shibata et al., 2010). Preferential localization of several sheet-associated proteins including Climp63 to the ER sheets is lost in cells treated with pactamycin or puromycin that inhibit translation but not in cells cycloheximide treatment that inhibits translation by stalling ribosomes (Shibata et al., 2010). These results and earlier findings that ER associated translation regulates ER morphology, make it tempting to speculate that the spatial arrangement of large polysome assemblies may restrict them to and help sculpt the ER sheets (Christensen and Bourne, 1999; Puhka et al., 2007; Shibata et al., 2010). The relevance of ER morphology to the overall cellular physiology is not clear. Whereas budding yeast cells lacking tubulating proteins do not exhibit obvious growth defects, mutations in genes regulating ER morphology have been linked to human nervous system diseases (Hu et al., 2008b; Prior et al., 2010). Interestingly, *S. pombe* cells lacking ER tubulating proteins mislocalize the cytokinetic regulator Mid1 during cell division and these defects are rescued when the peripheral ER is detached from the plasma membrane (Zhang et al., 2010, 2012) Thus the fine reticulation of the peripheral ER might be needed to

allow efficient communication between the cytosol and the plasma membrane (Zhang et al., 2012).

The ER exit sites (ERES), also referred to as transitional ER (tER), is another morphologically distinct ER subcompartment described as a ribosome free vesiculating ER surface designated for production of COPII vesicles that shuttle the ER proteins to Golgi apparatus (Orci et al., 1991; Shaywitz et al., 1995; Rossanese et al., 1999). Additionally, the phosphatidylinositol-4-phosphate biosynthesis preferentially occurs at the tER sites and aids production of COPII vesicles (Matsuoka et al., 1998; Blumental-Perry et al., 2006; Farhan et al., 2008). While *S. cerevisiae* and mammalian cells display numerous small tER sites, another budding yeast *Pichia pastoris* (*P. pastoris*) exhibits very few relatively large tER structures (Shaywitz et al., 1995; Rossanese et al., 1999; Hammond and Glick, 2000). The time-lapse studies of fluorescently tagged tER marker proteins in *P. pastoris* suggests that ERES sites are highly dynamic and may form *de novo*, undergo fusion as well as grow and shrink in size (Hammond and Glick, 2000). Findings that depolymerization of microtubules by nocodazole treatment causes clustering of the tER sites next to the Golgi apparatus in NRK cells led to a hypothesis that tER sites are in part defined by the retrograde transport from Golgi (Hammond and Glick, 2000). However, this mechanism needs further experimental support.

Membrane recruitment and activation of the small GTPase Sar1 by its transmembrane, ER localized GEF Sec12 is the trigger for COPII coat assembly (Barlowe and Schekman, 1993; Barlowe et al., 1994). When GTP-bound, Sar1 recruits the Sec23-Sec24 coatomer complex to the membrane

surface while Sec23 function as a Sar1-GAP establishes a feedback control of the vesicle budding (Barlowe et al., 1994; Kuehn et al., 1998; Bi et al., 2002). Sec24 also recruits cargo proteins through direct interactions or via adaptor proteins with distinct Sec24 paralogs implicated in recruiting different cargoes (Kuehn et al., 1998; Miller et al., 2002; Wendeler et al., 2007). Finally, Sec13-Sec31p outer coatomer proteins are recruited to complete the formation of the COPII vesicle typically 60-100 nm in diameter (Salama et al., 1993; Matsuoka et al., 2001). Sar1, Sec23, Sec24, Sec13 and Sec31 are the minimal requirements for *in vitro* reconstitution of the vesicle budding (Matsuoka et al., 1998). However, additional components are required *in vivo* for COPII vesicle formation such as the essential Sec16 (Espenshade et al., 1995). Sec16 localizes to tER sites in a Sar1 independent manner and has been proposed to function as a scaffold organizing and stabilizing COPII coat assembly (Connerly et al., 2005; Watson et al., 2006; Ivan et al., 2008). This hypothesis is supported by Sec16 ability to oligomerize and its physical interactions with Sec13, Sec31, Sec23 and Sec24 (Espenshade et al., 1995; Shaywitz et al., 1997; Whittle and Schwartz, 2010; Yorimitsu and Sato, 2012). *P. pastoris* ERES in the temperature sensitive *sec16^{dot1}* genetic background has appearance of many small spots as compared to two to six large tER sites present in wild-type cells (Connerly et al., 2005). Interestingly, in mammalian cells Sec16 has been identified as a target of MAPK signaling that regulates tER number and size (Farhan et al., 2008; Zacharogianni et al., 2011). Furthermore, changes in cargo load have been shown to influence both tER size and number (Farhan et al., 2008).

1.3.2. Golgi apparatus

The central role of the Golgi apparatus in glycosylation, sulfation, and proteolytic processing of both lipids and proteins transversing the secretory pathway has been long recognized (reviewed by Goldfischer, 1982; Freeze and Ng, 2011). Localization studies suggest that the cargo transiting the Golgi apparatus successively encounter resident Golgi enzymes that progressively carry out post-translational protein and lipid modifications (Rabouille et al., 1995). This model appears to be somewhat idealized since an overlap in distribution of Golgi enzymes carrying out successive processing steps has been reported and additional mechanisms probably ensure fidelity of posttranslational modifications (Nilsson et al., 1993; Mogelsvang et al., 2004). The Golgi compartment is also the sorting center of the secretory pathway that directs cargo to the appropriate subcellular destinations (reviewed by Anitei and Hoflack, 2011). More recently Golgi has received attention as a signaling center that recruits components of multiple signaling networks including those of Ras and cAMP/protein-kinase-A pathway (Nigg et al., 1985; Chiu et al., 2002; Shanks et al., 2002; Goodwin et al., 2005) (and reviewed by Mayinger, 2011). In fact, Golgi fragmentation in late G₂ phase in mammalian cells appears to be a prerequisite for mitotic entry (Sütterlin et al., 2002; Hidalgo Carcedo et al., 2004; Feinstein and Linstedt, 2007). Microinjection of a particular antibody against Golgi-Reassembly-And-Stacking-Protein GRASP55 prevents mitotic fragmentation of Golgi and induces a mitotic delay (Sütterlin et al., 2002). Strikingly, the effects of this *anti*-GRASP55 antibody on mitotic progression are overcome by artificially inducing Golgi

dispersal through treatment with nocodazole or Brefeldin A (Sütterlin et al., 2002).

The flattened cisternae are the basic functional unit of the Golgi apparatus. Higher order organization of the functionally distinct *cis*-, *medial*- and *trans*-Golgi cisternae varies greatly between different organisms. In mammalian cells homotypic cisternae connect laterally and stack with heterotypic Golgi cisternae to form the structure termed the Golgi ribbon that is also described as a set of laterally connected Golgi stacks (Ladinsky et al., 1999). In *Arabidopsis* and *Drosophila* individual Golgi stacks are scattered throughout the cytoplasm (Kondylis et al., 2007; Staehelin and Kang, 2008). Whereas stacking of individual Golgi cisternae is also observed in *P. pastoris*, several eukaryotes including *S. cerevisiae* have individual Golgi cisternae distributed throughout the cytoplasm (Preuss et al., 1992; Rossanese et al., 1999). In *S. pombe* electron microscopy studies report presence of both stacked and individual Golgi cisternae (Johnson et al., 1973; Ayscough et al., 1993). Organization of Golgi partially relies on a structural matrix visualized in electron micrographs of Golgi apparatus in several organisms including *P. pastoris* (Cluett and Brown, 1992; Slusarewicz et al., 1994; Seemann et al., 2000; Mogelsvang et al., 2003). Its components GRASP55, GRASP65 and golgin GM130 have all been implicated in maintaining the Golgi ribbon architecture possibly by physical linkage of neighboring cisternae (Barr et al., 1997; Shorter et al., 1999; Vasile et al., 2003; Xiang and Wang, 2010). Conversely, deletion of the sole GRASP homologue has no apparent effect on the early secretory pathway organization of budding yeasts *P. pastoris* and *S. cerevisiae* (Mogelsvang et al., 2003). Trafficking through Golgi is another

determinant of its structure. A pulse in traffic causes an increase in both number and size of Golgi cisternae in a stack (Trucco et al., 2004). Furthermore, impairment of trafficking through the secretory pathway by Brefeldin A treatment or through Sar1 inactivation causes dispersal of Golgi membranes and retrieval of *cis*- and *medial*-Golgi resident proteins to the ER (Lippincott-Schwartz et al., 1989, 1990; Storrie et al., 1998). *S. cerevisiae* cells with impaired Golgi trafficking due to a mutation of Sec7, a GEF of Arf-family GTPases, exhibit cisternae organized as stacks under certain conditions (Novick et al., 1981).

Eukaryotes utilize distinct strategies to ensure that Golgi complex is inherited by both daughter cells upon cell division. In *Trichomonas* a single Golgi apparatus grows through lateral extension and undergoes medial fission so that each daughter cell could obtain a copy (Benchimol et al., 2001). As mammalian cells prepare for cell division the Golgi ribbon breaks down into numerous small vesicles that reform the daughter Golgi apparatus only as cells exit mitosis. It is not clear whether these vesicles are only peripherally associated with the ER and serve as a template for Golgi assembly or they deliver their contents to the ER and daughter cells form Golgi *de novo* (reviewed by Barr, 2004). Mammalian cells are capable of what appears to be *de novo* Golgi biogenesis upon washout of drugs that simultaneously inhibit Golgi trafficking and disassemble the Golgi matrix (Puri and Linstedt, 2003). Sophisticated imaging techniques have shown that in yeast *cis*-Golgi cisternae may arise *de novo* and correlated these events to the tER dynamics (Bevis et al., 2002). The novel *cis*-Golgi elements are presumed to subsequently give rise to the later Golgi cisternae.

Mechanisms of trafficking through Golgi are heavily debated by five different models (reviewed by Glick and Luini, 2011). Neither of these models fully reconciles the experimental observations regarding Golgi structure and dynamics. The vesicular trafficking hypothesis postulates that individual Golgi cisternae are stable, biochemically distinct compartments that receive and dispatch cargo via vesicles (Farquhar, 1985; Rothman, 1994; Rabouille et al., 1995; Rothman and Wieland, 1996). Considering the size of COPI vesicles that are associated with Golgi trafficking this model is unable to explain how large cargo such as algal scales or procollagen aggregates traverses Golgi (Becker et al., 1995; Bonfanti et al., 1998). Conflicting data on whether COPI vesicles contain cargo proteins or resident Golgi enzymes makes it difficult to distinguish between vesicular trafficking and the competing cisternal maturation model (Dahan et al., 1994; Orci et al., 2000; Martinez-Menárguez et al., 2001; Malsam et al., 2005). The later model suggests that Golgi cisternae are transient structures that contain cargo while Golgi specific enzymes are delivered and dispatched in a stepwise manner (Grasse, 1957; Bonfanti et al., 1998; Glick and Malhotra, 1998). Time-lapse fluorescence microscopy in *S. cerevisiae* gives evidence of cis-Golgi cisternae that progressively lose an early Golgi marker protein and simultaneously receive a late Golgi marker (Losev et al., 2006; Matsuura-Tokita et al., 2006). It is inherent to this model that cargo between cisternae is not mixing and thus should exit Golgi with linear kinetics, a prediction that is discordant with the reports on exponential cargo export from Golgi (Patterson et al., 2008). Existence of tubular connections between heterotypic Golgi cisternae, proposed in a variant of the cisternal maturation model, could explain

exponential dynamics of Golgi export but only for small cargos (San Pietro et al., 2009). Such tubular connections between heterotypic cisternae have been reported by electron microscopy but only in mammalian cells (Marsh et al., 2004; Trucco et al., 2004). How identity of Golgi subcompartments would be maintained in the presence of tubular connections remains to be discovered. The rapid partitioning model proposes that Golgi would in fact operate as a single compartment that contains distinct membrane domains dedicated to processing and export (Patterson et al., 2008). Though reported kinetics of Golgi cargo export support this model, how the differential distribution of Golgi resident enzymes between *cis*- and *trans*-Golgi elements would be maintained is unclear. The cisternal progenitor model proposes that cargo exchange between cisternae is mediated by their fission and fusion (Pfeffer, 2010). Mechanistically this would rely on a Rab cascade where an early compartment specific Rab^{EARLY} would mediate recruitment of the late compartment specific Rab^{LATE}. The Rab^{LATE} would then partition and promote early cisterna fission to yield an intermediate subcompartment that would proceed to fuse with the late cisterna already populated by the Rab^{LATE}. Though this model was inspired by similar mechanisms operating in endosomal maturation it presently has little experimental support to function in Golgi (Rink et al., 2005; Poteryaev et al., 2010).

Though the role of COPI vesicles in anterograde versus retrograde transport is debated, the mechanism of their formation is better understood (reviewed by Popoff et al., 2011). In mammalian cells, recruitment of the Ras-like small GTPase Arf1 to Golgi membranes is mediated by Golgi proteins including p23 and the SNARE membrane (Gommel et al., 2001; Honda et al.,

2005). The GDP-GTP exchange that activates Arf1 is carried out by the Sec7 family GEFs (Claude et al., 1999; Spang et al., 2001). The GTP bound Arf1 promotes recruitment of the heptameric coatomer to which cargo proteins bind directly and indirectly (Donaldson et al., 1991; Serafini et al., 1991; Cosson and Letourneur, 1994; Hara-Kuge et al., 1994; Tu et al., 2008). The GTP-Arf1 and the heptameric coat reconstitute the vesicle budding from synthetic liposomes (Spang et al., 1998).

Membrane fusion at various subcellular locations is driven by interactions between the SNARE family of tail anchored proteins (Söllner et al., 1993). SNAREs are designated as vesicle, v-SNAREs that are monomeric and target membrane, t-SNAREs usually organizing complex of three proteins (Söllner et al., 1993; Fasshauer et al., 1997, 1998; Sutton et al., 1998). Pairing of v-SNARE and its cognate t-SNARE through a zipper-like mechanism is sufficient for *in vitro* fusion between membranes (Sutton et al., 1998; Melia et al., 2002; Pobbati et al., 2006). The SNARE complex is then engaged by soluble-NSF-attachment-factors (SNAPs) and hexameric ATPase N-ethylmaleimide-sensitive-factor (NSF) that resolve the complex and allows recycling of SNAREs (Block et al., 1988; Söllner et al., 1993; Mayer et al., 1996). The fusogenic SNARE complexes that drive liposome fusion *in vitro* are assembled only between specific pairs of v- and t- SNAREs and are thus proposed to help ensure specificity of vesicle and target membrane fusion (Weber et al., 1998; McNew et al., 2000; Parlati et al., 2000). Accordingly, several SNAREs exhibit a distinct subcellular distribution. Decreasing levels of the v-SNARE Bet1 from the *cis-* to *trans-*Golgi cisternae and the inverse localization pattern for the v-SNARE Sft1 suggest that they ensure specificity

of ER-to-Golgi and intra-Golgi trafficking respectively (Volchuk et al., 2004). Remarkably, Sec22 is a part of the t-SNARE complex at the Golgi membranes to promote ER-to-Golgi trafficking and has been suggested to function as the v-SNARE in the retrograde Golgi-to-ER trafficking, suggesting that a single SNARE can promote trafficking in one direction as a v-SNARE and in the other direction as a t-SNARE (Lewis et al., 1997; Xu et al., 2000, 2002; Burri et al., 2003).

Targeting specificity of the vesicular transport is further provided by tethering complexes that establish interactions between a vesicle and the target membranes prior to SNARE pairing (reviewed by Cai et al., 2007a). The transport-protein-particle-I (TRAPPI) mediated tethering of COPII vesicles depends on its subunit Bet3 that interacts with the coat protein Sec23 (Cai et al., 2007b). It has been shown that TRAPPI functions as a GEF for Ypt1, a Rab-family GTPase (Sacher et al., 2001; Cai et al., 2008). The subsequent interactions between active Ypt1 and its effector, a coiled-coil protein Uso1 is suggested to promote COPII vesicle tethering at the Golgi complex (Cao et al., 1998). It should be noted that in mammalian cells COPII vesicle fusion is a homotypic event that forms tubulo-vesicular network that precedes Golgi apparatus *sensu stricto* (Bannykh et al., 1996; Aridor et al., 2001; Mironov et al., 2003; Bentley et al., 2006). However yeast lack this compartment and COPII vesicles delivery to *cis*-Golgi is more direct (Bonifacino and Glick, 2004). The TRAPP II complex has been proposed to function in a similar manner to regulate intra-Golgi trafficking of COPI vesicles (reviewed by Barrowman et al., 2010). COPI retrograde flow to the ER involves a tethering

step mediated by the Dsl1 complex but with distinct mechanistic details (reviewed by Spang, 2012).

The cargo is sorted and exits the Golgi complex through *trans*-Golgi network (reviewed by Anitei and Hoflack, 2011). This subcompartment displays considerable differences from the earlier Golgi compartments in that it uses clathrin for vesicle budding, mixes with the endosomes and not the ER upon brefeldinA treatment and may segregate from other Golgi cisternae in some instances (Wood et al., 1991; Ladinsky et al., 2002; Donohoe et al., 2007; Toyooka et al., 2009).

1.3.3. Exocyst

Prior to fusing with the plasma membrane, secretory vesicles are tethered by the octameric complex termed the exocyst. The landmark screen for temperature-sensitive alleles in genes encoding regulators of secretion identified six exocyst components, Sec3, Sec5, Sec6, Sec8, Sec10 and Sec15, impairment of which caused cells to accumulate 80-100 nm vesicles (Novick et al., 1980). Subsequent biochemical approaches showed that these proteins form an evolutionarily conserved complex and identified two additional subunits, Exo70 and Exo84 (Hsu et al., 1996; TerBush et al., 1996). Crystal structure analyses of Exo70 and fragments of Exo84, Sec15 and Sec6 subunits suggests that exocyst belongs to the Complex-Associated-with-Tethering-Containing-Helical-Rods (CATCHR) family of protein complexes that have high structural but low sequence homology (Dong et al., 2005; Wu et al., 2005; Hamburger et al., 2006; Sivaram et al., 2006), reviewed by Yu and Hughson, 2010). Reportedly, each exocyst subunit directly engages several

others and electron microscopy of purified fixated complex suggests a Y-shaped structure (Hsu et al., 1998; Munson and Novick, 2006). On one hand, the exocyst subunit Sec15 has been reported to bind the GTP-bound Rab-family GTPases Sec4 localized to the secretory vesicles (Salminen and Novick, 1989; Roth et al., 1998; Guo et al., 1999). On the other hand, Sec3 and Exo70 are effectors of the active, plasma membrane allocated Rho-family GTPases (Adamo et al., 1999; Robinson et al., 1999; Guo et al., 2001; Zhang et al., 2001). Collectively, these and other findings have led to a working model where one short arm of the Y-shaped exocyst is comprised of Sec15 and interacts with the vesicle bound Rab while Rho mediated plasma membrane recruitment relies on Sec3 and Exo70 present at the other short arm and the stalk of the Y structure respectively (Munson and Novick, 2006).

In addition to its role in tethering secretory vesicles to the plasma membrane, exocyst has also been implicated in regulating SNARE activity in fusing two membranes (Grote et al., 2000). Overexpression of the plasma membrane t-SNAREs Sso1 and Sso2 relieves the temperature sensitive growth of specific Sec3, Sec5 and Sec15 but not Sec6, Sec8 and Sec10 mutants (Aalto et al., 1993). Sec6 interacts *in vitro* with the plasma membrane t-SNARE Sec9 and inhibits its binding with Sso1 (Boettcher et al., 2005). Furthermore, physical interactions between exocyst proteins and several SNARE regulators have been reported (Wiederkehr et al., 2004; Zhang, 2005).

In both *S. cerevisiae* and *S. pombe* the exocyst subunits localize to the sites of growth in interphase and are observed at the division site during cytokinesis (Finger et al., 1998; Wang et al., 2002). In *Drosophila* and mammalian neurons exocyst is present at the growth cones and sites of

synaptogenesis while in plants it has been observed at the growing tips of pollen tubes (Hazuka et al., 1999; Mehta et al., 2005; Hála et al., 2008). FRAP experiments of all exocyst subunits at the tip of growing *S.cerevisiae* bud show that Sec3 and Exo70 exhibit a relatively rapid recovery while other exocyst subunits have a comparatively slow turnover (Boyd et al., 2004). These results suggest that distinct mechanisms recruit different exocyst subunits to sites of polarized growth (reviewed by Heider and Munson, 2012). Mutation of *sec4* that partially impairs secretion also diminishes recovery of Sec8-GFP upon photo-bleaching suggesting that secretion is partially responsible for exocyst localization (Boyd et al., 2004). Electron microscopy on budding yeast cells immuno-gold stained for exocyst components have shown that most subunits are present at the secretory granules (Boyd et al., 2004). Furthermore, long-range Myo52 dependent movement of exocyst fluorescent punctae, presumably labeling secretory granules, from the cell interior to the tips has been reported in fission yeast (Bendezú et al., 2012). Disruption of F-actin by LatA treatment strongly reduces the turnover rate at *S. cerevisiae* bud tip of all exocyst subunits other than Sec3 and Exo70 (Boyd et al., 2004).

Polarized localization of the exocyst is also governed by phosphoinositides and the Rho-family GTPases. PI(4,5)P₂ concentrates at the plasma membrane in yeast cells in a PI4P 5-kinase Mss4/Its3 dependent manner (Zhang et al., 2000; Stefan et al., 2002). Impairment of Mss4/Its3 leads to decreased recruitment of Exo70, Sec3 and Sec8 and presumably of the entire exocyst to the plasma membrane (He et al., 2007; Bendezú et al., 2012). Furthermore, recombinant Exo70 and Sec3 fragments bind specifically to

liposomes carrying PI(4,5)P2 *in vitro* (He et al., 2007; Liu et al., 2007; Zhang et al., 2008). The N-terminal domain of Sec3 binds Cdc42 and Rho1 and interactions between Exo70 and Cdc42 and Rho3 have been reported (Robinson et al., 1999; Adamo et al., 2001; Guo et al., 2001; Zhang et al., 2001, 2008; Wu et al., 2010). The Cdc42 mediated recruitment of the exocyst to the plasma membrane is likely a part of the reinforcement mechanism that allows symmetry breaking (Wedlich-Soldner, 2003).

While all other subunits are essential, *S. pombe* cells lacking Sec3 or Exo70 are viable under certain conditions and polarize growth, but do exhibit a defect in septum cleavage (Wang et al., 2002; Bendezú et al., 2012). Deletion of the *sec3* gene slows down actomyosin ring constriction and leads to a defect in final abscission resolving daughter cells thus leaving a cytosolic bridge between daughter cells (Jourdain et al., 2012). Similarly, depletion of Sec5 from HeLa cells results in accumulation of secretory granules the proximity of the midbody and failure to efficiently perform abscission (Gromley et al., 2005). Multiple interactions between exocyst subunits and the extensive overlap between Sec3 and Exo70 in communicating plasma membrane signals could in principle explain why neither Sec3 nor Exo70 are individually essential to recruit other exocyst components to the growth sites in fission yeast (Bendezú et al., 2012). Removal of both Sec3 and Exo70 function is lethal and abolishes polarization of remaining exocyst subunits (Bendezú et al., 2012).

1.4. Objectives

Although protein secretion is essential to cell growth and division, the information on the secretory pathway organization in fission yeast is limited. The electron microscopy reports on Golgi organization in *S. pombe* (Johnson et al., 1973; Ayscough et al., 1993) suggest presence of both individual cisternae and stacks, making it a valuable system to test current hypotheses on the correlation between structural organization of the tER and Golgi apparatus (Papanikou and Glick, 2009). Furthermore, such cisternal arrangement would provide a system for *in vivo* visualization of Golgi trafficking and address whether the mechanisms previously reported solely in budding yeast are evolutionarily conserved (Losev et al., 2006; Matsuura-Tokita et al., 2006). Here I employ the fluorescently tagged proteins specific to distinct early secretory pathway compartments and characterize their organization and dynamics in fission yeast.

Targeted secretion is a vital determinant of cell polarity (Pruyne et al., 2004; Bendezú and Martin, 2011). The physiological relevance and mechanisms targeting secretory granules and the exocyst to the polarized cortical domains have been well documented (Pruyne et al., 2004; Bendezú et al., 2012). However, the extent of polarization of the secretion apparatus to the growth sites is presently unknown. Considering the functional continuum of the secretory pathway (reviewed by Guo and Novick, 2004), I was interested in investigating the spatial distribution of the ER and *cis*- and *trans*-Golgi during polarized tip growth and cell division, which represent major aspects of cellular polarity in fission yeast. Furthermore, I explore the role of the actin

cytoskeleton in positioning the ER and the putative molecular mechanisms linking filamentous actin to the early secretory pathway compartments.

Regulation and the cellular response to temperature increase is one of the most robust and evolutionarily conserved mechanisms in eukaryotes (reviewed by Richter et al., 2010). The molecular mechanisms of stress response are intensely explored but how they are integrated at the cellular level remains obscure. Here I employ fission yeast to explore dynamics of key polarity regulators during mild heat-stress and subsequent adaptation to elevated temperature. Since gene expression re-profiling is the landmark response to temperature elevation, I employed a genetic screen to isolate and characterize mutants with constitutively up-regulated heat-stress associated transcription. In this manner I aimed to address the specific contribution of the transcriptional response to temperature perturbations in regulating cell polarity.

In summary, in the course of my graduate studies I focused on exploring 1) the structural organization of the early secretory pathway, 2) its spatial distribution in respect to cell polarity and 3) the effects of environmental temperature on dynamics of cell polarity regulators.

CHAPTER II - Materials and methods

2.1. Drugs and staining reagents

Latrunculin A (LatA), a drug that prevents actin polymerization, was purchased from Biomol International LP (Plymouth Meeting, PA, USA). DNA fluorescent stain 4',6-diamidino-2-phenylindole (DAPI) and cell wall dyes Calcofluor White and FITC-Lectin were obtained from Sigma-Aldrich (St. Louis, MO, USA). The F-actin stain Alexa Fluor 593 Phalloidin was obtained from Invitrogen (Karlsruhe, Germany).

2.2. Growth media and conditions

Growth media were as described in (Moreno et al., 1991). Unless otherwise indicated cells were grown in YES media. Induction of gene expression from the *nmt* promoter was achieved by growing cells in the synthetic Minimal Medium (MM) lacking thiamine for 16 to 20 hrs. *nmt* promoter expression was suppressed by supplementing 5 μ M thiamine.

Genetic crosses and sporulation were performed on YPD agar plates.

Heat-stress experiments were performed as indicated in figure legends. Typically, a 30 ml cell suspension was grown to log-phase at constant temperature overnight (~16 hrs) with shaking at 200 r.p.m.. It should be noted that the cell suspension reached target temperature within 5 to 10 min and that this was important for the dynamics of the physiological response.

For long term imaging fission yeast cells were grown in liquid YES medium using ONIX perfusion chambers (CellASIC, Hayward, CA, USA) under the control of the proprietor software and the flow of 4 psi.

2.3. *S. pombe* strains

S. pombe strains used in this study and their genotypes are listed in Appendix I (pages A1 to A6).

2.4. Construction of *S. pombe* strains

The homologous recombination-based method was used to manipulate endogenous genes. The candidate marker proteins of various cellular subcompartments were selected based on their homologies to proteins characterized in other yeast systems. Accession numbers of genes previously uncharacterized in fission yeast and discussed in this thesis include: SPBC1734.04 (Anp1), SPAC27F1.07 (Ost1), SPAC22F8.08 (Sec24), SPBC36B7.03 (Sec63), SPAC30.01c (Sec72), SPAC144.18 (Vrg4), SPBC215.15 (Sec13), and SPBC8D2.20c (Sec31).

2.4.1. *S. pombe* transformation

The protocol for the fission yeast DNA transformation was adopted from (Kanter-Smoler et al., 1994). Approximately 2×10^8 cells (~10 O.D.595 units) were washed with water and BufferT1 (0.1M LiAc, 10 mM Tris-HCl, 1 mM EDTA, pH 7.5) and resuspended in 100 μ l of BufferT1. Approximately 1 to 5 μ g of target DNA was added together with 2 μ l of carrier DNA (sonicated salmon sperm DNA, Sigma) and incubated at room temperature for 10 min. The samples were gently mixed with BufferT2 (40% w/v polyethylene glycol (m.w. \approx 3550, Sigma), 100 mM LiAc, 10 mM Tris-HCl, 1 mM EDTA) and kept at 30°C for 45 min. After adding 43 μ l of dimethyl sulfoxide the cell

suspension was incubated for 5 min at 42°C, washed with 1 ml of water and plated on selective media.

2.4.2. Recombinant DNA technology and heterologous gene sequences

Yeast genomic DNA was extracted using DNA extraction kit purchased from Epicentre Biotechnologies (Madison, WI, USA).

Standard molecular biology protocols described by (Maniatis, 1982) were employed. Restriction enzymes were produced by New England Biolabs (Beverly, MA, USA), Roche (Basel, Switzerland) or Thermo Scientific (Waltham, MA, USA)

Plasmids, selection markers, gene expression promoters and DNA manipulation strategies used in the study are described by (Siam et al., 2004) and (Wang et al., 2004). pJK210 vector was used to target protein tags to the desired endogenous gene (Keeney and Boeke, 1994). pJK148 vector served to introduce additional gene copies or artificial gene constructs to the *leu1* genomic locus (Keeney and Boeke, 1994).

Properties of fluorophores used to visualize endogenous proteins are reviewed by (Straight, 2007). The heterologous c-Myc (Myc) and hemagglutinin (HA) antigen protein tags were also used.

The construct where GFP expression was driven by *hsp104* regulatory elements relied on a 1kb genomic fragment upstream of the Hsp104 start codon and 0.5kb downstream of the stop codon.

Fluorescent ER luminal markers GFP-AHDL and mCherry-AHDL are a kind gift from Dan Zhang (Zhang et al., 2010). The actin visualization tool LifeAct was a kind gift from Mohan Balasubramanian (Huang et al., 2012).

2.4.3 Genetic crosses

Classic genetic techniques were performed as described by (Moreno et al., 1991). Mating was carried out between heterothallic h^+ and h^- strain. Crosses and sporulation were performed on YPD agar plates. Prior to spore germination tetrad dissection was performed on YES plates using MSM micromanipulator (Singer Instruments, Somerset, UK). When yeast colonies developed, presence of selection markers was assayed by replica plating onto selective media plates.

Estimates of genetic linkage requires analysis of a large number of mating progeny and was performed using the free-spore assay (Moreno et al., 1991). Briefly, mating colonies were resuspended in water and treated with 0.5% glusulase at 36°C overnight. The vegetative cells were killed by a wash in 30% ethanol water solution and dilutions were plated on YES non-selective media.

2.4.4. Targeted mutagenesis of the *cdc15* genomic locus

To isolate novel *cdc15* mutants I employed the marker reconstitution mutagenesis strategy described by (Tang et al., 2011). Briefly, in the *his5* mutant genetic background I tagged the native *cdc15* genomic locus with the *his5* promoter and *his5* ORF fragment lacking the sequence encoding the C-terminus of the functional His5 protein. Simultaneously I employed error-prone PCR (I manipulated concentration of Mg^{2+} in the PCR reaction to control fidelity of DNA polymerase (Ling et al., 1991)) to amplify the *cdc15* genomic sequence fused to the sequence encoding the C-terminus of His5. Homologous recombination within both *cdc15* and *his5* encoding sequences

resulted in the replacement of the genomic *cdc15* with the PCR fragment and yeast cells that underwent such events could be selected for based on the his5+ phenotype. I proceeded to visually screen for temperature-sensitive *cdc15* alleles with impaired spatial distribution of the transitional ER.

2.5. Gene expression analysis

2.5.1. Microarray analysis

The gene expression profile of *mas5Δ* cells was obtained as previously described by (Peng et al., 2005). The significance of differential gene regulation between wild-type and *mas5Δ* cell was assessed by the Student's t-test (Fig. 3.3.5.1B). Only genes with $p < 0.05$ were included in subsequent analysis. The expression profiles for stress conditions was taken from (Chen et al., 2003).

Correspondence at the top plot was derived from (Irizarry et al., 2005). Briefly, the genes were sorted into a list according to how pronounced their up/down-regulation was in *mas5Δ* as compared to wild-type cells. The binomial test was then employed to generate p-values (Fig. 3.3.5.1B, y-axis) as a function of an increasing number of genes included (Fig. 3.3.5.1B, x-axis) into the comparison between *mas5Δ* expression profile and that of stressed cells.

2.5.2. Quantitative PCR

The RNA samples from *mas5Δ* and wild-type cells grown at 24°C or shifted to 36°C for 45 min were prepared using phenol-chlorophorm extraction described by (Peng et al., 2005) and reverse transcribed using SuperScript III

(Invitrogen) and random decamer primers (N10) at 50°C for 60min. The reverse transcriptase was inactivated at 70°C for 10min. cDNA samples were analyzed by quantitative real-time PCR (qPCR) using a StepOnePlus real-time PCR system (Applied Biosystems) and Fast SYBR Green Master Mix (Applied Biosystems) with 0.15 µM of each forward and reverse primers. The following cycling program was used: 95°C for 20 s, followed by 40 cycles of a three-step reaction, denaturation at 95°C for 5 s, annealing and extension at 60°C for 45 s. The primers used are listed in Appendix-II (page A7). Data shown were normalized to the expression levels of actin (act1, Fig. 3.3.4.1D) and similar results were obtained when using GAPDH (gpd1, data not shown) to normalize the data.

2.6. Fluorescence Activated Cell Sorting (FACS)

FACS was performed using a protocol described by (Sabatinos and Forsburg, 2009). Exponentially growing cells were pelleted and resuspended in 70% ethanol and kept for 1 hour at 4°C. Samples were washed three times with sterile 50 mM sodium citrate. Samples were incubated overnight on a rotator at room temperature in the citric solution with 10 mg/ml of RNase-A obtained from Roche (Basel, Switzerland). Samples were stained with 10 µg/ml final concentration propidium-iodide from Sigma-Aldrich (St. Louis, MO, USA) immediately prior to processing on on MACSQuant Analyzer (Miltenyi Biotec GmbH, Bergisch Gladbach, Germany).

2.7. Protein biochemistry techniques

2.7.1. Preparation of cell lysates and co-immunoprecipitation

Yeast cells were grown to log phase, harvested and washed with Buffer A (6 mM Na₂HPO₄, 4 mM NaH₂PO₄, 150 mM NaCl, 2 mM EDTA, 50 mM NaF, 0.1 mM Na₃VO₄, protease inhibitor cocktail (Roche)). Cell pellets were resuspended in 200 µl of Buffer A, mixed with glass beads and homogenized in a Mini Bead Beater (Biospec, Bartlesville, OK, USA) at 4°C. Total cell lysate were harvested and centrifuged (16,000 x g, 10 min) to remove cell debris. The protein concentration of the supernatant was measured by the Bradford assay (Bio-Rad Laboratories, Hercules, CA, USA). Soluble fractions were adjusted to same total protein concentration using Buffer A and 350µl were incubated with either mouse anti-Myc (Milipore, Billerica, MA, USA) antibodies and Protein A beads (Invitrogen, Carlsbad, CA, USA) or just GFP-Trap beads (ChromoTek, Munich, Germany) for 1 hour. Beads were washed 6 times with 1ml of Buffer A and resuspended in 50 µl of SDS-Loading buffer.

2.7.2. Trichloroacetic acid (TCA) precipitation

For total protein quantifications, cells were pelleted and resuspended in 200 µl of BufferB (1.85M NaOH, 1M β-mercaptoethanol,) and kept on ice for 10min. Subsequently, 450µl of water and 350µl of 6.1N trichloroacetic acid were added. The samples were incubated on ice for 10 min and centrifuged for 10 min at 4°C. The obtained pellet was washed with 0.5 M Tris-base, dissolved in gel loading buffer and kept at 65°C for 10min and 95°C for 3 min.

2.7.3. SDS-PAGE, Western blotting and antibodies

Protein samples were subjected to standard SDS-PAGE and western blotting analysis. Proteins of interest were probed by mouse *anti*-GFP (Roche), rabbit *anti*-HA (Roche) and mouse *anti*-Myc (Milipore). Rabbit *anti*-HistoneH3 (Abcam, Cambridge, MA, USA) probing served to monitor sample loading. IRDye800 conjugated *anti*-mouse and IRDye700 conjugated *anti*-rabbit antibodies were used prior to analysis on the Odyssey Infrared Imaging system, all purchased from LI-COR Biosciences (Lincoln, NE, USA).

2.8. Microscopy techniques

2.8.1. Epifluorescence and DIC microscopy

Epifluorescence and DIC images were collected using mercury or halogen lamp as an illumination source, respectively, with appropriate sets of filters on a Zeiss Axiovert 200M (Plan APOCHROMAT N.A.=1.4 objective) microscope equipped with CoolSnap camera (Photometrics) and Uniblitz shutter driver (Photronics, Rochester, NY, USA) under the control of Metamorph software package (Universal Imaging, Sunnyvale, CA, USA). Typically, we acquired image stacks that consisted of 9 sections of 0.5 μm spacing. Presented are the z-stack maximum projection images obtained by using Metamorph built-in module or ImageJ software.

2.8.2. Scanning confocal microscopy

Scanning confocal microscopy was performed on a Zeiss LSM510 microscope equipped with a Plan APOCHROMAT 100X, 1.4 N.A. objective lens, a 488-nm argon laser and a 543-nm HeNe laser. We acquired either

single z-planes or whole cell image stacks that consisted of 9 z-sections with 0.5 μm spacing.

Alternatively, scanning confocal microscopy was performed on a Leica DMI6000B microscope (HCX PLAN N.A.=1.35 objective) equipped with SP5 confocal system (Leica Microsystems, Mannheim, Germany) controlled by the proprietary software package. Z-stack images were taken with 0.5 μm spacing and reconstructed in three dimensions using the projection module.

Imaging was performed on *S. pombe* cells placed in sealed growth chambers containing 2% agarose YES media.

2.8.3. Spinning-disk confocal microscopy

Time-lapse fluorescent microscopy images were generated on a Zeiss Axiovert 200M (Plan APOCHROMAT N.A.=1.4 objective) microscope equipped with UltraView RS-3 confocal system: CSU21 confocal optical scanner, 12 bit digital cooled Hamamatsu Orca-ER camera (OPELCO, Sterling, VA) and krypton-argon triple line laser illumination source (488, 568 and 647 nm) under the control of UltraView software package (PerkinElmer Inc., Boston, MA, USA). Typically, we acquired image stacks that consisted of 9 0.5 μm spaced sections.

Alternatively, time-lapse fluorescent microscopy images were generated on Nikon TiE system (CFI Plan Apochromat VC 100XH 1.4 N.A. objective) equipped with Yokogawa CSU-X1-A1 spinning disk unit, the Photometrics CoolSNAP HQ2 camera and a DPSS 491nm 100mW and DPSS561nm 50 mW laser illumination under the control of Metamorph Premier.

Imaging was performed on *S. pombe* cells placed in sealed growth chambers containing 2% agarose YES media.

2.9. Image processing and analysis

2.9.1. 3D-rendered and projection images

The z-stack projection images were obtained either by Metamorph or ImageJ software package (<http://rsb.info.nih.gov/ij/>; National Institute of Health, Bethesda, MD, USA) built-in modules. Cubic-interpolation method was used when images were rotated.

Imaris (Bitplane, Zurich, Switzerland) and Volocity (Perkin Elmer, Waltham, MA, USA) software packages were used to create 3D-rendered images from z-stacks.

2.9.2. Analysis of the spatial distribution of the early secretory pathway compartments and Golgi maturation dynamics

Single cell maximum projection images obtained by epifluorescence microscopy were analyzed using customized CellProfiler image analysis software (Carpenter *et al.*, 2006). CellProfiler object processing modules were used to identify *S. pombe* cells. Longitudinal cell axes were approximated by linear regression of cell boundaries. Images were rotated by the angle of inclination of the cell axes to the x-axis, thus orienting cells horizontally. Next, images were cropped to cell boundaries. Using nearest-neighbor interpolation, image width was resized to the nearest multiple of 20 pixels, and image height to the nearest multiple of 10 pixels. The average intensity of an image field comprising 1/20th of the width and 1/10th of the height of this

image was represented as a single pixel, thus resulting in a 20x10 pixel image. Intensities were normalized and averaged over 50 images. Furthermore, we calculated intensities along longitudinal cell axes from mean column intensities of the 20x10 images. As above, these were averaged over 50 images and graphed. We determined the statistical significance of differences in fluorescence levels between two axial positions using the Kolmogorov-Smirnov test to calculate the p-values. The critical p-value ($p = 0.05$) was adjusted for multiple comparisons using Bonferroni correction.

Integrated intensity measurements were performed on maximum projection images obtained by time-lapse spinning-disk confocal microscopy using the Metamorph built-in module. The measurements were performed over three equal areas corresponding to cell tips and the cell middle. The fluorescence intensities were adjusted for bleaching using interphase cells fluorescence intensities ($n=4$ cells) assuming that the marker protein levels did not change during this time. Obtained values are presented as a time sequence of values relative to average intensity at cell tips and the moving average ($n=3$) time sequence.

For Golgi maturation analysis fluorescence intensities in both red and green channel were measured for individual cisternae from maximum projection images over the duration of the timelapse. Intensities were plotted and fitted with an exponential curve. The fitted curves ($n>8$) was used to calculate the fluorescence doubling time.

2.9.3. New-end growth analysis

Longitudinal growth in lectin stained cells was assessed manually as a distance from the cell tip to the lectin signal along the long cell axis (Fig. 3.3.1.1C).

New-cell-end growth was quantified from calcofluor stained cells as the distance from the birth scar to the proximal cell tip and expressed as a function of total cell length (Figures 4D and 7B). We employed ANCOVA analysis to assess the statistical significance of variation in new-end growth between cells with different genotypes ($n > 30$ cells per genotype). For simplified presentation we also estimated average new-end length in cells 12-15 μm long while making sure that the total cell length between samples was comparable, p-values were obtained using Welch's t-test.

2.9.4. Analysis of fluorescence intensity profiles

CRIB-GFP intensity profiles were created from background subtracted average intensity projections of scanning confocal z-stacks (7 sections, 0.5 μm spacing). ImageJ in-built line-scan module was used to create an intensity profile along the long axis of the cell. The positional information was normalized as the percentage of the cell length. The nuclear signal was set as one arbitrary unit since it did not vary significantly between samples analyzed (data not show).

Fluorescence levels of Cdc42 regulators at the cell tips were analyzed from background subtracted images by manually outlining the cell tips. Reported are the average fluorescence intensities.

CHAPTER III - Results

3.1. Characterization of the Secretory Pathway in Fission Yeast

3.1.1. The fission yeast tER is a distinct ER subcompartment present as numerous stable entities

The tER sites are morphologically and functionally distinct ER domains that serve as sites of COPII vesicle production. To monitor the COPII positive subcellular domains I constructed *S. pombe* strains expressing distinct COPII vesicle structural proteins C-terminally tagged with either GFP or mCherry at their genomic loci. The candidate marker proteins were selected based on their homologies to known COPII markers reported in other yeast (see Materials and Methods). Tagging of these proteins did not adversely affect their essential functions judging by the normal doubling time, cell morphology and division patterns (data not shown).

The COPII vesicle coat proteins Sec24-GFP, Sec13-GFP, Sec31-GFP were all found to localize to punctate structures (Fig. 3.1.1A and data not shown). I observed 80 ± 9 individual Sec24-GFP entities in interphase cells and 106 ± 11 of those in dividing cells ($n > 10$ cells; Fig. 3.1.1B). I found that cells contained a similar numbers of Sec31 positive structures (data not shown). Since imaging of Sec24-GFP provided the best signal-to-noise ratio I choose to use this marker protein in further studies.

I next explored Sec24-GFP dynamics using time-lapse microscopy. Single Z-sections acquired every 5 seconds in cells expressing Sec24-GFP and the nuclear envelope marker Uch2-mCherry (Li et al., 2000b) indicated that COPII positive entities were stable for periods extending 5 minutes during both cell growth and division (Fig. 3.1.1C and Movie 3.1.1). I was not able to

determine the average tER site life span due to technical limitations and the large number of these sites.

To explore how the Sec24-GFP punctae localized in respect to the ER I employed scanning confocal microscopy on cells co-expressing Sec24-GFP and mCherry-AHDL that labels the entire ER lumen (Zhang et al., 2010). The three-dimensional reconstruction of micrographs showed that the mCherry-AHDL and all Sec24-GFP positive punctae partially overlapped suggesting that in fission yeast Sec24-GFP labels an ER subdomain rather than individual COPII vesicles (Fig. 3.1.1C).

The ER is an intricate network of high and low curvature membranes designated as tubules and sheets respectively that share a common lumen. The ER tubules are characterized by the presence of ER shaping proteins such as the evolutionarily conserved Tts1 (Zhang et al., 2010) whereas the oligosaccharide transferase Ost1 (Silberstein et al., 1995) and the protein translocation complex subunit Sec63 (Deshaies et al., 1991) localize to the ER sheets. I analyzed the spatial distribution of the tER with respect to other ER subdomains by performing scanning confocal microscopy on cells co-expressing the Sec24-GFP and a marker protein of either ER tubules or sheets. The network of ER sheets and tubules, labeled by Tts1-mCherry and Ost1-mCherry respectively, appeared too interlaced to unambiguously correlate the spatial distributions of the ER subcompartments (Fig. 3.1.1E). Impairment in the function of an ER tubulating protein Rtn1 leads to a pronounced separation between ER morphological domains, with the majority of ER tubules localizing the cell tips while ER sheets become restricted to the lateral cell cortex of interphase cells (Zhang et al., 2010). Thus I examined the relative

distribution of the tER and ER marker proteins in *rtn1Δ* background. The Sec24-GFP sites accumulated towards the cell tips and could localize independently of the Ost1-mCherry in cells lacking Rtn1, even though many of the tER sites were still adjacent to the ER sheets (Fig. 3.1.1F, left panel). On the other hand, the tER was always juxtaposed to the ER tubules but not *vice versa* (n>100, Fig. 3.1.1F, right panel).

Taken together my data suggests that in fission yeast COPII coat protein Sec24-GFP labels a relatively stable subdomain of the ER. Considering rapid uncoating of coat proteins occurring from the fully assembled COPII vesicles (Antonny et al., 2001) I propose that in fission yeast Sec24-GFP marks the sites of COPII vesicles production, the tER. Furthermore the fission yeast tER appears to exist a distinct ER subcompartment positioned in the proximity to ER tubules and independently of ER sheets.

Figure 3.1.1. Characterization of the tER in fission yeast.

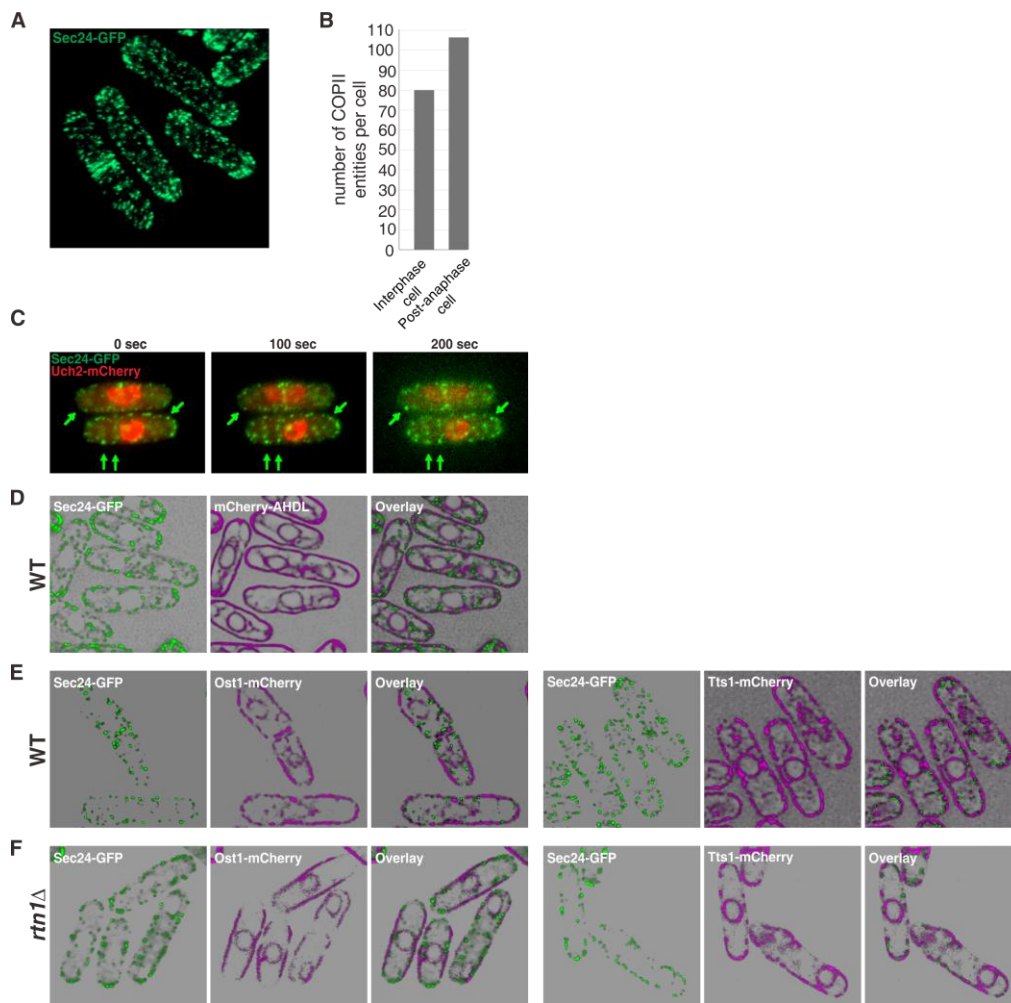


Figure Legend 3.1.1. Characterization of the tER in fission yeast.

(A) Three-dimensional reconstruction of nine 0.5 μm spaced Z-sections obtained using scanning confocal microscopy on fission yeast cells expressing tER marker Sec24-GFP.

(B) Quantification of the number of COPII punctae in fission yeast interphase and post-anaphase cells as visualized by scanning confocal imaging of Sec24-GFP (n= 10 cells per cell cycle stage).

(C) Representative frames from Supplemental Movie 3.1.1. Shown is the single focus plane images obtained by time-lapse epifluorescent microscopy of cells expressing Sec24-GFP and Uch2-mCherry. The arrows indicate COPII positive membranes that persisted throughout the course of the experiment.

(D) Three-dimensional reconstruction of three 0.25 μm spaced Z-sections obtained using scanning confocal microscopy on fission yeast cells expressing tER marker Sec24-GFP (green) and general ER marker mCherry-AHDL (magenta). tER sites were found distributed along the ER (overlay, right panel).

(E) Three-dimensional reconstruction of three 0.25 μm spaced Z-sections obtained using scanning confocal microscopy on wild- type fission yeast cells co-expressing tER marker Sec24-GFP (green) and tubular ER marker Tts1-mCherry (magenta, left panels) or Sec24-GFP and ER sheets marker Ost1-mCherry (magenta, right panels).

(F) Three-dimensional reconstruction of three 0.25 μm spaced Z-sections obtained using scanning confocal microscopy on *rtn1* Δ fission yeast cells co-expressing COPII vesicle marker Sec24-GFP (green) and tubular ER marker Tts1-mCherry (magenta, left panels) or Sec24-GFP and ER sheets marker Ost1-mCherry (magenta, right panels).

Movie Legend 3.1.1. COPII coat protein Sec24-GFP marks moderately stable tER sites in fission yeast.

Time-lapse sequence of cells expressing *cis*-Golgi marker Sec24-GFP. Arrows indicate stable tER sites. Shown are the single-plane epifluorescence microscopy images taken every 5 seconds.

3.1.2. The fission yeast Golgi apparatus is organized as stacks of cisternae and the dynamics of Golgi maturation in fission yeast are in accordance with the cisternal progression model

The electron microscopy studies suggested that in fission yeast Golgi cisternae may organize into stacks, as in *P. pastoris*, but could also exist as individual cisternae similar to *S. cerevisiae* (Ayscough et al., 1993). I argued that the modern fluorescence microscopy techniques would allow one to more carefully examine the Golgi organization in fission yeast. To that aim I fused a fluorescent protein to fission yeast homologues of proteins localizing to distinct Golgi subcompartments in other yeast (see Materials and Methods).

I analyzed the relative distribution of the *cis*-Golgi marker, a component of the mannosyltransferase complex, Anp1-mCherry (Fig. 3.1.1A, center panel, Jungmann and Munro, 1998) and the Arf GEF Sec72-GFP (Fig. 3.1.2A, left panel), a homologue of *S. cerevisiae* Sec7 that localizes to the late Golgi compartments in budding yeast (Franzusoff et al., 1991). I found that these proteins localized to several punctate structures (18 ± 3 *cis*- and 22 ± 3 *trans*-Golgi compartments during interphase and 23 ± 3 *cis*- and 26 ± 2 *trans*-Golgi compartments in dividing cells, n=10 cells). These two markers often partially overlapped or were found adjacent to each other consistent with their localization to the distinct cisternae within Golgi stacks (Fig. 3.1.2A, right panel and Fig. 3.1.2B). I also observed instances of several *cis*-Golgi cisternae adjacent to a single *trans*-Golgi structure. Individual cisternae were present albeit at a lower frequency (~10% of early and ~13% of late Golgi compartments, n=10 cells).

In order to explore the organization of tER structures and *cis*-Golgi with respect to each other, I simultaneously observed the localization of Sec24-GFP and the component of the Golgi mannosyltransferase complex Anp1-mCherry that served as a *cis*-Golgi marker protein (Fig. 3.1.2C, center panel). Due to the large number of the tER sites it was difficult to determine the fraction of adjacent COPII positive membranes and *cis*-Golgi compartments although I did observe such instances (Fig. 3.1.2B, right panel).

Using the spinning-disk confocal time-lapse microscopy I observed instances of early Golgi biogenesis without visible contribution from pre-existing cisternae, as judged by Anp1-mCherry dynamics (Fig. 3.1.2D and E, Movie 3.1.2.1). Moreover, I observed instances of cisternal identity change when Anp1-mCherry positive structures became predominantly occupied by Sec72-GFP (Fig. 3.1.2F, and Movie 3.1.2.2), in concordance with the Golgi cisternal progression models (reviewed by Glick and Luini, 2011). The quantification of the fluorescence signals associated with single cisternae maturation (Fig. 3.1.2G) suggested that this conversion occurred with the fluorescence ratio doubling time of approximately 30 ± 7 seconds (n=12 maturation events).

Taken together my data suggests that the Golgi apparatus in *S. pombe* cells exists as multiple entities comprising mainly stacks of few cisternae and some individual cisternae. Furthermore, *cis*-Golgi cisternae can form *de novo* in fission yeast and may give rise to late Golgi elements in accordance with the cisternal maturation model.

Figure 3.1.2. Characterization of the Golgi complex in *S. pombe*.

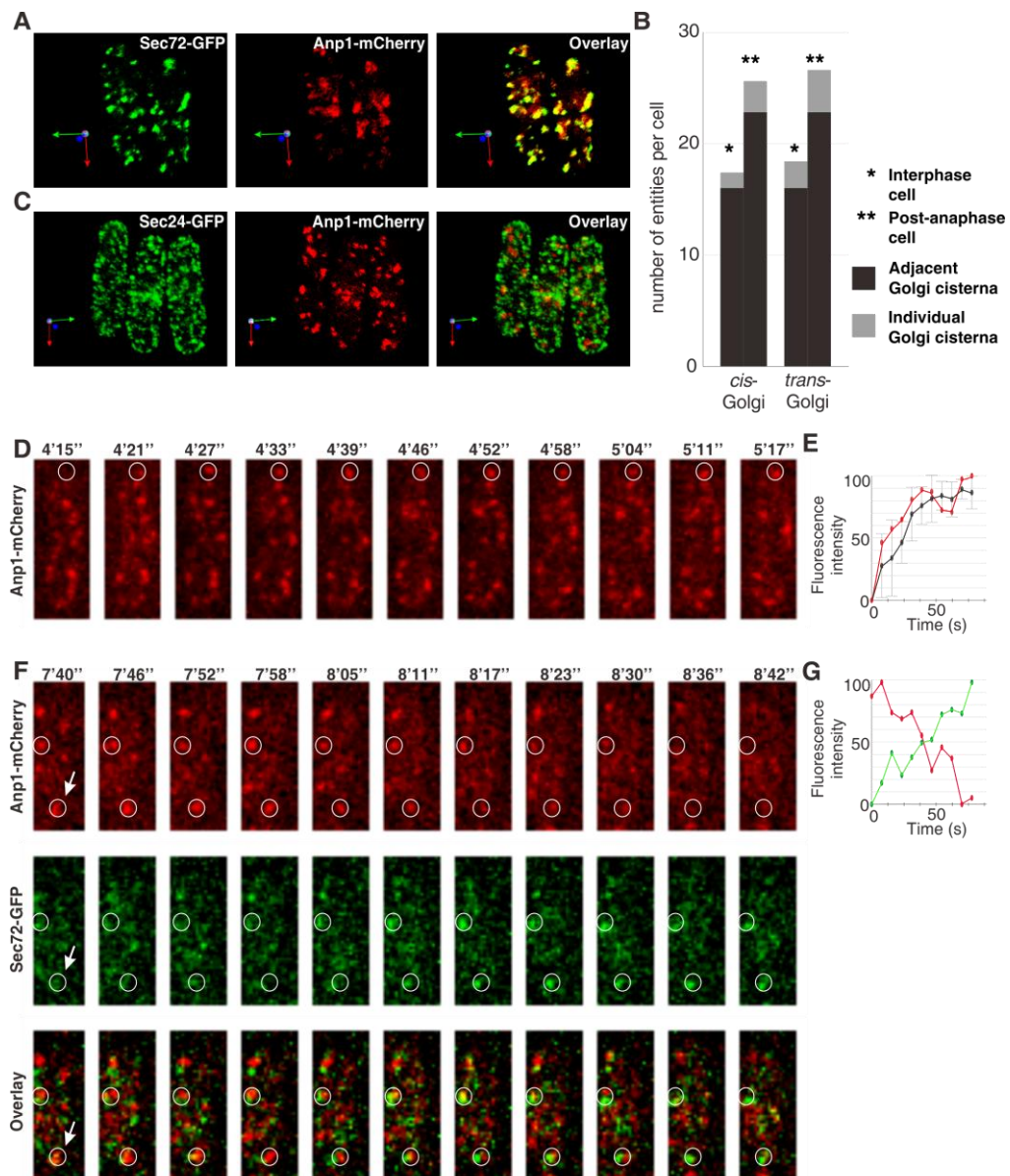


Figure Legend 3.1.2. Characterization of the Golgi complex in *S. pombe*.

(A) Three-dimensional reconstruction of scanning confocal microscopy images of *S. pombe* cells expressing *cis*-Golgi marker Anp1-mCherry (red) and *trans*-Golgi marker Sec72-GFP (green). The *trans*-Golgi localized as multiple separate cisternae that were in most cases partially overlapping or adjacent to the *cis*-Golgi cisternae (overlay). Arrows indicate the spatial orientation of objects in respect to x, y and z axis (green, red and blue respectively).

(B) Quantification of the number individual and adjacent *cis*- and *trans*-Golgi cisternae in fission yeast interphase and post-anaphase cells as visualized by scanning confocal imaging of Anp1-mCherry and Sec72GFP, respectively. (n= 10 cells per Golgi compartment per cell cycle stage)

(C) Three-dimensional reconstruction of scanning confocal microscopy images of *S. pombe* cells expressing COPII vesicle marker Sec24-GFP (green) and *cis*-Golgi marker Anp1-mCherry (red). Numerous punctate COPII entities and multiple separate *cis*-Golgi cisternae could be visualized, some of which were adjacent to each other (overlay). Arrows indicate the spatial orientation of objects in respect to x, y and z axis (green, red and blue respectively).

(D) Representative frames corresponding to Movie 3.1.2.1. Shown is the maximum projection image of the z-stack obtained by time-lapse spinning disk confocal imaging. Numbers refer to the time, in minutes(') and seconds ("). The encircled area indicates the site of *cis*-Golgi cisterna (Anp1-mCherry, red) biogenesis as visualized by time-lapse spinning disk confocal imaging.

(E) Quantification of Anp1-mCherry fluorescence intensity (red line) associated with *cis*-Golgi cisternae biogenesis event indicated in (E) and the fluorescence profile averaged over six biogenesis events (black line). The horizontal axis indicates time in seconds, and the vertical axis indicates fluorescence intensity as percentage of the maximal intensity observed. Error bars correspond to standard deviation.

(F) Representative frames corresponding to Supplemental Movie 3.1.2.2. Shown is the single focus plane image sampled from the z-stack obtained by time-lapse spinning disk confocal imaging. Numbers refer to the time, in minutes(') and seconds ("). Encircled areas indicate the single Golgi cisternae maturing from a *cis*-Golgi (Anp1-mCherry, red) to *trans*-Golgi identity (Sec72-GFP, green).

(G) Quantification of intensity of Anp1-mCherry (red) and Sec72-GFP (green) fluorescence associated with a Golgi cisterna maturation event indicated by the arrow in (F). Data is graphed as in (E).

Movie Legend 3.1.2.1. *cis*-Golgi cisternae can form *de novo* in *S. pombe*.

Time-lapse sequence of cells expressing *cis*-Golgi marker Anp1-mCherry (red). Arrows indicate sites of *cis*-Golgi cisternae biogenesis. Time-lapse images were generated using spinning-disk confocal imaging system. Image stacks consisted of 10 sections of 0.5 μm spacing taken every ~ 6 seconds. Three-dimensional images of each stack were combined into a QuickTime movie using Volocity software package.

Movie Legend 3.1.2.1. Golgi maturation dynamics are consistent with the cisternal maturation model

Time-lapse sequence of cells expressing *trans*-Golgi marker Sec72-GFP (green) and *cis*-Golgi marker Anp1-mCherry (red). Arrows indicate the site of a Golgi cisternae maturing. Time-lapse images were generated using spinning-disk confocal imaging system. Image stacks consisted of 9 sections of 0.5 μm spacing taken every ~ 6 seconds. Three-dimensional images of each stack were combined into a QuickTime movie using Volocity software package.

3.1.3. Early secretory pathway compartments accumulate at the division site

When characterizing the organization and the dynamics of the early secretory pathway compartments, I noticed a striking difference in the spatial distribution between interphase and dividing cells (Fig. 3.1.1A and C). To explore this matter further I performed epifluorescence microscopy analyses of live fission yeast cells expressing tER or Golgi markers fused to GFP and the actomyosin ring marker Rlc1 fused to RFP. A pronounced recruitment of secretory compartments to the cell division site became noticeable at the time of actomyosin ring formation. Notably, whereas the tER exhibited the highest levels of accumulation at this time (Fig. 3.1.3.1A), the Golgi apparatus appeared only moderately polarized towards the future division site (Fig. 3.1.3.1B and 3.1.3.1C). As cells progressed through septation all marker proteins attained maximum polarization levels. It should be noted that tER showed a fairly narrow region of intense accumulation, approximately 10% of mother cell length, while the Golgi marker proteins were enriched in the medial 30% of mother cell length. Thus, for further analyses cells exhibiting such accumulation of tER and Golgi markers respectively were considered polarized. Quantification of the fluorescence levels of tER and Golgi marker proteins suggested that their accumulation to the site of division was statistically significant (Fig. 3.1.3.2A-C, n=50 cells per marker per cell cycle stage; see Materials and Methods for details).

In a collaboration project with Zhang Dan, a graduate student in the Oliferenko lab, I analyzed the spatio-temporal dynamics of the ER tubules and sheets. Using the Rlc1-mCherry to determine the cell cycle stage of cells I

found that the ER sheets marked by Ost1-GFP or Sec63-GFP show no equatorial enrichment during cell division (Fig. 3.1.3.3A and data not shown). Conversely the ER tubules labeled by Tts1-GFP or Rtn1-GFP accumulated to the division site (Fig. 3.1.3.3B and data not shown). However, the enrichment of tER and ER tubules at the division site appear to be differentially regulated processes (see Results 3.2.8).

Taken together my data shows that the tubular ER, the tER and Golgi cisterane all polarize to the cell equator at the time of the actomyosin ring formation and remain enriched at the division site throughout the course of septation.

Figure Legend 3.1.3.1. Spatial distribution of the early secretory pathway throughout the cell cycle.

(A) tER localization marked by Sec24-GFP (top row) in interphase (first column), mitosis (second column), early and late septation (third and fourth column). The cell cycle stage was deduced by the morphology of the actomyosin ring marker Rlc1-mRFP (second row from the top) and the DIC image (not shown). Shown is the maximum projection image of the z-stack obtained by epifluorescence imaging. Epifluorescence maximum projection images of z-stacks of 50 individual cells at the same stage of the cell cycle expressing Sec24-GFP were standardized and compared to produce an averaged image (third row from the top, for details see Material and Methods). The horizontal axis indicates position along the cell axis in percentages of cell length and the vertical axis indicates fluorescence intensity in arbitrary units.

(B) *cis*-Golgi localization marked by Anp1-GFP, imaging and analysis as in (A).

(C) *trans*-Golgi localization marked by Sec72-GFP, imaging and analysis as in (A).

Figure 3.1.3.1. Spatial distribution of the early secretory pathway throughout the cell cycle.

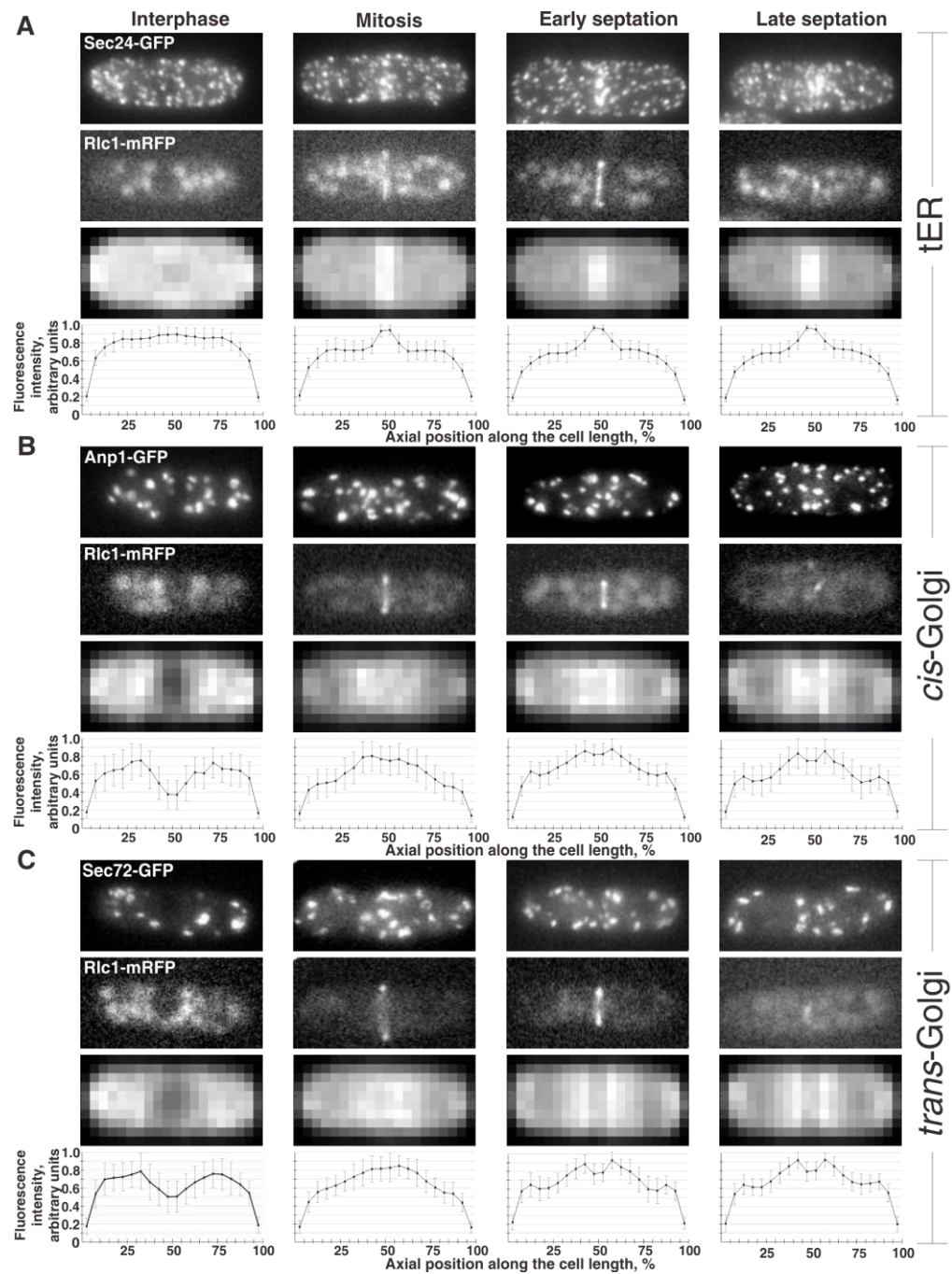


Figure 3.1.3.2. Accumulation of the early secretory pathway compartments at the site of division is statistically significant.

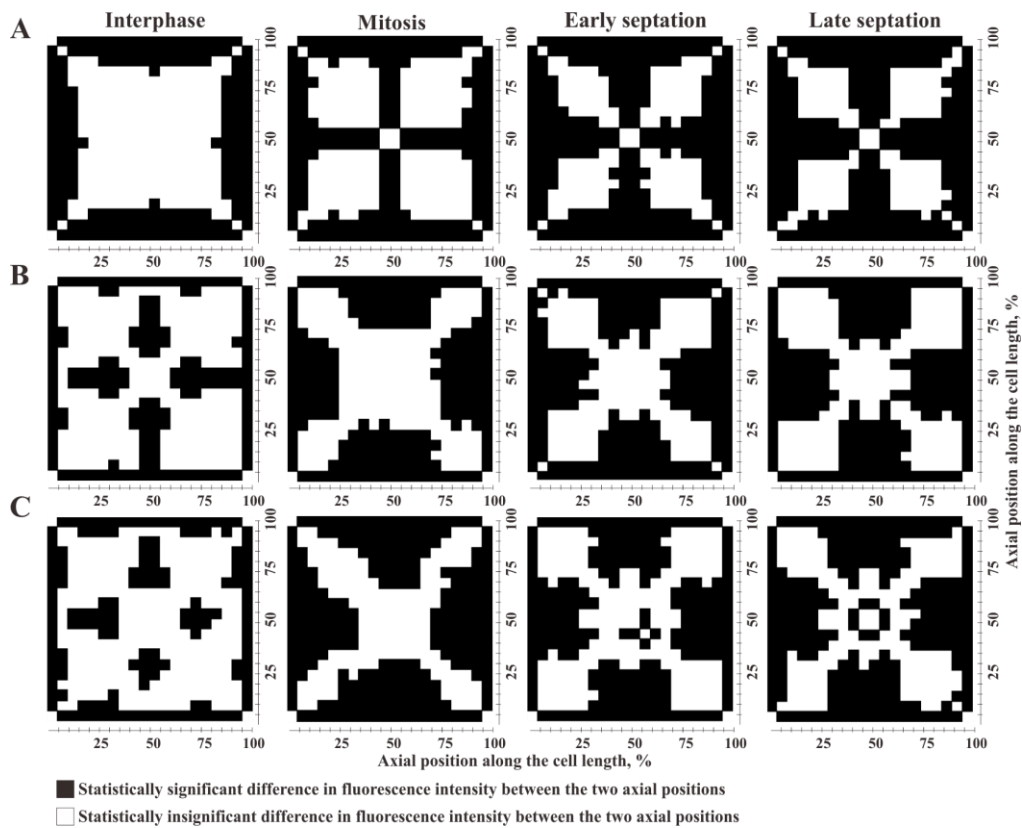


Figure Legend 3.1.3.2. Accumulation of the early secretory pathway compartments at the site of division is statistically significant.

(A) Statistical significance of differences in fluorescence signal between two axial positions in cells expressing tER marker Sec24-GFP during interphase (first column), mitosis (second column), early and late septation (third and fourth column). Epifluorescence maximum projection images of z-stacks of 50 individual cells at the same stage of the cell cycle (determined based on Rlc1-RFP signal and DIC images) were standardized and compared to produce the p-values (for details see Materials and Methods).

(B) Statistical significance of differences in fluorescence signal between two axial positions in cells expressing *cis*-Golgi marker Anp1-GFP, imaging and analysis as in (A).

(C) Statistical significance of differences in fluorescence signal between two axial positions in cells expressing *trans*-Golgi marker Sec72-GFP, imaging and analysis as in (A).

Figure 3.1.3.3. Spatial distribution of the ER sheets and tubules throughout the cell cycle.

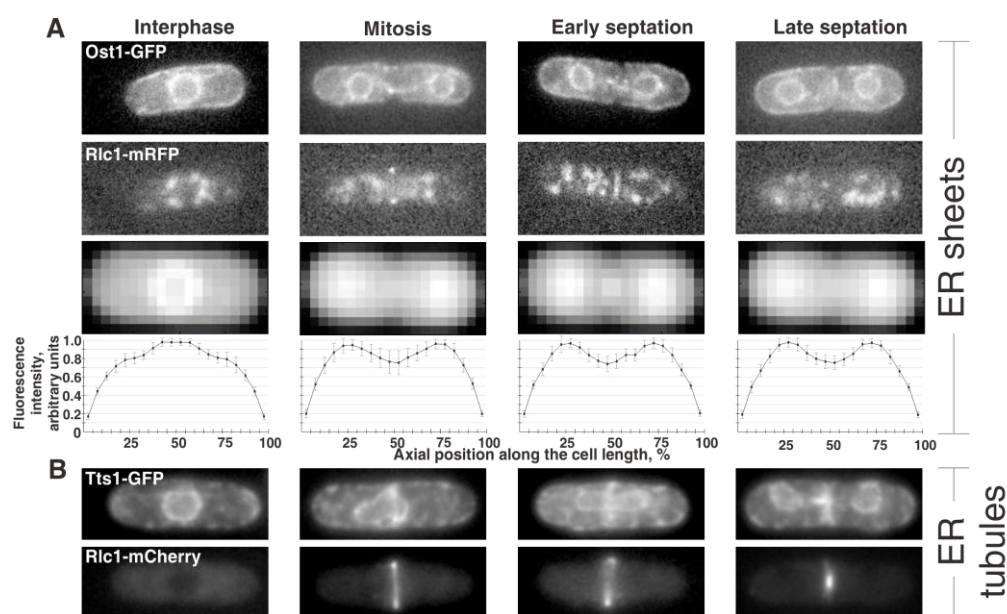


Figure Legend 3.1.3.3. Spatial distribution of the ER sheets and tubules throughout the cell cycle.

(A) Localization of the putative ER sheets marked by Ost1-GFP (top row of images) in interphase (first column), mitosis (second column), early and late septation (third and fourth column). The cell cycle stage was deduced by the morphology of the actomyosin ring marker Rlc1-mRFP (second row from the top) and the DIC image (not shown). Shown is the maximum projection image of the z-stack obtained by epifluorescence imaging. Epifluorescence images of 50 individual cells at the same stage of the cell cycle expressing Sec24-GFP were standardized and compared to produce an averaged image (third row from the top, for details see Materials and Methods). The horizontal axis indicates position along the cell axis in percentages of cell length and the vertical axis indicates fluorescence intensity in arbitrary units.

(B) Localization of the ER tubules marked by Tts1-GFP (top row of images) in interphase (first column), mitosis (second column), early and late septation (third and fourth column). The cell cycle stage was deduced by the morphology of the actomyosin ring marker Rlc1-mCherry (second row from the top) and the DIC image (not shown). Shown is the maximum projection image of the z-stack obtained by epifluorescence imaging.

3.2. Mechanisms of Spatial and Temporal Regulation of the Secretory Pathway in Fission Yeast

3.2.1. Actomyosin ring assembly is required for secretory machinery recruitment to the division site

Given that I observed the initial medial accumulation of both tER and Golgi compartments occurring concomitantly with actomyosin ring formation (Fig. 3.1.3.1A-C), I hypothesized that the ring itself might serve as a determinant for the early secretory pathway polarization. To explore this possibility, I introduced the fluorescent markers of the secretory pathway into the *cdc12-112* temperature-sensitive genetic background. The essential *S. pombe* formin Cdc12 plays a crucial role in actomyosin ring formation, and fission yeast cells are incapable of ring assembly when Cdc12 function is compromised (Chang et al., 1997). When grown at the restrictive temperature of 36°C, *cdc12-112* mutant cells undergo the nuclear division but are not capable of cytokinesis (Arai and Mabuchi, 2002). I synchronized exponentially growing cell cultures in early G₂ phase of the cell cycle by elutriation. Immediately upon elutriation cells were released into a fresh medium and grown at either permissive or restrictive temperatures. As judged by visualization of the Uch2-mCherry, anaphase cell population peaked at around 75 minutes and 90 minutes after elutriation for cultures grown at 24°C and 36°C, respectively. Samples were taken, fixed and stained for actin and DNA to confirm that cells were unable to form rings at the restrictive temperature (data not shown). By analyzing the spatial distribution of the secretory pathway marker proteins, I noticed a strikingly reduced medial accumulation of tER and Golgi cisternae (Fig. 3.2.1A-D). Under permissive

conditions ~90% and ~80% of cells exhibited tER and Golgi polarization, respectively, whereas under restrictive conditions only ~10% and ~25% of cells polarized these compartments. I confirmed that the actomyosin ring structure was essential for polarization of the early secretory compartments by exploring the spatial distribution of the tER and Golgi compartments in cells with compromised function of the myosin light chain Cdc4 (McCollum et al., 1995). The cells carrying the temperature sensitive *cdc4-8* allele lacked equatorial polarization of the early secretory pathway when grown at the restrictive temperature of 36°C (Fig. 3.2.1E-H). Thus, establishment of early secretory pathway polarization during mitosis depends on actomyosin ring formation.

Figure 3.2.1. Actomyosin ring assembly is required for secretory pathway recruitment to the division site.

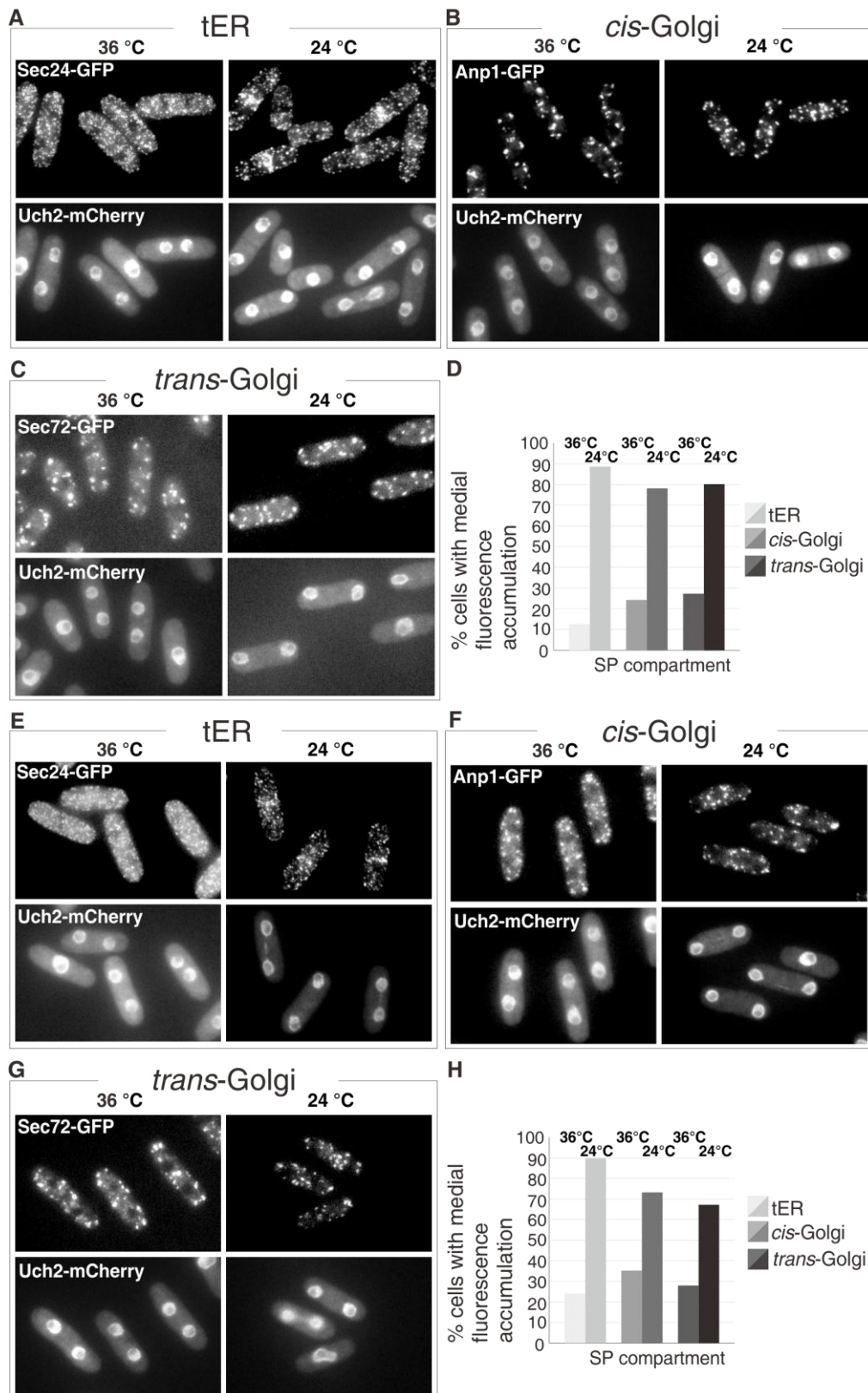


Figure Legend 3.2.1. Actomyosin ring assembly is required for secretory pathway recruitment to the division site.

(A) Temperature sensitive *cdc12-112* mutant cells expressing Sec24-GFP (top row) and the nuclear marker Uch2-mCherry (bottom row) were imaged upon entry into anaphase after previously being synchronized in G₂ by elutriation, transferred into fresh medium and allowed to grow at 36°C (left column) and 24°C (right column). Shown is the maximum projection image of the z-stack obtained by epifluorescence imaging.

(B) Temperature sensitive *cdc12-112* mutant cells expressing Anp1-GFP (top row) and the nuclear marker Uch2-mCherry (bottom row) were treated as in (A).

(C) Temperature sensitive *cdc12-112* mutant cells expressing Sec72-GFP (top row) and the nuclear marker Uch2-mCherry (bottom row) were treated as in (A).

(D) Quantitation of Sec24-GFP, Anp1-GFP and Sec72-GFP polarization under experimental conditions described in (A) (n=250 cells per sample).

(E) Temperature sensitive *cdc4-8* mutant cells expressing Sec24-GFP (top row) and the nuclear marker Uch2-mCherry (bottom row) were imaged upon entry into anaphase after previously being synchronized in G₂ by elutriation, transferred into fresh medium and allowed to grow at 36°C (left column) and 24°C (right column). Shown is the maximum projection image of the z-stack obtained by epifluorescence imaging.

(F) Temperature sensitive *cdc4-8* mutant cells expressing Anp1-GFP (top row) and the nuclear marker Uch2-mCherry (bottom row) were treated as in (A).

(G) Temperature sensitive *cdc4-8* mutant cells expressing Sec72-GFP (top row) and the nuclear marker Uch2-mCherry (bottom row) were treated as in (A).

(H) Quantitation of Sec24-GFP, Anp1-GFP and Sec72-GFP polarization under experimental conditions described in (A) (n=250 cells per sample).

3.2.2. Maintenance of a polarized state of the early secretory pathway compartments requires an intact actin cytoskeleton

My observations indicated that the establishment of the polarized distribution of the early secretory pathway compartments required actomyosin ring assembly. However, the polarized state persisted throughout septation at the time when the ring is disassembled. Thus it was possible that other factors could be employed for maintenance of the polarized tER and Golgi distribution. Since actin patches localize at the site of septation following ring constriction, I probed the importance of an intact actin cytoskeleton for this phenomenon. To this end, I analyzed the behavior of the early secretory pathway marker proteins in asynchronously growing cell cultures treated with Latrunculin A (LatA), a drug that prevents actin polymerization. 10 μ M LatA has been shown to cause a rapid depolymerization of the actin cytoskeleton in *S. pombe* (Karagiannis et al., 2005). I observed that cells treated with LatA for 15 minutes underwent a significant decrease in polarization of all secretory pathway compartments (Fig. 3.2.2A-D). The binucleate mitotic cells treated with LatA did not show any degree of either tER or Golgi accumulation, likely due to their inability to assemble the actomyosin ring. While some septating cells exhibited polarization 15 minutes after drug application, 30 minutes of LatA treatment completely abolished the medial accumulation of the secretory pathway compartments. I confirmed that both division rings and interphase actin structures were eliminated by LatA treatment (Fig. 3.2.2E). These data confirmed that the actomyosin ring was essential for establishment of tER and Golgi compartments polarization, and suggested that an intact actin cytoskeleton was required for its maintenance during septation.

Figure 3.2.2. Maintenance of the secretory pathway polarization to the site of cell division requires an intact actin cytoskeleton.

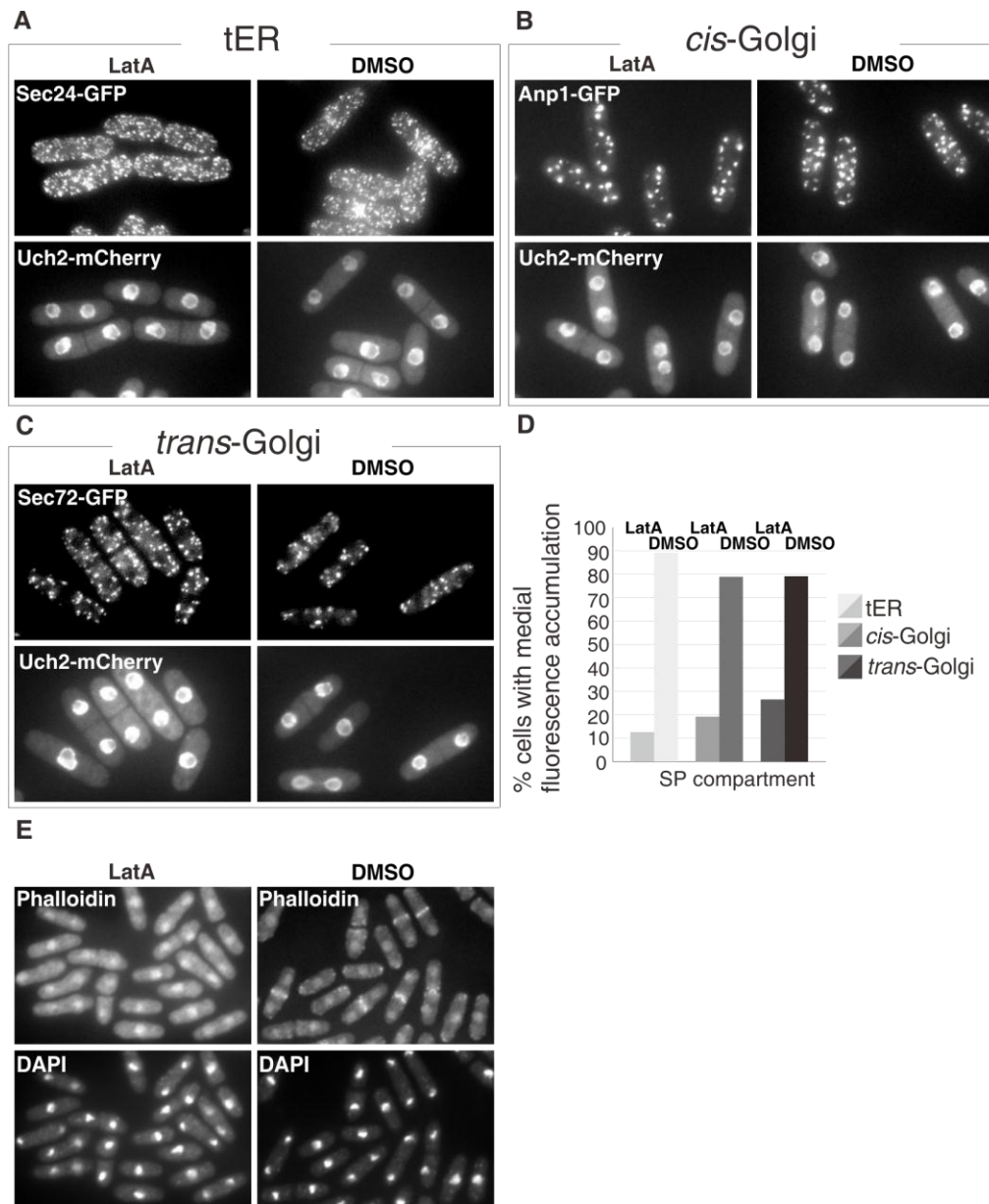


Figure Legend 3.2.2. Maintenance of the secretory pathway polarization to the site of cell division requires an intact actin cytoskeleton.

(A) Cells expressing Sec24-GFP (top row) and Uch2-mCherry (bottom row) were treated with 10 μ M LatA (left column) or DMSO (right column) for 30 minutes. Shown is the maximum projection image of the z-stack obtained by epifluorescence imaging.

(B) Cells expressing Anp1-GFP (top row) and Uch2-mCherry (bottom row) were treated as in (A).

(C) Cells expressing Sec72-GFP (top row) and Uch2-mCherry (bottom row) were treated as in (A).

(D) Graph quantifying the proportion of cells exhibiting Sec24-GFP, Anp1-GFP and Sec72-GFP polarization under experimental conditions described in (A), n=250 cells per sample.

(E) Cells expressing Sec24-GFP and Uch2-mCherry were grown overnight at 24°C and treated for 30 minutes with either 10 μ M LatA dissolved in DMSO (left column) or DMSO alone (right column). Culture samples were taken and stained for actin (phalloidin, top row) and DNA (DAPI, bottom row) indicating that 30 minute treatment with 10 μ M LatA is sufficient for complete depolymerization of the actin cytoskeleton in *S. pombe*. Identical results were obtained for wild-type cells (data not shown).

3.2.3. The recruitment of the early secretory compartments to the actomyosin ring and the septation site is not under direct regulation of cell cycle

To explore whether accumulation of the secretory compartments to the division site was dependent on the cell cycle stage, I analyzed the behavior of both the tER and the Golgi apparatus in the *cdc16-116* temperature-sensitive genetic background. Cdc16 is a subunit of the two-component GTPase-activating module for the small GTPase Spg1 and thus serves as a negative regulator of the SIN pathway (Furge et al., 1998). Loss of function of Cdc16 untimely activates the SIN pathway resulting in cell cycle independent, successive rounds of actomyosin ring formation and constriction accompanied by septum deposition (Minet et al., 1979). Asynchronously growing *cdc16-116* cells expressing GFP fusions with the early secretory pathway markers were shifted to the restrictive temperature of 36°C and imaged one hour after temperature shift-up. I found that Sec24-GFP, Anp1-GFP and Sec72-GFP, that represent tER, early and late Golgi compartments respectively, accumulated in the vicinity of most ectopic septa (Fig. 3.2.3A-C). Considering that some cells simultaneously exhibited more than one ectopic septum, I quantified the number of ectopic septa that recruited the secretory compartments rather than the proportion of cells showing such accumulation (Fig. 3.2.3D). I concluded that early secretory pathway accumulation spatially and temporally coincided with contractile ring and septum formation independently of the cell cycle.

Figure 3.2.3. The recruitment of the early secretory compartments to the actomyosin ring and the septation site is not under direct regulation of cell cycle.

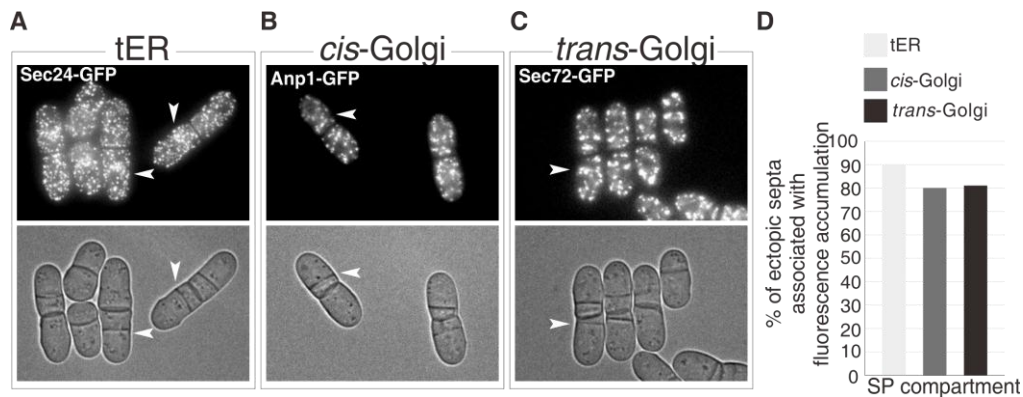


Figure Legend 3.2.3. The recruitment of the early secretory compartments to the actomyosin ring and the septation site is not under direct regulation of cell cycle.

(A) Epifluorescence and DIC images (top and bottom, respectively) of temperature sensitive *cdc16-116* mutant cells expressing Sec24-GFP grown at 36°C. Shown is the maximum projection image of the z-stack obtained by epifluorescence imaging.

(B) Epifluorescence and DIC images (top and left column, respectively) of temperature sensitive *cdc16-116* mutant cells expressing Anp1-GFP grown at 36° C.

(C) Epifluorescence and DIC images (top and left column, respectively) of temperature sensitive *cdc16-116* mutant cells expressing Sec72-GFP grown at 36° C.

(D) Quantitation of Sec24-GFP, Anp1-GFP and Sec72-GFP polarization under experimental conditions described in (A) above (n=250 ectopic septa per sample).

3.2.4. The Septation Initiation Network is required for maintenance but not for the initial recruitment of the early secretory pathway compartments at the division site

To explore the possibility that the SIN pathway was directly responsible for the polarization of the early secretory compartments I observed the spatial distribution of the tER and Golgi marker proteins in the *sid2-250* temperature-sensitive mutant background. Sid2 is the downstream effector kinase of SIN signaling (Sparks et al., 1999), and loss of its activity leads to septation failure. Using elutriation I synchronized cells in the manner described above and observed the localization of Sec24-GFP, Anp1-GFP and Sec72-GFP in anaphase cells (Fig. 3.2.4.1A-C) also expressing the nuclear envelope marker, Uch2-mCherry, at both 24°C and 36°C. As indicated by the marker proteins, in mitotic cells all three compartments, including the tER, *cis*-Golgi and *trans*-Golgi, exhibited medial accumulation independently of whether the SIN function was compromised (Fig. 3.2.4.1D). It should be noted that medial accumulation of the tER and Golgi compartments did decrease upon longer incubation at the restrictive temperature, suggesting that maintenance of the actomyosin ring executed by the SIN pathway throughout anaphase and cytokinesis was essential for ensuring the continuous localization of the secretory compartments to the site of septation. To confirm that the SIN pathway activity was not essential for the initial secretory machinery recruitment but was required for maintenance of its polarization state I performed the time-lapse imaging of *sid2-250* mutant cells expressing secretory pathway GFP tagged marker proteins and Uch2-mCherry, growing either at the permissive temperature of 24°C or shifted to the restrictive

temperature of 36°C for 1 hour (Fig. 3.2.4.2A-C). I found that anaphase cells (as indicated by the nuclear envelope marker Uch2-mCherry) growing at both 24°C and 36°C exhibited initial medial accumulation of the secretory compartments. While this accumulation persisted in cells grown at 24°C (7/8, 5/6 and 5/5 cells for tER, *cis*-Golgi and *trans*-Golgi respectively), it was abolished at 36°C (only 2/8, 0/4 and 0/4 cells exhibited some residual accumulation in case of tER, *cis*-Golgi and *trans*-Golgi respectively). In conclusion, my findings implied that the medial recruitment of the early secretory pathway was SIN independent while its maintenance relied on SIN regulated cellular processes.

Figure 3.2.4.1. The Septation Initiation Network is required for maintenance but not for the initial recruitment of the early secretory pathway compartments at the division site.

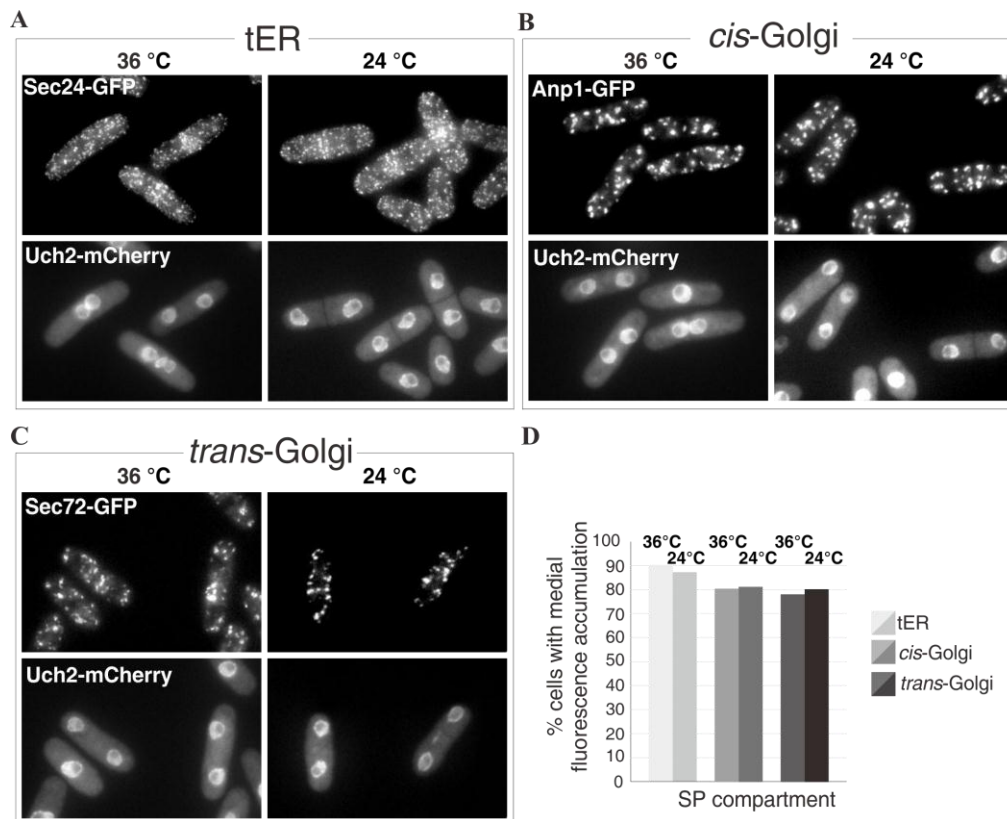


Figure Legend 3.2.4.1. The Septation Initiation Network is required for maintenance but not for the initial recruitment of the early secretory pathway compartments at the division site.

(A) Temperature sensitive *sid2-250* mutant cells expressing Sec24-GFP (top row) and the nuclear marker Uch2-mCherry (bottom row), were imaged upon entry into anaphase after previously being synchronized in G₂ by elutriation, transferred into fresh medium and allowed to grow at 36° (left column) and 24°C (right column). Shown is the maximum projection image of the z-stack obtained by epifluorescence imaging.

(B) Temperature sensitive *sid2-250* mutant cells expressing Anp1-GFP (top row) and the nuclear marker Uch2-mCherry (bottom row) were treated as in (A).

(C) Temperature sensitive *sid2-250* mutant cells expressing Sec72-GFP (top row) and the nuclear marker Uch2-mCherry (bottom row) were treated as in (A).

(D) Graph quantifying the proportion of cells exhibiting Sec24-GFP, Anp1-GFP and Sec72-GFP polarization under experimental conditions described in (A), n=250 cells per sample.

Figure 3.2.4.2. The Septation Initiation Network is required for maintenance but not for the initial recruitment of the early secretory pathway compartments at the division site.

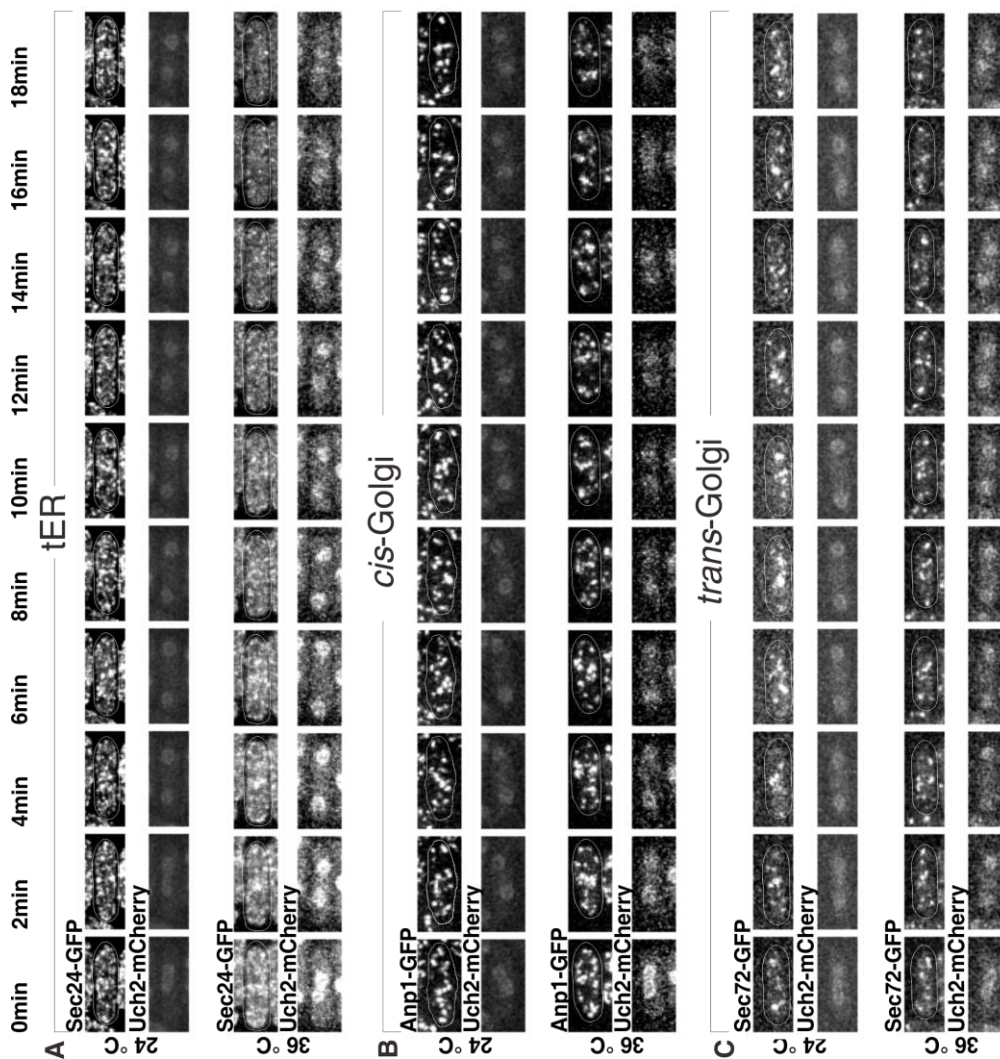


Figure Legend 3.2.4.2. The Septation Initiation Network is required for maintenance but not for the initial recruitment of the early secretory pathway compartments at the division site.

(A) *sid2-250* cells expressing Sec24-GFP (first and third row from the top) and Uch2-mCherry (second and fourth row from the top) were grown overnight at 24°C and imaged at either 24°C (top two panels) or shifted to 36°C (bottom two panels) for 1 hour prior to imaging.. Shown is the maximum projection image of the z-stack obtained by time-lapse spinning disk confocal imaging. Numbers correspond to time in minutes.

(B) *sid2-250* cells expressing Anp1-GFP (first and third row from the top) and Uch2-mCherry (second and fourth row from the top) treated as in (A).

(C) *sid2-250* cells expressing Sec72-GFP (first and third row from the top) and Uch2-mCherry (second and fourth row from the top) treated as in (A).

3.2.5. The EFC domain protein Cdc15 is required for tER recruitment to the division site

My results showed that the actomyosin ring is required for the tER and Golgi polarization during mitosis. Cdc15 is a component of the actomyosin ring and is the member of the EFC domain family characterized by an EFC domain at the N-terminus and an SH3-domain at the C-terminus (Fankhauser et al., 1995; Tsujita et al., 2006). Cdc15 essential function in stabilizing contractile rings is exhibited only upon SIN signaling activation (Wachtler et al., 2006). At restrictive temperatures, cells carrying the conditional *cdc15* alleles are capable of forming transient actomyosin rings early in mitosis (Fankhauser et al., 1995; Chang et al., 1996; Balasubramanian et al., 1998). Interestingly, the EFC protein family members were shown to couple membrane deformation to the actin cytoskeleton, providing a potential link to COPII vesicle biogenesis (Lee et al., 2005; Tsujita et al., 2006). Thus, I set out to investigate whether Cdc15 functioned during establishment of the polarized state of tER and Golgi during cell division.

Although not essential for actomyosin ring formation in metaphase, Cdc15 is necessary for its maintenance upon SIN activation (Wachtler et al., 2006). Thus, to assess the specific contribution of Cdc15 independently from the actomyosin ring, I observed the spatial distribution of the secretory pathway proteins in wild-type and temperature sensitive *cdc15-140* mutant cells arrested in metaphase by overexpression of the spindle assembly checkpoint component Mad2 under the *nmt1* promoter (Maundrell, 1990; He et al., 1997). Briefly, Mad2 overexpression was induced for 20 hours at the permissive temperature of 24°C followed by the temperature shift-up for 4

hours at 36°C. Samples were taken from cell cultures and stained by phalloidin and DAPI indicating that under the experimental conditions described ~38% of cells contained actomyosin ring with ~85% of these appearing arrested in metaphase. I analyzed the distribution of the early secretory pathway markers in live cells exhibiting Rlc1-mRFP rings. I observed a marginal difference in the spatial distribution of *cis*- and the *trans*-Golgi compartments between wild-type and *cdc15-140* mutant cells at both 24°C and 36°C, with approximately 50% and 55% cells exhibiting polarization of early and late Golgi elements, respectively (Fig. 3.2.5B and C, respectively). On the other hand, the tER marker protein Sec24-GFP exhibited a more complex distribution (Fig. 3.2.5A). In wild-type cells, at both 24°C and 36°C, approximately 80% of cells displaying Rlc1-mRFP ring exhibited a clear recruitment of Sec24-GFP to the narrow medial band, while ~10% of these cells showed some degree of accumulation in a broader, less defined medial region (Fig. 3.2.5A, center panel). Sec24-GFP appeared non-polarized in ~10% under these conditions. I observed a striking reduction in the number of cells exhibiting clear polarization of the tER in *cdc15-140* cells already at the permissive temperature of 24°C (Fig. 3.2.5A, bottom panel) suggesting that under these circumstances the mutant Cdc15 protein behaved as a hypomorph. Amongst *cdc15-140* cells grown at 24°C and displaying the Rlc1-RFP, approximately 40%, 40% and 20% of exhibited the polarized, marginally polarized and unpolarized localization of Sec24-GFP respectively. Upon temperature shift-up to 36°C, the number of *cdc15-140* mutant cells with Rlc1-mRFP rings exhibiting clearly polarized Sec24-GFP localization further decreased to ~20% whereas approximately 40% showed no polarization and

the rest exhibited only marginal medial localization. I concluded that Sec24-GFP accumulation at the division site was impaired in metaphase arrested *cdc15-140* cells in spite of their ability to assemble actomyosin rings, implicating Cdc15 in tER polarization during cell division.

To further explore the role of Cdc15 in polarization of the tER at the level of individual cells I performed the time-lapse analyses of either wild-type or *cdc15-140* cells expressing Sec24-GFP and Rlc1-mCherry grown overnight at 24°C and shifted to 36°C for 1 hour (Fig. 3.2.5D and E). The wild-type cells entered mitosis and formed an actomyosin ring that persisted and eventually constricted. I observed a marked and persistent recruitment of tER occurring concomitantly with the actomyosin ring assembly (8/8 cells). The *cdc15-140* cells could form actomyosin rings upon entry into mitosis, but these rings neither persisted nor constricted. Formation of the actomyosin ring in *cdc15-140* cells did not correlate with marked Sec24-GFP polarization (Fig. 3.2.5E, 5/8 cells). Incomplete inactivation of Cdc15 temperature-sensitive protein could be a reason behind weak and transient Sec24-GFP accumulation detected in remaining cells.

Figure 3.2.5. The EFC domain protein Cdc15 was required for the recruitment of the tER to the division site.

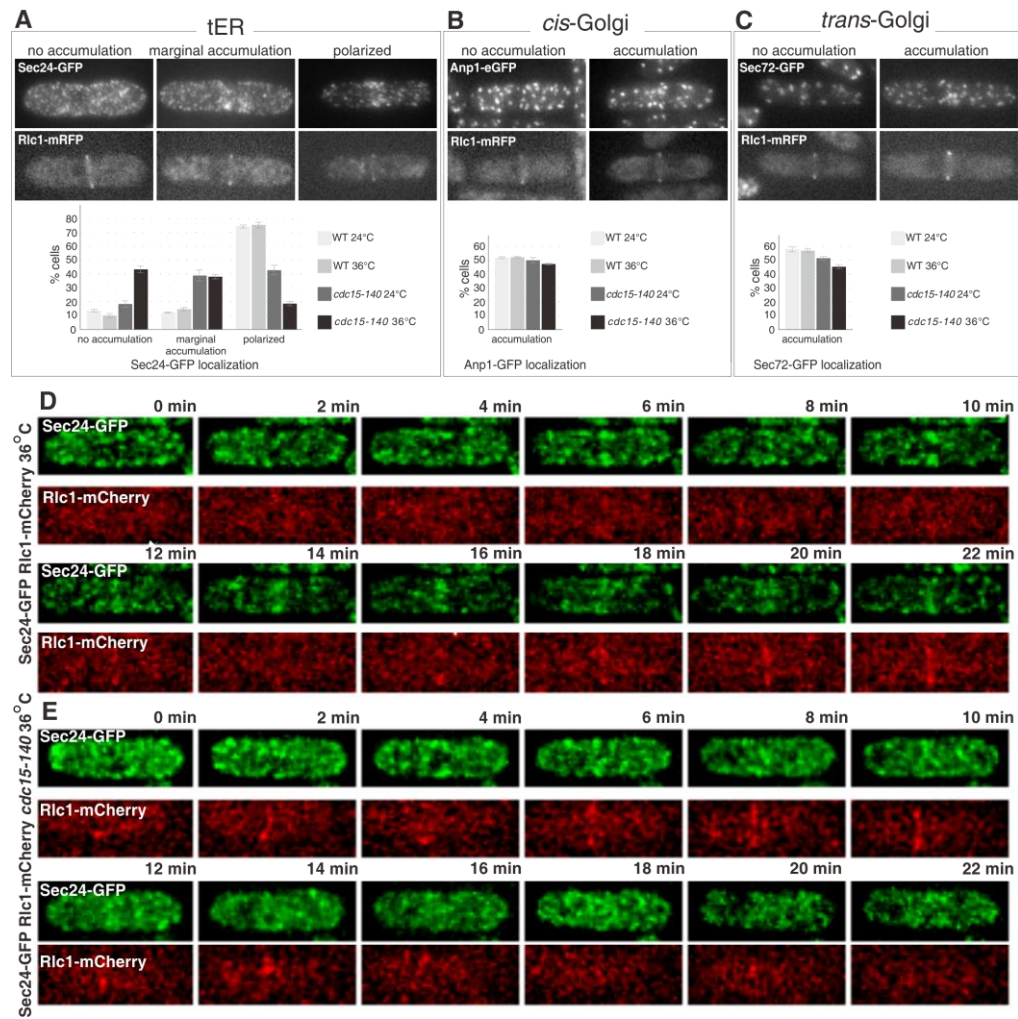


Figure Legend 3.2.5. The EFC domain protein Cdc15 was required for the recruitment of the tER to the division site.

(A) pREP1-mad2⁺ cells co-expressing Sec24-GFP and Rlc1-RFP in wild-type or *cdc15-140* mutant background were grown for 20 hours in the absence of thiamine to induce metaphase arrest by overproduction of Mad2 and additionally allowed to grow for 4 hours at either 24°C or 36°C. In each sample, cells displaying Rlc1-mRFP rings (second row from the top) exhibited three distinct phenotypes of Sec24-GFP localization (top row of images). Shown is the maximum projection image of the z-stack obtained by epifluorescence imaging. Quantitation of Sec24-GFP localization profiles under experimental conditions described is presented in the graph (n=250 cells per sample).

(B) pREP1-mad2⁺ cells co-expressing Anp1-GFP and Rlc1-RFP in wild-type or *cdc15-140* mutant background were treated as in (A). In each sample, cells displaying Rlc1mRFP rings (second row from the top) exhibited distinct phenotypes of Anp1-GFP localization (top row of images). Shown is the maximum projection image of the z-stack obtained by epifluorescence imaging. Quantitation of Anp1-GFP localization profiles under experimental conditions described are presented in the graph (n=250 cells per sample).

(C) pREP1-mad2⁺ cells co-expressing Sec72-GFP and Rlc1-RFP in wild-type or *cdc15-140* mutant background were treated as in (A). In each sample, cells displaying Rlc1mRFP rings (second row from the top) exhibited distinct phenotypes of Sec72-GFP localization (top row of images). Shown is the maximum projection image of the z-stack obtained by epifluorescence imaging. Quantitation of Sec72-GFP localization profiles under experimental conditions described are presented in the graph (n=250 cells per sample).

(D) Wild-type cells expressing Sec24-GFP (green) and Rlc1-mCherry (red) were grown overnight at 24°C and shifted to 36°C for 1 hour prior to imaging. Shown is the maximum projection image of the z-stack obtained by time-lapse spinning disk confocal imaging.

(E) *cdc15-140* mutant cells expressing Sec24-GFP (green) and Rlc1-mCherry (red) were grown overnight at 24°C and shifted to 36°C for 1 hour prior to imaging. Shown is the maximum projection image of the z-stack obtained by time-lapse spinning disk confocal imaging.

3.2.6. Overexpression of Cdc15 is sufficient to promote relocalization of the tER to the cell equator in interphase cells

It has been shown that overexpression of Cdc15 causes actin relocalization to the equatorial region in interphase cells (Fankhauser et al., 1995). To assess whether this is sufficient for the early secretory pathway compartments polarization, I overexpressed Cdc15 under the *nmt1* promoter in cells arrested in interphase by the use of *cdc25-22* genetic background (Gould and Nurse, 1989). The *cdc25-22* arrest at restrictive temperature was evident from the increased cell length and Cdc15 overexpression induced for a total of 16 hours (12 hours at 24°C and 4 hours at 36°C) resulted in approximately 35% of interphase arrested cells with relocalized actin to the cell middle, as judged by DAPI and phalloidin staining. Only few of these cells formed an organized ring as judged by localization of Rlc1-mRFP. I did not observe medial accumulation of either *cis*- and *trans*-Golgi compartments (data not shown). Interestingly, a total of $37 \pm 4\%$ interphase arrested cells showed a marked accumulation of tER at the medial region, a number which corresponded to the percentage of cells that relocalized actin (Fig. 3.2.6A and B). Most cells exhibiting the tER polarization did not assemble the Rlc1-mRFP-positive actomyosin ring structures (Fig. 3.2.6A bottom panel). Taken together, my experiments imply that the EFC domain protein Cdc15 is specifically required for the COP II vesicle polarization at the division site.

Figure 3.2.6. Overexpression of Cdc15 is sufficient to induce medial tER accumulation in interphase.

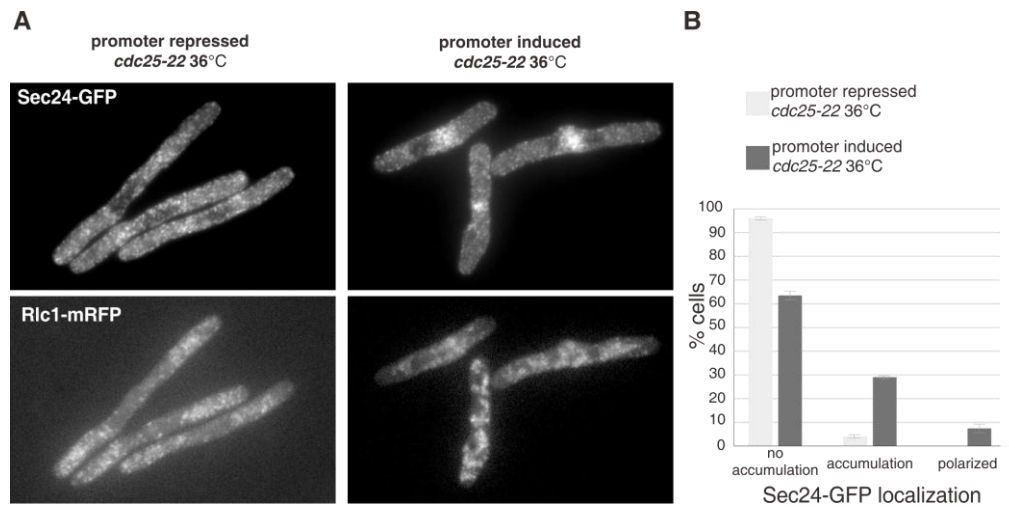


Figure Legend 3.2.6. Overexpression of Cdc15 is sufficient to induce medial tER accumulation in interphase.

(A) *cdc25-22 pREP1-cdc15⁺* cells expressing Sec24-GFP (top row) and Rlc1-mRFP (bottom row) were grown for 12 hours at 24°C and for 4 hours at 36° in the absence or presence of thiamine (left and right column respectively). Shown is the maximum projection image of the z-stack obtained by epifluorescence imaging.

(B) Quantitation of Sec24-GFP polarization under experimental conditions described above (n=250 cells per sample).

3.2.7. Cdc15 is required for the tER polarization to the post-metaphase actomyosin rings.

Having shown that the medial accumulation of the tER at metaphase is dependent on the intact function of the Cdc15 (Fig. 3.2.5), I was interested if Cdc15 might also maintain tER polarization after anaphase onset. Since actomyosin ring is required for maintenance of tER polarization and the available Cdc15 mutants disassemble the ring at the onset of cytokinesis, I sought to identify novel Cdc15 alleles that uncouple its roles in regulating the actomyosin ring and the tER. In collaboration with Dr Maria Makarova, a postdoctoral fellow in the Oliferenko lab, I randomly mutagenized the *cdc15* open reading frame in cells expressing Sec24-GFP and visually screened for strains that would be unable to polarize tER to the septum at 36°C (see Materials and Methods). Though most temperature sensitive strains obtained in the screen failed to septate, three strains could form septa that were not associated with Sec24-GFP accumulation (data not shown). I chose one of these mutant strains for further studies. Genetic analysis confirmed that the temperature sensitivity and tER polarization defects were linked to the *cdc15* locus and I termed this novel recessive allele *cdc15-22* (data not shown). While Sec24-GFP efficiently polarized to the Rlc1-mCherry labeled actomyosin rings in wild-type cells grown at 24° and 36°C, tER polarization was impaired at 24°C and fully abolished at 36° in the *cdc15-22* genetic background (Fig. 3.2.7A and data not shown). Surprisingly, I found that the actomyosin rings in *cdc15-22* cells labeled by Rlc1-mCherry were slow to constrict at 24°C and fully arrested at 36°C (Fig. 3.2.7B and data not show). After 3 hrs at 36°C, the actomyosin rings in *cdc15-22* mutants were seen

falling apart and cells failed septation (data not shown). The *cdc15-22* mutant protein carried three amino acid substitutions and lacked the C-terminus of Cdc15 (Fig. 3.2.7C). Introduction of individual *cdc15-22* mutations to the wild-type *cdc15* locus indicated that the premature STOP codon was responsible for the failure of tER polarization and ring constriction defects in *cdc15-22* cells (data not shown).

The western blot analysis with anti-Cdc15 sera, performed in collaboration with the Kathleen Gould lab, showed that the *cdc15-22* mutation lead to production of a truncated protein at increased levels as compared to the wild-type Cdc15 (Fig. 3.2.7D). The phosphatase treatment of the cell lysates obtained from wild-type and *cdc15-22* cells indicated that the mutant protein underwent extensive phosphorylation similar to wild-type. The C-terminal GFP tagged versions of both wild-type Cdc15 and the mutant Cdc15-22 localized efficiently to the actomyosin ring visualized by Rlc1-mCherry (Fig. 3.2.7E).

Next I sought to better understand the slow ring constriction phenotype of *cdc15-22* mutant cells (Fig. 3.2.7B). Mutations in the cell wall synthase Cps1/Bgs1 lead to a similar arrest in actomyosin ring constriction (Liu et al., 1999). Both wild-type and *cdc15-22* cells efficiently recruited GFP tagged Cps1 to the division site (Fig. 3.2.7F). To explore if SIN signaling was intact in *cdc15-22* cells, I introduced the GFP tagged SIN signaling kinase Sid2 and Rlc1-mCherry into wild-type and mutant genetic background. By visualizing Pcp1-mCherry I also monitored the SPBs that nucleate the mitotic spindle and move apart as the spindle elongates in anaphase B. After being shifted to 36°C for 3 hours, wild-type post-metaphase cells with well separated SPBs

efficiently recruited Sid2-GFP to the division site and to both SPBs as previously reported (Fig. 3.2.7G, left panels and Sparks et al., 1999). Under same conditions the recruitment of Sid2-GFP to the division site was abolished in all post-metaphase *cdc15-22* cells even though the signal could be clearly visualized on separated SPBs (Fig. 3.2.7G, right panels). I concluded that *cdc15-22* cells were defective in putative transmission of SIN signaling between the SPBs and the actomyosin ring mediated by the Sid2 kinase.

Since Sid2 activity is presumed to be under control of the upstream Sid1 kinase and Sid2-GFP fails to localize to the equatorial ring in *sid1-239* mutants (Sparks et al., 1999), I proceeded to analyze anaphase localization of GFP-tagged Sid1 in wild-type and *cdc15-22* cells. The cell cycle stage was monitored by simultaneously visualizing Pcp1-mCherry and Rlc1-mCherry. Sid1-GFP was found properly localized to a single SPB in post-metaphase wild-type and *cdc15-22* mutant cells (Fig. 3.2.7H). Mitotic SPB-recruitment of Sid1 requires activity of the SIN regulatory kinase Cdc7 that also localizes to a single SPB during septation (Guertin et al., 2000). The SPB localization of the Cdc7-GFP appeared intact in septating *cdc15-22* cells (Fig. 3.2.7H). I concluded that *cdc15-22* cells have a defect in SIN signaling downstream of Cdc7 mediated recruitment of Sid1 to the SPB.

To gain further insight into potential roles of Cdc15 in ring constriction and tER polarization I exploited the temperature sensitivity of *cdc15-22* and performed a high-copy suppressor screen. The screen resulted in the isolation of two high copy suppressors of *cdc15-22* temperature sensitive growth, the C2 domain protein Fic1 and zinc finger protein Cps3 (data not shown). Future analyses on genetic interactions of *cdc15* with *fic1* and *eps3* might provide

insight on the roles of Cdc15 in ring constriction and secretory pathway regulation.

Figure 3.2.7. Characterization of the *cdc15-22* mutants

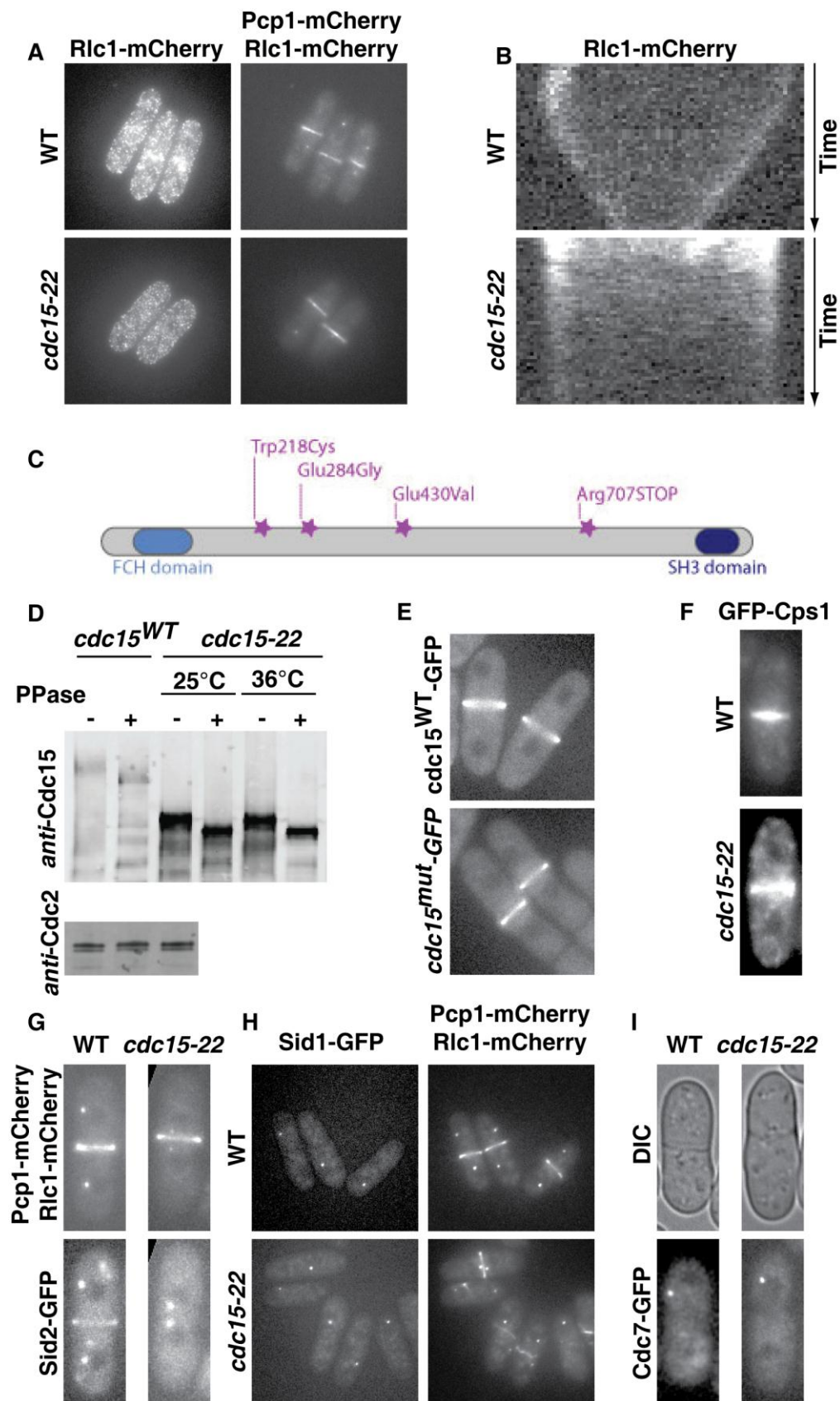


Figure Legend 3.2.7. Characterization of the *cdc15-22* mutants

(A) Wild-type and *cdc15-22* cells expressing Sec24-GFP (left column) and mCherry tagged Rlc1 and Pcp1 (right column) were grown for 16 hours at 24°C and for 3 hours at 36°C. Shown is the maximum projection image of the z-stack obtained by epifluorescence imaging.

(B) Kymographs illustrating Rlc1-mCherry dynamics in wild-type (top) and *cdc55-22* (bottom) shifted to 36°C for one hour and imaged by spinning-disk confocal fluorescence microscopy.

(C) Graphical illustration of mutations in the Cdc15-22 allele as compared to wild-type Cdc15. The positions of the FCH and SH3 domains are indicated

(D) Western blotting analysis using *anti*-Cdc15 sera of the wild-type Cdc15 and mutant Cdc15-22. The total cell lysates were obtained from cells grown under indicated conditions and treated with protein phosphatase as indicated.

(E) Wild-type Cdc15 and mutant Cdc15-22 were tagged with GFP and subjected to epifluorescence imaging. Shown is the maximum projection image of the nine 0.5 µm spaced z-sections.

(F) Wild-type and *cdc15-22* cells expressing GFP-Cps1 were grown for 16 hours at 24°C and for 3 hours at 36°C. Shown is the maximum projection image of the z-stack obtained by epifluorescence imaging.

(G) Wild-type and *cdc15-22* cells expressing Sid2-GFP (bottom panels) and mCherry tagged Rlc1 and Pcp1 (top panels) were grown for 16 hours at 24°C and for 3 hours at 36°C. Shown is the maximum projection image of the z-stack obtained by epifluorescence imaging.

(H) Wild-type and *cdc15-22* cells expressing Sid1-GFP (bottom panels) and mCherry tagged Rlc1 and Pcp1 (top panels) were grown for 16 hours at 24°C and for 3 hours at 36°C. Shown is the maximum projection image of the z-stack obtained by epifluorescence imaging.

(I) Wild-type and *cdc15-22* cells expressing Sid1-GFP were grown for 16 hours at 24°C and for 3 hours at 36°C. Shown is the DIC image (top panels) and maximum projection image of z-stacks obtained by epifluorescence imaging (bottom panels).

3.2.8. tER and ER tubules polarization to the division site have distinct molecular requirements

As previously mentioned, tubular ER also exhibits equatorial accumulation during cell division (Fig 3.1.3B). I was interested whether mitotic dynamics of the ER tubules share similar requirements to those of the tER. In collaboration with Zhang Dan, I analyzed the medial recruitment of the tubular ER marker protein Tts1-GFP in wild-type and temperature sensitive *cdc12-112* cells dividing at 36°C. I simultaneously imaged Uch2-mCherry to monitor the nuclear division and thus infer the cell cycle stage. I found that 87% of wild-type cells that underwent nuclear division accumulated Tts1 positive membranes to the cell equator (Fig. 3.2.8A, top panel and Fig. 3.2.8B). However, medial enrichment of ER tubules was observed in only 7% of cells compromised in actomyosin ring assembly due to the *cdc12-112* mutation (Fig. 3.2.8A, bottom panel and Fig. 3.2.8B). Thus the actomyosin ring assembly is required for recruitment of the tubular ER to the division site.

I next employed the time-lapse microscopy to monitor the dynamics of the Tts1-GFP in wild-type and *cdc15-140* cells dividing at 36°C. The Tts1-GFP allowed us to simultaneously visualize nuclear division and thus infer the cell cycle stage. Surprisingly, I found that cells with a compromised Cdc15 function accumulated the ER tubules to the cell equator during nuclear division as efficiently as wild-type cells (Fig. 3.2.8C). Time-lapse imaging of *cdc15-140* cells co-expressing Tts1-GFP and Rlc1-mCherry confirmed that the medial accumulation of the tubular ER occurred in cells in which the

actomyosin rings disassembled due to impairment of Cdc15 function (Fig. 3.2.8D).

The tubular ER enrichment at the division site depends on the anilin-like protein Mid1 (Zhang et al., 2010 and Fig. 3.2.8E) and I was interested if mitotic tER polarization might have the same requirement. I introduced the Sec24-GFP into *mid1* Δ cells that misposition the actomyosin ring that I visualized using the Rlc1-mCherry fluorescent protein. Interestingly, I found that Sec24-GFP was efficiently recruited to the proximity of the actomyosin ring even when the rings were severely displaced from the cell equator (Fig. 3.2.8F).

Finally I analyzed the distribution of the Sec24-GFP signal in dividing cells that lack the ER tubulating proteins Tts1, Yop1 and Rtn1. The ER of *tts1* Δ *rtn1* Δ *yop1* Δ cells has a largely sheet-like morphology (Shibata et al., 2010; Zhang et al., 2010) and these cells misposition the actomyosin ring (Zhang et al., 2010). However, the tER labeled by Sec24-GFP and Golgi cisternae labeled by Vrg4-GFP both efficiently polarized towards the mispositioned septation site in *tts1* Δ *rtn1* Δ *yop1* Δ cells (Fig. 3.2.8G-I)

I concluded that the equatorial recruitment of the ER tubules and the tER are distinctly regulated processes that both require an intact actomyosin ring. Whereas the medial accumulation of the ER tubules depends on Mid1, the tER polarization requires Cdc15 function.

Figure 3.2.8. The dynamics of the tubular ER and the tER are distinct differentially regulated processes

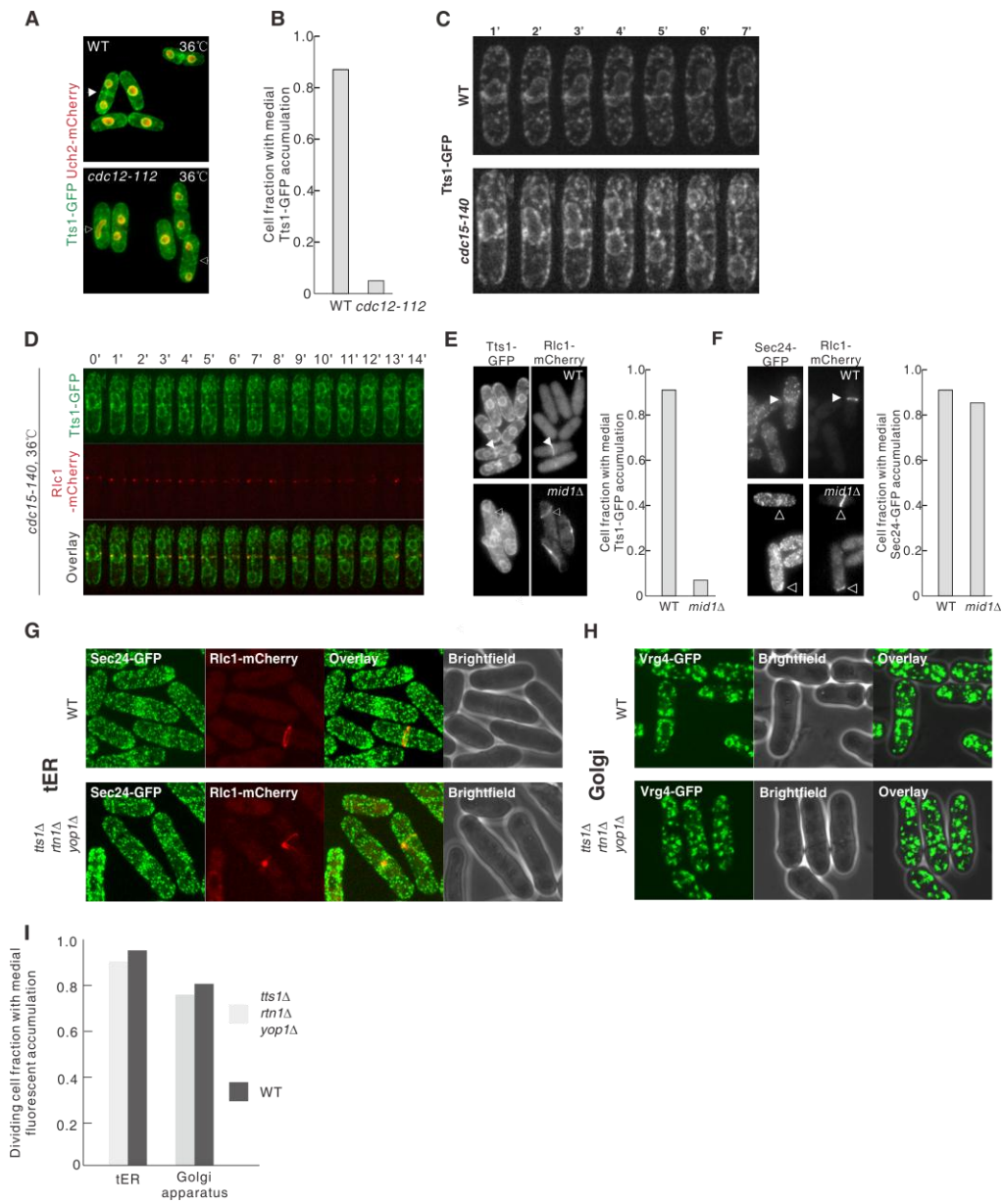


Figure Legend 3.2.8. The dynamics of the tubular ER and the tER are distinct differentially regulated processes

(A) Wild-type (top) and *cdc12-112* (bottom) mutant cells expressing Tts1-GFP and Uch2-mCherry were grown overnight at 24°C and shifted to 36°C for 1 hour prior to imaging. Shown is the maximum projection image of the z-stack obtained by epifluorescence microscopy. Solid arrows indicate accumulation of Tts1-GFP to the division site and outlined arrows indicate division sites lacking tubular ER accumulation.

(B) Quantitation of Tts1-GFP medial accumulation during division in wild-type and *cdc12-112* cells (n=250 cells per sample).

(C) Wild-type (top) and *cdc15-140* (bottom) mutant cells expressing Tts1-GFP were grown overnight at 24°C and shifted to 36°C for 1 hour prior to imaging. Shown is the maximum projection image of the z-stack obtained by time-lapse spinning disk confocal imaging.

(D) *cdc15-140* (bottom) mutant cells expressing Tts1-GFP (green) and Rlc1-mCherry (red) were grown overnight at 24°C and shifted to 36°C for 1 hour prior to imaging. Shown is the maximum projection image of the z-stack obtained by time-lapse spinning disk confocal imaging.

(E) Localization of Tts1-GFP in wild-type (top) and *mid1Δ* (bottom) cells during mitosis, as indicated by Rlc1-mCherry. The graph quantifies the medial accumulation of Tts1-GFP in binucleate cells, n = 100. The arrows indicate Tts1 GFP accumulation at the division site in WT and its absence in *mid1Δ* cells.

(F) Localization of Sec24-GFP in wild-type (top) and *mid1Δ* (bottom) cells during mitosis, as indicated by Rlc1-mCherry. The graph quantifies the medial accumulation of Sec24-GFP in binucleate cells, n = 100. The arrows indicate Sec24-GFP accumulation at the division site in both WT and *mid1Δ* cells.

(G) Scanning confocal micrographs of wild-type (top panel) and *tts1Δrtn1Δyop1Δ* (*tryΔ*, bottom) cells co-expressing the tER marker Sec24-GFP (green) at various stages of the cell cycle as indicated by Rlc1-mCherry (red) and brightfield images.

(H) Scanning confocal micrographs of wild-type (top panel) and *tts1Δrtn1Δyop1Δ* (*tryΔ*, bottom) cells expressing the Golgi marker Vrg4-GFP (green) and brightfield images.

(I) Quantitation of Sec24-GFP and Vrg4-GFP polarization in wild-type and *tts1Δrtn1Δyop1Δ* cells (n=250 cells per sample).

3.2.9. Polarization of the tER to the division site does not depend on net centripetal movement of pre-existing COPII positive membranes using type-V myosins.

Cdc15 could be involved in targeting the preexisting COPII-positive membranes to the division site. Alternatively, Cdc15 might directly promote tER biogenesis in the vicinity of the actomyosin ring. I assessed whether the COPII structures in dividing cells exhibited the net centripetal movement towards the actomyosin ring by dual color image analyses of Sec24-GFP and Rlc1-mCherry (Fig. 3.2.9A). Measurements of integrated fluorescence intensities of Sec24-GFP in areas representing both cell tips and cell middle throughout cell division showed that COPII positive structures accumulated at the division site concurrently with actomyosin ring formation (Fig. 3.2.9B, red line). At the same time, the fluorescence intensity of Sec24-GFP remained unchanged at cell tips (Fig. 3.2.9B, green and blue lines; see also Fig. 3.2.9C, n=5 cells). Importantly, Sec24-GFP accumulated at the division site in cells lacking both type-V myosins, Myo51 and Myo52, suggesting that actin cable-directed transport was not required for tER polarization (Fig. 12D, 70% cells exhibited medial accumulation of tER compartments, n = 150 cells). Taken together, my data indicated that Cdc15 could promote tER biogenesis at the division site.

Figure 3.2.9. Polarization of the tER to the division site does not depend on net centripetal movement of pre-existing COPII positive membranes using type-V myosins.

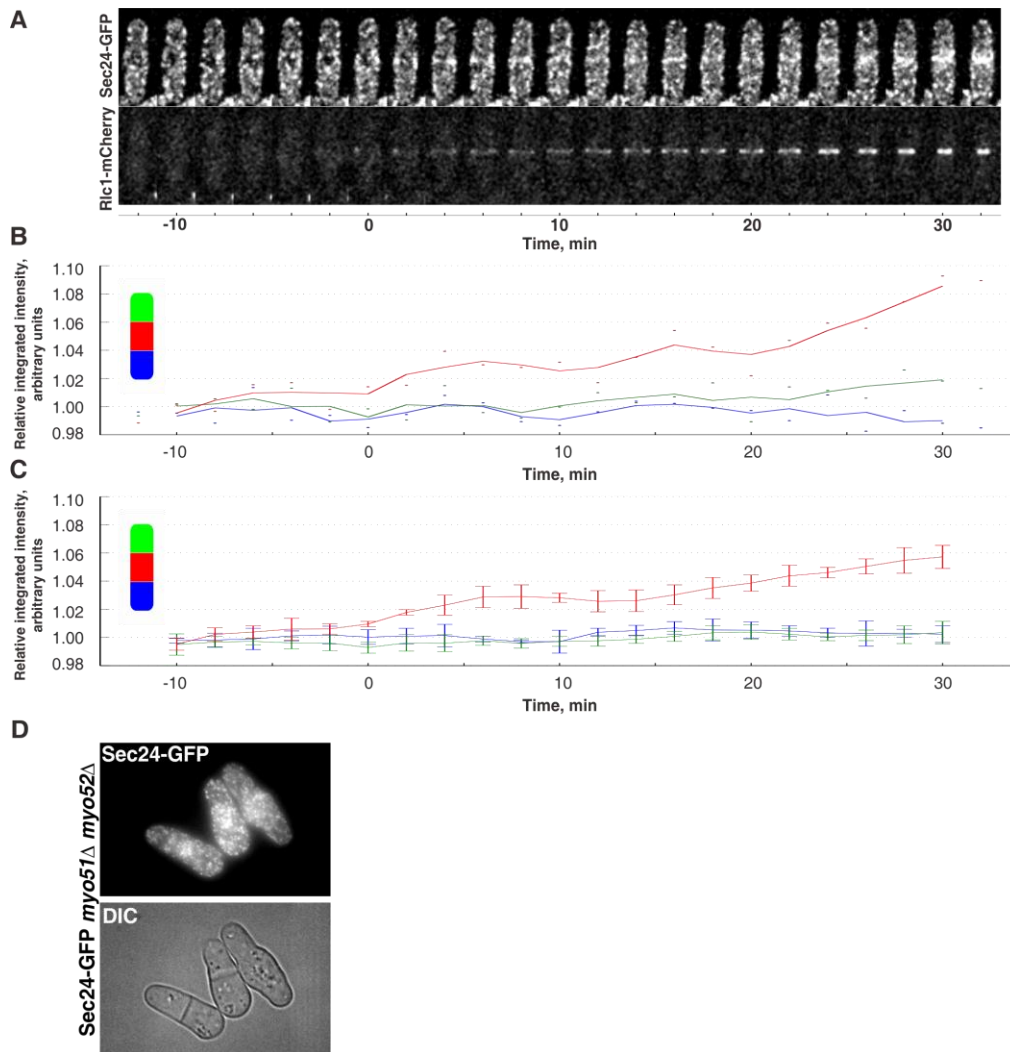


Figure Legend 3.2.9. Polarization of the tER to the division site does not depend on net centripetal movement of pre-existing COPII positive membranes using type-V myosins.

(A) Shown is the maximum projection image of the z-stacks obtained by time-lapse spinning disk confocal imaging of cells expressing Sec24-GFP (top row) and Rlc1-mCherry (bottom row) grown at 24°C.

(B) Quantitation of the relative integrated fluorescence intensities of Sec24-GFP in tips (green, blue) and the center (red) of the cell presented in (A). Dots indicate the measured values at distinct time points and the graph lines represent the moving average values (for details see Material and Methods).

(C) Quantitation of the relative integrated fluorescence intensities of Sec24-GFP in tips (green, blue) and the center (red) of the five cell. y-axis is scaled relative to average intensity at cell tips. The graph lines represent the moving average values and error bars correspond to the standard error (for details see Material and Methods).

(D) *myo51Δmyo52Δ* cells expressing Sec24-GFP were grown overnight at 24°C and imaged in DIC (bottom, single plane image) and by epifluorescence (top, maximum projection image of the z-stack) microscopy.

3.2.10. Type-V myosin along actin cables recruits ER to the cell tips in interphase *S. pombe* cells.

In collaboration with Zhang Dan, I investigated the ER dynamics during interphase. Upon time-lapse imaging of cells expressing the general ER marker GFP-AHDL, I observed dynamic remodeling of the ER at the growing cell tips of interphase cells (Fig. 3.2.10A). The ER underwent repeated attachment and detachment from the cell tips but appeared stably associated to the lateral cell cortex. In cells co-expressing GFP-AHDL and the artificial actin marker LifeAct-mCherry (Huang et al., 2012), I was able to observe rapid “stretching” of ER elements along an actin cable towards cell tips. The velocity of ER movement ($0.40 \pm 0.11 \mu\text{m/s}$, $n=15$ events) roughly corresponded to the speed of type-V myosin based ER delivery to the growing buds in *S. cerevisiae* (Estrada et al., 2003; Grallert et al., 2007).

I next explored the ER organization in interphase cells lacking actin cables due to deletion of the formin For3 (Feierbach and Chang, 2001). I simultaneously monitored the actin structures associated with the growing cell tips by visualizing LifeAct-mCherry. Whereas GFP-AHDL was observed forming a laced network of elements at the growing tips of wild-type cells (Fig. 3.2.10B, left panels, $n=100$), 58% of interphase *for3* Δ cells lacked ER at the growing cell tips (Fig. 3.2.10B, middle panels, $n=100$). Likewise, 58% of *myo51* Δ *myo52* Δ cells failed to recruit the ER to the growing cell tips. The ER remained stably attached to the lateral cell cortex in both *for3* Δ and *myo51* Δ *myo52* Δ cells. Taken together these data suggest that type-V myosin transport along actin cables functions to recruit the ER to the growing cell tips in *S. pombe*.

Figure 3.2.10. Type-V myosin along actin cables recruits ER to the cell tips in interphase *S. pombe* cells.

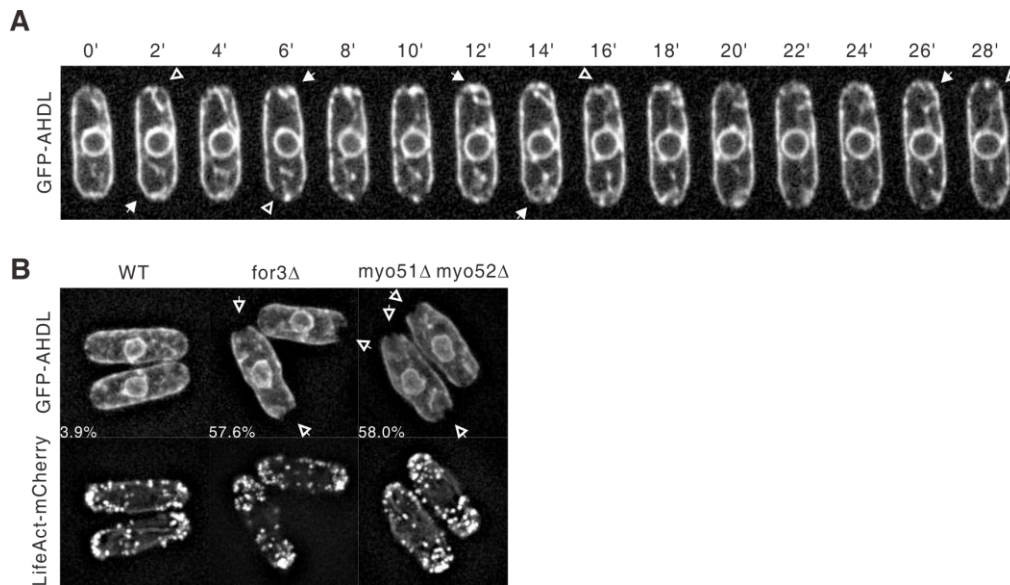


Figure Legend 3.2.10. Type-V myosin along actin cables recruits ER to the cell tips in interphase *S. pombe* cells.

(A) Shown is the single z-section image obtained by time-lapse spinning disk confocal imaging of cells expressing GFP-AHDL. The time is indicated in minutes. Arrows point to dynamic remodeling of the ER at the cell tips. Full arrows point to the events of ER recruitment to the cell tip and arrowheads point to events of ER detachment from the cell tips.

(B) Shown are the deconvolved maximum z-section images obtained by epifluorescence imaging of cells co-expressing GFP-AHDL (top row) and LifeAct-mCherry (bottom row) in the indicated genetic background. Arrows point to tips of *for3Δ* and *myo51Δ myo52Δ* cells lacking the underlying cortical ER.

Movie Legend 3.2.10. Type-V myosin along actin cables recruits ER to the cell tips in interphase *S. pombe* cells.

Shown is the single z-section image obtained by time-lapse spinning disk confocal imaging of cells co-expressing GFP-AHDL and Lifeact-mCherry. Arrows point to the rapid ER tubule stretching along actin cables towards cell tips.

3.3. Remodeling of Cell Polarity Under Heat-stress in Fission Yeast Cells

Fission yeast efficiently maintain rod-shaped morphology when grown at different temperatures but their cell polarity is transiently impaired upon heat-stress (Mitchison and Nurse, 1985; Petersen and Hagan, 2005). In the following sections I analyze dynamics of key regulators of cell polarity in *S. pombe* cells during mild heat-stress and when cells are adapted to ambient temperature.

3.3.1. Heat-stress induces transient loss of polarized growth succeeded by monopolar growth pattern in cells adapting to elevated temperature.

As previously mentioned, the tER was enriched at both cell tips in cells during late G₂ stage of the cell cycle (Fig. 3.1.3.1A, left panel and Fig. 3.3.1.1A, left panel). I observed that when wild-type cells expressing Sec24-GFP were shifted from 24°C to 36°C for 45 minutes the tip accumulation of the tER was absent from interphase cells (Fig. 3.3.1.1A, middle panel). Interestingly, the tER exhibit enrichment to only one cell tip in interphase cells shifted from 24°C to 36°C for 45 minutes (Fig. 3.3.1.1A, right panel). Given that tER accumulation appears to spatially correlate to the sites of active cell wall remodeling, the cell tips and site of septation, I decided to investigate further the effects of temperature transition on growth of fission yeast cells.

Lectins bind polysaccharides of the yeast cell wall with high affinity but without impairing cell growth (Hayes and Goldstein, 1974). Thus, sites of cell wall deposition subsequent to fluorophore coupled lectin staining are readily visualized as a dip in fluorescence intensity (May and Mitchison, 1986). To monitor cell growth upon heat-stress I stained log-phase wild-type cells growing at 24°C with FITC-Lectin, washed-out the excess dye and

immediately shifted cells to 36°C or allowed them to grow at 24°C (Fig. 3.3.1.1B). Samples were collected every 30min, fixed and subjected to fluorescence microscopy. Cells continuously growing at 24°C were observed to elongate 2.51 ± 0.77 μm an hour after the dye washout. Conversely, cells shifted to 36°C for one hour fully arrested longitudinal growth (Fig. 3.3.1.1B and B, $n > 60$ cells per sample, $p^{\text{Welch's t-test}} = 4.10 \cdot 10^{-17}$). Interestingly the diameter of heat-stressed cells increased (Fig. 3.3.1.1B and D, width increased by $9 \pm 7\%$, $n > 60$ cells per sample, $p^{\text{Welch's t-test}} = 7.45 \cdot 10^{-15}$) and the FITC-Lectin staining of the cell slightly decreased (data not shown) suggesting that the cell wall underwent remodeling throughout the cell periphery rather than at the cell tips.

Cells resumed polarized growth 90min after the temperature increase and subsequently elongated at a rate $\sim 28\%$ greater than cells grown at 24°C (Fig. 3.3.1.1C and data not shown). Among unstressed population of cells longer than $9 \mu\text{m}$ (likely, the late G_2 phase cells) only 18% were monopolar (Fig. 3.3.1.1B and E). However, the majority of heat-stressed cells elongated only at one cell tip. Two-and-a-half hours after the shift from 24°C to 36°C it became evident that 75% of heat-stressed late G_2 cells grew in a monopolar fashion (Fig. 3.3.1.1B and E). When propagated overnight at 36°C, 83% of wild-type cells were bipolar (Fig. 3.3.1.2A). I concluded that in fission yeast heat-stress leads to a temporary arrest of longitudinal growth followed by an adaptation response in which cells re-establishing polarity undergo a period of monopolar growth.

To explore effects the heat-stress might have on key regulators of cell growth and polarity, I employed a set of fission yeast strains expressing

distinct marker proteins fused to a fluorophore at their native genomic loci. Localization of the fluorophore tagged marker proteins was analyzed in cells grown at 24°C, and in cells shifted to 36°C for 45 min and 105 min.

Subcellular distribution of polarity markers Tea1-YFP, Tea4-GFP and Pom1-GFP was not affected by the temperature change as these markers exhibited bipolar localization in ~95% of late G₂ phase cells at both 24°C and 36°C within the observed timeframe (Fig. 3.3.1.1F and Fig. 3.3.1.2B and C, respectively). In contrast, β -glucan synthase GFP-Cps1, which localized to both cell tips in late G₂ cells at 24°C, could be observed throughout the cell cortex 45 min after cells were shifted to 36°C (Fig. 3.3.1.1G). At this point the GFP-Cps1 cortical signal also had decreased intensity. Incubating cells at 36°C for 105 min allowed all cells to repolarize GFP-Cps1 to the cell tips albeit in a monopolar fashion (Fig. 3.3.1.1G, 60% of heat-stressed late G₂ cells localized GFP-Cps1 predominantly to one cell tip as compared to 35% in unstressed cells).

Secretion of cell wall enzymes is specified by both localizing the exocyst and by orienting actin-based long-range transport of secretory vesicles (Bendezú and Martin, 2011). An exocyst component Sec6-GFP localized to both cell tips in 79% of late G₂ phase cells grown at 24°C but was observed throughout the cell cortex in cells shifted to 36°C for 45 min (Fig. 3.3.1.2D). Cells growing at 36°C for 105 min did repolarize Sec6-GFP but 47% of late G₂ phase cells confined it to only one cell tip (Fig. 3.3.1.2D). Thus exocyst mediated vesicle secretion is also responsive to heat-stress and exhibits dynamics in line with the observed behavior of cell wall enzymes.

As in budding yeast (Delley and Hall, 1999), polarization of LifeAct-GFP marked actin structures in cells grown at 24°C was completely abolished in cells shifted to 36°C for 45 min (Fig. 3.3.1.2E). Cells were able to re-polarize actin cytoskeleton after 105 min at 36°C but most of late G₂ phase cells had F-actin structures unequally distributed between the two tips (Fig. 3.3.1.2D). Similarly, fluorophore tagged formin For3 and a type-V myosin Myo52 both lost tip localization and were readily seen spreading towards the cell equator upon heat-stress (Fig. 3.3.1.1H and Fig. 3.3.1.2G). In cells grown at 36°C for 105 min polarity of the For3-GFP and Myo52-GFP was re-established, albeit in a monopolar fashion (11% and 17% of unstressed G₂ phase cells localized For3-GFP and Myo52-GFP to one cell tip as compared to 43% and 52% of late G₂ phase cells shifted from 24°C to 36°C for 105 min). I concluded that heat-stress leads to transient loss of polarized F-actin distribution that is restored in a monopolar manner as cells adapt to elevated temperature.

Both F-actin distribution and exocyst localization are governed by the activity of a Rho-family GTPase Cdc42 (Bendezú and Martin, 2011). Given that fluorescent protein tagging impairs Cdc42 function, I decided to monitor the active Cdc42 *in vivo* during heat-stress by observing GFP tagged CRIB domain reported to bind the active Cdc42 (Tatebe et al., 2008). CRIB-GFP localized to narrow zones at both cell tips in 98% of late G₂ phase cells grown at 24°C but was found throughout the cell cortex 45min after the cell culture was shifted to 36°C (Fig. 3.3.1.1I). Cells grown at 36°C for 105min re-polarized Cdc42 activity but with 37% of late G₂ phase cells exhibited a

strictly monopolar CRIB-GFP distribution. Heat stress did not affect the localization of CRIB-GFP to the division site in mitotic cells (data not show).

Taken together my results suggest that processes confining the growth machinery to the polarisome demarcated cell tips are perturbed by temperature increase. Taking into account the instructive role of Cdc42 in positioning the actin cytoskeleton and the exocyst (Bendezú and Martin, 2011) I speculated that upon heat-stress the active Cdc42 relocates throughout the lateral cell cortex and recruits the downstream growth machinery thus allowing for the entire cell wall remodeling. As cells adapt to elevated temperature Cdc42 activity is frequently restricted to only one cell tip of late G₂ phase cells resulting in a monopolar growth pattern.

Figure Legend 3.3.1.1. Heat-stress induces transient longitudinal growth arrest succeeded by monopolar growth.

(A) Shown are maximum projections of seven z-sections of Sec24-GFP expressing cells grown at 24°C (left panel) or shifted to 36°C for 45 minutes (middle panel) or 105 minutes (right panel).

(B) Shown are single z-plane epifluorescence micrographs of FITC-Lectin stained cells grown at indicated temperatures and imaged immediately (left panel), 60 min (middle panels) and 150 min upon dye washout (right panels).

(C) Quantification of longitudinal cell growth of cells represented in (C). Circles represent individual cells grown at 24°C (gray) or shifted to 36°C (blue) for indicated time points. n>25 per sample per time point, p-values were derived by Welch's test.

(D) Percentage of monopolar late G₂ phase cells in a cell suspensions treated as described in (C), n>250 per sample.

(E-I) Shown are whole cell maximum intensity z-projections of scanning confocal micrographs of log-phase wild-type cells expressing indicated fluorophore tagged marker proteins grown at 24°C (left panels) or shifted to 36°C for 45min (middle panels) or 105min (right panels). The arrows point out localization of the marker proteins to lateral cell cortex. Image contrast is reported using corresponding gray wedges. All scale bars refer to 5 µm.

Figure 3.3.1.1. Heat-stress induces transient longitudinal growth arrest succeeded by monopolar growth.

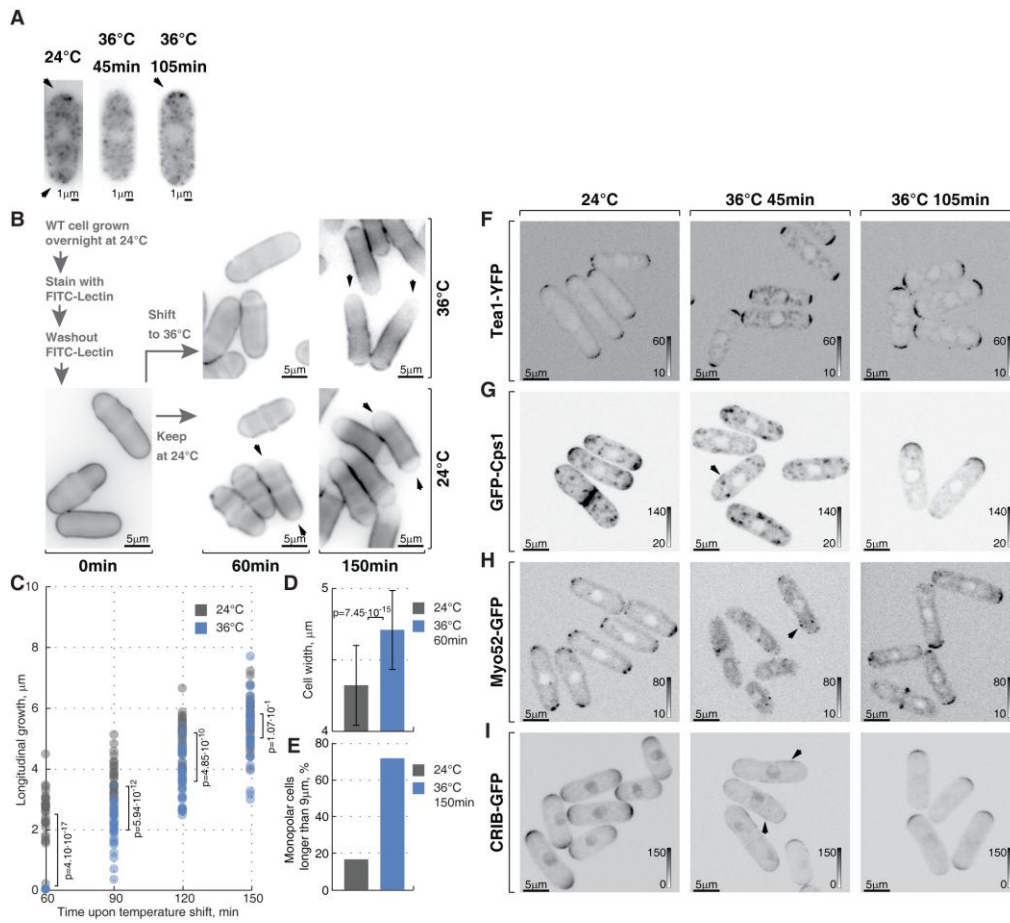


Figure 3.3.1.2. Heat-stress leads to a transient loss of cell polarity succeeded by monopolar growth.

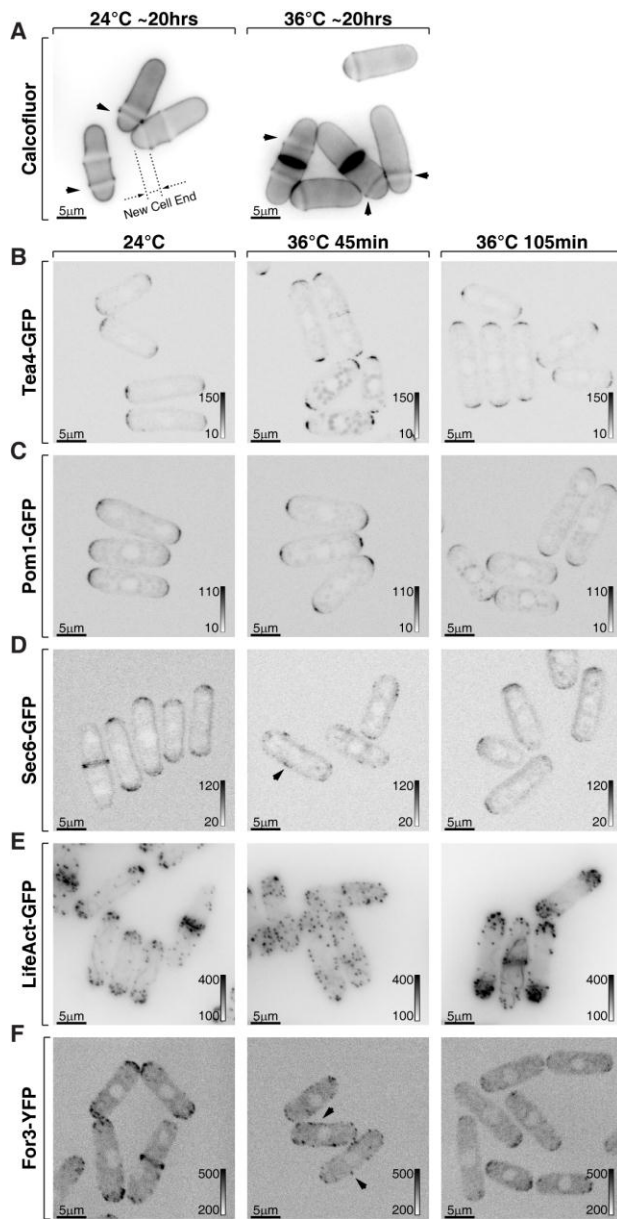


Figure Legend 3.3.1.2. Heat-stress leads to a transient loss of cell polarity succeeded by monopolar growth.

(A-F) Shown are whole cell maximum intensity *z*-projections of confocal micrographs of log-phase wild-type cells expressing indicated fluorophore tagged marker proteins grown at 24°C (left panels) or shifted to 36°C for 45min (middle panels) or 105min (right panels). The arrows point out localization of the marker proteins to lateral cell cortex. Image contrast is reported using corresponding gray wedges. All scale bars refer to 5 μ m.

3.3.2. Cortical association of Cdc42 GEFs and GAP is modulated by temperature

As monitored by CRIB-GFP, late G₂ phase cells grown at 24°C focus the Cdc42 activity to the cell tips with moderate oscillations in its levels (Das et al., 2012 and Fig. 3.3.2.1A, top panel). In contrast, minutes after cells were shifted from 24°C to 36°C CRIB-GFP was seen spreading from the cell tips towards the cell equator establishing zones of Cdc42-activity at the cell sides (Fig. 3.3.2.1A, bottom panel). Since activity of Cdc42 is primarily regulated by its GEFs and GAPs I analyzed their spatial dynamics.

Both Cdc42-GEFs are restricted to the cell tips in unstressed cells with Gef1-3YFP and Scd1-GFP observed at both cell tips in late G₂ cells (Fig. 3.3.2.1B and C, 86% and 73% of cells longer than 9µm respectively). 45 min upon temperature shift from 24°C to 36°C, Scd1-GFP was no longer detectable at the cell cortex whereas the Gef1-3YFP localized to patches distributed throughout the cell cortex (Fig. 3.3.2.1B and C). I also noticed that upon heat-stress both Scd1-GFP and Gef1-3YFP localized to intracellular structures (Fig. 3.3.2.1B and C). After 105 min at 36°C both GEFs became confined to cell tips but majority of late G₂ cells displayed a monopolar Scd1-GFP and Gef1-3YFP signal (68% and 67% of cells longer than 9µm respectively, Fig. 3.3.2.1B and C). I also noticed that Scd1-GFP and Gef1-3YFP signal was severely diminished at the cortex of cells repolarizing growth at elevated temperature (Fig. 3.3.2.1B and C). The average intensity of Scd1-GFP at a single cell tip decreased by 49±23% ($p^{\text{Welch's t-test}} = 1.43 \cdot 10^{-7}$, $n > 25$ cells per sample) whereas Gef1-3YFP signal dipped by 65±17% ($p^{\text{Welch's t-test}} = 7.34 \cdot 10^{-12}$, $n > 25$ cells per sample).

The sole identified fission yeast Cdc42-GAP Rga4 localizes to the lateral cell cortex and to the new cell end in pre-NETO cells (Das et al., 2007; Tatebe et al., 2008). Upon heat-stress the Rga4-GFP localization remained restricted to the lateral cell cortex of ~90% of late G₂ cells throughout the course of the experiment (Fig. 3.3.2.1D). A 34±22% ($p^{\text{Welch's t-test}} = 7.35 \cdot 10^{-8}$, $n > 25$ cells per sample) decrease in cortically associated levels was also observed for the Rga4-GFP 105min upon shifting cells from 24°C to 36°C (Fig. 3.3.2.1D).

The diminished cortical levels of Cdc42 regulators in cells exposed to elevated temperature were not a consequence of gross decrease in total amount of these proteins. (Fig. 3.3.2.2A-C). Thus recruitment of the Cdc42 regulators in cells adapting to elevated temperature appears to involve a more complex regulation, possibly involving protein targeting and/or post-translational modifications.

To explore the effects decreased activity Cdc42 regulators might have on cell polarity I employed the recently developed model correlating the cell length and the bipolar Cdc42 activation (Das et al., 2012, Fig. 3.3.2.2D-G). Mathematical simulations predict that cells with decreased positive feedback, proposed to function through Cdc42-GEFs (Kozubowski et al., 2008; Das et al., 2012), would require increased cell length to sustain bipolar activity of Cdc42 (Fig. 3.3.2.2E). Conversely, the decrease of negative feedback promotes bipolar growth (Fig. 3.3.2.2F). Finally, the model predicts that a decrease of the positive relative to the negative Cdc42 feedback would result in an increased proportion of monopolar cells population of fission yeast cells (Fig. 3.3.2.2G).

Since heat-stressed fission yeast cells eventually resume bipolar growth (Fig. 3.3.1.2A) I went on to analyze cortical levels of active Cdc42, Cdc42-GAP and GEFs in cells growing overnight at 36°C. The cortical CRIB-GFP, Gef1-3YFP and Scd1-GFP did assume bipolar localization in late G₂ cells growing overnight at 36°C and the cortical recruitment of CRIB-GFP was comparable to that of cells growing at 24°C (data not shown). To my surprise, the Gef1-3YFP and Scd1-GFP average signal intensity per cell tip remained relatively low, as did Rga4-GFP levels at the lateral cortex (data not shown). In fact, the cortical levels of the three Cdc42 regulators proteins inversely correlated to the growth temperature even though tip recruitment of CRIB was not affected (Fig. 3.3.2.2H-L). Western blotting analysis of the SDS-PAGE resolved cell lysates prepared from cells grown to log-phase at 18°C, 24°C, 30°C and 36°C indicated a similar trend in total protein levels of Scd1-GFP, Gef1-3YFP and Rga4-GFP (Fig. 3.3.2.2M-O). Thus it appears that cells adapt levels of Cdc42 regulators according to temperature but maintain comparable levels of active Cdc42 at the cell cortex.

Taken together these results suggest that activation of the Cdc42 by Gef1 could occur throughout the cell cortex upon temperature increase. The monopolar growth of recovering heat-stressed cells may be a function of altered Cdc42 feedback mechanisms reflected in the cortical recruitment of the Cdc42-GEFs Scd1 and Gef1. It appears that cells adjust the levels of Cdc42 regulators in accordance to the environmental temperature. Interestingly, the mechanisms regulating cortical recruitment of Cdc42 GEFs and GAPs are likely different in cells recovering from heat-stress and cells fully adapted to different environmental temperatures.

Figure 3.3.2.1. Heat-stress leads to a transient loss of cell polarity succeeded by monopolar growth.

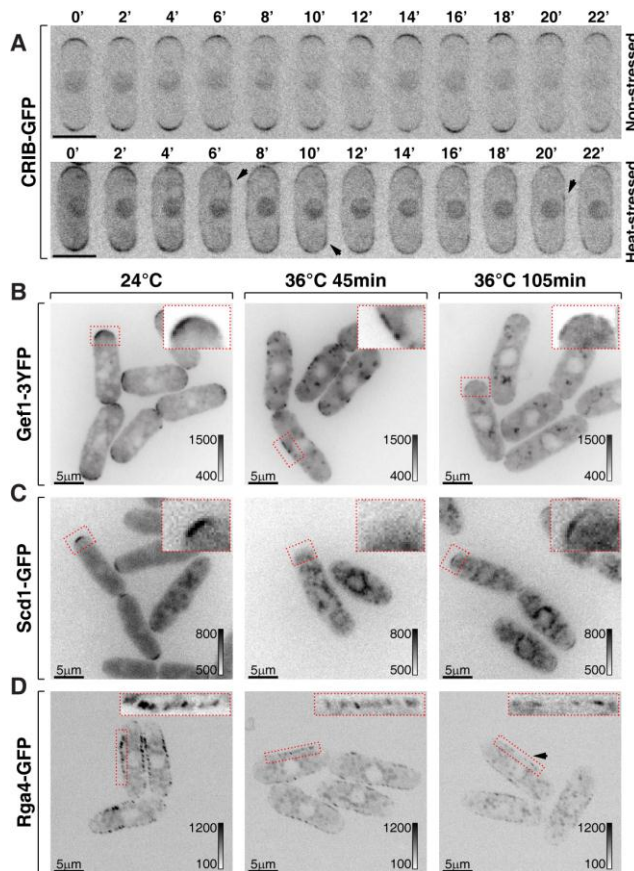


Figure Legend 3.3.2.1. Heat-stress leads to a transient loss of cell polarity succeeded by monopolar growth.

(A) Single *z*-plane spinning disk confocal microscopy time-lapse images of CRIB-GFP expressing wild-type cells grown at room temperature (top panel) or shifted to 36°C at the start of imaging (bottom panel). The arrows point to relatively stable sites of laterally localized CRIB-GFP.

(B-D) Shown are single *z*-plane micrographs of log-phase wild-type cells expressing indicated fluorophore tagged marker proteins grown at 24°C (left panels) or shifted to 36°C for 45min (middle panels) or 105min (right panels). The insets represent zoomed in and re-contrasted main image segments outlined in red. Gray wedges report the main image contrasting. All scale bars refer to 5 μm.

Figure 3.3.2.2. Recruitment of the Cdc42 regulators to the cell cortex is regulated by temperature.

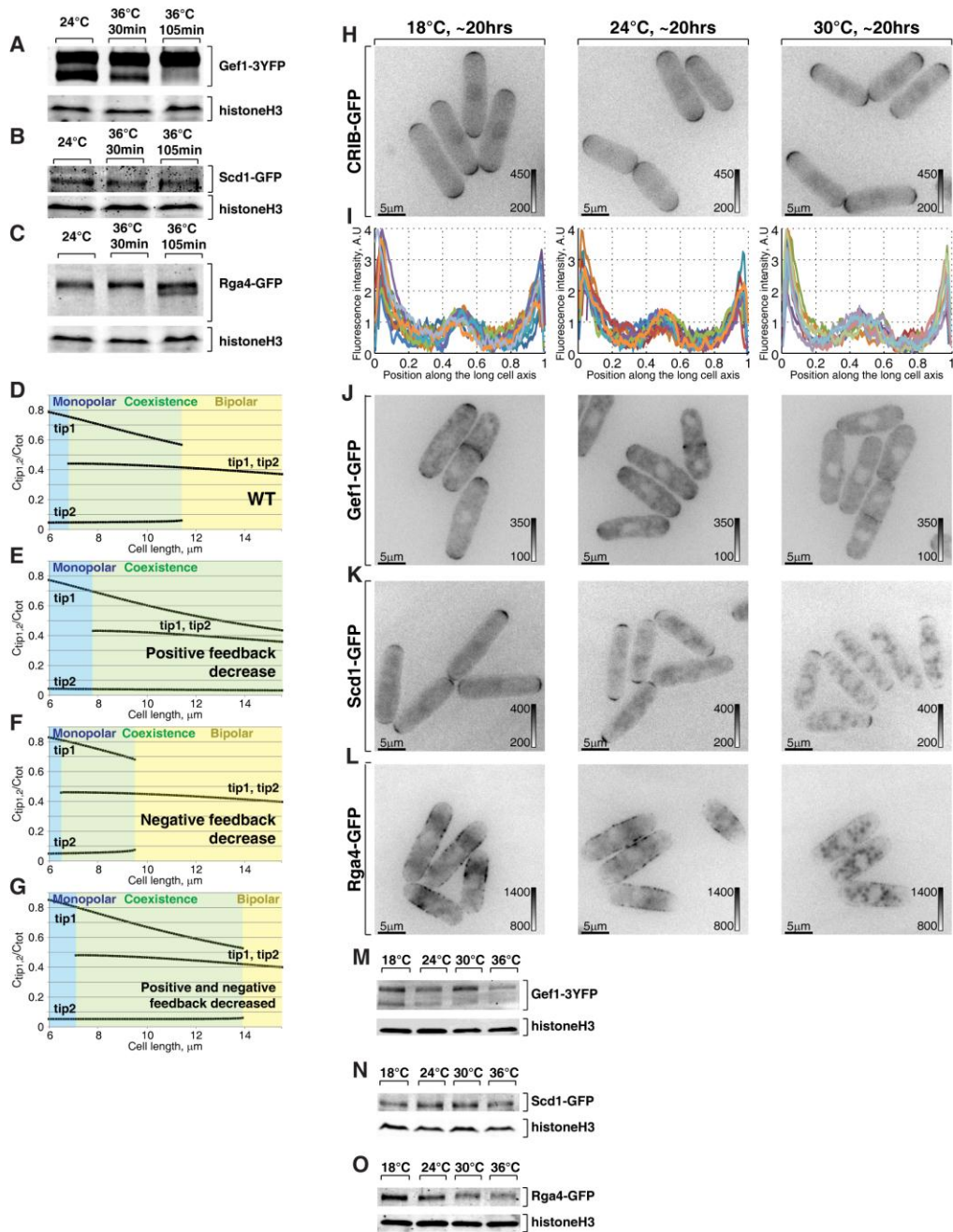


Figure Legend 3.3.2.2. Recruitment of the Cdc42 regulators to the cell cortex is regulated by temperature.

(A) Wild-type cells expressing Gef1-3YFP were grown to log-phase at 24°C prior to total protein extraction. SDS-PAGE resolved protein samples were subjected to western blotting using *anti-GFP* antibodies (top panels). HistoneH3 probing (bottom panels) served as a sample loading control.

(B) Wild-type cells expressing Scd1-GFP were treated as in (A)

(C) Wild-type cells expressing Rga4-GFP were treated as in (A)

(D-G) The dependency of bipolar growth onset on cell length under indicated values for positive and negative Cdc42-feedback. Please refer to (Das et al., 2012) for details.

(H-I) Cells expressing indicated fluorophore tagged proteins grown overnight at 18°C (left panels), 24°C (middle panels) or 30°C (right panels). All images shown are epifluorescence micrographs of log-phase cells with image contrast reported using corresponding gray wedges. All scale bars refer to 5 µm.

(J-L) Wild-type cells expressing Gef1-3YFP (left panels), Scd1-GFP (middle panels) or Rga4-GFP (right panels) were grown overnight to log-phase (O.D.⁵⁹⁵ ≈ 0.4) at indicated temperatures prior to total protein extraction. SDS-PAGE resolved protein samples were subjected to western blotting using *anti-GFP* antibodies (top panels). HistoneH3 probing (bottom panels) served as a sample loading control.

(M) Wild-type cells expressing Gef1-3YFP were grown overnight to log-phase at indicated temperatures prior to total protein extraction. SDS-PAGE resolved protein samples were subjected to western blotting using *anti-GFP* antibodies (top panels). HistoneH3 probing (bottom panels) served as a sample loading control.

(N) Wild-type cells expressing Scd1-GFP were treated as in (M)

(O) Wild-type cells expressing Rga4-GFP were treated as in (M)

3.3.3. Cdc42 activation at the lateral cell cortex upon heat-stress is mediated by Cdc42-GEFs and counteracted by the Cdc42-GAP

To better understand the involvement of GEFs and GAPs in Cdc42 dynamics during heat-stress, I investigated whether Scd1, Gef1 and Rga4 could play a role in localizing the active Cdc42 to the lateral cell cortex observed within the first hour upon temperature shift from 24°C to 36°C (Fig. 3.3.2.1A and Fig. 3.3.3A). As monitored by CRIB-GFP, cells lacking Gef1 effectively polarize Cdc42 activity but frequently at only one cell tip (Coll et al., 2003). Strikingly, when shifted from 24°C to 36°C for 30 min *gef1*Δ cells fully lost CRIB-GFP signal at the cell cortex (Fig. 3.3.3B). Similarly, 30 minutes upon temperature shift 18% of *scd1*Δ cells lost cortical CRIB-GFP signal whereas the remaining cells localized the CRIB-GFP throughout the cell cortex albeit with a signal intensity decreased as compared to that of WT cells under the same conditions (Fig. 3.3.3C). These results are in line with my imaging analysis of Gef1 and Scd1 localization upon heat-stress (Fig. 3.3.2.1B and C, middle panels) and suggest that Cdc42 activity at the lateral cortex could be promoted by GEF mediated activation with the relative contribution of Gef1 exceeding that of Scd1. Cells lacking a Cdc42-GEF were observed recruiting CRIB-GFP to the cell tips approximately 90 minutes after temperature shift (data not shown).

Cells lacking Rga4 have an increased cell diameter and localize CRIB-GFP to a relatively wide crescent at the cell tips (Das et al., 2007, Fig. 3.3.3D). Interestingly, not only did the transition from 24°C to only 36°C lead to a strong CRIB-GFP localization throughout the lateral cell cortex in *rga4*Δ cells, but so did the shift to 30°C which did not affect CRIB-GFP localization

in other strains explored (Fig. 3D, 79% of *rga4* Δ cells localized CRIB-GFP to the lateral cell cortex, n>250). These data imply that Rga4 functions in counteracting the localization of active Cdc42 both during steady-state and upon heat-stress.

Next, I was interested whether localization of the active Cdc42 to the lateral cell cortex during heat-stress is a consequence of its activation, promoted by Gef1, or lack of its negative regulation by Rga4. To that aim I monitored the CRIB-GFP localization in *gef1* Δ *rga4* Δ cells upon temperature shift. Although frequently monopolar, unperturbed *gef1* Δ *rga4* Δ cells efficiently polarized Cdc42 activity to cell tips (Fig. 3.3.3E, left panel). Temperature shift to 36°C led to a complete depletion of the CRIB-GFP signal from the cell cortex within 30min and a temperature increase of 6°C had no observable effect on its localization (Fig. 3.3.3E, middle and right panels).

I wondered if upregulation of Rga4 could prevent the Cdc42 activation at the cell sides. To this end, I placed *rga4-mCherry* construct under repressible *nmt41* promoter and monitored the localization of CRIB-GFP during temperature transition in otherwise wild-type cells. Presence of thiamine in the growth medium fully suppressed expression of Rga4-mCherry and cells effectively localized CRIB-GFP to the cell tips at 24°C and redistributed it throughout the cell upon shift-up to 36°C for 30 min (Fig. 3.3.3F, left panels). In line with earlier reports (Das et al., 2007; Tatebe et al., 2008), upon upregulation of the Rga4-mCherry expression cells became slightly thinner and the CRIB-GFP localized to a narrow crescent at the tips of unstressed cells. Rga4-mCherry overexpressing cells efficiently maintained

CRIB-GFP signal at the cell tips when shifted to 36°C for 30 minutes (Fig. 3.3.3F, right panels, 82% of the cells localized CRIB-GFP to cell tips n>250).

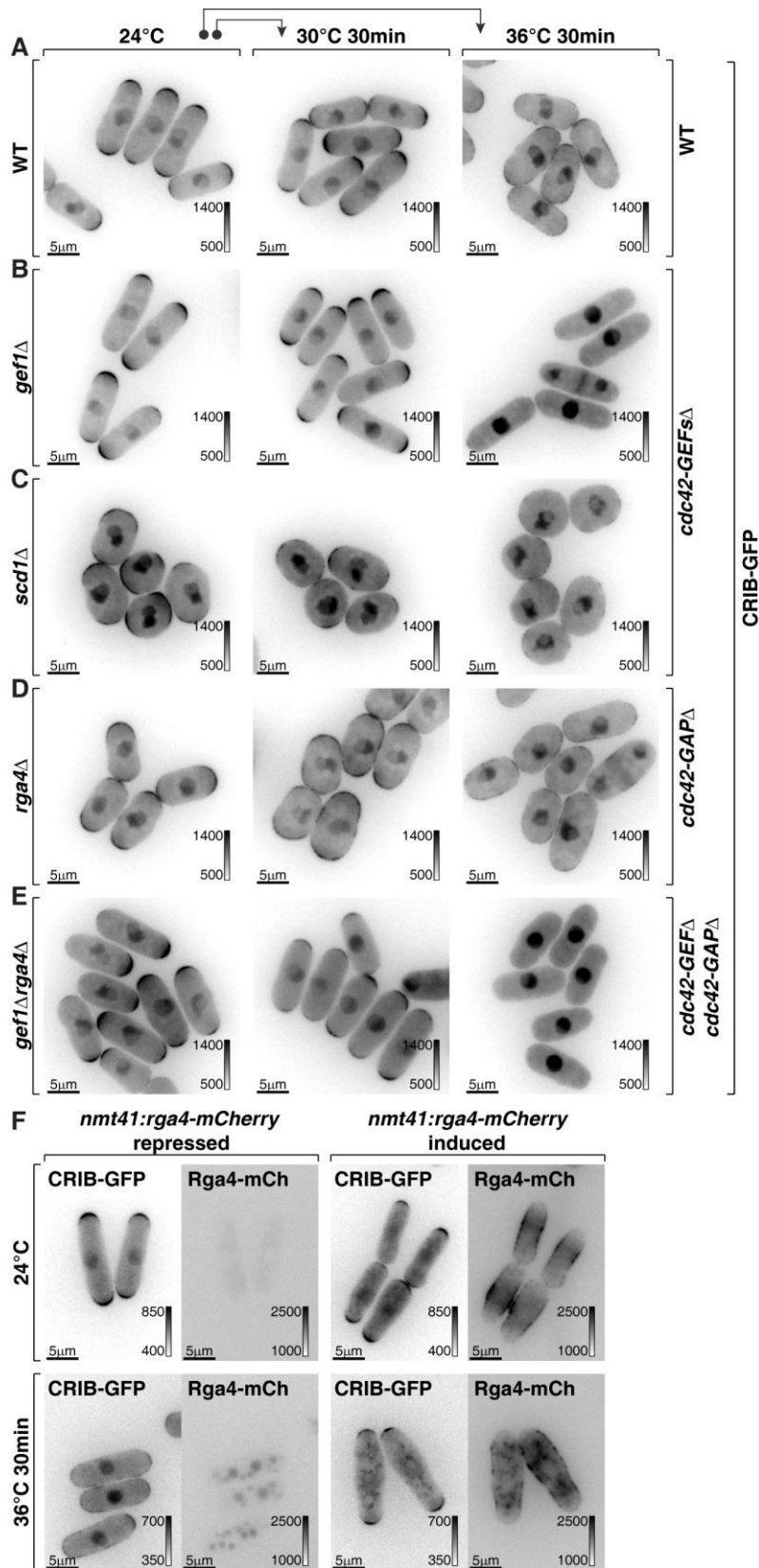
Taken together my results imply that the Cdc42 activity throughout the cell cortex of cells experiencing heat-stress requires Cdc42-GEF mediated activation to overcome the negative regulation conferred by the Cdc42-GAPs.

Figure Legend 3.3.3. Cdc42 activity at the lateral cell cortex upon heat-stress is enabled by cdc42-GEFs and counteracted by the cdc42-GAP.

(A-E) Single *z*-plane epifluorescence micrographs of CRIB-GFP in cells with indicated genotypes grown at 24°C (left panels), shifted to 30°C (middle panels) or 36°C for 30min (right panels).

(F) CRIB-GFP expressing cells transformed with *rga4-mCherry* construct under the regulation of thiamine responsive *nmt41* promoter were grown for 20 hours at 24°C in presence (left panels) or absence of thiamine (right) and imaged before (top panels) and 30min after transition to 36°C (bottom panels). Shown are single *z*-plane epifluorescence micrographs. Gray wedges report image contrasting and all scale bars refer to 5 μm.

Figure 3.3.3. Cdc42 activity at the lateral cell cortex upon heat-stress is enabled by *cdc42*-GEFs and counteracted by the *cdc42*-GAP.



3.3.4. Heat-stress associated transcription is essential to polarize growth at elevated temperature and sufficient to induce monopolar growth pattern

Heat-stress leads to extensive changes in transcriptional activity in various organisms including fission yeast (Chen et al., 2003; Richter et al., 2010). To explore if heat-stress associated transcriptional response also regulates cell polarity upon temperature increase I transiently blocked transcription in cells exposed to heat-stress. As outlined in Figure 3.3.4A, wild-type cells expressing CRIB-GFP were grown at 24°C to log-phase and treated with a transcriptional inhibitor actinomycin D (ActD) or solvent 5 min prior to raising temperature to 36°C or maintaining it at 24°C. The drug was washed out 25min later and cells were allowed to continue growth at respective temperatures. ActD did not affect the localization of CRIB-GFP to narrow tip zones in unstressed cells during the course of the experiment (Fig. 3.3.4B and C). CRIB-GFP was seen spreading along the cell sides in both ActD and ethanol treated cells shifted for 30min to 36°C (Fig. 3.3.4B and C). 90 min upon temperature shift virtually all ethanol treated cells but only 62% of ActD treated cells re-established polarity of the CRIB-GFP (Fig. 3.3.4B and 4C). Majority cells transiently treated with ActD and grown at 36°C did re-polarize CRIB-GFP although with almost an hour delay as compared to wild-type cells (Fig. 3.3.4B and C). None of the heat-stressed cells were able to re-polarize CRIB-GFP within two hours if I continuously applied ActD, even though a two hour ActD treatment did not perturb the tip localization of CRIB-GFP in unstressed cells (data not shown).

Heat-stress associated transcription is primarily mediated by a transient activation of the Hsf1 family of transcription factors (reviewed by Akerfelt et al., 2010) only one of which is present in the fission yeast genome. I was

interested how cell polarity is affected by Hsf1 transcriptional activity alone, without the coupled temperature change. To that aim I replaced the fission yeast *hsf1* genomic promoter with a strong, thiamine responsive *nmt1* promoter. Overexpression of Hsf1 appeared to elevate its transcriptional activity since I could readily observe increased levels of a heat-stress induced protein Hsp104 C-terminally tagged with GFP at its native locus (Fig. 3.3.4D and S4E). Strikingly, calcofluor staining revealed that upregulation of *hsf1* caused decreased new-cell-end growth as compared to wild-type cells (Fig. 3.3.4F and G, on average the new-end length decreased by $59\pm 22\%$ in *nmt1:hsf1* cells as compared to wild-type cells, $p^{\text{Welch's t-test}} = 4.58 \cdot 10^{-10}$, $n > 50$ cells per sample). Prolonged Hsf1 overexpression caused cells to fully arrest growth as long, unseptated cells (data not shown). Furthermore, in the absence of thiamine *nmt1:hsf1* cells recruited CRIB-GFP predominantly to one cell tip at decreased levels as compared to cells growing in the presence of thiamine (Fig. 3.3.4H and I). I concluded that the increasing Hsf1 activity is sufficient to induce a transition to a monopolar growth pattern

Taken together my results suggest that the heat-stress associated transcription, required to efficiently re-establish cell polarity upon temperature increase, must be eventually repressed to allow bipolar growth.

Figure 3.3.4. Heat-stress associated transcription regulates growth pattern in fission yeast

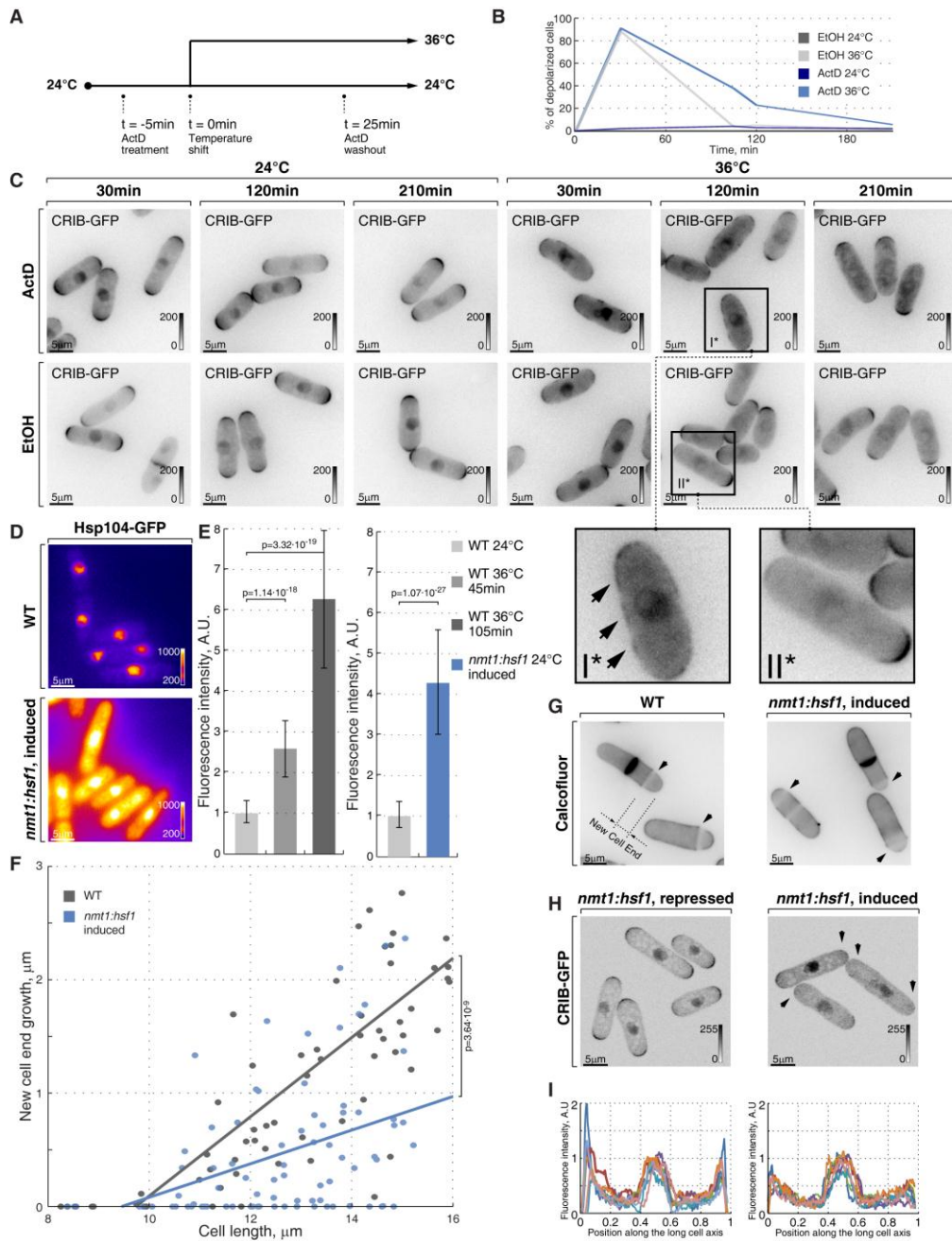


Figure Legend 3.3.4. Heat-stress associated transcription regulates growth pattern in fission yeast

(A) Scheme of the experimental design used in (B) and (C); Log-phase wild-type cells expressing CRIB-GFP were grown at 24°C and treated with either a transcriptional inhibitor actinomycin D (ActD) or ethanol 5min prior to splitting each cell culture into equal fractions. One half of each cell culture was allowed to continue growth at 24°C and the other was shifted to 36°C and this time is denoted as t_0 . Cells were washed with fresh media of matching temperature 25min later. Imaging was done at 0, 30, 90, 105, 120 and 210 min timepoints.

(B) Quantification of interphase cells with depolarized CRIB-GFP at indicated timepoints under conditions described in (A).

(C) Shown are single z-plane epifluorescence micrographs of cells described in (A) for indicated treatment, temperature and timepoints. Insets I* and II* are enlarged views of indicated cells to allow better view of CRIB-GFP signal localized to the lateral cell cortex as pointed out by arrows.

(D) Hsp104-GFP fluorescence in cells with *hsf1* ORF under the control of the wild-type or *nmt1* promoter grown to log phase in minimal media without thiamine. Shown are pseudocolored average intensity whole cell z-projections of Hsp104-GFP epifluorescence.

(E) Quantification of Hsp104-GFP fluorescence in log-phase wild-type cells grown at 24°C and shifted to 36°C for 45min or 105min (left panel) and between the wild-type and *nmt1::hsf1* cells grown to log phase in absence of thiamine.

(F) New-cell-end length as a function of cell length for wild-type (black) and cells over-expressing Hsf1 from the thiamine responsive *nmt1* promoter (blue). Dots represent individual late G₂ phase cells and lines represent linear regressions for cells analyzed (n>30). p-values were obtained through ANCOVA analysis.

(G) Single z-plane images of calcofluor stained wild-type and cells with Hsf1 over-expression driven by *nmt1* promoter induced for 20hrs by removal of thiamine. Arrows point to birth-scars and the new-cell-end length was determined as a distance from the birth-scar to the proximal cell tip.

(H) Shown are whole cell maximum intensity z-projections of scanning confocal micrographs of log-phase *nmt1::hsf1* cells expressing CRIB-GFP grown in the presence or absence of thiamine for 20 hrs (left and right panels). Arrows point to cell tips with low or no Cdc42 activity. Gray wedges report image contrasting and all scale bars refer to 5 μ m.

(I) Quantification of CRIB-GFP intensities along the long cell axis in log-phase w *nmt1::hsf1* treated as in (H).

3.3.5. Cells with impaired Hsp70•Hsp40 complex Mas5•Ssa2 have elevated levels of heat-stress associated transcription.

In fission yeast, *hsf1* is an essential gene and artificial up- or down-regulation of its expression levels renders cells defective in germination (Gallo et al., 1993 and data not shown). I sought to isolate a fission yeast mutants with elevated heat-stress associated transcription but amenable to genetic analysis. Hsp90 and Hsp70 family proteins are known repressors of Hsf1 activity but have been proposed to engage a large number of target proteins (Gong et al., 2009; Akerfelt et al., 2010) . I reasoned that using their mutants to modulate heat-stress associated transcription might give ambiguous results. Instead, I decided to screen the deletion library of sixteen non-essential genes encoding putative nucleo-cytoplasmic Hsp70-binding proteins including DnaJ subfamily of chaperones that serve as activators and specificity factors of Hsp70 chaperones (Table 3.3.5). Two screening strategies were employed.

First approach was based on my findings that Hsf1 overexpression leads to decreased growth rates and eventually a growth arrest (data not shown). I hypothesized that mutant strains with elevated levels of heat-stress associated transcription would have decreased growth rates at 24°C and likely arrest growth at 36°C. A growth assay indicated that within the deletion library of nonessential Hsp70-binding proteins only the strain lacking the DnaJ chaperone Mas5 exhibited such growth pattern (Fig. 3.3.5.1A).

I employed a second screening strategy exploiting the fact that a mild heat-stress increases survival upon a subsequent severe heat-shock. Presumably, activation of heat-stress response by moderate temperature elevation increases ability of cells to combat protein aggregation caused by

acute heat-shock (Li and Werb, 1982). As outlined in Figure 3.3.5.1B, wild-type and cells from the deletion library were grown to log-phase at 24°C and aliquots were either allowed to continue growth at 24°C or shifted to 50°C for 15min before returning them to 24°C. Additionally, a sample of wild-type cells was shifted to 36°C for 45min before being exposed to 50°C. Survival was measured by assessing the number of colony forming units in each culture and a spotting assay (Fig. 3.3.5.1C and D). Wild-type and most mutant fission yeast strains investigated had a survival rate below 0.5% when shifted from 24°C to 50°C for 15min (n>200 CFU per strain). Conversely, 29% of wild-type cells survived if a mild heat-stress preceded severe heat-shock. Unlike *ssa1Δ* cells, *ssa2Δ* mutants showed increased resilience to acute exposure to 50°C with the survival rate of 6% (Fig. 3.3.5.1C and D). Cells lacking Mas5 had a comparable 8% survival rate when shifted directly from 24°C to 50°C for 15min (Fig. 3.3.5.1C and D). Thus, both *ssa2Δ* and *mas5Δ* cells are resilient to extreme heat-shock even though they arrest growth at 36°C.

In collaboration with Jianhua Liu lab, I investigated gene expression of *mas5Δ* cells using microarray analysis (see Materials and Methods) and identified over 300 significantly up- or down-regulated genes (Fig. 3.3.5.1E, $p^{\text{Welch-test}} < 0.05$). Next, I compared the expression profile of *mas5Δ* cells to that of wild-type cells under five different abiotic stresses (Chen et al., 2003, Fig. 3.3.5.1F-I). The correlation between expression profiles was analyzed in a manner derived from (Irizarry et al., 2005) and demonstrated good agreement between expression profiles of *mas5Δ* cells and wild-type cells exposed to heat or cadmium ($\rho^{\text{Spearman's}} > 0.6$, Fig. 3.3.5.1F-H). DNA damage, osmotic

and oxidative stress induced expression profiles correlated poorly to the expression pattern of cells lacking Mas5 (Fig. 3.3.5.1F-H). A modified correspondence at the top (CAT) plot was used to assess the significance ($p^{\text{binomial test}}$) of similarity between expression profiles for the most up-/down-regulated genes in *mas5Δ* cells (Fig. 3.3.5.1G). Consistent with the concept of the general stress response (Gasch et al., 2000), the 70 most up-/down-regulated genes in *mas5Δ* cells showed likewise regulation during most stress conditions examined (Fig. 3.3.5.1G). As an increasing number of genes was included into the analysis, the significance was strengthened only for the similarity between *mas5Δ* cells and cells exposed to heat or cadmium. MAPK signaling is also activated by heat-stress through Sty1 kinase (Shiozaki et al., 1998). The CAT profile comparing gene expression of *mas5Δ* cells to that of heat-stressed *sty1Δ* cells were similar with high significance (Fig. 3.3.5.1G) suggesting that gene expression of *mas5Δ* correlates to heat-stress associated transcription largely independent of MAPK signaling.

The Bahler lab identified fission yeast genes exclusively induced or super-induced in response to a specific stress (Chen et al., 2003). Only the heat-stress specific genes were consistently up-regulated in *mas5Δ* cells ($p^{\text{binomial test}} = 3.17 \cdot 10^{-3}$) but not the genes characteristic other types of stress ($p^{\text{binomial test}} = 0.80, 0.64$ and 0.71 for oxidative, osmotic stress and cadmium treatment respectively, Fig. 3.3.5.1I).

The qPCR analysis of RNA samples prepared from *mas5Δ* cells, wild-type cells exponentially growing at 24°C and wild-type cells shifted from 24°C to 36°C for 45min supported my microarray data (Fig. 3.3.5.2A). Genes specifically induced or super-induced in response to heat-stress (*aha1*, *dpp5*,

fes1, *sti1*, *tps3*) were up-regulated in *mas5Δ* cells and genes down-regulated during heat-stress (*rpl24-3*, *fas2*, *dbp2*, *ght8*) had also lowered expression in *mas5Δ* cells. I concluded that the transcriptional profile of *mas5Δ* cells qualitatively matches the heat-stress gene expression signature.

The budding yeast homologue of Mas5, Ydj1 has been shown to interact with SSA subfamily of Hsp70s (Cyr and Douglas, 1994; Cyr, 1995; Gong et al., 2009). My co-immunoprecipitation experiments on lysates from cells with differentially tagged Mas5 and an SSA chaperone expressed from their native promoters loci suggested that both *Ssa2* and *Ssa1* interact with Mas5 (Fig. 3.3.5.2B and C).

I went on to explore if either of the two SSA chaperones function to represses heat-stress associated transcription. To that aim I tagged the heat-responsive proteins with GFP at their native loci and analyzed fluorescence levels in log-phase wild-type, *ssa1Δ*, *ssa2Δ* and *mas5Δ* cells growing at 24°C in addition to wild-type cells shifted from 24°C to 36°C for 45min. Hsp104-GFP, Swo1-mCherry and Psi1-GFP levels were all increased upon heat-stress and also exhibited elevated levels in *mas5Δ* and *ssa2Δ* but not in *ssa1Δ* cells (Fig. 3.3.5.2D and data not shown). To exclude the possibility that elevated fluorescence levels ere due to selective stabilization of heat-responsive proteins in mutant cells I also analyzed fluorescence of the GFP under the control of 5' and 3' UTRs of *hsp104* gene (Fig. 3.3.5.2E). The UTRs^{Hsp104}:GFP levels rose in response to temperature increase and were also elevated in both *ssa2Δ* and *mas5Δ* cells whereas deletion of the *ssa1* gene had no apparent effect.

In summary, my screening strategy, microarray analysis, qPCR results, and imaging of heat-stress responsive proteins pointed to elevated levels of heat-stress associated transcription in *mas5* Δ and *ssa2* Δ cells. These results combined with data obtained from co-immunoprecipitation experiments suggest that the Ssa2 and Mas5 function as a complex to repress the heat-stress associated transcription.

Table 3.3.5. Overview of putative Hsp70-binding chaperones in fission yeast

Viability (Kim et al., 2010)	Cellular subcompartment (Matsuyama et al., 2006)	Systematic Id	Product	Description	
Inviabile	Endoplasmic reticulum	SPBC1347.05c		DNAJ domain protein Scj1 (predicted)	Absent from the screening library
Inviabile	Endoplasmic reticulum	SPAC17A5.12	ucp7	UBA/TPR/DNAJ domain protein Ucp7	
Inviabile	Golgi	SPCC4G3.14	mdj1	mitochondrial DNAJ domain protein Mdj1 (predicted)	
Not determined	Mitochondrial	SPAC824.06	tim14	TIM23 translocase complex subunit Tim14 (predicted)	
Viable	Endoplasmic reticulum	SPBC36B7.03	sec63	ER protein translocation subcomplex subunit Sec63 (predicted)	
Viable	Mitochondrial	SPAC144.08		mitochondrial DNAJ domain protein Jac1 (predicted)	
Viable	Mitochondrial	SPAC24H6.02c		TIM23 translocase complex subunit Tim15 (predicted)	
Viable	Nucleo-cytoplasmic	SPBC1773.09c	mug184	meiotically upregulated gene Mug184	
Viable	Nucleo-cytoplasmic	SPBC1734.05c	spf31	DNAJ protein Spf31 (predicted)	
Viable	Nucleo-cytoplasmic	SPAC1071.09c		DNAJ domain protein, DNAJC9 family (predicted)	
Viable	Nucleo-cytoplasmic	SPAC2E1P5.03		DNAJ domain protein Erj5 (predicted)	
Viable	Nucleo-cytoplasmic	SPAC4G9.19		DNAJ domain protein DNAJB family (predicted)	
Viable	Nucleo-cytoplasmic	SPAC4H3.01		DNAJ domain protein Caj1/Djp1 type (predicted)	
Viable	Nucleo-cytoplasmic	SPAC6B12.08	mug185	Co-chaperone for ATPase activity (predicted)	
Viable	Nucleo-cytoplasmic	SPAC926.05c	dph4	diphthamide biosynthesis protein Dph4 (predicted)	
Viable	Nucleo-cytoplasmic	SPBC11B10.05c	rsp1	random septum position protein Rsp1	
Viable	Nucleo-cytoplasmic	SPBC1734.11	mas5	DNAJ domain protein Mas5 (predicted)	
Viable	Nucleo-cytoplasmic	SPBC1778.01c	zuo1	zootin (predicted)	
Viable	Nucleo-cytoplasmic	SPBC17A3.05c		DNAJ/DUF1977 DNAJB12 homolog (predicted)	
Viable	Nucleo-cytoplasmic	SPBC3E7.11c		DNAJ protein Caj1/Djp1-type (predicted)	
Viable	Nucleo-cytoplasmic	SPBC405.06		DNAJ protein Xdj1 (predicted)	
Viable	Nucleo-cytoplasmic	SPBC543.02c		DNAJ/TPR domain protein DNAJC7 family	
Viable	Nucleo-cytoplasmic	SPCC10H11.02	cwf23	DNAJ domain protein Cwf23	
Viable	Nucleo-cytoplasmic	SPCC63.03		DNAJ domain protein, DNAJC11 family	
Viable	Nucleo-cytoplasmic	SPCC63.13		DNAJ domain protein	
Viable	Nucleo-cytoplasmic	SPCC830.07c	psi1	DNAJ domain protein, involved in translation initiation Psi1	

Figure 3.3.5.1. Cells with impaired function of the Ssa2•Mas5 complex have elevated levels of heat-stress associated transcription.

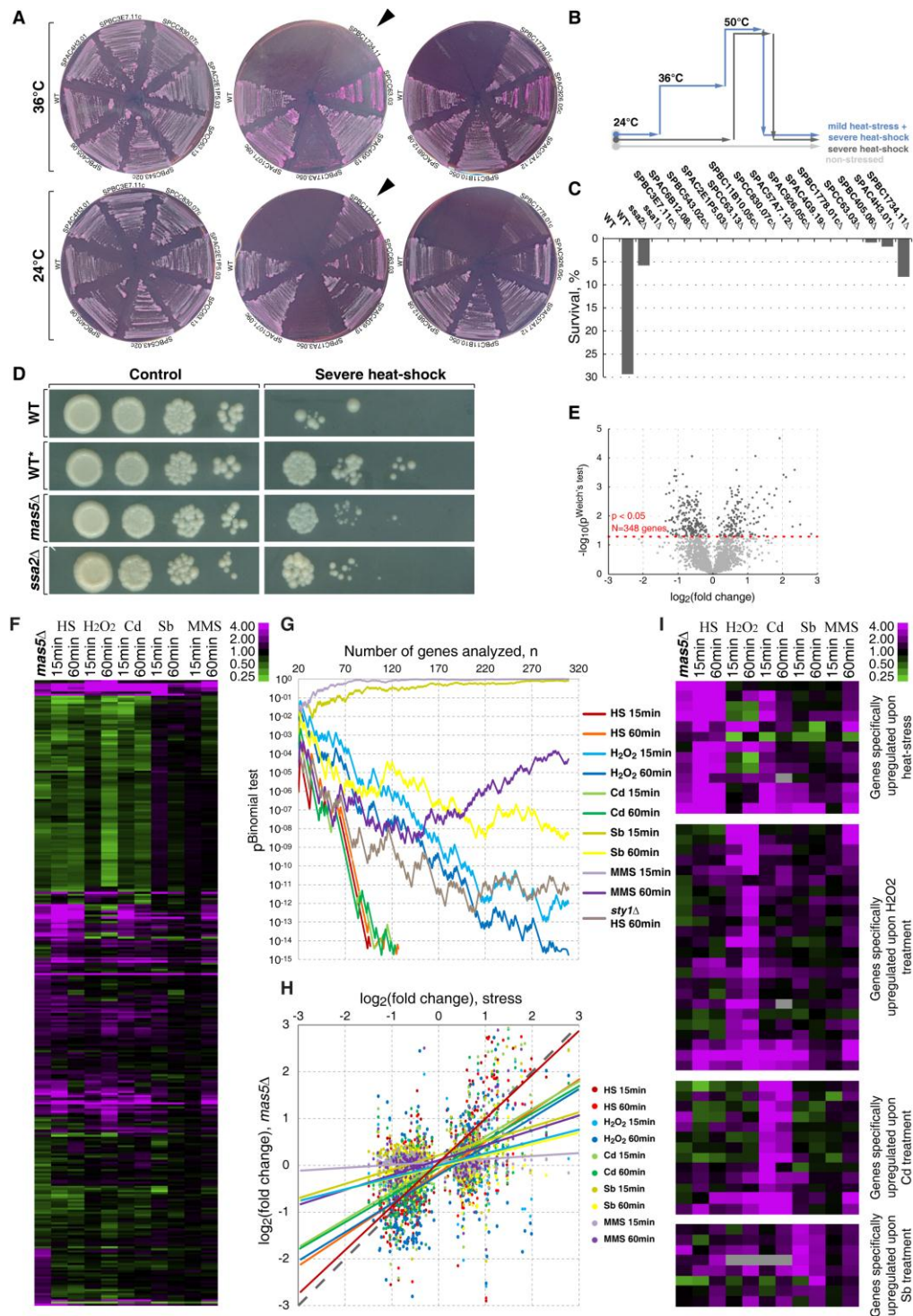


Figure Legend 3.3.5.1. Cells with impaired function of the Ssa2•Mas5 complex have elevated levels of heat-stress associated transcription.

(A) Fission yeast strains lacking indicated non-essential nucleocytoplasmic Hsp70-interacting proteins were streaked out onto YES plates containing phloxineB and grown at 24°C or 36°C. Arrowheads points to the strain lacking DnaJ chaperone Mas5.

(B) Outline of the screening strategy used to identify strains with elevated levels of heat-stress associated transcription. Cells were grown to log-phase at 24°C and aliquots were either allowed to continue growth at 24°C (light-gray line) or shifted to 50°C for 15min (dark-gray line). An additional sample of wild-type cells was shifted to 36°C for 45min before being transferred to 50°C for 15min. Number of colony forming units was measured for each sample and used to calculate survival rates.

(C) Survival rate upon extreme heat-shock (50°C for 15min) of wild-type cells (WT), wild-type cells pre-exposed to mild heat stress (WT^{*}) and cells lacking individual SSA subfamily chaperones or indicated non-essential nucleocytoplasmic Hsp70-interacting proteins.

(D) Spotting assay of wild-type cells (WT), wild-type cells pre-exposed to mild heat-stress (WT^{*}) and cells lacking Mas5 or Ssa2 grown at 24°C (left panels) and exposed to 50°C for 15min prior to plating (right panels).

(E) Volcano plot denoting significance of change in mRNA levels for individual genes analyzed by the microarray comparison of *mas5Δ* to wild-type cells. Red line represents $p^{\text{Welch's test}} = 0.05$.

(F) Comparison between gene expression profiles of *mas5Δ* and wild-type cells under indicated environmental stresses (Chen et al., 2003).

(G) CAT plot analyzing significance of similarity between gene expression profiles of *mas5Δ* cells and wild-type cells under indicated environmental stresses.

(H) Correlation analysis between gene expression profiles of *mas5Δ* cells and wild-type cells under indicated environmental stress. Individual dots represent individual genes.

(I) Expression profiles of genes specifically upregulated by distinct environmental stresses in *mas5Δ* cells and wild-type cells under indicated environmental stresses.

Figure 3.3.5.2. Cells lacking a DnaJ chaperone Mas5 have elevated levels of heat-stress associated transcription.

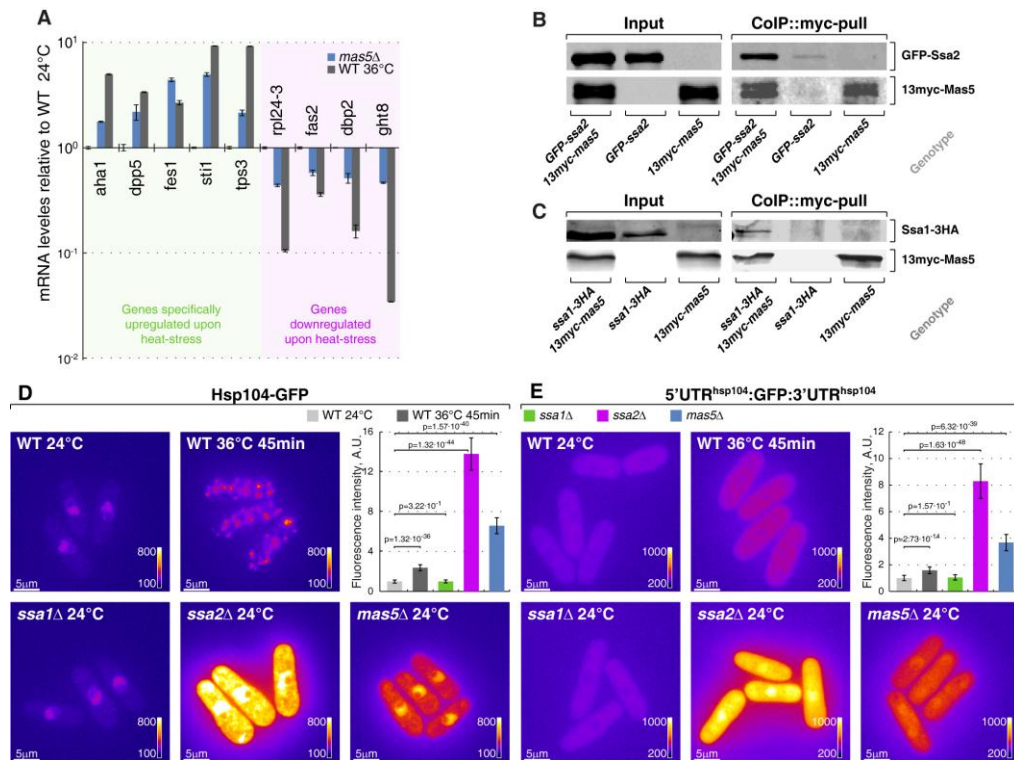


Figure Legend 3.3.5.2. Cells lacking a DnaJ chaperone Mas5 have elevated levels of heat-stress associated transcription.

(A) Expression levels of genes specifically induced and genes repressed during heat-stress in wild-type cells grown at 24°C, shifted to 36°C for 45min and *mas5*Δ cells as measured by qPCR. Expression levels are normalized to wild-type cells grown at 24°C.

(B, C) Lysates prepared from cells with indicated genotypes were incubated with *anti-myc* antibodies and subsequently with beads coupled to protein-G. Proteins that remained associated with the beads after multiple buffer washes were resolved by SDS-PAGE and prepared for western blotting with *anti-myc* and *anti-GFP* or *anti-HA* antibodies.

(D) Pseudocolored average *z*-projection epifluorescence images of Hsp104-GFP in wild-type, *ssa1*Δ, *ssa2*Δ and *mas5*Δ cells grown in indicated conditions. The graph represents quantification of Hsp104-GFP fluorescence intensity in indicated genetic backgrounds.

(E) Pseudocolored average *z*-projection epifluorescence images of the GFP under the regulation of *hsp104* 5'UTR and 3'UTR in wild-type, *ssa1*Δ, *ssa2*Δ and *mas5*Δ cells grown in indicated conditions. The graph represents quantification of GFP fluorescence intensity in indicated genetic backgrounds. Image contrast is reported using corresponding gray wedges and all scale bars correspond to 5μm.

3.3.6. Ssa2•Mas5 complex regulates nucleo-cytoplasmic shuttling of the Hsp90 chaperone Swo1 and its target protein Hsf1

Transcriptional response upon heat-stress is largely mediated by the HSF family of transcription factors (Akerfelt et al., 2010). Thus I wondered whether Ssa2•Mas5 complex could modulate Hsf1 function. I analyzed the subcellular distribution of GFP tagged Hsf1 expressed from its native promoter in wild-type, *mas5Δ*, *ssa2Δ* and *ssa1Δ* genetic background. I simultaneously monitored the localization of the Hsf1 inhibitor, Hsp90 family protein Swo1 tagged at its native locus with a C-terminal mCherry fluorophore. In log-phase wild-type cells growing at 24°C GFP-Hsf1 localized to the nucleus and weakly to the cytoplasm. Swo1-mCherry was distributed throughout the cellular volume of log-phase wild-type cells (Fig. 3.3.6A, left panels). In contrast, when shifted to 36°C for 45min the nuclear GFP-Hsf1 signal diminished and the cytoplasmic signal increased suggesting active nuclear export. Simultaneously, Swo1-mCherry accumulated in the nucleus of heat-stressed wild-type cells (Fig. 3.3.6A, right panels). These results suggest that 45 minutes upon temperature shift cells actively repress the Hsf1 transcriptional activity by both exporting Hsf1 from the nucleus and importing its inhibitor Swo1. My results are in line with proposed dynamics of Hsf1 transcriptional activity during heat-stress in other model systems whereby rapid activation of Hsf1 occurs within minutes of temperature change and is subsequently repressed (Gasch et al., 2000; Chen et al., 2003; Rieger et al., 2005; Zobeck et al., 2010; Ghosh et al., 2011).

In both *ssa2Δ* and *mas5Δ* cells exponentially growing at 24°C GFP-Hsf1 localized to the nucleus and displayed a weak cytoplasmic signal (Fig.

3.3.6B and C, left panels). The ratio between the nuclear and cytoplasmic Swo1-mCherry signal was strongly lowered in cells lacking Mas5 or Ssa2 as compared to wild-type cells (Fig. 3.3.6B and C, left panels). Furthermore, when *ssa2* Δ and *mas5* Δ cells were shifted to 36°C for 45min the nuclear GFP-Hsf1 signal remained strong and the Swo1-mCherry was not seen accumulating in the nucleus (Fig. 3.3.6B and C, right panels). These defects in the nucleo-cytoplasmic shuttling of GFP-Hsf1 and Swo1-mCherry in *mas5* Δ cells were observed when cells were expressing individual fluorophores as well (data not shown). Cells lacking Ssa1 exhibited GFP-Hsf1 and Swo1-mCherry localization indistinguishable from wild-type cells in all experimental conditions (Fig. 3.3.6D). GFP-Mas5 and GFP-Ssa2 were present throughout the cellular volume in both unstressed and heat-stressed cells. However, temperature increase did stimulate recruitment of both GFP-Mas5 and GFP-Ssa2 to faint cytosolic foci (Fig. 3.3.6E and F). My data suggests that *ssa2* Δ and *mas5* Δ cells 1) exhibit a defect in the nucleo-cytoplasmic shuttling of Swo1 during both steady-state growth and heat-stress conditions and 2) fail to export of Hsf1 from the nucleus upon heat-stress.

Neither GFP-Ssa2 nor 13myc-Mas5 was detected to form a complex with GFP-Hsf1 (data not shown) but both readily co-immunoprecipitated with Swo1-3HA (Fig. 3.3.6G and H). Interestingly, *swo1-w1* mutant cells shifted to 36°C also failed to export GFP-Hsf1 from the nucleus (Fig. 3.3.6I).

Taken together my results are consistent with a hypothesis that elevated levels of heat-stress associated transcription in *ssa2* Δ and *mas5* Δ cells are a consequence of impaired Hsf1 dynamics. One possibility is that

Ssa2•Mas5 complex regulates nucleo-cytoplasmic shuttling of Swo1, which in turn could modulate localization and activity of Hsf1.

Figure Legend 3.3.6. Ssa2•Mas5 complex regulates nuclear shuttling of Hsf1 and Swo1.

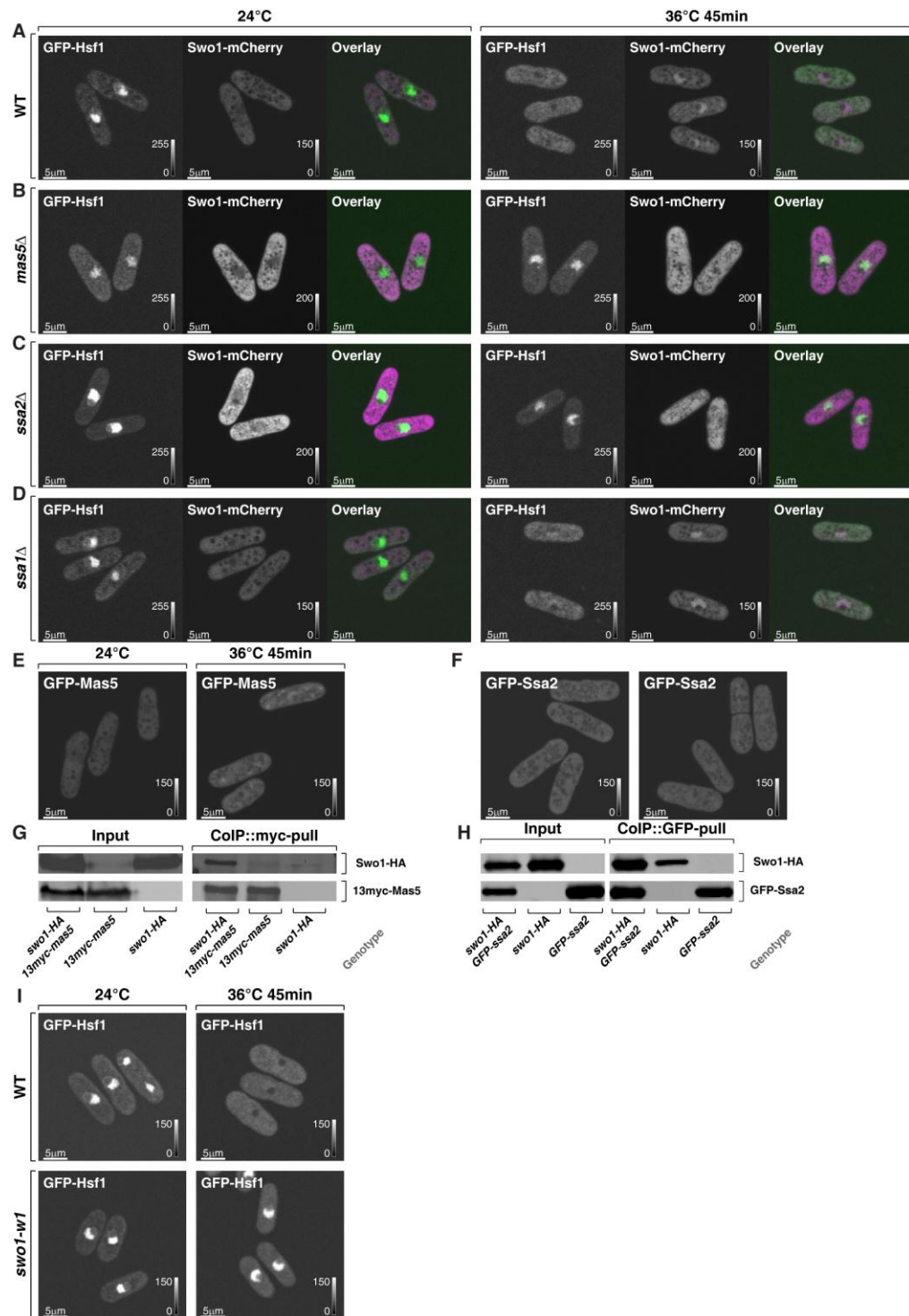
(A-D) Shown are whole cell maximum intensity *z*-projections of scanning confocal micrographs of log-phase cells with indicated genotypes co-expressing Swo1-mCherry and GFP-Hsf1 grown at 24°C (left panels) or shifted to 36°C for 45min (right panels).

(E, F) Shown are whole cell maximum intensity *z*-projections of scanning confocal micrographs of indicated chaperones with N-terminally fused GFP expressed from their native loci in cells grown at 24°C (left panels) or shifted to 36°C for 45min (right panels).

(G, H) Lysates prepared from cells with indicated genotypes were incubated with denoted antibodies and subsequently with beads coupled to protein-G. Proteins that remained associated with the beads after multiple buffer washes were resolved by SDS-PAGE and prepared for western blotting with *anti*-HA and *anti*-GFP or *anti*-myc antibodies.

(I) Shown are whole cell maximum intensity *z*-projections of scanning confocal micrographs of log-phase wild-type (top panels) and *swo1-w1* (bottom panels) cells expressing GFP-Hsf1 grown at 24°C (left panels) or shifted to 36°C for 45min (right panels). Image contrast is reported using corresponding color wedges. All scale bars refer to 5 μ m.

Figure 3.3.6. Ssa2•Mas5 complex regulates nuclear shuttling of Hsf1 and Swo1.



3.3.7. Cells lacking the Mas5•Ssa2 complex exhibit an intermittent, monopolar growth pattern

Having established that lack of Mas5 or Ssa2 activates the heat-stress associated transcription, I investigated the growth pattern of *mas5Δ* and *ssa2Δ* cells. As compared to wild-type cells, log-phase *mas5Δ* and *ssa2Δ* cell growing at 24°C had approximately 30% and 100% longer doubling time, respectively (Fig. 3.3.7.2A top panel, $p^{\text{Welch's t-test}} = 1.61 \cdot 10^{-2}$ and $7.16 \cdot 10^{-3}$, $n = 3$). However, cells lacking Mas5 or Ssa2 divided at $85 \pm 10\%$ and $93 \pm 12\%$ of the length of wild-type cells (Fig. 3.3.7.2A bottom panel, $p^{\text{Welch's t-test}} = 8.12 \cdot 10^{-24}$ and $2.76 \cdot 10^{-11}$, $n \approx 100$ per genotype). Calcofluor staining suggested that as compared to wild-type cells both *ssa2Δ* and *mas5Δ* cells underwent significantly decreased new-cell-end growth (Fig. 3.3.7.1A and B, on average, *mas5Δ* and *ssa2Δ* cells reduced the new-end growth by $50 \pm 24\%$ and $78 \pm 93\%$ respectively, $p^{\text{Welch's t-test}} = 2.28 \cdot 10^{-28}$ and $2.46 \cdot 10^{-11}$, $n > 60$ per genotype).

Progression through the cell cycle was not affected in *mas5Δ* and *ssa2Δ* mutants as evaluated by FACS (Fluorescence Activated Cell Sorting) analysis (Fig. 3.3.7.2B) suggesting that there was no G₂ entry delay to account for the monopolar growth of these mutants.

I analyzed the localization of fluorescently tagged polarity and growth marker proteins in wild-type and *mas5Δ* genetic background. Subcellular distribution of polarisome components Tea1-YFP, Tea4-GFP and Pom1-GFP was unaffected by *mas5* gene deletion (Fig. 3.3.7.2C-E). In contrast, late into the G₂ phase of the cell cycle GFP-Cps1 localized to both cell tips in 68% of wild-cells and only 8%, *mas5Δ* cells (Fig. 3.3.7.2F). Thus it appears that in

mas5Δ cells mechanisms specifying cell tips remain intact yet the recruitment of cell wall remodeling enzymes to one of the cell tip fails.

The bipolar recruitment of the exocyst was also impaired in cells lacking Mas5. Late into the G₂ phase of the cell cycle Sec6-GFP localized to both cell tips in 79% of wild-type cells and only 46% of *mas5Δ* cells (Fig. 3.3.7.2G). Furthermore, imaging of LifeAct-GFP showed that the actin cytoskeleton predominantly localized to one cell tip of late G₂ phase *mas5Δ* cells (Fig. 3.3.7.2H). Consistently, For3-GFP and Myo52-GFP which were monopolar in 25% and 22% of late G₂ phase wild-type-cells, localized to only one cell tip in 69% and 61% of *mas5Δ* cells of similar size (Fig. 3.3.7.2I and J).

Next I performed live imaging on wild-type, *ssa2Δ* and *mas5Δ* cells grown in a perfusion chamber at room temperature (Movie 3.3.7, see Materials and Methods). After an initial monopolar growth phase, newly born wild-type cells underwent NETO and assumed bipolar growth pattern clearly seen in the kymograph (Fig. 3.3.7.1C). As previously reported (Mata and Nurse, 1997), *teal1Δ* cells maintained the growth pattern attained at the time of birth and were rarely seen undergoing NETO (Fig. 3.3.7.1C). Consistent with the data presented earlier, over 90% of *ssa2Δ* and *mas5Δ* cells grew only at the old cell tip. Surprisingly, all mutant cells had an intermittent growth pattern with periods of complete growth arrests lasting from five to over thirty minutes followed by growth bursts lasting five and over thirty minutes (Fig. 3.3.7.1C and Fig. 3.3.7.2K).

The activity of Cdc42, as reported by CRIB-GFP, was also localized to one cell tip in cells lacking Mas5 or Ssa2 (Fig. 3.3.7.1D, 3% of wild-type,

93% of *ssa2Δ* and 58% of *mas5Δ* late G₂ phase of the cell). Furthermore, the levels of CRIB-GFP at the cell tip were strongly diminished in *ssa2Δ* and *mas5Δ* cells (Fig. 3.3.7.1D and E). The time-lapse spinning-disk confocal microscopy revealed that the CRIB-GFP recruitment to the cell tips was unstable in *mas5Δ* and *ssa2Δ* cells (Fig. 3.3.7.1F). In wild-type cells, CRIB-GFP signal at the continuously growing old-cell-end displayed only minor oscillations in intensity during the course of the imaging. CRIB-GFP levels at the new-cell-end of wild-type cells went through major, on-off oscillations prior to NETO but eventually stabilized and exhibited only minor oscillations (Fig. 3.3.7.1F, left panel). However, in *ssa2Δ* and *mas5Δ* cells CRIB-GFP levels underwent on-off oscillations at both cell tips throughout the cell cycle. I observed that CRIB-GFP levels at the old-cell-end were relatively high only for periods of time during which the tip growth was also carried out (Fig. 3.3.7.1F, middle and right panels, see arrows). CRIB-GFP levels at the new-cell-end of *ssa2Δ* and *mas5Δ* cells underwent on-off oscillations that would rarely stabilize to allow for noticeable tip elongation during the course of imaging. These results suggest that the intermittent growth pattern of *ssa2Δ* and *mas5Δ* cells is a consequence of the unstable Cdc42 activity at the cell tips. Furthermore, the decreased Cdc42 activity at the new-cell-end could explain the monopolar growth pattern of mutants lacking Ssa2 or Mas5 function.

The low levels of active Cdc42 in *mas5Δ* cells prompted us to explore the distribution of the Cdc42-GAP and GEFs in the mutant. In late G₂ phase of the cell cycle, Gef1-3YFP was noticeable at both cell tips in 89% of wild-type but only 45% of *mas5Δ* cells (Fig. 3.3.7.1G). Likewise, Scd1-GFP was bipolar

in 72% of late wild-type cells but could be observed at both cell tips in only 18% of cells lacking Mas5 (Fig. 3.3.7.1H). The Cdc42-GAP, Rga4-GFP, was restricted to the lateral cell cortex in ~90% of both wild-type and *mas5*Δ cells (Fig. 3.3.7.1F).

Interestingly, levels of cortically associated Cdc42 regulators appeared decreased in *mas5*Δ cells as compared to wild-type cells. The average intensity of Gef1-3YFP at a cell tip was decreased by 38±28% whereas Scd1-GFP signal diminished by 53±27% (Fig. 3.3.7.1G and H, $p^{\text{Welch's t-test}} = 2.51 \cdot 10^{-6}$ and $7.94 \cdot 10^{-7}$ respectively, $n > 25$ cells per sample). A 20±22% decrease in cortically associated levels was also observed for the Rga4-GFP in cells lacking Mas5 (Fig. 3.3.7.1I, $p^{\text{Welch's t-test}} = 2.71 \cdot 10^{-4}$, $n > 25$ cells per sample). The total protein levels of the three examined Cdc42 regulators were also lower in *mas5*Δ than wild-type cells (Fig. 3.3.7.2L-N). Gef1-3YFP and Scd1-GFP levels decreased by 18% and 48% respectively and a 21% decrease was observed for Rga4-GFP.

Taken together my results suggest that fission yeast cells with impaired Ssa2•Mas5 complex efficiently specify cell poles but fail to maintain the Cdc42 activity at the cell tips. The decreased levels of the Cdc42-GAP and GEFs in *mas5*Δ are possibly insufficient to allow for continuous activity of Cdc42 at the cell tips and bipolar growth in these mutants.

Figure 3.3.7.1. Cells with impaired Ssa2•Mas5 complex have decreased cortical Cdc42 activity and exhibit monopolar intermittent growth pattern.

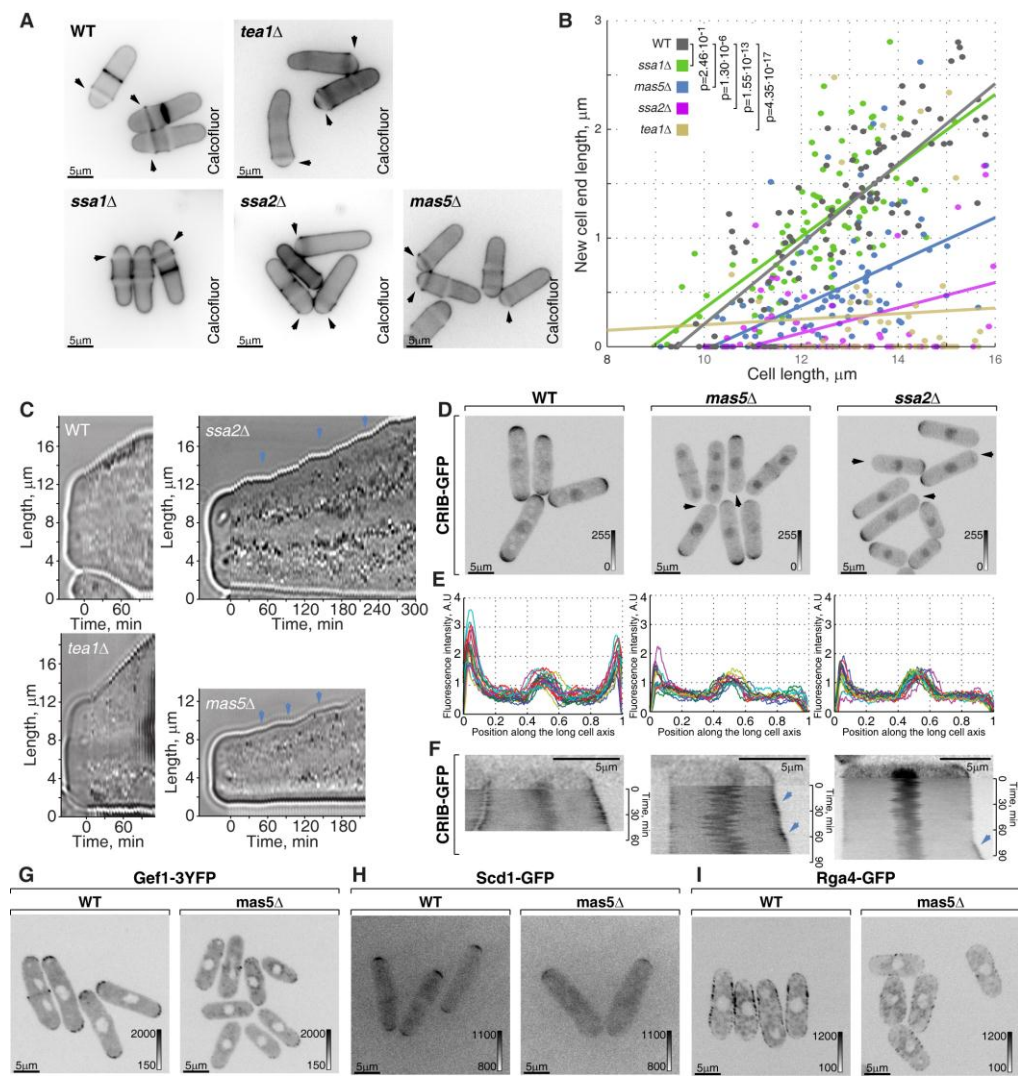


Figure Legend 3.3.7.1. Cells with impaired Ssa2•Mas5 complex have decreased cortical Cdc42 activity and exhibit monopolar intermittent growth pattern.

(A) Single z-plane images of calcofluor stained log-phase cells with indicated genotypes. Arrows point to birth-scars.

(B) New-cell-end length as a function of cell length for cells with noted genotype. Points represent individual cells, lines represent the linear regression of a sample and p-values were obtained through ANCOVA.

(C) Kymographs of brightfield microscopy time-lapse of cells with the indicated genetic background grown in a perfusion chamber at room temperature. Arrows point to growth pauses characteristic to *ssa2Δ* and *mas5Δ* cells only.

(D) Shown are whole cell maximum intensity z-projections of scanning confocal micrographs of log-phase cells with indicated genotypes expressing CRIB-GFP, arrows point to cell tips lacking Cdc42 activity.

(E) Quantification of CRIB-GFP intensities along the long cell axis in log-phase wild-type (left panel), *mas5Δ* (middle panel) and *ssa2Δ* cells (right panels). Individual lines correspond to individual cells.

(F) Kymograph of single z-plane spinning disk confocal microscopy time-lapse of wild-type (left panel), *mas5Δ* (middle panel) and *ssa2Δ* cells (right panels) grown at room temperature. Arrows point to intermittent Cdc42 activity bursts associated with longitudinal growth seen in *mas5Δ* and *ssa2Δ* cells only.

(G-I) Shown are single z-plane micrographs of log-phase wild-type (left panels) or *mas5Δ* (right panels) cells expressing indicated fluorophore tagged marker proteins grown at 24°C. Image contrast is reported using corresponding color wedges. All scale bars refer to 5 μm.

Figure 3.3.7.2. Cells lacking DnaJ chaperone Mas5 exhibit monopolar intermittent growth in G₂ phase of the cell cycle.

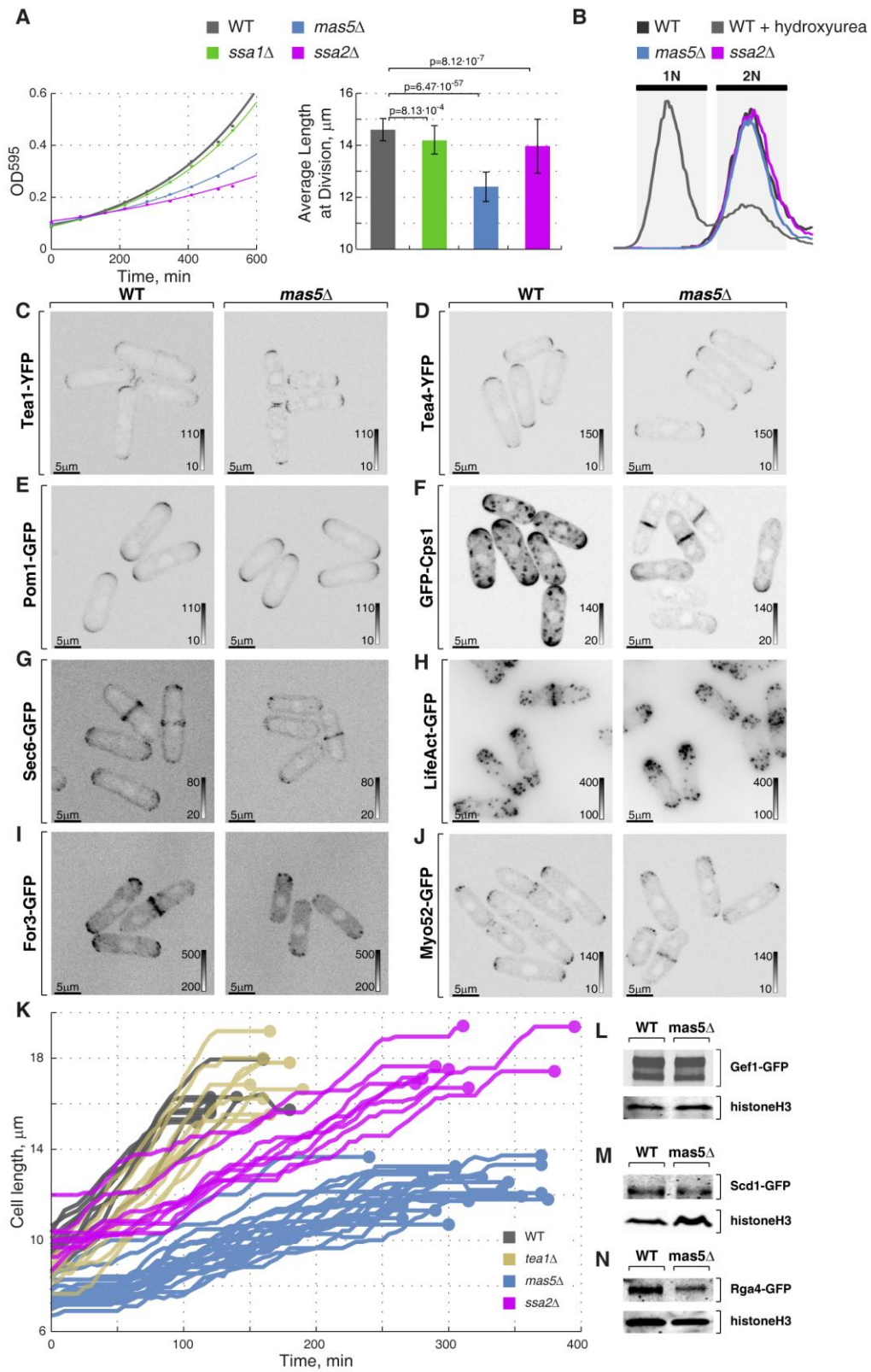


Figure Legend 3.3.7.2. Cells lacking DnaJ chaperone Mas5 exhibit monopolar intermittent growth in G₂ phase of the cell cycle.

(A) O.D.⁵⁹⁵ measurements of a log-phase cell culture with indicated genotypes grown at 24°C (left panel) and average division length at O.D.⁵⁹⁵ = 0.5 (right panel)

(B) FACS sorting analysis of DNA content for log-phase wild-type cells (black), wild-type cells arrested in S phase using hydroxyurea (gray) and log-phase *ssa2Δ* (purple) and *mas5Δ* cells (blue).

(C-J) Shown are whole cell maximum intensity z-projections of scanning confocal micrographs of log-phase wild-type (left panels) and *mas5Δ* (right panels) cells expressing indicated fluorophore tagged marker proteins grown at 24°C. Percentage of late G₂ phase cells with monopolar distribution of the indicated marker proteins are denoted for the corresponding genetic background. Image contrast is reported using corresponding color wedges. All scale bars refer to 5 μm.

(K) Quantification of longitudinal growth of cells with indicated genotypes placed in a perfusion chamber at room temperature. Individual lines correspond to individual cells.

(L-N) Wild-type and *mas5Δ* cells expressing indicated marker proteins were grown overnight to log-phase at 24°C prior to total protein extraction. SDS-PAGE resolved protein samples were subjected to western blotting using *anti-GFP* antibodies (top panels). HistoneH3 probing (bottom panels) served as a sample loading control.

CHAPTER IV - Discussion

4.1. Organization of the early secretory pathway compartments in fission yeast

As indicated by the COPII marker Sec24-GFP (Fig. 3.1.1A; and Sec13-GFP and Sec31-mCherry data not shown), the tER of *S. pombe* is not organized as several discrete structures in *P. pastoris* but resembles the delocalized tER of budding yeast (Rossanese et al., 1999). My data suggest that the tER is an ER subdomain distinct from ER sheets and tubules (Fig. 3.1.1D-F). Interestingly, when the ER sheets and tubules were sufficiently resolved in *rtn1*Δ cells I observed that the spatial distribution of the tER correlates to the ER tubules but not sheets (Fig 3.1.1F). In root meristem cells it was reported that the COPII vesicles form on multiple ER tubules (Staehelin and Kang, 2008). Possibly, the tER proteins such as the Arf-family GTPase Sar1 that have membrane bending capacity (Lee et al., 2005) could passively segregate to high curvature membranes (McMahon and Gallop, 2005; Voeltz et al., 2006). It is not clear if tER distribution proximal to tubules is functionally relevant. *S. cerevisiae* cells lacking the reticulons and Yop1 are not reported to exhibit secretion defects (De Craene et al., 2006; Voeltz et al., 2006), suggesting that the tER function in secretion does not require tubulated ER structure. I did notice a more pronounced tip recruitment of the tER and ER tubules in *rtn1*Δ cells suggesting that spatial distribution of the two ER subcompartment might rely on a common mechanism in interphase cells. Type-V myosin transport that regulates ER dynamics in various species including fission yeast could be involved (Fig. 3.2.10 and Estrada et al., 2003; Ueda et al., 2010; Wagner et al., 2011). In fact, the type-V myosin has been reported to deliver ER to the

growing bud (Estrada et al., 2003) and electron tomography suggests that these elements are primarily pulled as tubules (West et al., 2011). The putative myosin receptor linking the ER to type-V myosin is currently unknown but could localize specifically to the ER tubules.

My colocalization studies of two different Golgi compartments, marked by Anp1 and Sec72 (Fig. 3.1.2A and B), support the electron microscopy evidence (Johnson et al., 1973; Ayscough et al., 1993) of the Golgi apparatus in fission yeast being predominantly organized as adjacent stacks of few cisternae. In the view of Rossanese and colleagues, the difference in Golgi organization between two budding yeast species could arise from the difference in tER structure. Thus, the stable tER structure of *P. pastoris* would consecutively produce the novel *cis*-Golgi cisternae at a fixed location and maturation of these cisternae would give rise to a stacked Golgi apparatus structure. Absence of the long-lived, discrete tER sites in *S. cerevisiae* would cause the formation of novel Golgi cisternae at random locations, yielding dispersed Golgi entities. My results suggest that in fission yeast a relatively disorganized and yet stable tER is present as multiple entities that are accompanied by considerably fewer coherent Golgi stacks (Fig. 3.1.2A-C). Such structural organization of the early secretory pathway might reflect the possible involvement of the Golgi matrix (review by Barr and Short, 2003) or tether (Cai et al., 2007b) proteins in maintaining attachment between Golgi cisternae, a function that was lost in *S. cerevisiae* but is present in fission yeast. Deletion of the sole GRASP homologue does not alter the early secretory pathway organization of budding yeasts *P. pastoris* and *S. cerevisiae* (Levi et al., 2010).

Recent advances in high-speed microscopy have allowed the study of Golgi biogenesis and maturation (for review see Glick and Luini, 2011). My data provide further evidence supporting the cisternal progression model of Golgi maturation (Fig. 3.1.2F). Time required for Golgi cisternae identity change in fission yeast (Fig. 3.1.2G) was consistent with maturation dynamics reported previously in *S. cerevisiae* (Losev et al., 2006; Matsuura-Tokita et al., 2006). As judged by the dynamics of the early Golgi marker protein, Anp1-mCherry, *cis*-Golgi cisternae could also arise *de novo* (Fig. 3.1.2D and E), but the relationship of these biogenesis events to tER was more difficult to establish because of the large number of Sec24-GFP entities.

4.2. Polarization of the secretory pathway to the division site

The secretory pathway is a major player during cell polarization in many organisms including epithelial polarization in *Drosophila* embryos (Lecuit and Wieschaus, 2000), axon outgrowth in cultured rat embryonic neurons (Bradke and Dotti, 1997) and bud development in *S. cerevisiae* (reviewed by Finger and Novick, 1998). However, polarized secretion has been mainly studied with respect to the most downstream elements of the secretory pathway, such as the exocytotic machinery and the secretory vesicles. For instance, it was shown that the early buds of the budding yeast *S. cerevisiae* contain numerous secretory vesicles that are rarely observed in the mother cell (Preuss et al., 1992). Fission yeast cells with impaired exocyst components still form complete septa but exhibit defects in septum cleavage (Wang et al., 2002). To investigate secretory pathway spatial distribution I observed the spatial distribution of the fluorescently tagged proteins specific

to distinct early secretory pathway compartments during the cell cycle. Although I did not observe relocation of the ER sheets to the site of septation as judged by Ost1-GFP or Sec63-GFP (Fig. 3.1.3.3A and data not shown), I found a marked accumulation of tER and ER tubules (Fig. 3.1.3.1A and 3.1.3.3B). Surprisingly, polarization of the transitional and tubular ER subdomain is achieved through distinct molecular pathways reliant on Cdc15 and Mid1 functions respectively (Fig. 3.2 8).

Both *cis*- and *trans*-Golgi also established preferential localization to the division site in *S. pombe* (Fig. 3.1.3.1B and C). Thus it would be of interest to investigate the manner of ER subdomains distribution in other instances where Golgi accumulation at the growth sites was reported, such as *Candida albicans* (Rida et al., 2006). Golgi cisternae were reported to localize close to the incipient bud in *S. cerevisiae* (Preuss et al., 1992) and Golgi elements in *P. pastoris* were observed preferentially tracking towards the budding site (Bevis et al., 2002). Interestingly, the Golgi and the secretory vesicles accumulated at the sites of cell wall formation as judged by three-dimensional reconstruction of reverting *S. pombe* protoplasts (Osumi et al., 1998).

Given that the Golgi polarization during cell division is Cdc15-independent and less pronounced than that of tER, it is possible that the physiological role of tER equatorial accumulation is independent of the secretory pathway. The importance of ER recruitment has been reported in a study on the role of the gene *jagunal* in *Drosophila* oocyte development (Lee and Cooley, 2007). This study highlighted the importance of ER reorganization to the subcortical clusters as essential for increased exocytic membrane traffic that is vital for oocyte development. It was recently

proposed that the fine reticulation of the cortical ER, maintained by the ER shaping proteins, is required to allow efficient communication between the plasma membrane and the cytosol in cells with prominent plasma membrane-ER contacts (Zhang et al., 2012).

How could such polarization be achieved? One obvious solution is the recruitment of the secretion machinery by cytoskeletal elements. In *S. cerevisiae*, compromised function of actin cytoskeleton components abolishes polarized secretion (reviewed by Finger and Novick, 1998). In particular, polarized secretion at the bud requires intact actin cables and the type-V myosin Myo2 (Govindan et al., 1995). In *S. pombe*, both actin cables (Feierbach and Chang, 2001) and the type V myosins (Motegi et al., 2001) are necessary for the establishment of proper cell morphology. Indeed, I show that efficient cell tip recruitment of the ER in *S. pombe* relies on type-V myosin transport along actin cables (Fig. 3.2.10). However, it remains unclear what promotes the observed events of the ER detachment from the cell tips. It was recently shown that endocytic vesicle formation in budding yeast is initiated at the plasma membrane sites lacking the attached ER (Stradalova et al., 2012). The tight coupling between endocytosis and F-actin could explain my observations that actin patches and tip associated ER never colocalize (data not shown). Interestingly equatorial polarization of the tER does not require type-V myosin transport (Fig. 3.2.9D).

My results are consistent with the possibility that the EFC domain protein Cdc15 might function as the actomyosin ring component promoting biogenesis of the tER at the site of division. Lee et al. (2005) have shown that the COPII coat proteins alone were defective in forming COPII vesicles in

vitro and required Sar1 function to vesiculate lipid membranes. They suggested that the formation of membrane curvature by components other than COPII vesicle proteins might be vital to the formation of the vesicles. They also suggested that factors such as the microtubule-driven membrane deformation characteristic of mammalian cells could generate curvature that could be subsequently acted upon by the cytosolic coat proteins. Cdc15 possesses an EFC domain that has been shown to induce membrane tubulation in other proteins (Tsujita et al., 2006). As I neither observed any net movement of COPII-positive membranes toward the division site (Fig. 3.2.9A-C) nor involvement of type V myosins (Fig. 3.2.9D) in this phenomenon, an exciting possibility is that Cdc15 might be involved in generating membrane curvature and thus promote tER formation in the vicinity of the actomyosin ring. I found that Cdc15 was necessary and sufficient for the medial accumulation of the tER (Fig. 3.2.5 and 3.2.6). Overexpression of the Cdc15 EFC domain alone or of Cdc15 lacking the EFC domain was not sufficient for the induction of tER recruitment to the equatorial region in interphase cells (data not shown). Alternative, less direct mechanisms could also be envisioned. Sec16 phosphorylation by MAPK has been proposed to regulate the number and size of tER sites (Farhan et al., 2008; Zacharogianni et al., 2011). Interestingly, the MAPK Pmk1 localizes to the division site in fission yeast (Madrid et al., 2006) and *pmk1Δ* cells have a cell separation defect (Toda et al., 1996).

Analysis of the novel *cdc15-22* allele suggests that Cdc15 is also required for the tER polarization in post-metaphase cells (Fig. 3.2.7). The slow ring constriction phenotype was previously noted in cells where Cdc15 lacked

the SH3 domain but the tER spatial distribution was not analyzed in this genetic background (Roberts-Galbraith et al., 2009). It is tempting to speculate that loss of tER polarization to the division site impedes secretion and thus delays septum formation. Alternatively, defects in Sid2 recruitment to the division site might be responsible for altered ring dynamics (Fig. 3.2.7G). Cdc15 was not required for localization of Golgi cisternae, suggesting that the recruitment of tER and Golgi to the division site may occur through different mechanisms. My experiments together with the published research suggest that actin structures could possibly act as a delivery or anchor system for Golgi apparatus.

The SIN pathway has been shown to be vital for targeted secretion because its inactivation hinders secretion of the septum material at the division site (Liu et al., 2002). My data show that the early secretory pathway polarization occurs before SIN activation and does not require its function (Fig. 3.2.4.1 and 3.2.4.2), therefore suggesting that recruitment of the early secretory machinery and post-Golgi secretion are differentially regulated. Thus it seems that SIN functions in activating most downstream secretion events, such as post-Golgi vesicle trafficking. It has been suggested that Cdc15 functions downstream of SIN in regulating septum assembly (Marks et al., 1992; Wachtler et al., 2006) and proper ring formation (Hachet and Simanis, 2008). My analysis of the *cdc15-22* mutant suggests that Cdc15 might also be involved in promoting Sid2 localization to the division site (Fig. 3.2.7G). It is important to note here that SIN signaling integrity is essential to post-metaphase ring maintenance in *cps1-191* mutants (Liu et al., 1999).

In conclusion, my work identifies the fission yeast *S. pombe* as an interesting system for studying the phenomena of secretion and polarity establishment. I propose that the polarization of both tER and Golgi might fulfill the need for massive vesicle trafficking events occurring at the division site. It would be interesting to gain a better understanding of the role of Cdc15 and to identify additional molecular determinants of the process in future.

4.3. Remodeling of cell polarity in response to ambient temperature

On one hand, robust polarity mechanisms ensure consistent cell morphology. Conversely, cells must dynamically reorient polarity axes in response to environmental stimuli such as chemoattractants (Li et al., 2003; Bendezú and Martin, 2012) or localized injury (Kono et al., 2012). A variety of stresses, including heat and osmolytes, cause a biphasic relocalization of the yeast cell wall remodeling machinery (Bickle et al., 1998; Bao, 2001; Petersen and Hagan, 2005; Robertson and Hagan, 2008). After rapidly redistributing the growth machinery throughout the cell cortex, both fission and budding yeast restore polarity at elevated temperature (Bickle et al., 1998; Petersen and Hagan, 2005 and Fig. 3.3.1.1 and 3.3.1.2). Interestingly, my results suggest that heat-stress distinctly affects cell tip specification and recruitment of the growth machinery to cell poles.

Osmotic-stress leads to stalling of microtubule dynamics suggesting that the cell tip specification might be impaired under these conditions (Tatebe et al., 2008). However, I did not observe a similar phenomenon upon temperature shift (data not shown). In fact, none of the landmark proteins investigated in this study relocalized in response to elevated temperature (Fig.

3.3.1.1F, 3.3.1.2B and C). Pom1 function in restricting Rga4 to the lateral cell cortex of late G₂ cells also remained intact (Tatebe et al., 2008, Fig. 3.3.2.1D). Primarily involved in initiating bipolar growth, the Tea4 recruitment of For3 to cell tips is an auxiliary mechanism of localizing actin cable nucleation to cell tips (Martin et al., 2005). Whereas several types of stresses have been shown to promote branching of *tea* mutants (Mata and Nurse, 1997; Bähler and Pringle, 1998; Tatebe et al., 2005), I never observed ectopic growth sites in heat-stressed wild-type cells nor in mutants with elevated levels of heat-stress associated transcription (data not shown).

Upon heat-stress, the mechanisms restricting Cdc42 activity to the cell tips are overridden and the active Cdc42 redistributes throughout the cell cortex (Fig. 3.3.1.1I). Cdc42 is likely to contribute to the recruitment of both F-actin and the exocyst to the cell sides thus allowing redistribution of the cell wall remodeling machinery throughout the cell cortex (Fig. 3.3.1.1G-I and 3.3.1.2D-F). Dominant negative forms of Rac and Cdc42 have been reported to impair F-actin remodeling upon hypertonic stress in CHO cells (Ciano et al., 2002). The role of Cdc42 in cytoskeletal dynamics upon stress has not been reported in the budding yeast where research efforts focused on the closely related small GTPase Rho1. The cell wall sensors Wsc1 and Mid2 have been shown to interact with Rom2 GEF and stimulate the Rho1 nucleotide exchange (Philip and Levin, 2001). I find that activity of Cdc42 during heat-stress similarly requires intact Cdc42-GEFs with Gef1 playing a more prominent role than Scd1 (Fig. 3.3.3B and C). One possibility is that the heat-stress increases lateral diffusion of the Cdc42 activated exclusively at the cell tips. However, the reported diffusion rates of the membrane bound Cdc42

render this explanation insufficient (Marco et al., 2007). My GEF localization analyses are consistent with an alternative model where Cdc42 activation occurs at the lateral cell cortex during heat stress (Fig. 3.3.2.1B and C). Since Gef1 overexpression is sufficient to activate Cdc42 throughout the cell cortex (Coll et al., 2003), identification of pathways promoting Gef1 nucleotide exchange function would be an interesting direction to pursue. In this respect the MOR signaling kinase Orb6 is of particular interest. Inhibition of Orb6 kinase activity promotes relocalization of active Cdc42 and Gef1, but not Scd1 to the lateral cell cortex (Das et al., 2009). Furthermore, Gef1 is an *in vitro* Orb6 target (Das et al., 2009). The Orb6 regulator, Nak1/Orb3 kinase is a fission yeast homologue of the Germinal-Center Kinases (GCK) implicated in stress response as well as apoptosis and cancer (Kanai et al., 2005, reviewed by Dan et al., 2001; Boyce and Andrianopoulos, 2011). Whether and how Rho1 and Cdc42 modules are coordinated during heat-stress remains to be explored with potential links involving regulators such as RhoGDI, RhoGAP Rga8 (Sinha and Yang, 2008; Tiedje et al., 2008) or effectors such as formins (Nakano et al., 2002; Dong, 2003). The Cdc42-GAP Rga4 apparently counteracts Cdc42 activation at the lateral cell cortex and thus likely preventing precocious delocalization of Cdc42 activity (Fig. 3.3.3D and F).

A budding yeast study where osmotic stabilizers and hyper-activation of the MAPK signaling pathways rescue specific Hsf1 mutants suggests a role for the heat-stress associated transcription in maintaining cell wall integrity (Imazu and Sakurai, 2005). Here I present evidence that Hsf1 mediated transcription might also modulates cell polarity (Fig. 3.3.4F-I). However, my analysis of cells with elevated levels of heat-associated transcription did not

indicate significant repression nor activation of genes encoding known key regulators of cell polarity. Hsp90 mediated stabilization of kinases regulating cell polarity could mediate the Hsf1 regulation of morphogenesis (Taipale et al., 2012). Hsf1 induction of small chaperones that sever actin filaments might also play a role (reviewed by Mounier and Arrigo, 2002). Furthermore, polo kinase Plo1 has been shown to play a role in repolarizing actin upon stress in fission yeast (Petersen and Hagan, 2005). Isolation and characterization of *mas5* Δ cells provides a framework for better understanding of the roles heat-stress associated transcription has in polarized growth.

The complex Hsf1 regulation allows a rapid response to diverse environmental stressors (reviewed by Akerfelt et al., 2010). The SSA subfamily chaperones are likely primary sensors for some of the stressors such as thiol-reactive compounds. The putative roles of the Hsp40 chaperones during stress remain vague. A recent screening has isolated the budding yeast Mas5 and Ssa2 homologues as potent repressors of Hsf1 (Brandman et al., 2012), but did not address the underlying mechanism. Furthermore, human Mas5 and Ssa2 homologues have been shown to bind Hsf1 *in vitro* (Shi et al., 1998), an interaction I was unable to detect in fission yeast possibly due to low binding affinities or the transient nature of interaction. The cell biological studies of Hsf1 suggest regulation at the level of nucleo-cytoplasmic shuttling (Baler et al., 1993; Zandi et al., 1997; Vujanac and Fenaroli, 2005). However, the Hsp90 regulation of the Hsf1 nuclear export and involvement of Hsp70•Hsp40 complex have not been previously described (Fig. 3.3.6). Notably, several types of stress decrease the importin- α and β mediated nuclear import (Furuta et al., 2004; Miyamoto et al., 2004; Kelley and Paschal,

2007) but promote Hsp70 nuclear localization through an alternative mechanism reliant on a conserved protein Hikeshi (Kose et al., 2012). Interestingly this pathway is necessary for attenuation and reversal of the thermal stress response (Kose et al., 2012). The rapid nuclear efflux of Hsf1 in heat-stressed cells is in line with dynamic studies of Hsf1 activity (Gasch et al., 2000; Chen et al., 2003; Rieger et al., 2005; Zobeck et al., 2010). Though much of heat shock associated transcription is transient, more recent transcriptomics analysis of HSP transcripts indicates deviation from this dynamic pattern and existence of genes with expression constitutively regulated by temperature (Gasch et al., 2000).

The budding yeast Mas5 homologue, Ydj1 has been recently reported as a growth rate sensor that regulates mitotic commitment (Vergés et al., 2007; Ferrezuelo et al., 2012). Taking into account my findings, it is tempting to speculate on the role of Mas5 in the crosstalk between stress and growth. Interesting in that regard is the observation that slow growing cells are cross-protected for heat-shock (Lu et al., 2009). In fact, slow growth of budding yeast cells lacking Hsp70 chaperones SSA1 and SSA2 is rescued by an inactivating mutation of Hsf1 (Halladay and Craig, 1995).

I find that cell adapting to growth at elevated temperature undergo a stage of monopolar growth (Fig. 3.3.1.1B and E). Transition to bipolar growth requires cells to enter the G₂ stage of the cell cycle (Mitchison and Nurse, 1985). Stress has been shown to modulate cell cycle by stabilizing the Wee kinase Swe1 in budding yeast but fission yeast *wee1* mutants commence bipolar growth at the same cell size as wild-type cells (Mitchison and Nurse, 1985). Furthermore, transient depolymerization of actin cytoskeleton by LatA

treatment also stalls the cell cycle progression (Rupes et al., 2001) yet allows for transition to bipolar growth in monopolar *ssp1Δ* mutants (Rupes et al., 1999). Mutations in genes involved in tip specification cause impaired NETO (Mata and Nurse, 1997; Bähler and Pringle, 1998; Tatebe et al., 2005) but, as discussed above, my results suggests that these mechanisms are largely unaffected by heat-stress. Importantly, NETO defects have been reported in cells with perturbed regulation of the Cdc42 activity. The GFP-Cdc42 hypomorph cells exhibit monopolar growth (data not shown). Cells lacking *Gef1* have been shown to delay NETO (Coll et al., 2003). The *orb2-34* cells carrying a point mutation in the Cdc42 effector PAK kinase (Verde et al., 1995; Das et al., 2012) are also monopolar. The budding yeast PAK homologues physically interact with the scaffold protein Bem1 to recruit the Cdc42-GEF and thus promote positive feedback (Kozubowski et al., 2008). Simultaneously, PAK kinases modulate Cdc42-GEF function through direct phosphorylation (Bose, 2000; Gulli et al., 2000). The observed decrease in cortical levels of Cdc42-GEFs (Fig. 3.3.2.1B and C) could provide an explanation for the monopolar growth in cells recovering from heat-stress. This hypothesis is further supported by my findings that late G₂ phase *mas5Δ* cells are monopolar despite having properly specified cell tips (Fig. 3.3.7.1A-B and 3.3.7.2C-E). The decreased cortical levels of Cdc42-GEFs might underlie the observations that active Cdc42 could be recruited to both cell ends in *mas5Δ* cells, but only the old cell end was capable of maintaining high Cdc42 activity for periods sufficient to promote growth (Fig. 3.3.7.1C-F). I also observed diminished cortical levels of Rga4 upon heat-stress, in cells grown at elevated temperature and *mas5Δ* cells (Fig. 3.3.2.1D, 3.3.2.2L and

3.3.7.1I). Since Rga4 down- and up-regulation lead to increased and decreased cell diameter (Das et al., 2007; Tatebe et al., 2008 and data not shown), it is possible that decrease of GAP cortical levels accommodates the maintenance of a constant cell diameter in cells with diminished cortical GEFs due to increased heat-stress associated transcription. Interestingly, the decrease in cortical levels of Cdc42-GEFs and GAP upon heat-stress is not a consequence of diminished protein levels but might be a consequence of their posttranslational modifications (Fig. 3.3.2.2A-C) or recruitment to intracellular structures (Fig. 3.3.2.1B-D).

The total and cortically associated protein levels of Cdc42-GEFs and GAP exhibit an inverse correlation to the environmental temperature in unstressed cells (Fig. 3.3.2.2J-O), yet cells efficiently maintain active Cdc42 at the cell tips and undergo NETO at all temperatures examined (Fig. 3.3.2.2H and I). These results point to potential mechanism allowing temperature compensation of the Cdc42-GTPase module. The eukaryotic circadian clocks are complex feedback networks that buffer the oscillation period against temperature (reviewed by Hogenesch and Ueda, 2011). The temperature compensation of the *Neurospora* circadian clock relies on phosphorylation of the key regulator Frq by the casein-kinase2 (Mehra et al., 2009) a gene isolated as Orb5 in a fission yeast morphogenesis screen (Snell and Nurse, 1994). Furthermore, Hsf1 regulates temperature compensation of the mammalian circadian clocks (Buhr et al., 2010). Polarity establishment and maintenance are also regulated through complex feedback networks of the Cdc42-GTPase module that might require temperature compensation. In that context the low levels of Cdc42 activity and NETO defects in *mas5Δ* and

ssa2Δ cells might be a consequence of inadequate regulation of the temperature compensation of the Cdc42-GTPase module. Taken together my results are consistent with a hypothesis where cells adjust the Cdc42GTPase module to allow for efficient polarized growth at different environmental temperatures.

4.4. Conclusions and perspectives

The research focus of my graduate studies has been placed on investigating the structural and spatial organization of the secretory pathway and the mechanisms governing cell polarity upon temperature perturbations.

I show that in *S. pombe* the tER is present as multiple stable ER subdomains that are distinct from both ER sheets and tubules. Though I could observe spatial correlation between transitional and tubular ER I did not observe a functional relationship. Investigating the role of recently isolated ER shaping proteins such as Sey1 and Lnp1 in tER dynamics might provide further insight. My analyses of the distinct Golgi subcompartment fluorescent marker proteins support electron microscopy results that in fission yeast, the Golgi cisternae organize into stacks of several elements though individual cisternae can also exist. Thus mechanisms regulating Golgi cisternae stacking might be particularly dynamic in *S. pombe* and possibly prone to genetic and experimental perturbations shifting the balance between stacked and unstacked Golgi. Future work in this respect should address the function of putative structural Golgi proteins such as GRASPs and the effects of increased and decreased trafficking. I also show that *cis*-Golgi elements can form *de novo* and mature in accordance with the cisternal maturation model suggesting that the mechanisms reported in budding yeast exhibit a degree of evolutionary conservation.

I have shown that in fission yeast the Golgi apparatus and both tubular and transitional ER become polarized during cell division in an actomyosin ring dependent manner. Data presented here show that tubular and transitional ER accumulation to the division site are distinct phenomena with the former

relying on the anilin-like protein Mid1 and the later requiring the EFC domain protein Cdc15. In a visual screen I have isolated a novel *cdc15* allele that allowed me to conclude that Cdc15 function is required to polarize the tER throughout the course of cytokinesis. Furthermore, I show that Cdc15 overexpression in interphase-arrested cells is sufficient to promote tER equatorial accumulation. The correlation between tER polarization and ring constriction defects in *cdc15-22* cells suggests that the tight coupling of ring formation and secretory pathway polarization could be necessary for fission yeast to timely prime the site for intense secretion that is associated with building a septum across the cylindrical cell. Modern high-throughput screening strategies that are coupled to automated imaging make it feasible to conduct a genome wide screening for mutants impaired in tER spatial distribution. Furthermore, *in vitro* studies on COPII vesicle budding efficiency could assess whether Cdc15 is directly involved in promoting tER polarization. Interestingly, while type-V myosin transport along actin cables is required for ER attachment to the cell tips, the tER recruitment to the division site is independent of it.

I propose that although different organisms could undergo polarization of the secretory pathway at various stages of its biogenesis, the common feature of the examples available in the published literature could be a necessity for a rapid increase in cell surface area. It is conceivable that such intense events might require massive trafficking that could be achieved by concentrating the entire secretory machinery to the proximity of the secretion site, rather than relying on a long-range delivery of post-Golgi vesicles.

Fission yeast cells robustly maintain rod-shaped morphology under different environmental conditions. Here I show that upon mild heat-stress, activity of Cdc42 is no longer confined to the cortical domains specified by the polarisome. The transient redistribution of the Cdc42 activity is accompanied by relocalization of its effectors regulating cellular growth. I show that active Cdc42 recruitment to the lateral cell cortex upon heat-stress relies on its GEFs. However, the physiological significance of such a mechanism is unclear. Redistribution of actin cytoskeleton upon heat-stress has been reported in multiple species and it is tempting to speculate that it might be a part of an evolutionarily conserved response rather than a passive consequence of stress. Relocalizing the growth machinery to the cell sides might allow cell wall reinforcement. Thus it would be interesting to employ electron microscopy and explore the cell wall structure in heat-stressed *gef1Δ* cells as well as their survival under these conditions.

How Gef1 is stimulated to promote transient recruitment of active Cdc42 to the cell sides remains unexplored. In budding yeast the cell wall integrity pathway has been suggested to promote Rho1 relocalization during heat-stress by engaging its GEF Rom2. A crosstalk between Rho-GTPases has been reported and might also regulate Cdc42 activity under stress. Alternatively, cell wall integrity pathways may act more directly on the Cdc42-GTPase module. Characterizing heat-stress response in mutants of these molecular pathways is likely to provide further insight. An intriguing possibility is that temperature passively affects the rates of biochemical processes mediating positive feedback between Cdc42 and its regulators and

in such a manner the mechanisms confining Cdc42 activity to the cell tips fail upon temperature increase.

In initial stages of adaptation the cells attain monopolar growth but eventually restore growth at both cell tips. I show that Hsf1 overexpression also induces monopolar growth in late G₂ cells suggesting that repression of Hsf1 transcriptional activity after heat-stress might be required for bipolar growth. Analysis of *mas5Δ* and *ssa2Δ* cells also suggests that increased levels of heat-stress associated transcription impede bipolar growth. However, analysis of gene expression profiles in cells with elevated heat-stress associated transcription has not singled out a particular gene or a group of genes responsible and further studies with this aim will be required. I show that the cortical levels of Cdc42 GEFs and GAP are decreased in *mas5Δ* and *ssa2Δ* cells that are unable to maintain active Cdc42 at the cell tips. However, as wild-type cells restore polarized growth and adapt to elevated temperature, the cortical levels of the Cdc42 GEFs and GAP are drastically decreased while the active Cdc42 levels at the tips of cells growing at different temperature remain comparable. How this is achieved remains to be explored but expanding analysis of the temperature effect on other Cdc42-GTPase module components could provide further insights into this interesting problem.

Based on these results I propose that the temperature sensitive regulation of the Cdc42 GTPase module allows efficient growth at different environmental temperatures.

Bibliography

- Aalto, M.K., Ronne, H., and Keränen, S. (1993). Yeast syntaxins Sso1p and Sso2p belong to a family of related membrane proteins that function in vesicular transport. *The EMBO Journal* *12*, 4095–4104.
- Adamo, J.E., Moskow, J.J., Gladfelter, A.S., Viterbo, D., Lew, D.J., and Brennwald, P.J. (2001). Yeast Cdc42 functions at a late step in exocytosis, specifically during polarized growth of the emerging bud. *The Journal of Cell Biology* *155*, 581–592.
- Adamo, J.E., Rossi, G., and Brennwald, P. (1999). The Rho GTPase Rho3 has a direct role in exocytosis that is distinct from its role in actin polarity. *Molecular Biology of the Cell* *10*, 4121–4133.
- Akerfelt, M., Morimoto, R.I., and Sistonen, L. (2010). Heat shock factors: integrators of cell stress, development and lifespan. *Nature Reviews. Molecular Cell Biology* *11*, 545–555.
- Alberts, A.S. (2001). Identification of a carboxyl-terminal diaphanous-related formin homology protein autoregulatory domain. *The Journal of Biological Chemistry* *276*, 2824–2830.
- Alberts, B., Johnson, A., Lewis, J., Raff, M., Roberts, K., and Walter, P. (2007). *Molecular Biology of the Cell* (Garland Science).
- Almonacid, M., Moseley, J.B., Janvore, J., Mayeux, A., Fraiser, V., Nurse, P., and Paoletti, A. (2009). Spatial control of cytokinesis by Cdr2 kinase and Mid1/anillin nuclear export. *Current Biology : CB* *19*, 961–966.
- Alvarez-Tabares, I., Grallert, a., Ortiz, J.-M., and Hagan, I.M. (2007). *Schizosaccharomyces pombe* protein phosphatase 1 in mitosis, endocytosis and a partnership with Wsh3/Tea4 to control polarised growth. *Journal of Cell Science* *120*, 3589–3601.
- Ambrose, J.C., and Cyr, R. (2008). Mitotic spindle organization by the preprophase band. *Molecular Plant* *1*, 950–960.
- Anitei, M., and Hoflack, B. (2011). Exit from the trans-Golgi network: from molecules to mechanisms. *Current Opinion in Cell Biology* *23*, 443–451.
- Antonny, B., Madden, D., Hamamoto, S., Orci, L., and Schekman, R. (2001). Dynamics of the COPII coat with GTP and stable analogues. *Nature Cell Biology* *3*, 531–537.
- Arai, R., and Mabuchi, I. (2002). F-actin ring formation and the role of F-actin cables in the fission yeast *Schizosaccharomyces pombe*. *Journal of Cell Science* *115*, 887–898.
- Arasada, R., and Pollard, T.D. (2011). Distinct roles for F-BAR proteins Cdc15p and Bzz1p in actin polymerization at sites of endocytosis in fission yeast. *Current Biology : CB* *21*, 1450–1459.
- Aridor, M., Fish, K.N., Bannykh, S., Weissman, J., Roberts, T.H., Lippincott-Schwartz, J., and Balch, W.E. (2001). The Sar1 GTPase coordinates biosynthetic cargo selection with endoplasmic reticulum export site assembly. *The Journal of Cell Biology* *152*, 213–229.

- Ayscough, K., Hajibagheri, N.M., Watson, R., and Warren, G. (1993). Stacking of Golgi cisternae in *Schizosaccharomyces pombe* requires intact microtubules. *Journal of Cell Science* *106* (Pt 4, 1227–1237.
- Balasubramanian, M.K., Bi, E., and Glotzer, M. (2004). Comparative analysis of cytokinesis in budding yeast, fission yeast and animal cells. *Current Biology* : CB *14*, R806–18.
- Balasubramanian, M.K., McCollum, D., Chang, L., Wong, K.C., Naqvi, N.I., He, X., Sazer, S., and Gould, K.L. (1998). Isolation and characterization of new fission yeast cytokinesis mutants. *Genetics* *149*, 1265–1275.
- Baler, R., Dahl, G., and Voellmy, R. (1993). Activation of Human Heat Shock Genes Is Accompanied by Oligomerization , Modification , and Rapid Translocation of Heat Shock Transcription Factor HSF1. *13*, 2486–2496.
- Bannykh, S.I., Rowe, T., and Balch, W.E. (1996). The organization of endoplasmic reticulum export complexes. *The Journal of Cell Biology* *135*, 19–35.
- Bao, S. (2001). The Highly Conserved Protein Methyltransferase, Skb1, Is a Mediator of Hyperosmotic Stress Response in the Fission Yeast *Schizosaccharomyces pombe*. *Journal of Biological Chemistry* *276*, 14549–14552.
- Barlowe, C., Orci, L., Yeung, T., Hosobuchi, M., Hamamoto, S., Salama, N., Rexach, M.F., Ravazzola, M., Amherdt, M., and Schekman, R. (1994). COPII: a membrane coat formed by Sec proteins that drive vesicle budding from the endoplasmic reticulum. *Cell* *77*, 895–907.
- Barlowe, C., and Schekman, R. (1993). SEC12 encodes a guanine-nucleotide-exchange factor essential for transport vesicle budding from the ER. *Nature* *365*, 347–349.
- Barr, F. a, and Gruneberg, U. (2007). Cytokinesis: placing and making the final cut. *Cell* *131*, 847–860.
- Barr, F.A. (2004). Golgi inheritance: shaken but not stirred. *The Journal of Cell Biology* *164*, 955–958.
- Barr, F.A., Puype, M., Vandekerckhove, J., and Warren, G. (1997). GRASP65, a protein involved in the stacking of Golgi cisternae. *Cell* *91*, 253–262.
- Barr, F.A., and Short, B. (2003). Golgins in the structure and dynamics of the Golgi apparatus. *Current Opinion in Cell Biology* *15*, 405–413.
- Barrowman, J., Bhandari, D., Reinisch, K., and Ferro-Novick, S. (2010). TRAPP complexes in membrane traffic: convergence through a common Rab. *Nature Reviews. Molecular Cell Biology* *11*, 759–763.
- Becker, B., Bölinger, B., and Melkonian, M. (1995). Anterograde transport of algal scales through the Golgi complex is not mediated by vesicles. *Trends in Cell Biology* *5*, 305–307.
- Behrens, R., and Nurse, P. (2002). Roles of fission yeast tea1p in the localization of polarity factors and in organizing the microtubular cytoskeleton. *The Journal of Cell Biology* *157*, 783–793.

- Bement, W.M., Benink, H.A., and Von Dassow, G. (2005). A microtubule-dependent zone of active RhoA during cleavage plane specification. *The Journal of Cell Biology* *170*, 91–101.
- Benchimol, M., Ribeiro, K.C., Mariante, R.M., and Alderete, J.F. (2001). Structure and division of the Golgi complex in *Trichomonas vaginalis* and *Tritrichomonas foetus*. *European Journal of Cell Biology* *80*, 593–607.
- Bendezú, F.O., and Martin, S.G. (2011). Actin cables and the exocyst form two independent morphogenesis pathways in the fission yeast. *Molecular Biology of the Cell* *22*, 44–53.
- Bendezú, F.O., and Martin, S.G. (2012). Cdc42 Explores the Cell Periphery for Mate Selection in Fission Yeast. *Current Biology* : CB 1–6.
- Bendezú, F.O., Vincenzetti, V., and Martin, S.G. (2012). Fission yeast Sec3 and Exo70 are transported on actin cables and localize the exocyst complex to cell poles. *PLoS One* *7*, e40248.
- Bentley, M., Liang, Y., Mullen, K., Xu, D., Sztul, E., and Hay, J.C. (2006). SNARE status regulates tether recruitment and function in homotypic COPII vesicle fusion. *The Journal of Biological Chemistry* *281*, 38825–38833.
- Berro, J., Sirotkin, V., and Pollard, T.D. (2010). Mathematical modeling of endocytic actin patch kinetics in fission yeast: disassembly requires release of actin filament fragments. *Molecular Biology of the Cell* *21*, 2905–2915.
- Bevis, B.J., Hammond, A.T., Reinke, C.A., and Glick, B.S. (2002). De novo formation of transitional ER sites and Golgi structures in *Pichia pastoris*. *Nature Cell Biology* *4*, 750–756.
- Bi, X., Corpina, R.A., and Goldberg, J. (2002). Structure of the Sec23/24-Sar1 pre-budding complex of the COPII vesicle coat. *Nature* *419*, 271–277.
- Bicho, C.C., Kelly, D.A., Snaith, H. a, Goryachev, A.B., and Sawin, K.E. (2010). A catalytic role for Mod5 in the formation of the Tea1 cell polarity landmark. *Current Biology* : CB *20*, 1752–1757.
- Bickle, M., Delley, P., Schmidt, A., and Hall, M.N. (1998). Cell wall integrity modulates RHO1 activity via the exchange factor ROM2. *17*, 2235–2245.
- Bieling, P., Laan, L., Schek, H., Munteanu, E.L., Sandblad, L., Dogterom, M., Brunner, D., and Surrey, T. (2007). Reconstitution of a microtubule plus-end tracking system in vitro. *Nature* *450*, 1100–1105.
- Block, M.R., Glick, B.S., Wilcox, C.A., Wieland, F.T., and Rothman, J.E. (1988). Purification of an N-ethylmaleimide-sensitive protein catalyzing vesicular transport. *Proceedings of the National Academy of Sciences of the United States of America* *85*, 7852–7856.
- Blumental-Perry, A., Haney, C.J., Weixel, K.M., Watkins, S.C., Weisz, O. a, and Aridor, M. (2006). Phosphatidylinositol 4-phosphate formation at ER exit sites regulates ER export. *Developmental Cell* *11*, 671–682.
- Boettcher, A.J., Munson, M., Sivaram, M.V.S., Saporita, J.A., Furgason, M.L.M., Boettcher, A.J., and Munson, M. (2005). Dimerization of the Exocyst Protein Sec6p and Its Interaction with the t-SNARE Sec9p. *Biochemistry* *44*, 6302–6311.

- Bonfanti, L., Mironov, A.A., Martínez-Menárguez, J.A., Martella, O., Fusella, A., Baldassarre, M., Buccione, R., Geuze, H.J., and Luini, A. (1998). Procollagen traverses the Golgi stack without leaving the lumen of cisternae: evidence for cisternal maturation. *Cell* 95, 993–1003.
- Bonifacino, J.S., and Glick, B.S. (2004). The mechanisms of vesicle budding and fusion. *Cell* 116, 153–166.
- Bose, I. (2000). Assembly of Scaffold-mediated Complexes Containing Cdc42p, the Exchange Factor Cdc24p, and the Effector Cla4p Required for Cell Cycle-regulated Phosphorylation of Cdc24p. *Journal of Biological Chemistry* 276, 7176–7186.
- Boyce, K.J., and Andrianopoulos, A. (2011). Ste20-related kinases: effectors of signaling and morphogenesis in fungi. *Trends in Microbiology* 19, 400–410.
- Boyd, C., Hughes, T., Pypaert, M., and Novick, P. (2004). Vesicles carry most exocyst subunits to exocytic sites marked by the remaining two subunits, Sec3p and Exo70p. *The Journal of Cell Biology* 167, 889–901.
- Bradke, F., and Dotti, C.G. (1997). Neuronal polarity: vectorial cytoplasmic flow precedes axon formation. *Neuron* 19, 1175–1186.
- Brandman, O., Stewart-Ornstein, J., Wong, D., Larson, A., Williams, C.C., Li, G.-W., Zhou, S., King, D., Shen, P.S., Weibezahn, J., et al. (2012). A Ribosome-Bound Quality Control Complex Triggers Degradation of Nascent Peptides and Signals Translation Stress. *Cell* 151, 1042–1054.
- Bringmann, H., and Hyman, A. a (2005). A cytokinesis furrow is positioned by two consecutive signals. *Nature* 436, 731–734.
- Browning, H., and Hackney, D.D. (2005). The EB1 homolog Mal3 stimulates the ATPase of the kinesin Tea2 by recruiting it to the microtubule. *The Journal of Biological Chemistry* 280, 12299–12304.
- Browning, H., Hackney, D.D., and Nurse, P. (2003). Targeted movement of cell end factors in fission yeast. *Nature Cell Biology* 5, 812–818.
- Browning, H., Hayles, J., Mata, J., Aveline, L., Nurse, P., and McIntosh, J.R. (2000). Tea2p is a kinesin-like protein required to generate polarized growth in fission yeast. *The Journal of Cell Biology* 151, 15–28.
- Brunner, D., and Nurse, P. (2000). CLIP170-like tip1p spatially organizes microtubular dynamics in fission yeast. *Cell* 102, 695–704.
- Buhr, E.D., Yoo, S.-H., and Takahashi, J.S. (2010). Temperature as a universal resetting cue for mammalian circadian oscillators. *Science (New York, N.Y.)* 330, 379–385.
- Burbelo, P.D., Drechsel, D., and Hall, A. (1995). A conserved binding motif defines numerous candidate target proteins for both Cdc42 and Rac GTPases. *The Journal of Biological Chemistry* 270, 29071–29074.
- Burkard, M.E., Randall, C.L., Larochele, S., Zhang, C., Shokat, K.M., Fisher, R.P., and Jallepalli, P. V (2007). Chemical genetics reveals the requirement for Polo-like kinase 1 activity in positioning RhoA and triggering cytokinesis

- in human cells. *Proceedings of the National Academy of Sciences of the United States of America* *104*, 4383–4388.
- Burri, L., Varlamov, O., Doege, C.A., Hofmann, K., Beilharz, T., Rothman, J.E., Söllner, T.H., and Lithgow, T. (2003). A SNARE required for retrograde transport to the endoplasmic reticulum. *Proceedings of the National Academy of Sciences of the United States of America* *100*, 9873–9877.
- Busch, K.E., and Brunner, D. (2004). The microtubule plus end-tracking proteins mal3p and tip1p cooperate for cell-end targeting of interphase microtubules. *Current Biology : CB* *14*, 548–559.
- Busch, K.E., Hayles, J., Nurse, P., and Brunner, D. (2004). Tea2p kinesin is involved in spatial microtubule organization by transporting tip1p on microtubules. *Developmental Cell* *6*, 831–843.
- Bähler, J., and Pringle, J.R. (1998). Pom1p, a fission yeast protein kinase that provides positional information for both polarized growth and cytokinesis. *Developmental Cell* *5*, 1356–1370.
- Bähler, J., Steever, A.B., Wheatley, S., Wang, Y. I., Pringle, J.R., Gould, K.L., and McCollum, D. (1998). Role of polo kinase and Mid1p in determining the site of cell division in fission yeast. *The Journal of Cell Biology* *143*, 1603–1616.
- Cai, H., Reinisch, K., and Ferro-Novick, S. (2007a). Coats, tethers, Rabs, and SNAREs work together to mediate the intracellular destination of a transport vesicle. *Developmental Cell* *12*, 671–682.
- Cai, H., Yu, S., Menon, S., Cai, Y., Lazarova, D., Fu, C., Reinisch, K., Hay, J.C., and Ferro-Novick, S. (2007b). TRAPP1 tethers COPII vesicles by binding the coat subunit Sec23. *Nature* *445*, 941–944.
- Cai, Y., Chin, H.F., Lazarova, D., Menon, S., Fu, C., Cai, H., Sclafani, A., Rodgers, D.W., De La Cruz, E.M., Ferro-Novick, S., et al. (2008). The structural basis for activation of the Rab Ypt1p by the TRAPP membrane-tethering complexes. *Cell* *133*, 1202–1213.
- Canman, J.C., Lewellyn, L., Laband, K., Smerdon, S.J., Desai, A., Bowerman, B., and Oegema, K. (2008). Inhibition of Rac by the GAP activity of centralspindlin is essential for cytokinesis. *Science (New York, N.Y.)* *322*, 1543–1546.
- Cao, X., Ballew, N., and Barlowe, C. (1998). Initial docking of ER-derived vesicles requires Uso1p and Ypt1p but is independent of SNARE proteins. *The EMBO Journal* *17*, 2156–2165.
- Carnahan, R.H., and Gould, K.L. (2003). The PCH family protein, Cdc15p, recruits two F-actin nucleation pathways to coordinate cytokinetic actin ring formation in *Schizosaccharomyces pombe*. *The Journal of Cell Biology* *162*, 851–862.
- Castrillon, D.H., and Wasserman, S.A. (1994). Diaphanous is required for cytokinesis in *Drosophila* and shares domains of similarity with the products of the limb deformity gene. *Development (Cambridge, England)* *120*, 3367–3377.

- Cavalier-Smith, T. (2006). Cell evolution and Earth history: stasis and revolution. *Philosophical Transactions of the Royal Society of London. Series B, Biological Sciences* 361, 969–1006.
- Celton-Morizur, S., Racine, V., Sibarita, J.-B., and Paoletti, A. (2006). Pom1 kinase links division plane position to cell polarity by regulating Mid1p cortical distribution. *Journal of Cell Science* 119, 4710–4718.
- Chang, E., Bartholomeusz, G., Pimental, R., Chen, J., Lai, H., Wang, L. h, Yang, P., and Marcus, S. (1999). Direct binding and In vivo regulation of the fission yeast p21-activated kinase shk1 by the SH3 domain protein scd2. *Molecular and Cellular Biology* 19, 8066–8074.
- Chang, E.C., Barr, M., Wang, Y., Jung, V., Xu, H.-P.P., and Wigler, M.H. (1994). Cooperative interaction of *S. pombe* proteins required for mating and morphogenesis. *Cell* 79, 131–141.
- Chang, F., Drubin, D., and Nurse, P. (1997). cdc12p, a protein required for cytokinesis in fission yeast, is a component of the cell division ring and interacts with profilin. *The Journal of Cell Biology* 137, 169–182.
- Chang, F., Woollard, A., and Nurse, P. (1996). Isolation and characterization of fission yeast mutants defective in the assembly and placement of the contractile actin ring. *Journal of Cell Science* 109 (Pt 1), 131–142.
- Chang, L., and Gould, K.L. (2000). Sid4p is required to localize components of the septation initiation pathway to the spindle pole body in fission yeast. *Proceedings of the National Academy of Sciences of the United States of America* 97, 5249–5254.
- Chant, J. (1999). Cell polarity in yeast. *Annual Review of Cell and Developmental Biology* 15, 365–391.
- Chen, C., Li, Y., and Chen, J. (1999). Moe1, a conserved protein in *Schizosaccharomyces pombe*, interacts with a Ras effector, Scd1, to affect proper spindle formation. *Proceedings of the ...* 96, 517–522.
- Chen, D., Toone, W.M., Mata, J., Lyne, R., Burns, G., Kivinen, K., Brazma, A., Jones, N., and Bähler, J. (2003). Global transcriptional responses of fission yeast to environmental stress. *Molecular Biology of the Cell* 14, 214–229.
- Chen, S., Novick, P., and Ferro-Novick, S. (2012). ER network formation requires a balance of the dynamin-like GTPase Sey1p and the Lunapark family member Lnp1p. *Nature Cell Biology* 14, 707–716.
- Chiu, V.K., Bivona, T., Hach, A., Sajous, J.B., Silletti, J., Wiener, H., Johnson, R.L., Cox, A.D., and Philips, M.R. (2002). Ras signalling on the endoplasmic reticulum and the Golgi. *Nature Cell Biology* 4, 343–350.
- Christensen, a K., and Bourne, C.M. (1999). Shape of large bound polysomes in cultured fibroblasts and thyroid epithelial cells. *The Anatomical Record* 255, 116–129.
- Chvatchko, Y., Howald, I., and Riezman, H. (1986). Two yeast mutants defective in endocytosis are defective in pheromone response. *Cell* 46, 355–364.

- Ciano, C. Di, Nie, Z., and Szászi, K. (2002). Osmotic stress-induced remodeling of the cortical cytoskeleton. *American Journal of Physiology - Cell Physiology* 283, C850–C865.
- Claude, A., Zhao, B.P., Kuziemy, C.E., Dahan, S., Berger, S.J., Yan, J.P., Arnold, A.D., Sullivan, E.M., and Melançon, P. (1999). GBF1: A novel Golgi-associated BFA-resistant guanine nucleotide exchange factor that displays specificity for ADP-ribosylation factor 5. *The Journal of Cell Biology* 146, 71–84.
- Cleary, A., and Gunning, B. (1992). Microtubule and F-actin dynamics at the division site in living *Tradescantia* stamen hair cells. *Journal of Cell*
- Cleary, A.L., and Smith, L.G. (1998). The Tangled1 gene is required for spatial control of cytoskeletal arrays associated with cell division during maize leaf development. *The Plant Cell* 10, 1875–1888.
- Clifford, D.M., Wolfe, B. a, Roberts-Galbraith, R.H., McDonald, W.H., Yates, J.R., and Gould, K.L. (2008). The Clp1/Cdc14 phosphatase contributes to the robustness of cytokinesis by association with anillin-related Mid1. *The Journal of Cell Biology* 181, 79–88.
- Cluett, E.B., and Brown, W.J. (1992). Adhesion of Golgi cisternae by proteinaceous interactions: intercisternal bridges as putative adhesive structures. *Journal of Cell Science* 103 (Pt 3, 773–784.
- Coll, P.M., Rincon, S. a, Izquierdo, R. a, and Perez, P. (2007). Hob3p, the fission yeast ortholog of human BIN3, localizes Cdc42p to the division site and regulates cytokinesis. *The EMBO Journal* 26, 1865–1877.
- Coll, P.M., Trillo, Y., Ametzazurra, A., and Perez, P. (2003). Gef1p , a New Guanine Nucleotide Exchange Factor for Cdc42p , Regulates Polarity in *Schizosaccharomyces pombe*. 14, 313–323.
- Connerly, P.L., Esaki, M., Montegna, E.A., Strongin, D.E., Levi, S., Soderholm, J., and Glick, B.S. (2005). Sec16 is a determinant of transitional ER organization. *Current Biology : CB* 15, 1439–1447.
- Cosson, P., and Letourneur, F. (1994). Coatamer interaction with di-lysine endoplasmic reticulum retention motifs. *Science (New York, N.Y.)* 263, 1629–1631.
- Cotteret, S., and Chernoff, J. (2002). The evolutionary history of effectors downstream of Cdc42 and Rac. *Genome Biology* 3, REVIEWS0002.
- De Craene, J.-O., Coleman, J., Estrada de Martin, P., Pypaert, M., Anderson, S., Yates, J.R., Ferro-Novick, S., and Novick, P. (2006). Rtn1p is involved in structuring the cortical endoplasmic reticulum. *Molecular Biology of the Cell* 17, 3009–3020.
- Cyr, D.M. (1995). Cooperation of the molecular chaperone Ydj1 with specific Hsp70 homologs to suppress protein aggregation. *FEBS Letters* 359, 129–132.
- Cyr, D.M., and Douglas, M.G. (1994). Differential regulation of Hsp70 subfamilies by the eukaryotic DnaJ homologue YDJ1. *The Journal of Biological Chemistry* 269, 9798–9804.

- Daga, R.R., and Chang, F. (2005). Dynamic positioning of the fission yeast cell division plane. *Proceedings of the National Academy of Sciences of the United States of America* *102*, 8228–8232.
- Dahan, S., Ahluwalia, J.P., Wong, L., Posner, B.I., and Bergeron, J.J. (1994). Concentration of intracellular hepatic apolipoprotein E in Golgi apparatus saccular distensions and endosomes. *The Journal of Cell Biology* *127*, 1859–1869.
- Van Damme, D. (2009). Division plane determination during plant somatic cytokinesis. *Current Opinion in Plant Biology* *12*, 745–751.
- Dan, I., Watanabe, N.M., and Kusumi, A. (2001). The Ste20 group kinases as regulators of MAP kinase cascades. *Trends in Cell Biology* *11*, 220–230.
- Das, M., Drake, T., Wiley, D.J., Buchwald, P., Vavylonis, D., and Verde, F. (2012). Oscillatory dynamics of Cdc42 GTPase in the control of polarized growth. *Science (New York, N.Y.)* *337*, 239–243.
- Das, M., Wiley, D.J., Chen, X., Shah, K., and Verde, F. (2009). The conserved NDR kinase Orb6 controls polarized cell growth by spatial regulation of the small GTPase Cdc42. *Current Biology : CB* *19*, 1314–1319.
- Das, M., Wiley, D.J., Medina, S., Vincent, H.A., Larrea, M., Oriolo, A., and Verde, F. (2007). Regulation of Cell Diameter, For3p Localization, and Cell Symmetry by Fission Yeast Rho-GAP Rga4p. *PLoS Biol* *5*, 2090–2101.
- Von Dassow, G., Verbrugghe, K.J.C., Miller, A.L., Sider, J.R., and Bement, W.M. (2009). Action at a distance during cytokinesis. *The Journal of Cell Biology* *187*, 831–845.
- Dean, S.O., Rogers, S.L., Stuurman, N., Vale, R.D., and Spudich, J.A. (2005). Distinct pathways control recruitment and maintenance of myosin II at the cleavage furrow during cytokinesis. *Proceedings of the National Academy of Sciences of the United States of America* *102*, 13473–13478.
- Delley, P., and Hall, M.N. (1999). Cell Wall Stress Depolarizes Cell Growth Via Hyperactivation of RHO1. *PLoS Biol* *17*, 163–174.
- DerMardirossian, C., and Bokoch, G.M. (2005). GDIs: central regulatory molecules in Rho GTPase activation. *Trends in Cell Biology* *15*, 356–363.
- Deshaies, R.J., Sanders, S.L., Feldheim, D.A., and Schekman, R. (1991). Assembly of yeast Sec proteins involved in translocation into the endoplasmic reticulum into a membrane-bound multisubunit complex. *Nature* *349*, 806–808.
- Dettmer, J., and Friml, J. (2011). Cell polarity in plants: when two do the same, it is not the same.... *Current Opinion in Cell Biology* *23*, 686–696.
- Dodgson, J., Brown, W., Rosa, C.A., and Armstrong, J. (2010). Reorganization of the growth pattern of *Schizosaccharomyces pombe* in invasive filament formation. *Eukaryotic Cell* *9*, 1788–1797.
- Donaldson, J.G., Kahn, R.A., Lippincott-Schwartz, J., and Klausner, R.D. (1991). Binding of ARF and beta-COP to Golgi membranes: possible regulation by a trimeric G protein. *Science (New York, N.Y.)* *254*, 1197–1199.

- Dong, G., Hutagalung, A.H., Fu, C., Novick, P., and Reinisch, K.M. (2005). The structures of exocyst subunit Exo70p and the Exo84p C-terminal domains reveal a common motif. *Nature Structural & Molecular Biology* *12*, 1094–1100.
- Dong, Y. (2003). Formin-dependent actin assembly is regulated by distinct modes of Rho signaling in yeast. *The Journal of Cell Biology* *161*, 1081–1092.
- Donohoe, B.S., Kang, B.-H., and Staehelin, L.A. (2007). Identification and characterization of COPIa- and COPIb-type vesicle classes associated with plant and algal Golgi. *Proceedings of the National Academy of Sciences of the United States of America* *104*, 163–168.
- Doyle, A., Martín-García, R., Coulton, A.T., Bagley, S., and Mulvihill, D.P. (2009). Fission yeast Myo51 is a meiotic spindle pole body component with discrete roles during cell fusion and spore formation. *Journal of Cell Science* *122*, 4330–4340.
- D'souza, V.M., Naqvi, N.I., Wang, H., and Balasubramanian, M.K. (2001). Interactions of Cdc4p, a myosin light chain, with IQ-domain containing proteins in *Schizosaccharomyces pombe*. *Cell Structure and Function* *26*, 555–565.
- Echard, A., Hickson, G.R.X., Foley, E., and O'Farrell, P.H. (2004). Terminal cytokinesis events uncovered after an RNAi screen. *Current Biology : CB* *14*, 1685–1693.
- Eliáš, M., and Klimeš, V. (2012). *Rho GTPases* (New York, NY: Springer New York).
- Ellenbroek, S.I.J., Iden, S., and Collard, J.G. (2012). Cell polarity proteins and cancer. *Seminars in Cancer Biology* *22*, 208–215.
- Endo, M., Shirouzu, M., and Yokoyama, S. (2003). The Cdc42 binding and scaffolding activities of the fission yeast adaptor protein Scd2. *The Journal of Biological Chemistry* *278*, 843–852.
- Espenshade, P., Gimeno, R.E., Holzmacher, E., Teung, P., and Kaiser, C.A. (1995). Yeast SEC16 gene encodes a multidomain vesicle coat protein that interacts with Sec23p. *The Journal of Cell Biology* *131*, 311–324.
- Estrada, P., Kim, J., Coleman, J., Walker, L., Dunn, B., Takizawa, P., Novick, P., and Ferro-Novick, S. (2003). Myo4p and She3p are required for cortical ER inheritance in *Saccharomyces cerevisiae*. *The Journal of Cell Biology* *163*, 1255–1266.
- Estravís, M., Rincón, S. a, Santos, B., and Pérez, P. (2011). Cdc42 regulates multiple membrane traffic events in fission yeast. *Traffic (Copenhagen, Denmark)* *12*, 1744–1758.
- Etienne-Manneville, S. (2004). Cdc42--the centre of polarity. *Journal of Cell Science* *117*, 1291–1300.
- Faix, J., and Grosse, R. (2006). Staying in shape with formins. *Developmental Cell* *10*, 693–706.
- Fankhauser, C., Marks, J., Reymond, A., and Simanis, V. (1993). The *S. pombe* cdc16 gene is required both for maintenance of p34cdc2 kinase activity

- and regulation of septum formation: a link between mitosis and cytokinesis? *The EMBO Journal* *12*, 2697–2704.
- Fankhauser, C., Reymond, A., Cerutti, L., Utzig, S., Hofmann, K., and Simanis, V. (1995). The *S. pombe cdc15* gene is a key element in the reorganization of F-actin at mitosis. *Cell* *82*, 435–444.
- Fankhauser, C., and Simanis, V. (1994). The *cdc7* protein kinase is a dosage dependent regulator of septum formation in fission yeast. *The EMBO Journal* *13*, 3011–3019.
- Farhan, H., Weiss, M., Tani, K., Kaufman, R.J., and Hauri, H.-P. (2008). Adaptation of endoplasmic reticulum exit sites to acute and chronic increases in cargo load. *The EMBO Journal* *27*, 2043–2054.
- Farquhar, M.G. (1985). Progress in unraveling pathways of Golgi traffic. *Annual Review of Cell Biology* *1*, 447–488.
- Fasshauer, D., Bruns, D., Shen, B., Jahn, R., and Brünger, A.T. (1997). A structural change occurs upon binding of syntaxin to SNAP-25. *The Journal of Biological Chemistry* *272*, 4582–4590.
- Fasshauer, D., Sutton, R.B., Brunger, A.T., and Jahn, R. (1998). Conserved structural features of the synaptic fusion complex: SNARE proteins reclassified as Q- and R-SNAREs. *Proceedings of the National Academy of Sciences of the United States of America* *95*, 15781–15786.
- Feierbach, B. (2004). Regulation of a formin complex by the microtubule plus end protein tealp. *The Journal of Cell Biology* *165*, 697–707.
- Feierbach, B., and Chang, F. (2001). Roles of the fission yeast formin for3p in cell polarity, actin cable formation and symmetric cell division. *Current Biology* : *CB 11*, 1656–1665.
- Feinstein, T.N., and Linstedt, A.D. (2007). Mitogen-activated protein kinase kinase 1-dependent Golgi unlinking occurs in G2 phase and promotes the G2/M cell cycle transition. *Molecular Biology of the Cell* *18*, 594–604.
- Feltham, J.L., Dötsch, V., Raza, S., Manor, D., Cerione, R.A., Sutcliffe, M.J., Wagner, G., and Oswald, R.E. (1997). Definition of the switch surface in the solution structure of Cdc42Hs. *Biochemistry* *36*, 8755–8766.
- Feoktistova, A., Morrell-Falvey, J., Chen, J.-S., Singh, N.S., Balasubramanian, M.K., and Gould, K.L. (2012). The fission yeast septation initiation network (SIN) kinase, Sid2, is required for SIN asymmetry and regulates the SIN scaffold, Cdc11. *Molecular Biology of the Cell* *23*, 1636–1645.
- Ferrezuelo, F., Colomina, N., Palmisano, A., Garí, E., Gallego, C., Csikász-Nagy, A., and Aldea, M. (2012). The critical size is set at a single-cell level by growth rate to attain homeostasis and adaptation. *Nature Communications* *3*, 1012.
- Field, M.C., and Dacks, J.B. (2009). First and last ancestors: reconstructing evolution of the endomembrane system with ESCRTs, vesicle coat proteins, and nuclear pore complexes. *Current Opinion in Cell Biology* *21*, 4–13.

- Field, M.C., Sali, A., and Rout, M.P. (2011). Evolution: On a bender--BARs, ESCRTs, COPs, and finally getting your coat. *The Journal of Cell Biology* 193, 963–972.
- Finger, F.P., Hughes, T.E., and Novick, P. (1998). Sec3p Is a Spatial Landmark for Polarized Secretion in Budding Yeast. *Cell* 92, 559–571.
- Finger, F.P., and Novick, P. (1998). Spatial regulation of exocytosis: lessons from yeast. *The Journal of Cell Biology* 142, 609–612.
- Franzusoff, A., Redding, K., Crosby, J., Fuller, R.S., and Schekman, R. (1991). Localization of components involved in protein transport and processing through the yeast Golgi apparatus. *The Journal of Cell Biology* 112, 27–37.
- Freeze, H.H., and Ng, B.G. (2011). Golgi glycosylation and human inherited diseases. *Cold Spring Harbor Perspectives in Biology* 3, a005371.
- Frost, A., Perera, R., Roux, A., Spasov, K., Destaing, O., Egelman, E.H., De Camilli, P., and Unger, V.M. (2008). Structural basis of membrane invagination by F-BAR domains. *Cell* 132, 807–817.
- Fujiwara, T., Bandi, M., Nitta, M., Ivanova, E. V, Bronson, R.T., and Pellman, D. (2005). Cytokinesis failure generating tetraploids promotes tumorigenesis in p53-null cells. *Nature* 437, 1043–1047.
- Furge, K.A., Cheng, Q.C., Jwa, M., Shin, S., Song, K., and Albright, C.F. (1999). Regions of Byr4, a regulator of septation in fission yeast, that bind Spg1 or Cdc16 and form a two-component GTPase-activating protein with Cdc16. *The Journal of Biological Chemistry* 274, 11339–11343.
- Furge, K.A., Wong, K., Armstrong, J., Balasubramanian, M., and Albright, C.F. (1998). Byr4 and Cdc16 form a two-component GTPase-activating protein for the Spg1 GTPase that controls septation in fission yeast. *Current Biology* : CB 8, 947–954.
- Furuta, M., Kose, S., Koike, M., Shimi, T., Hiraoka, Y., Yoneda, Y., Haraguchi, T., and Imamoto, N. (2004). Heat-shock induced nuclear retention and recycling inhibition of importin alpha. *Genes to Cells : Devoted to Molecular & Cellular Mechanisms* 9, 429–441.
- Gallo, G.J., Prentice, H., and Kingston, R.E. (1993). Heat Shock Factor Is Required for Growth at Normal Temperatures in the Fission Yeast *Schizosaccharomyces pombe*. 13, 749–761.
- Garcia, P., Tajadura, V., and Sanchez, Y. (2009). The Rho1p Exchange Factor Rgf1p Signals Upstream from the Pmk1 Mitogen-activated Protein Kinase Pathway in Fission Yeast. 20, 721–731.
- Gasch, A.P., Spellman, P.T., Kao, C.M., Carmel-harel, O., Eisen, M.B., Storz, G., Botstein, D., and Brown, P.O. (2000). Genomic Expression Programs in the Response of Yeast Cells to Environmental Changes □. 11, 4241–4257.
- Ghosh, S.K.B., Missra, A., and Gilmour, D.S. (2011). Negative elongation factor accelerates the rate at which heat shock genes are shut off by facilitating dissociation of heat shock factor. *Molecular and Cellular Biology* 31, 4232–4243.

- Gillies, T.E., and Cabernard, C. (2011). Cell division orientation in animals. *Current Biology* : CB 21, R599–609.
- Glick, B.S., and Luini, A. (2011). Models for Golgi traffic: a critical assessment. *Cold Spring Harbor Perspectives in Biology* 3, a005215.
- Glick, B.S., and Malhotra, V. (1998). The curious status of the Golgi apparatus. *Cell* 95, 883–889.
- Glotzer, M. (2005). The molecular requirements for cytokinesis. *Science (New York, N.Y.)* 307, 1735–1739.
- Goldfischer, S. (1982). The internal reticular apparatus of Camillo Golgi: a complex, heterogeneous organelle, enriched in acid, neutral, and alkaline phosphatases, and involved in glycosylation, secretion, membrane flow, lysosome formation, and intracellular digestion. *The Journal of Histochemistry and Cytochemistry : Official Journal of the Histochemistry Society* 30, 717–733.
- Gommel, D.U., Memon, A.R., Heiss, A., Lottspeich, F., Pfannstiel, J., Lechner, J., Reinhard, C., Helms, J.B., Nickel, W., and Wieland, F.T. (2001). Recruitment to Golgi membranes of ADP-ribosylation factor 1 is mediated by the cytoplasmic domain of p23. *The EMBO Journal* 20, 6751–6760.
- Gong, Y., Kakihara, Y., Krogan, N., Greenblatt, J., Emili, A., Zhang, Z., and Houry, W. a (2009). An atlas of chaperone-protein interactions in *Saccharomyces cerevisiae*: implications to protein folding pathways in the cell. *Molecular Systems Biology* 5, 275.
- Goodwin, J.S., Drake, K.R., Rogers, C., Wright, L., Lippincott-Schwartz, J., Philips, M.R., and Kenworthy, A.K. (2005). Depalmitoylated Ras traffics to and from the Golgi complex via a nonvesicular pathway. *The Journal of Cell Biology* 170, 261–272.
- Gould, K.L., and Nurse, P. (1989). Tyrosine phosphorylation of the fission yeast *cdc2+* protein kinase regulates entry into mitosis. *Nature* 342, 39–45.
- Govindan, B., Bowser, R., and Novick, P. (1995). The role of Myo2, a yeast class V myosin, in vesicular transport. *The Journal of Cell Biology* 128, 1055–1068.
- Grallert, A., Martín-García, R., Bagley, S., and Mulvihill, D.P. (2007). In vivo movement of the type V myosin Myo52 requires dimerisation but is independent of the neck domain. *Journal of Cell Science* 120, 4093–4098.
- Grasse, P.P. (1957). [Ultrastructure, polarity and reproduction of Golgi apparatus]. *Comptes Rendus Hebdomadaires Des Séances De l'Académie Des Sciences* 245, 1278–1281.
- Gromley, A., Yeaman, C., Rosa, J., Redick, S., Chen, C.-T., Mirabelle, S., Guha, M., Sillibourne, J., and Doxsey, S.J. (2005). Centriolin anchoring of exocyst and SNARE complexes at the midbody is required for secretory-vesicle-mediated abscission. *Cell* 123, 75–87.
- Grote, E., Carr, C.M., and Novick, P.J. (2000). Ordering the final events in yeast exocytosis. *The Journal of Cell Biology* 151, 439–452.

- Guertin, D.A., Chang, L., Irshad, F., Gould, K.L., and McCollum, D. (2000). The role of the *sid1p* kinase and *cdc14p* in regulating the onset of cytokinesis in fission yeast. *The EMBO Journal* *19*, 1803–1815.
- Guertin, D.A., Venkatram, S., Gould, K.L., and McCollum, D. (2002). *Dma1* prevents mitotic exit and cytokinesis by inhibiting the septation initiation network (SIN). *Developmental Cell* *3*, 779–790.
- Gulli, M., Jaquenoud, M., Shimada, Y., Niederha, G., Wiget, P., Peter, M., and Boveresses, C. (2000). Phosphorylation of the Cdc42 Exchange Factor Cdc24 by the PAK-like Kinase Cla4 May Regulate Polarized Growth in Yeast. *6*, 1155–1167.
- Guo, C., Tommasi, S., Liu, L., Yee, J.-K., Dammann, R., and Pfeifer, G.P. (2007). RASSF1A is part of a complex similar to the Drosophila Hippo/Salvador/Lats tumor-suppressor network. *Current Biology : CB* *17*, 700–705.
- Guo, S., Shen, X., Yan, G., Ma, D., Bai, X., Li, S., and Jiang, Y. (2009). A MAP kinase dependent feedback mechanism controls Rho1 GTPase and actin distribution in yeast. *PloS One* *4*, e6089.
- Guo, W., and Novick, P. (2004). The exocyst meets the translocon: a regulatory circuit for secretion and protein synthesis? *Trends in Cell Biology* *14*, 61–63.
- Guo, W., Roth, D., Walch-Solimena, C., and Novick, P. (1999). The exocyst is an effector for Sec4p, targeting secretory vesicles to sites of exocytosis. *The EMBO Journal* *18*, 1071–1080.
- Guo, W., Tamanoi, F., and Novick, P. (2001). Spatial regulation of the exocyst complex by Rho1 GTPase. *Nature Cell Biology* *3*, 353–360.
- Hachet, O., Berthelot-Grosjean, M., Kokkoris, K., Vincenzetti, V., Moosbrugger, J., and Martin, S.G. (2011). A phosphorylation cycle shapes gradients of the DYRK family kinase Pom1 at the plasma membrane. *Cell* *145*, 1116–1128.
- Hachet, O., and Simanis, V. (2008). Mid1p/anillin and the septation initiation network orchestrate contractile ring assembly for cytokinesis. *Genes & Development* *22*, 3205–3216.
- Hales, K.G., Bi, E., Wu, J.Q., Adam, J.C., Yu, I.C., and Pringle, J.R. (1999). Cytokinesis: an emerging unified theory for eukaryotes? *Current Opinion in Cell Biology* *11*, 717–725.
- Halladay, J.T., and Craig, E.A. (1995). A Heat Shock Transcription Factor with Reduced Activity Suppresses a Yeast HSP70 Mutant. *15*, 4890–4897.
- Hamburger, Z.A., Hamburger, A.E., West, A.P., and Weis, W.I. (2006). Crystal structure of the *S.cerevisiae* exocyst component Exo70p. *Journal of Molecular Biology* *356*, 9–21.
- Hammer, J. a, and Sellers, J.R. (2012). Walking to work: roles for class V myosins as cargo transporters. *Nature Reviews. Molecular Cell Biology* *13*, 13–26.

Hammond, A.T., and Glick, B.S. (2000). Dynamics of transitional endoplasmic reticulum sites in vertebrate cells. *Molecular Biology of the Cell* *11*, 3013–3030.

Hara-Kuge, S., Kuge, O., Orci, L., Amherdt, M., Ravazzola, M., Wieland, F.T., and Rothman, J.E. (1994). En bloc incorporation of coatamer subunits during the assembly of COP-coated vesicles. *The Journal of Cell Biology* *124*, 883–892.

Hayes, E., and Goldstein, I.J. (1974). An a-D-Galactosyl-binding 33andeiraea simplicifolia Lectin Seeds from. 1904–1914.

Hazuka, C.D., Foletti, D.L., Hsu, S.C., Kee, Y., Hopf, F.W., and Scheller, R.H. (1999). The sec6/8 complex is located at neurite outgrowth and axonal synapse-assembly domains. *The Journal of Neuroscience : the Official Journal of the Society for Neuroscience* *19*, 1324–1334.

He, B., Xi, F., Zhang, X., Zhang, J., and Guo, W. (2007). Exo70 interacts with phospholipids and mediates the targeting of the exocyst to the plasma membrane. *The EMBO Journal* *26*, 4053–4065.

He, X., Patterson, T.E., and Sazer, S. (1997). The Schizosaccharomyces pombe spindle checkpoint protein mad2p blocks anaphase and genetically interacts with the anaphase-promoting complex. *Proceedings of the National Academy of Sciences of the United States of America* *94*, 7965–7970.

Heider, M.R., and Munson, M. (2012). Exorcising the exocyst complex. *Traffic (Copenhagen, Denmark)* *13*, 898–907.

Hidalgo Carcedo, C., Bonazzi, M., Spanò, S., Turacchio, G., Colanzi, A., Luini, A., and Corda, D. (2004). Mitotic Golgi partitioning is driven by the membrane-fissioning protein CtBP3/BARS. *Science (New York, N.Y.)* *305*, 93–96.

Higgins, D., and Dworkin, J. (2012). Recent progress in Bacillus subtilis sporulation. *FEMS Microbiology Reviews* *36*, 131–148.

Hirata, D. (2002). Fission yeast Mor2/Cps12, a protein similar to Drosophila Furry, is essential for cell morphogenesis and its mutation induces Wee1-dependent G2 delay. *The EMBO Journal* *21*, 4863–4874.

Hirono, M., Nakamura, M., Tsunemoto, M., Yasuda, T., Ohba, H., Numata, O., Watanabe, Y., and Cells, T. (1987). Tetrahymena actin: localization and possible biological roles of actin in Tetrahymena cells. *Journal of Biochemistry* *102*, 537–545.

Hogenesch, J.B., and Ueda, H.R. (2011). Understanding systems-level properties: timely stories from the study of clocks. *Nature Reviews. Genetics* *12*, 407–416.

Honda, A., Al-Awar, O.S., Hay, J.C., and Donaldson, J.G. (2005). Targeting of Arf-1 to the early Golgi by membrin, an ER-Golgi SNARE. *The Journal of Cell Biology* *168*, 1039–1051.

Hoshino, H., Yoneda, A., Kumagai, F., and Hasezawa, S. (2003). Roles of actin-depleted zone and preprophase band in determining the division site of

- higher-plant cells, a tobacco BY-2 cell line expressing GFP-tubulin. *Protoplasma* 222, 157–165.
- Hou, M.-C., Wiley, D.J., Verde, F., and McCollum, D. (2003). Mob2p interacts with the protein kinase Orb6p to promote coordination of cell polarity with cell cycle progression. *Journal of Cell Science* 116, 125–135.
- Howell, A.S., Jin, M., Wu, C.-F., Zyla, T.R., Elston, T.C., and Lew, D.J. (2012). Negative feedback enhances robustness in the yeast polarity establishment circuit. *Cell* 149, 322–333.
- Howell, A.S., and Lew, D.J. (2012). Morphogenesis and the cell cycle. *Genetics* 190, 51–77.
- Hsu, S.C., Hazuka, C.D., Roth, R., Foletti, D.L., Heuser, J., and Scheller, R.H. (1998). Subunit composition, protein interactions, and structures of the mammalian brain sec6/8 complex and septin filaments. *Neuron* 20, 1111–1122.
- Hsu, S.C., Ting, a E., Hazuka, C.D., Davanger, S., Kenny, J.W., Kee, Y., and Scheller, R.H. (1996). The mammalian brain rsec6/8 complex. *Neuron* 17, 1209–1219.
- Hu, C.-K., Coughlin, M., Field, C.M., and Mitchison, T.J. (2008a). Cell polarization during monopolar cytokinesis. *The Journal of Cell Biology* 181, 195–202.
- Hu, F., Wang, Y., Liu, D., Li, Y., Qin, J., and Elledge, S.J. (2001). Regulation of the Bub2/Bfa1 GAP complex by Cdc5 and cell cycle checkpoints. *Cell* 107, 655–665.
- Hu, J., Shibata, Y., Voss, C., Shemesh, T., Li, Z., Coughlin, M., Kozlov, M.M., Rapoport, T. a, and Prinz, W. a (2008b). Membrane proteins of the endoplasmic reticulum induce high-curvature tubules. *Science (New York, N.Y.)* 319, 1247–1250.
- Hu, J., Shibata, Y., Zhu, P.-P., Voss, C., Rismanchi, N., Prinz, W. a, Rapoport, T. a, and Blackstone, C. (2009). A class of dynamin-like GTPases involved in the generation of the tubular ER network. *Cell* 138, 549–561.
- Huang, J., Huang, Y., Yu, H., Subramanian, D., Padmanabhan, A., Thadani, R., Tao, Y., Tang, X., Wedlich-Soldner, R., and Balasubramanian, M.K. (2012). Nonmedially assembled F-actin cables incorporate into the actomyosin ring in fission yeast. *The Journal of Cell Biology* 199, 831–847.
- Huang, T.Y., Renaud-Young, M., and Young, D. (2005). Nak1 interacts with Hob1 and Wsp1 to regulate cell growth and polarity in *Schizosaccharomyces pombe*. *Journal of Cell Science* 118, 199–210.
- Huang, Y., Chew, T.G., Ge, W., and Balasubramanian, M.K. (2007). Polarity determinants Tea1p, Tea4p, and Pom1p inhibit division-septum assembly at cell ends in fission yeast. *Developmental Cell* 12, 987–996.
- Huang, Y., Yan, H., and Balasubramanian, M.K. (2008). Assembly of normal actomyosin rings in the absence of Mid1p and cortical nodes in fission yeast. *The Journal of Cell Biology* 183, 979–988.

- Humbel, B.M., Konomi, M., Takagi, T., Kamasawa, N., Ishijima, S.A., and Osumi, M. (2001). In situ localization of beta-glucans in the cell wall of *Schizosaccharomyces pombe*. *Yeast (Chichester, England)* *18*, 433–444.
- Hutterer, A., Glotzer, M., and Mishima, M. (2009). Clustering of centralspindlin is essential for its accumulation to the central spindle and the midbody. *Current Biology : CB* *19*, 2043–2049.
- Hála, M., Cole, R., Synek, L., Drdová, E., Pecenková, T., Nordheim, A., Lamkemeyer, T., Madlung, J., Hochholdinger, F., Fowler, J.E., et al. (2008). An exocyst complex functions in plant cell growth in *Arabidopsis* and tobacco. *The Plant Cell* *20*, 1330–1345.
- Iden, S., and Collard, J.G. (2008). Crosstalk between small GTPases and polarity proteins in cell polarization. *Nature Reviews. Molecular Cell Biology* *9*, 846–859.
- Imazu, H., and Sakurai, H. (2005). *Saccharomyces cerevisiae* Heat Shock Transcription Factor Regulates Cell Wall Remodeling in Response to Heat Shock. *4*, 1050–1056.
- Iraoqui, J.E., Gladfelter, A.S., and Lew, D.J. (2003). Scaffold-mediated symmetry breaking by Cdc42p. *Nature Cell Biology* *5*, 1062–1070.
- Irizarry, R.A., Warren, D., Spencer, F., Kim, I.F., Biswal, S., Frank, B.C., Gabrielson, E., Garcia, J.G.N., Geoghegan, J., Germino, G., et al. (2005). Multiple-laboratory comparison of microarray platforms. *2*, 345–349.
- Itoh, T., Erdmann, K.S., Roux, A., Habermann, B., Werner, H., and De Camilli, P. (2005). Dynamin and the actin cytoskeleton cooperatively regulate plasma membrane invagination by BAR and F-BAR proteins. *Developmental Cell* *9*, 791–804.
- Ivan, V., De Voer, G., Xanthakis, D., Spoorendonk, K.M., Kondylis, V., and Rabouille, C. (2008). *Drosophila* Sec16 mediates the biogenesis of tER sites upstream of Sar1 through an arginine-rich motif. *Molecular Biology of the Cell* *19*, 4352–4365.
- Jin, Y., Sultana, A., Gandhi, P., Franklin, E., Hamamoto, S., Khan, A.R., Munson, M., Schekman, R., and Weisman, L.S. (2011). Myosin V transports secretory vesicles via a Rab GTPase cascade and interaction with the exocyst complex. *Developmental Cell* *21*, 1156–1170.
- Jochová, J., Rupes, I., and Streiblová, E. (1991). F-actin contractile rings in protoplasts of the yeast *Schizosaccharomyces*. *Cell Biology International Reports* *15*, 607–610.
- Johnson, A.E., and Gould, K.L. (2011). Dma1 ubiquitinates the SIN scaffold, Sid4, to impede the mitotic localization of Plo1 kinase. *The EMBO Journal* *30*, 341–354.
- Johnson, B.F., Yoo, B.Y., and Calleja, G.B. (1973). Cell division in yeasts: movement of organelles associated with cell plate growth of *Schizosaccharomyces pombe*. *Journal of Bacteriology* *115*, 358–366.
- Johnson, J.L., Erickson, J.W., and Cerione, R.A. (2009). New insights into how the Rho guanine nucleotide dissociation inhibitor regulates the interaction

- of Cdc42 with membranes. *The Journal of Biological Chemistry* 284, 23860–23871.
- Johnson, J.M., Jin, M., and Lew, D.J. (2011). Symmetry breaking and the establishment of cell polarity in budding yeast. *Current Opinion in Genetics & Development* 21, 740–746.
- Jourdain, I., Dooley, H.C., and Toda, T. (2012). Fission yeast sec3 bridges the exocyst complex to the actin cytoskeleton. *Traffic (Copenhagen, Denmark)* 13, 1481–1495.
- Jungmann, J., and Munro, S. (1998). Multi-protein complexes in the cis Golgi of *Saccharomyces cerevisiae* with alpha-1,6-mannosyltransferase activity. *The EMBO Journal* 17, 423–434.
- Kamasaki, T., Arai, R., Osumi, M., and Mabuchi, I. (2005). Directionality of F-actin cables changes during the fission yeast cell cycle. *Nature Cell Biology* 7, 916–917.
- Kamasaki, T., Osumi, M., and Mabuchi, I. (2007). Three-dimensional arrangement of F-actin in the contractile ring of fission yeast. *The Journal of Cell Biology* 178, 765–771.
- Kanai, M., Kume, K., Miyahara, K., Sakai, K., Nakamura, K., Leonhard, K., Wiley, D.J., Verde, F., Toda, T., and Hirata, D. (2005). Fission yeast MO25 protein is localized at SPB and septum and is essential for cell morphogenesis. *The EMBO Journal* 24, 3012–3025.
- Kang, P.J., Sanson, A., Lee, B., and Park, H.O. (2001). A GDP/GTP exchange factor involved in linking a spatial landmark to cell polarity. *Science (New York, N.Y.)* 292, 1376–1378.
- Kanter-Smoler, G., Dahlkvist, A., and Sunnerhagen, P. (1994). Improved method for rapid transformation of intact *Schizosaccharomyces pombe* cells. *BioTechniques* 16, 798–800.
- Karagiannis, J., Bimbó, A., Rajagopalan, S., Liu, J., and Balasubramanian, M.K. (2005). The nuclear kinase Lsk1p positively regulates the septation initiation network and promotes the successful completion of cytokinesis in response to perturbation of the actomyosin ring in *Schizosaccharomyces pombe*. *Molecular Biology of the Cell* 16, 358–371.
- Keeney, J.B., and Boeke, J.D. (1994). Efficient targeted integration at *leu1-32* and *ura4-294* in *Schizosaccharomyces pombe*. *Genetics* 136, 849–856.
- Kelley, J.B., and Paschal, B.M. (2007). Hyperosmotic stress signaling to the nucleus disrupts the Ran gradient and the production of RanGTP. *Molecular Biology of the Cell* 18, 4365–4376.
- Kelly, F.D., and Nurse, P. (2011). De novo growth zone formation from fission yeast spheroplasts. *PloS One* 6, e27977.
- Kim, H., Yang, P., Catanuto, P., Verde, F., Lai, H., Du, H., Chang, F., and Marcus, S. (2003). The kelch repeat protein, Tea1, is a potential substrate target of the p21-activated kinase, Shk1, in the fission yeast, *Schizosaccharomyces pombe*. *The Journal of Biological Chemistry* 278, 30074–30082.

- Kimura, K., Ito, M., Amano, M., Chihara, K., Fukata, Y., Nakafuku, M., Yamamori, B., Feng, J., Nakano, T., Okawa, K., et al. (1996). Regulation of myosin phosphatase by Rho and Rho-associated kinase (Rho-kinase). *Science (New York, N.Y.)* *273*, 245–248.
- Kinoshita, M., Field, C.M., Coughlin, M.L., Straight, A.F., and Mitchison, T.J. (2002). Self- and actin-templated assembly of Mammalian septins. *Developmental Cell* *3*, 791–802.
- Ten Klooster, J.P., Jansen, M., Yuan, J., Oorschot, V., Begthel, H., Di Giacomo, V., Colland, F., De Koning, J., Maurice, M.M., Hornbeck, P., et al. (2009). Mst4 and Ezrin induce brush borders downstream of the Lkb1/Strad/Mo25 polarization complex. *Developmental Cell* *16*, 551–562.
- Kondylis, V., Van Nispen tot Pannerden, H.E., Herpers, B., Friggi-Grelin, F., and Rabouille, C. (2007). The golgi comprises a paired stack that is separated at G2 by modulation of the actin cytoskeleton through Abi and Scar/WAVE. *Developmental Cell* *12*, 901–915.
- Kono, K., Saeki, Y., Yoshida, S., Tanaka, K., and Pellman, D. (2012). Proteasomal degradation resolves competition between cell polarization and cellular wound healing. *Cell* *150*, 151–164.
- Kose, S., Furuta, M., and Imamoto, N. (2012). Hikeshi, a nuclear import carrier for Hsp70s, protects cells from heat shock-induced nuclear damage. *Cell* *149*, 578–589.
- Kovar, D.R., Harris, E.S., Mahaffy, R., Higgs, H.N., and Pollard, T.D. (2006). Control of the assembly of ATP- and ADP-actin by formins and profilin. *Cell* *124*, 423–435.
- Kozminski, K.G., Beven, L., Angerman, E., Tong, A.H.Y., Boone, C., and Park, H.-O. (2003). Interaction between a Ras and a Rho GTPase couples selection of a growth site to the development of cell polarity in yeast. *Molecular Biology of the Cell* *14*, 4958–4970.
- Kozubowski, L., Saito, K., Johnson, J.M., Howell, A.S., Zyla, T.R., and Lew, D.J. (2008). Symmetry-Breaking Polarization Driven by a Cdc42p GEF-PAK Complex. *Current Biology* *18*, 1719–1726.
- Krapp, A., Cano, E., and Simanis, V. (2004a). Analysis of the *S. pombe* signalling scaffold protein Cdc11p reveals an essential role for the N-terminal domain in SIN signalling. *FEBS Letters* *565*, 176–180.
- Krapp, A., Gulli, M.-P., and Simanis, V. (2004b). SIN and the art of splitting the fission yeast cell. *Current Biology : CB* *14*, R722–30.
- Krapp, A., Schmidt, S., Cano, E., and Simanis, V. (2001). *S. pombe* cdc11p, together with sid4p, provides an anchor for septation initiation network proteins on the spindle pole body. *Current Biology : CB* *11*, 1559–1568.
- Krapp, A., and Simanis, V. (2008). An overview of the fission yeast septation initiation network (SIN). *Biochemical Society Transactions* *36*, 411–415.
- Kuehn, M.J., Herrmann, J.M., and Schekman, R. (1998). COPII-cargo interactions direct protein sorting into ER-derived transport vesicles. *Nature* *391*, 187–190.

- Kumar, P., and Wittmann, T. (2012). +TIPs: SxIPping along microtubule ends. *Trends in Cell Biology* 22, 418–428.
- Kurischko, C., Kuravi, V.K., Wannissorn, N., Nazarov, P.A., Husain, M., Zhang, C., Shokat, K.M., McCaffery, J.M., and Luca, F.C. (2008). The yeast LATS/Ndr kinase Cbk1 regulates growth via Golgi-dependent glycosylation and secretion. *Molecular Biology of the Cell* 19, 5559–5578.
- Kurisu, S., and Takenawa, T. (2009). The WASP and WAVE family proteins. *Genome Biology* 10, 226.
- Kübler, E., and Riezman, H. (1993). Actin and fimbrin are required for the internalization step of endocytosis in yeast. *The EMBO Journal* 12, 2855–2862.
- Ladinsky, M.S., Mastronarde, D.N., McIntosh, J.R., Howell, K.E., and Staehelin, L.A. (1999). Golgi structure in three dimensions: functional insights from the normal rat kidney cell. *The Journal of Cell Biology* 144, 1135–1149.
- Ladinsky, M.S., Wu, C.C., McIntosh, S., McIntosh, J.R., and Howell, K.E. (2002). Structure of the Golgi and distribution of reporter molecules at 20 degrees C reveals the complexity of the exit compartments. *Molecular Biology of the Cell* 13, 2810–2825.
- Lammers, M., Rose, R., Scrima, A., and Wittinghofer, A. (2005). The regulation of mDial by autoinhibition and its release by Rho*GTP. *The EMBO Journal* 24, 4176–4187.
- Laporte, D., Coffman, V.C., Lee, I.-J., and Wu, J.-Q. (2011). Assembly and architecture of precursor nodes during fission yeast cytokinesis. *The Journal of Cell Biology* 192, 1005–1021.
- Lechler, T., Jonsdottir, G.A., Klee, S.K., Pellman, D., and Li, R. (2001). A two-tiered mechanism by which Cdc42 controls the localization and activation of an Arp2/3-activating motor complex in yeast. *The Journal of Cell Biology* 155, 261–270.
- Lecuit, T., and Wieschaus, E. (2000). Polarized insertion of new membrane from a cytoplasmic reservoir during cleavage of the *Drosophila* embryo. *The Journal of Cell Biology* 150, 849–860.
- Lee, C., and Chen, L.B. (1988). Dynamic behavior of endoplasmic reticulum in living cells. *Cell* 54, 37–46.
- Lee, M.C.S., Orci, L., Hamamoto, S., Futai, E., Ravazzola, M., and Schekman, R. (2005). Sar1p N-terminal helix initiates membrane curvature and completes the fission of a COPII vesicle. *Cell* 122, 605–617.
- Lee, S., and Cooley, L. (2007). Jagunal is required for reorganizing the endoplasmic reticulum during *Drosophila* oogenesis. *The Journal of Cell Biology* 176, 941–952.
- Lee, W.L., Bezanilla, M., and Pollard, T.D. (2000). Fission yeast myosin-I, Myo1p, stimulates actin assembly by Arp2/3 complex and shares functions with WASp. *The Journal of Cell Biology* 151, 789–800.

- Leonhard, K., and Nurse, P. (2005). Ste20/GCK kinase Nak1/Orb3 polarizes the actin cytoskeleton in fission yeast during the cell cycle. *Journal of Cell Science* *118*, 1033–1044.
- Levi, S.K., Bhattacharyya, D., Strack, R.L., Austin, J.R., and Glick, B.S. (2010). The yeast GRASP Grh1 colocalizes with COPII and is dispensable for organizing the secretory pathway. *Traffic (Copenhagen, Denmark)* *11*, 1168–1179.
- Lewis, M.J., Rayner, J.C., and Pelham, H.R. (1997). A novel SNARE complex implicated in vesicle fusion with the endoplasmic reticulum. *The EMBO Journal* *16*, 3017–3024.
- Li, C., Furge, K.A., Cheng, Q.C., and Albright, C.F. (2000a). Byr4 localizes to spindle-pole bodies in a cell cycle-regulated manner to control Cdc7 localization and septation in fission yeast. *The Journal of Biological Chemistry* *275*, 14381–14387.
- Li, F., and Higgs, H.N. (2003). The mouse Formin mDia1 is a potent actin nucleation factor regulated by autoinhibition. *Current Biology : CB* *13*, 1335–1340.
- Li, G.C., and Werb, Z. (1982). Correlation between synthesis of heat shock proteins and development of thermotolerance in Chinese hamster fibroblasts. *Proceedings of the National Academy of Sciences of the United States of America* *79*, 3218–3222.
- Li, T., Naqvi, N.I., Yang, H., and Teo, T.S. (2000b). Identification of a 26S proteasome-associated UCH in fission yeast. *Biochemical and Biophysical Research Communications* *272*, 270–275.
- Li, Z., Hannigan, M., Mo, Z., Liu, B., Lu, W., Wu, Y., Smrcka, A. V, Wu, G., Li, L., Liu, M., et al. (2003). Directional sensing requires G beta gamma-mediated PAK1 and PIX alpha-dependent activation of Cdc42. *Cell* *114*, 215–227.
- Lind, G.E., Raiborg, C., Danielsen, S.A., Rognum, T.O., Thiis-Evensen, E., Hoff, G., Nesbakken, A., Stenmark, H., and Lothe, R.A. (2011). SPG20, a novel biomarker for early detection of colorectal cancer, encodes a regulator of cytokinesis. *Oncogene* *30*, 3967–3978.
- Ling, L.L., Keohavong, P., Dias, C., and Thilly, W.G. (1991). Optimization of the polymerase chain reaction with regard to fidelity: modified T7, Taq, and vent DNA polymerases. *PCR Methods and Applications* *1*, 63–69.
- Lippincott-Schwartz, J., Donaldson, J.G., Schweizer, A., Berger, E.G., Hauri, H.P., Yuan, L.C., and Klausner, R.D. (1990). Microtubule-dependent retrograde transport of proteins into the ER in the presence of brefeldin A suggests an ER recycling pathway. *Cell* *60*, 821–836.
- Lippincott-Schwartz, J., Yuan, L.C., Bonifacino, J.S., and Klausner, R.D. (1989). Rapid redistribution of Golgi proteins into the ER in cells treated with brefeldin A: evidence for membrane cycling from Golgi to ER. *Cell* *56*, 801–813.
- Liu, J., Tang, X., Wang, H., Oliferenko, S., and Balasubramanian, M.K. (2002). The localization of the integral membrane protein Cps1p to the cell

- division site is dependent on the actomyosin ring and the septation-inducing network in *Schizosaccharomyces pombe*. *Molecular Biology of the Cell* *13*, 989–1000.
- Liu, J., Wang, H., and Balasubramanian, M.K. (2000). A checkpoint that monitors cytokinesis in *Schizosaccharomyces pombe*. *Journal of Cell Science* *113* (Pt 7, 1223–1230.
- Liu, J., Wang, H., McCollum, D., and Balasubramanian, M.K. (1999). Drc1p/Cps1p, a 1,3-beta-glucan synthase subunit, is essential for division septum assembly in *Schizosaccharomyces pombe*. *Genetics* *153*, 1193–1203.
- Liu, J., Zuo, X., Yue, P., and Guo, W. (2007). Phosphatidylinositol 4,5-bisphosphate mediates the targeting of the exocyst to the plasma membrane for exocytosis in mammalian cells. *Molecular Biology of the Cell* *18*, 4483–4492.
- Lord, M., and Pollard, T.D. (2004). UCS protein Rng3p activates actin filament gliding by fission yeast myosin-II. *The Journal of Cell Biology* *167*, 315–325.
- Losev, E., Reinke, C.A., Jellen, J., Strongin, D.E., Bevis, B.J., and Glick, B.S. (2006). Golgi maturation visualized in living yeast. *Nature* *441*, 1002–1006.
- Lu, C., Brauer, M.J., and Botstein, D. (2009). Slow Growth Induces Heat-Shock Resistance in Normal and Respiratory-deficient Yeast. *20*, 891–903.
- Ma, Y., Kuno, T., Kita, A., Asayama, Y., and Sugiura, R. (2006). Rho2 Is a Target of the Farnesyltransferase Cpp1 and Acts Upstream of Pmk1 Mitogen-activated Protein Kinase Signaling in Fission Yeast. *17*, 5028–5037.
- Macara, I.G., and Mili, S. (2008). Polarity and differential inheritance--universal attributes of life? *Cell* *135*, 801–812.
- Maddox, A.S., Lewellyn, L., Desai, A., and Oegema, K. (2007). Anillin and the septins promote asymmetric ingression of the cytokinetic furrow. *Developmental Cell* *12*, 827–835.
- Madrid, M., Soto, T., Khong, H.K., Franco, A., Vicente, J., Pérez, P., Gacto, M., and Cansado, J. (2006). Stress-induced response, localization, and regulation of the Pmk1 cell integrity pathway in *Schizosaccharomyces pombe*. *The Journal of Biological Chemistry* *281*, 2033–2043.
- Maerz, S., and Seiler, S. (2010). Tales of RAM and MOR: NDR kinase signaling in fungal morphogenesis. *Current Opinion in Microbiology* *13*, 663–671.
- Malsam, J., Satoh, A., Pelletier, L., and Warren, G. (2005). Golgin tethers define subpopulations of COPI vesicles. *Science (New York, N.Y.)* *307*, 1095–1098.
- Maniatis, T. (1982). *Molecular cloning: A laboratory manual* (Cold Spring Harbor Laboratory).
- Marco, E., Wedlich-Soldner, R., Li, R., Altschuler, S.J., and Wu, L.F. (2007). Endocytosis optimizes the dynamic localization of membrane proteins that regulate cortical polarity. *Cell* *129*, 411–422.

- Marks, J., Fankhauser, C., and Simanis, V. (1992). Genetic interactions in the control of septation in *Schizosaccharomyces pombe*. *Journal of Cell Science* *101* (Pt 4, 801–808.
- Marks, J., Hagan, I.M., and Hyams, J.S. (1986). Growth polarity and cytokinesis in fission yeast: the role of the cytoskeleton. *Journal of Cell Science*. Supplement 5, 229–241.
- Marks, J., and Hyams, J.S. (1985). Localization of F-actin through the cell division cycle of *Schizosaccharomyces pombe*. *European Journal of Cell Biology* 27–32.
- Marsh, B.J., Volkman, N., McIntosh, J.R., and Howell, K.E. (2004). Direct continuities between cisternae at different levels of the Golgi complex in glucose-stimulated mouse islet beta cells. *Proceedings of the National Academy of Sciences of the United States of America* *101*, 5565–5570.
- Martin, S., Rincón, S., and Basu, R. (2007). Regulation of the Formin for3p by cdc42p and bud6p. *Molecular Biology of the ...* *18*, 4155–4167.
- Martin, S.G. (2009). Microtubule-dependent cell morphogenesis in the fission yeast. *Trends in Cell Biology* *19*, 447–454.
- Martin, S.G., and Chang, F. (2006). Dynamics of the formin for3p in actin cable assembly. *Current Biology : CB* *16*, 1161–1170.
- Martin, S.G., McDonald, W.H., Yates, J.R., and Chang, F. (2005). Tea4p links microtubule plus ends with the formin for3p in the establishment of cell polarity. *Developmental Cell* *8*, 479–491.
- Martin, W. (1999). A briefly argued case that mitochondria and plastids are descendants of endosymbionts, but that the nuclear compartment is not. *Proceedings of the Royal Society B: Biological Sciences* *266*, 1387–1395.
- Martinez-Menárguez, J.A., Prekeris, R., Oorschot, V.M., Scheller, R., Slot, J.W., Geuze, H.J., and Klumperman, J. (2001). Peri-Golgi vesicles contain retrograde but not anterograde proteins consistent with the cisternal progression model of intra-Golgi transport. *The Journal of Cell Biology* *155*, 1213–1224.
- Mata, J., and Nurse, P. (1997). tea1 and the microtubular cytoskeleton are important for generating global spatial order within the fission yeast cell. *Cell* *89*, 939–949.
- Matsuoka, K., Orci, L., Amherdt, M., Bednarek, S.Y., Hamamoto, S., Schekman, R., and Yeung, T. (1998). COPII-coated vesicle formation reconstituted with purified coat proteins and chemically defined liposomes. *Cell* *93*, 263–275.
- Matsuoka, K., Schekman, R., Orci, L., and Heuser, J.E. (2001). Surface structure of the COPII-coated vesicle. *Proceedings of the National Academy of Sciences of the United States of America* *98*, 13705–13709.
- Matsuura-Tokita, K., Takeuchi, M., Ichihara, A., Mikuriya, K., and Nakano, A. (2006). Live imaging of yeast Golgi cisternal maturation. *Nature* *441*, 1007–1010.

- Maundrell, K. (1990). *nmt1* of fission yeast. A highly transcribed gene completely repressed by thiamine. *The Journal of Biological Chemistry* 265, 10857–10864.
- Maurer, S.P., Fourniol, F.J., Bohner, G., Moores, C. a, and Surrey, T. (2012). EBs recognize a nucleotide-dependent structural cap at growing microtubule ends. *Cell* 149, 371–382.
- May, J.W., and Mitchison, J.M. (1986). Length growth in fission yeast cells measured by two novel techniques. *Nature* 322, 752–754.
- Mayer, A., Wickner, W., and Haas, A. (1996). Sec18p (NSF)-driven release of Sec17p (alpha-SNAP) can precede docking and fusion of yeast vacuoles. *Cell* 85, 83–94.
- Mayinger, P. (2011). Signaling at the Golgi. *Cold Spring Harbor Perspectives in Biology* 3,.
- McCollum, D., Balasubramanian, M.K., Pelcher, L.E., Hemmingsen, S.M., and Gould, K.L. (1995). *Schizosaccharomyces pombe cdc4+* gene encodes a novel EF-hand protein essential for cytokinesis. *The Journal of Cell Biology* 130, 651–660.
- McMahon, H.T., and Gallop, J.L. (2005). Membrane curvature and mechanisms of dynamic cell membrane remodelling. *Nature* 438, 590–596.
- McNew, J.A., Parlati, F., Fukuda, R., Johnston, R.J., Paz, K., Paumet, F., Söllner, T.H., and Rothman, J.E. (2000). Compartmental specificity of cellular membrane fusion encoded in SNARE proteins. *Nature* 407, 153–159.
- Mehra, A., Shi, M., Baker, C.L., Colot, H. V, Loros, J.J., and Dunlap, J.C. (2009). A role for casein kinase 2 in the mechanism underlying circadian temperature compensation. *Cell* 137, 749–760.
- Mehta, S.Q., Hiesinger, P.R., Beronja, S., Zhai, R.G., Schulze, K.L., Verstreken, P., Cao, Y., Zhou, Y., Tepass, U., Crair, M.C., et al. (2005). Mutations in *Drosophila sec15* reveal a function in neuronal targeting for a subset of exocyst components. *Neuron* 46, 219–232.
- Melia, T.J., Weber, T., McNew, J.A., Fisher, L.E., Johnston, R.J., Parlati, F., Mahal, L.K., Sollner, T.H., and Rothman, J.E. (2002). Regulation of membrane fusion by the membrane-proximal coil of the t-SNARE during zippering of SNAREpins. *The Journal of Cell Biology* 158, 929–940.
- Miller, E., Antonny, B., Hamamoto, S., and Schekman, R. (2002). Cargo selection into COPII vesicles is driven by the Sec24p subunit. *The EMBO Journal* 21, 6105–6113.
- Miller, P.J., and Johnson, D.I. (1994). Cdc42p GTPase is involved in controlling polarized cell growth in *Schizosaccharomyces pombe*. *Molecular and Cellular Biology* 14, 1075–1083.
- Minc, N., Bratman, S. V, Basu, R., and Chang, F. (2009). Establishing new sites of polarization by microtubules. *Current Biology : CB* 19, 83–94.
- Minet, M., Nurse, P., Thuriaux, P., and Mitchison, J.M. (1979). Uncontrolled septation in a cell division cycle mutant of the fission yeast *Schizosaccharomyces pombe*. *Journal of Bacteriology* 137, 440–446.

- Minoshima, Y., Kawashima, T., Hirose, K., Tonozuka, Y., Kawajiri, A., Bao, Y.C., Deng, X., Tatsuka, M., Narumiya, S., May, W.S., et al. (2003). Phosphorylation by aurora B converts MgcRacGAP to a RhoGAP during cytokinesis. *Developmental Cell* 4, 549–560.
- Mironov, A.A., Beznoussenko, G. V, Trucco, A., Lupetti, P., Smith, J.D., Geerts, W.J.C., Koster, A.J., Burger, K.N.J., Martone, M.E., Deerinck, T.J., et al. (2003). ER-to-Golgi carriers arise through direct en bloc protrusion and multistage maturation of specialized ER exit domains. *Developmental Cell* 5, 583–594.
- Mitchison, J.M., and Nurse, P. (1985). Growth in cell length in the fission yeast *Schizosaccharomyces pombe*. *Journal of Cell Science* 75, 357–376.
- Miyamoto, Y., Saiwaki, T., Yamashita, J., Yasuda, Y., Kotera, I., Shibata, S., Shigeta, M., Hiraoka, Y., Haraguchi, T., and Yoneda, Y. (2004). Cellular stresses induce the nuclear accumulation of importin alpha and cause a conventional nuclear import block. *The Journal of Cell Biology* 165, 617–623.
- Mogelsvang, S., Gomez-Ospina, N., Soderholm, J., Glick, B.S., and Staehelin, L.A. (2003). Tomographic evidence for continuous turnover of Golgi cisternae in *Pichia pastoris*. *Molecular Biology of the Cell* 14, 2277–2291.
- Mogelsvang, S., Marsh, B.J., Ladinsky, M.S., and Howell, K.E. (2004). Predicting function from structure: 3D structure studies of the mammalian Golgi complex. *Traffic (Copenhagen, Denmark)* 5, 338–345.
- Mondal, S., Burgute, B., Rieger, D., Müller, R., Rivero, F., Faix, J., Schleicher, M., and Noegel, A.A. (2010). Regulation of the actin cytoskeleton by an interaction of IQGAP related protein GAPA with filamin and cortexillin I. *PloS One* 5, e15440.
- Moreno, S., Klar, A., and Nurse, P. (1991). Molecular genetic analysis of fission yeast *Schizosaccharomyces pombe*. *Methods in Enzymology* 194, 795–823.
- Morrell, J.L., Tomlin, G.C., Rajagopalan, S., Venkatram, S., Feoktistova, A.S., Tasto, J.J., Mehta, S., Jennings, J.L., Link, A., Balasubramanian, M.K., et al. (2004). Sid4p-Cdc11p assembles the septation initiation network and its regulators at the S. *pombe* SPB. *Current Biology : CB* 14, 579–584.
- Moseley, J.B., and Goode, B.L. (2006). The yeast actin cytoskeleton: from cellular function to biochemical mechanism. *Microbiology and Molecular Biology Reviews : MMBR* 70, 605–645.
- Moseley, J.B., Mayeux, A., Paoletti, A., and Nurse, P. (2009). A spatial gradient coordinates cell size and mitotic entry in fission yeast. *Nature* 459, 857–860.
- Motegi, F., Arai, R., and Mabuchi, I. (2001). Identification of Two Type V Myosins in Fission Yeast, One of Which Functions in Polarized Cell Growth and Moves Rapidly in the Cell. *Mol. Biol. Cell* 12, 1367–1380.
- Motegi, F., Mishra, M., Balasubramanian, M.K., and Mabuchi, I. (2004). Myosin-II reorganization during mitosis is controlled temporally by its dephosphorylation and spatially by Mid1 in fission yeast. *The Journal of Cell Biology* 165, 685–695.

- Mott, H.R., Owen, D., Nietlispach, D., Lowe, P.N., Manser, E., Lim, L., and Laue, E.D. (1999). Structure of the small G protein Cdc42 bound to the GTPase-binding domain of ACK (Nature Publishing Group).
- Mounier, N., and Arrigo, A. (2002). Actin cytoskeleton and small heat shock proteins: how do they interact? *Cell Stress & Chaperones* 7, 167–176.
- Mukhina, S., Wang, Y.-L., and Murata-Hori, M. (2007). Alpha-actinin is required for tightly regulated remodeling of the actin cortical network during cytokinesis. *Developmental Cell* 13, 554–565.
- Munn, A.L., Stevenson, B.J., Geli, M.I., and Riezman, H. (1995). end5, end6, and end7: mutations that cause actin delocalization and block the internalization step of endocytosis in *Saccharomyces cerevisiae*. *Molecular Biology of the Cell* 6, 1721–1742.
- Munson, M., and Novick, P. (2006). The exocyst defrocked, a framework of rods revealed. *Nature Structural & Molecular Biology* 13, 577–581.
- Murata, T., and Wada, M. (1991). Effects of centrifugation on preprophase-band formation in *Adiantum protonemata*. *Planta* 183,.
- Murone, M., and Simanis, V. (1996). The fission yeast *dma1* gene is a component of the spindle assembly checkpoint, required to prevent septum formation and premature exit from mitosis if spindle function is compromised. *The EMBO Journal* 15, 6605–6616.
- Murphy, P.M. (1994). The molecular biology of leukocyte chemoattractant receptors. *Annual Review of Immunology* 12, 593–633.
- Murthy, K., and Wadsworth, P. (2005). Myosin-II-dependent localization and dynamics of F-actin during cytokinesis. *Current Biology : CB* 15, 724–731.
- Nakano, K., Bunai, F., and Numata, O. (2005). Stg 1 is a novel SM22/transgelin-like actin-modulating protein in fission yeast. *FEBS Letters* 579, 6311–6316.
- Nakano, K., Imai, J., Arai, R., Toh-E, A., Matsui, Y., and Mabuchi, I. (2002). The small GTPase Rho3 and the diaphanous/formin For3 function in polarized cell growth in fission yeast. *Journal of Cell Science* 115, 4629–4639.
- Naqvi, N.I., Eng, K., Gould, K.L., and Balasubramanian, M.K. (1999). Evidence for F-actin-dependent and -independent mechanisms involved in assembly and stability of the medial actomyosin ring in fission yeast. *The EMBO Journal* 18, 854–862.
- Nelson, B., Kurischko, C., Horecka, J., Mody, M., Nair, P., Pratt, L., Zougman, A., McBroom, L.D.B., Hughes, T.R., Boone, C., et al. (2003). RAM: a conserved signaling network that regulates Ace2p transcriptional activity and polarized morphogenesis. *Molecular Biology of the Cell* 14, 3782–3803.
- Nelson, W.J. (2003). Adaptation of core mechanisms to generate cell polarity. *Nature* 422, 766–774.
- Nigg, E.A., Hilz, H., Eppenberger, H.M., and Dutly, F. (1985). Rapid and reversible translocation of the catalytic subunit of cAMP-dependent protein

- kinase type II from the Golgi complex to the nucleus. *The EMBO Journal* 4, 2801–2806.
- Niyya, F., Xie, X., Lee, K.S., Inoue, H., and Miki, T. (2005). Inhibition of cyclin-dependent kinase 1 induces cytokinesis without chromosome segregation in an ECT2 and MgcRacGAP-dependent manner. *The Journal of Biological Chemistry* 280, 36502–36509.
- Nilsson, T., Pypaert, M., Hoe, M.H., Slusarewicz, P., Berger, E.G., and Warren, G. (1993). Overlapping distribution of two glycosyltransferases in the Golgi apparatus of HeLa cells. *The Journal of Cell Biology* 120, 5–13.
- Nishimura, Y., and Yonemura, S. (2006). Centralspindlin regulates ECT2 and RhoA accumulation at the equatorial cortex during cytokinesis. *Journal of Cell Science* 119, 104–114.
- Novick, P., Ferro, S., and Schekman, R. (1981). Order of events in the yeast secretory pathway. *Cell* 25, 461–469.
- Novick, P., Field, C., and Schekman, R. (1980). Identification of 23 complementation groups required for post-translational events in the yeast secretory pathway. *Cell* 21, 205–215.
- Ogata, T., and Yamasaki, Y. (1997). Ultra-high-resolution scanning electron microscopy of mitochondria and sarcoplasmic reticulum arrangement in human red, white, and intermediate muscle fibers. *The Anatomical Record* 248, 214–223.
- Ohkura, H., Hagan, I.M., and Glover, D.M. (1995). The conserved *Schizosaccharomyces pombe* kinase *plp1*, required to form a bipolar spindle, the actin ring, and septum, can drive septum formation in G1 and G2 cells. *Genes & Development* 9, 1059–1073.
- Oliferenko, S., Chew, T.G., and Balasubramanian, M.K. (2009). Positioning cytokinesis. *Genes & Development* 23, 660–674.
- Orci, L., Ravazzola, M., Meda, P., Holcomb, C., Moore, H.P., Hicke, L., and Schekman, R. (1991). Mammalian Sec23p homologue is restricted to the endoplasmic reticulum transitional cytoplasm. *Proceedings of the National Academy of Sciences of the United States of America* 88, 8611–8615.
- Orci, L., Ravazzola, M., Volchuk, A., Engel, T., Gmachl, M., Amherdt, M., Perrelet, A., Sollner, T.H., and Rothman, J.E. (2000). Anterograde flow of cargo across the golgi stack potentially mediated via bidirectional “percolating” COPI vesicles. *Proceedings of the National Academy of Sciences of the United States of America* 97, 10400–10405.
- Osumi, M., Sato, M., Ishijima, S.A., Konomi, M., Takagi, T., and Yaguchi, H. (1998). Dynamics of cell wall formation in fission yeast, *Schizosaccharomyces pombe*. *Fungal Genetics and Biology : FG & B* 24, 178–206.
- Ozbudak, E.M., Becskei, A., and Van Oudenaarden, A. (2005). A system of counteracting feedback loops regulates Cdc42p activity during spontaneous cell polarization. *Developmental Cell* 9, 565–571.

- Padmanabhan, A., Bakka, K., Sevugan, M., Naqvi, N.I., D'souza, V., Tang, X., Mishra, M., and Balasubramanian, M.K. (2011). IQGAP-related Rng2p organizes cortical nodes and ensures position of cell division in fission yeast. *Current Biology* : CB 21, 467–472.
- Paoletti, A., and Chang, F. (2000). Analysis of mid1p, a protein required for placement of the cell division site, reveals a link between the nucleus and the cell surface in fission yeast. *Molecular Biology of the Cell* 11, 2757–2773.
- Papanikou, E., and Glick, B.S. (2009). The yeast Golgi apparatus: insights and mysteries. *FEBS Letters* 583, 3746–3751.
- Park, H.O., Bi, E., Pringle, J.R., and Herskowitz, I. (1997). Two active states of the Ras-related Bud1/Rsr1 protein bind to different effectors to determine yeast cell polarity. *Proceedings of the National Academy of Sciences of the United States of America* 94, 4463–4468.
- Parlati, F., McNew, J.A., Fukuda, R., Miller, R., Söllner, T.H., and Rothman, J.E. (2000). Topological restriction of SNARE-dependent membrane fusion. *Nature* 407, 194–198.
- Patterson, G.H., Hirschberg, K., Polishchuk, R.S., Gerlich, D., Phair, R.D., and Lippincott-Schwartz, J. (2008). Transport through the Golgi apparatus by rapid partitioning within a two-phase membrane system. *Cell* 133, 1055–1067.
- Pavicic-Kaltenbrunner, V., Mishima, M., and Glotzer, M. (2007). Cooperative assembly of CYK-4/MgcRacGAP and ZEN-4/MKLP1 to form the centralspindlin complex. *Molecular Biology of the Cell* 18, 4992–5003.
- Pendin, D., McNew, J. a, and Daga, A. (2011). Balancing ER dynamics: shaping, bending, severing, and mending membranes. *Current Opinion in Cell Biology* 23, 435–442.
- Peng, X., Karuturi, R.K.M., Miller, L.D., Lin, K., Jia, Y., Kondu, P., Wang, L., Wong, L., Liu, E.T., Balasubramanian, M.K., et al. (2005). Identification of Cell Cycle-regulated Genes in Fission Yeast □. 16, 1026–1042.
- Petersen, J., and Hagan, I.M. (2005). Polo kinase links the stress pathway to cell cycle control and tip growth in fission yeast. *Nature* 435, 507–512.
- Peterson, J., Zheng, Y., Bender, L., Myers, A., Cerione, R., and Bender, A. (1994). Interactions between the bud emergence proteins Bem1p and Bem2p and Rho-type GTPases in yeast. *The Journal of Cell Biology* 127, 1395–1406.
- Petronczki, M., Glotzer, M., Kraut, N., and Peters, J.-M. (2007). Polo-like kinase 1 triggers the initiation of cytokinesis in human cells by promoting recruitment of the RhoGEF Ect2 to the central spindle. *Developmental Cell* 12, 713–725.
- Pfeffer, S.R. (2010). How the Golgi works: a cisternal progenitor model. *Proceedings of the National Academy of Sciences of the United States of America* 107, 19614–19618.
- Philip, B., and Levin, D.E. (2001). Wsc1 and Mid2 are cell surface sensors for cell wall integrity signaling that act through Rom2, a guanine nucleotide exchange factor for Rho1. *Molecular and Cellular Biology* 21, 271–280.

- Phillips, M.J., Calero, G., Chan, B., Ramachandran, S., and Cerione, R.A. (2008). Effector proteins exert an important influence on the signaling-active state of the small GTPase Cdc42. *The Journal of Biological Chemistry* 283, 14153–14164.
- Phillips, R., Ursell, T., Wiggins, P., and Sens, P. (2009). Emerging roles for lipids in shaping membrane-protein function. *Nature* 459, 379–385.
- Piekny, A.J., and Glotzer, M. (2008). Anillin is a scaffold protein that links RhoA, actin, and myosin during cytokinesis. *Current Biology : CB* 18, 30–36.
- Piel, M., and Tran, P.T. (2009). Cell shape and cell division in fission yeast. *Current Biology : CB* 19, R823–7.
- Pobbati, A. V., Stein, A., and Fasshauer, D. (2006). N- to C-terminal SNARE complex assembly promotes rapid membrane fusion. *Science (New York, N.Y.)* 313, 673–676.
- Popoff, V., Adolf, F., Brügger, B., and Wieland, F. (2011). COPI budding within the Golgi stack. *Cold Spring Harbor Perspectives in Biology* 3, a005231.
- Poteryaev, D., Datta, S., Ackema, K., Zerial, M., and Spang, A. (2010). Identification of the switch in early-to-late endosome transition. *Cell* 141, 497–508.
- Presti, L. Lo, Chang, F., and Martin, S.G. (2012). Myosin Vs organize actin cables in fission yeast. *Molecular Biology of the Cell* 23, 4579–4591.
- Lo Presti, L., and Martin, S.G. (2011). Shaping fission yeast cells by rerouting actin-based transport on microtubules. *Current Biology : CB* 21, 2064–2069.
- Preuss, D., Mulholland, J., Franzusoff, A., Segev, N., and Botstein, D. (1992). Characterization of the *Saccharomyces* Golgi complex through the cell cycle by immunoelectron microscopy. *Molecular Biology of the Cell* 3, 789–803.
- Prior, M., Shi, Q., Hu, X., He, W., Levey, A., and Yan, R. (2010). RTN/Nogo in forming Alzheimer's neuritic plaques. *Neuroscience and Biobehavioral Reviews* 34, 1201–1206.
- Pruyne, D., Legesse-Miller, A., Gao, L., Dong, Y., and Bretscher, A. (2004). Mechanisms of polarized growth and organelle segregation in yeast. *Annual Review of Cell and Developmental Biology* 20, 559–591.
- Pruyne, D.W., Schott, D.H., and Bretscher, A. (1998). Tropomyosin-containing actin cables direct the Myo2p-dependent polarized delivery of secretory vesicles in budding yeast. *The Journal of Cell Biology* 143, 1931–1945.
- Puhka, M., Vihinen, H., Joensuu, M., and Jokitalo, E. (2007). Endoplasmic reticulum remains continuous and undergoes sheet-to-tubule transformation during cell division in mammalian cells. *The Journal of Cell Biology* 179, 895–909.
- Puri, S., and Linstedt, A.D. (2003). Capacity of the golgi apparatus for biogenesis from the endoplasmic reticulum. *Molecular Biology of the Cell* 14, 5011–5018.

- Rabouille, C., Hui, N., Hunte, F., Kieckbusch, R., Berger, E.G., Warren, G., and Nilsson, T. (1995). Mapping the distribution of Golgi enzymes involved in the construction of complex oligosaccharides. *Journal of Cell Science* *108* (Pt 4, 1617–1627.
- Rasmussen, C.G., Humphries, J. a, and Smith, L.G. (2011). Determination of symmetric and asymmetric division planes in plant cells. *Annual Review of Plant Biology* *62*, 387–409.
- Ray, S., Kume, K., Gupta, S., Ge, W., Balasubramanian, M., Hirata, D., and McCollum, D. (2010). The mitosis-to-interphase transition is coordinated by cross talk between the SIN and MOR pathways in *Schizosaccharomyces pombe*. *The Journal of Cell Biology* *190*, 793–805.
- Reynwar, B.J., Illya, G., Harmandaris, V. a, Müller, M.M., Kremer, K., and Deserno, M. (2007). Aggregation and vesiculation of membrane proteins by curvature-mediated interactions. *Nature* *447*, 461–464.
- Richter, K., Haslbeck, M., and Buchner, J. (2010). The heat shock response: life on the verge of death. *Molecular Cell* *40*, 253–266.
- Rida, P.C.G., Nishikawa, A., Won, G.Y., and Dean, N. (2006). Yeast-to-hyphal transition triggers formin-dependent Golgi localization to the growing tip in *Candida albicans*. *Molecular Biology of the Cell* *17*, 4364–4378.
- Rieger, T.R., Morimoto, R.I., and Hatzimanikatis, V. (2005). Mathematical modeling of the eukaryotic heat-shock response: dynamics of the hsp70 promoter. *Biophysical Journal* *88*, 1646–1658.
- Rink, J., Ghigo, E., Kalaidzidis, Y., and Zerial, M. (2005). Rab conversion as a mechanism of progression from early to late endosomes. *Cell* *122*, 735–749.
- Rittinger, K., Walker, P.A., Eccleston, J.F., Smerdon, S.J., and Gamblin, S.J. (1997). Structure at 1.65 Å of RhoA and its GTPase-activating protein in complex with a transition-state analogue. *Nature* *389*, 758–762.
- Rivero, F., and Cvrcková, F. (2000). Origins and Evolution of the Actin Cytoskeleton.
- Roberts-Galbraith, R.H., Chen, J.-S., Wang, J., and Gould, K.L. (2009). The SH3 domains of two PCH family members cooperate in assembly of the *Schizosaccharomyces pombe* contractile ring. *The Journal of Cell Biology* *184*, 113–127.
- Roberts-Galbraith, R.H., Ohi, M.D., Ballif, B.A., Chen, J.-S., McLeod, I., McDonald, W.H., Gygi, S.P., Yates, J.R., and Gould, K.L. (2010). Dephosphorylation of F-BAR protein Cdc15 modulates its conformation and stimulates its scaffolding activity at the cell division site. *Molecular Cell* *39*, 86–99.
- Robertson, a. M., and Hagan, I.M. (2008). Stress-regulated kinase pathways in the recovery of tip growth and microtubule dynamics following osmotic stress in *S. pombe*. *Journal of Cell Science* *121*, 4055–4068.
- Robinson, N.G., Guo, L., Imai, J., Toh-E, A., Matsui, Y., and Tamanoi, F. (1999). Rho3 of *Saccharomyces cerevisiae*, which regulates the actin

- cytoskeleton and exocytosis, is a GTPase which interacts with Myo2 and Exo70. *Molecular and Cellular Biology* *19*, 3580–3587.
- Rodriguez, O.C., Schaefer, A.W., Mandato, C.A., Forscher, P., Bement, W.M., and Waterman-Storer, C.M. (2003). Conserved microtubule-actin interactions in cell movement and morphogenesis. *Nature Cell Biology* *5*, 599–609.
- Romero, S., Le Clainche, C., Didry, D., Egile, C., Pantaloni, D., and Carlier, M.-F. (2004). Formin is a processive motor that requires profilin to accelerate actin assembly and associated ATP hydrolysis. *Cell* *119*, 419–429.
- Rosario, C.O., Ko, M.A., Haffani, Y.Z., Gladdy, R.A., Paderova, J., Pollett, A., Squire, J.A., Dennis, J.W., and Swallow, C.J. (2010). Plk4 is required for cytokinesis and maintenance of chromosomal stability. *Proceedings of the National Academy of Sciences of the United States of America* *107*, 6888–6893.
- Rosenberg, J.A., Tomlin, G.C., McDonald, W.H., Snydsman, B.E., Muller, E.G., Yates, J.R., and Gould, K.L. (2006). Ppc89 links multiple proteins, including the septation initiation network, to the core of the fission yeast spindle-pole body. *Molecular Biology of the Cell* *17*, 3793–3805.
- Rossanese, O.W., Soderholm, J., Bevis, B.J., Sears, I.B., O'Connor, J., Williamson, E.K., and Glick, B.S. (1999). Golgi structure correlates with transitional endoplasmic reticulum organization in *Pichia pastoris* and *Saccharomyces cerevisiae*. *The Journal of Cell Biology* *145*, 69–81.
- Rossmann, K.L., Der, C.J., and Sodek, J. (2005). GEF means go: turning on RHO GTPases with guanine nucleotide-exchange factors. *Nature Reviews. Molecular Cell Biology* *6*, 167–180.
- Roth, D., Guo, W., and Novick, P. (1998). Dominant negative alleles of SEC10 reveal distinct domains involved in secretion and morphogenesis in yeast. *Molecular Biology of the Cell* *9*, 1725–1739.
- Rothman, J.E. (1994). Mechanisms of intracellular protein transport. *Nature* *372*, 55–63.
- Rothman, J.E., and Wieland, F.T. (1996). Protein sorting by transport vesicles. *Science (New York, N.Y.)* *272*, 227–234.
- Royer, C., and Lu, X. (2011). Epithelial cell polarity: a major gatekeeper against cancer? *Cell Death and Differentiation* *18*, 1470–1477.
- Rupes, I., Jia, Z., and Young, P.G. (1999). Ssp1 promotes actin depolymerization and is involved in stress response and new end take-off control in fission yeast. *Molecular Biology of the Cell* *10*, 1495–1510.
- Rupes, I., Webb, B.A., Mak, A., and Young, P.G. (2001). G2/M arrest caused by actin disruption is a manifestation of the cell size checkpoint in fission yeast. *Molecular Biology of the Cell* *12*, 3892–3903.
- Sabatino, S.A., and Forsburg, S.L. (2009). Measuring DNA content by flow cytometry in fission yeast. *Methods in Molecular Biology (Clifton, N.J.)* *521*, 449–461.

- Sabherwal, N., and Papalopulu, N. (2012). Apicobasal polarity and cell proliferation during development. *Essays in Biochemistry* 53, 95–109.
- Sacher, M., Barrowman, J., Wang, W., Horecka, J., Zhang, Y., Pypaert, M., and Ferro-Novick, S. (2001). TRAPP I implicated in the specificity of tethering in ER-to-Golgi transport. *Molecular Cell* 7, 433–442.
- Sagona, A.P., and Stenmark, H. (2010). Cytokinesis and cancer. *FEBS Letters* 584, 2652–2661.
- Salama, N.R., Yeung, T., and Schekman, R.W. (1993). The Sec13p complex and reconstitution of vesicle budding from the ER with purified cytosolic proteins. *The EMBO Journal* 12, 4073–4082.
- Salimova, E., Sohrmann, M., Fournier, N., and Simanis, V. (2000). The *S. pombe* orthologue of the *S. cerevisiae* *mob1* gene is essential and functions in signalling the onset of septum formation. *Journal of Cell Science* 113 (Pt 1, 1695–1704.
- Salminen, A., and Novick, P.J. (1989). The Sec15 protein responds to the function of the GTP binding protein, Sec4, to control vesicular traffic in yeast. *The Journal of Cell Biology* 109, 1023–1036.
- Samejima, I., Lourenço, P.C.C., Snaith, H.A., and Sawin, K.E. (2005). Fission yeast *mto2p* regulates microtubule nucleation by the centrosomin-related protein *mto1p*. *Molecular Biology of the Cell* 16, 3040–3051.
- San Pietro, E., Capestrano, M., Polishchuk, E. V, DiPentima, A., Trucco, A., Zizza, P., Mariggì, S., Pulvirenti, T., Sallese, M., Tete, S., et al. (2009). Group IV phospholipase A(2)alpha controls the formation of inter-cisternal continuities involved in intra-Golgi transport. *PLoS Biology* 7, e1000194.
- Sawin, K.E., and Snaith, H. a (2004). Role of microtubules and *tea1p* in establishment and maintenance of fission yeast cell polarity. *Journal of Cell Science* 117, 689–700.
- Schmidt, S., Sohrmann, M., Hofmann, K., Woollard, A., and Simanis, V. (1997). The *Spg1p* GTPase is an essential, dosage-dependent inducer of septum formation in *Schizosaccharomyces pombe*. *Genes & Development* 11, 1519–1534.
- Seemann, J., Jokitalo, E., Pypaert, M., and Warren, G. (2000). Matrix proteins can generate the higher order architecture of the Golgi apparatus. *Nature* 407, 1022–1026.
- Segall, J.E. (1993). Polarization of yeast cells in spatial gradients of alpha mating factor. *Proceedings of the National Academy of Sciences of the United States of America* 90, 8332–8336.
- Serafini, T., Stenbeck, G., Brecht, A., Lottspeich, F., Orci, L., Rothman, J.E., and Wieland, F.T. (1991). A coat subunit of Golgi-derived non-clathrin-coated vesicles with homology to the clathrin-coated vesicle coat protein beta-adaptin. *Nature* 349, 215–220.
- Shanks, R.A., Steadman, B.T., Schmidt, P.H., and Goldenring, J.R. (2002). AKAP350 at the Golgi apparatus. I. Identification of a distinct Golgi apparatus

- targeting motif in AKAP350. *The Journal of Biological Chemistry* 277, 40967–40972.
- Shaywitz, D. a, Orci, L., Ravazzola, M., Swaroop, a, and Kaiser, C. a (1995). Human SEC13Rp functions in yeast and is located on transport vesicles budding from the endoplasmic reticulum. *The Journal of Cell Biology* 128, 769–777.
- Shaywitz, D.A., Espenshade, P.J., Gimeno, R.E., and Kaiser, C.A. (1997). COPII subunit interactions in the assembly of the vesicle coat. *The Journal of Biological Chemistry* 272, 25413–25416.
- Shi, Y., Mosser, D.D., and Morimoto, R.I. (1998). Molecular chaperones as HSF1-specific transcriptional repressors. 654–666.
- Shibata, Y., Shemesh, T., Prinz, W. a, Palazzo, A.F., Kozlov, M.M., and Rapoport, T. a (2010). Mechanisms determining the morphology of the peripheral ER. *Cell* 143, 774–788.
- Shimada, A., Niwa, H., Tsujita, K., Suetsugu, S., Nitta, K., Hanawa-Suetsugu, K., Akasaka, R., Nishino, Y., Toyama, M., Chen, L., et al. (2007). Curved EFC/F-BAR-domain dimers are joined end to end into a filament for membrane invagination in endocytosis. *Cell* 129, 761–772.
- Shiozaki, K., Shiozaki, M., and Russell, P. (1998). Heat stress activates fission yeast Spc1/StyI MAPK by a MEKK-independent mechanism. *Molecular Biology of the Cell* 9, 1339–1349.
- Shohat, M., Janossy, G., and Dourmashkin, R.R. (1973). Development of rough endoplasmic reticulum in mouse splenic lymphocytes stimulated by mitogens. *European Journal of Immunology* 3, 680–687.
- Shorter, J., Watson, R., Giannakou, M.E., Clarke, M., Warren, G., and Barr, F.A. (1999). GRASP55, a second mammalian GRASP protein involved in the stacking of Golgi cisternae in a cell-free system. *The EMBO Journal* 18, 4949–4960.
- Siam, R., Dolan, W.P., and Forsburg, S.L. (2004). Choosing and using *Schizosaccharomyces pombe* plasmids. *Methods (San Diego, Calif.)* 33, 189–198.
- Siegrist, S.E., and Doe, C.Q. (2007). Microtubule-induced cortical cell polarity. *Genes & Development* 21, 483–496.
- Silberstein, S., Collins, P.G., Kelleher, D.J., Rapiejko, P.J., and Gilmore, R. (1995). The alpha subunit of the *Saccharomyces cerevisiae* oligosaccharyltransferase complex is essential for vegetative growth of yeast and is homologous to mammalian ribophorin I. *The Journal of Cell Biology* 128, 525–536.
- Sinha, S., and Yang, W. (2008). Cellular signaling for activation of Rho GTPase Cdc42. *Cellular Signalling* 20, 1927–1934.
- Sirotkin, V., Beltzner, C.C., Marchand, J.-B., and Pollard, T.D. (2005). Interactions of WASp, myosin-I, and verprolin with Arp2/3 complex during actin patch assembly in fission yeast. *The Journal of Cell Biology* 170, 637–648.

- Sirotkin, V., Berro, J., Macmillan, K., Zhao, L., and Pollard, T.D. (2010). Quantitative analysis of the mechanism of endocytic actin patch assembly and disassembly in fission yeast. *Molecular Biology of the Cell* *21*, 2894–2904.
- Sivaram, M.V.S., Furgason, M.L.M., Brewer, D.N., and Munson, M. (2006). The structure of the exocyst subunit Sec6p defines a conserved architecture with diverse roles. *Nature Structural & Molecular Biology* *13*, 555–556.
- Skau, C.T., and Kovar, D.R. (2010). Fimbrin and tropomyosin competition regulates endocytosis and cytokinesis kinetics in fission yeast. *Current Biology : CB* *20*, 1415–1422.
- Slusarewicz, P., Nilsson, T., Hui, N., Watson, R., and Warren, G. (1994). Isolation of a matrix that binds medial Golgi enzymes. *The Journal of Cell Biology* *124*, 405–413.
- Snaith, H.A., Samejima, I., and Sawin, K.E. (2005). Multistep and multimode cortical anchoring of tea1p at cell tips in fission yeast. *The EMBO Journal* *24*, 3690–3699.
- Snaith, H.A., and Sawin, K.E. (2003). Fission yeast mod5p regulates polarized growth through anchoring of tea1p at cell tips.x. *Nature* *423*, 647–651.
- Snell, V., and Nurse, P. (1994). Genetic analysis of cell morphogenesis in fission yeast--a role for casein kinase II in the establishment of polarized growth. *The EMBO Journal* *13*, 2066–2074.
- Sohrmann, M., Schmidt, S., Hagan, I., and Simanis, V. (1998). Asymmetric segregation on spindle poles of the *Schizosaccharomyces pombe* septum-inducing protein kinase Cdc7p. *Genes & Development* *12*, 84–94.
- Song, K., Mach, K.E., Chen, C.Y., Reynolds, T., and Albright, C.F. (1996). A novel suppressor of ras1 in fission yeast, byr4, is a dosage-dependent inhibitor of cytokinesis. *The Journal of Cell Biology* *133*, 1307–1319.
- Spang, A. (2012). The DSL1 complex: the smallest but not the least CATCHR. *Traffic (Copenhagen, Denmark)* *13*, 908–913.
- Spang, A., Herrmann, J.M., Hamamoto, S., and Schekman, R. (2001). The ADP ribosylation factor-nucleotide exchange factors Gea1p and Gea2p have overlapping, but not redundant functions in retrograde transport from the Golgi to the endoplasmic reticulum. *Molecular Biology of the Cell* *12*, 1035–1045.
- Spang, A., Matsuoka, K., Hamamoto, S., Schekman, R., and Orci, L. (1998). Coatamer, Arf1p, and nucleotide are required to bud coat protein complex I-coated vesicles from large synthetic liposomes. *Proceedings of the National Academy of Sciences of the United States of America* *95*, 11199–11204.
- Sparks, C.A., Moprhew, M., and McCollum, D. (1999). Sid2p, a spindle pole body kinase that regulates the onset of cytokinesis. *The Journal of Cell Biology* *146*, 777–790.
- Spoerner, M., Herrmann, C., Vetter, I.R., Kalbitzer, H.R., and Wittinghofer, A. (2001). Dynamic properties of the Ras switch I region and its importance for binding to effectors. *Proceedings of the National Academy of Sciences of the United States of America* *98*, 4944–4949.

- Staehelein, L.A., and Kang, B.-H. (2008). Nanoscale architecture of endoplasmic reticulum export sites and of Golgi membranes as determined by electron tomography. *Plant Physiology* *147*, 1454–1468.
- Stefan, C.J., Audhya, A., and Emr, S.D. (2002). The yeast synaptojanin-like proteins control the cellular distribution of phosphatidylinositol (4,5)-bisphosphate. *Molecular Biology of the Cell* *13*, 542–557.
- Storrie, B., White, J., Röttger, S., Stelzer, E.H., Sukanuma, T., and Nilsson, T. (1998). Recycling of golgi-resident glycosyltransferases through the ER reveals a novel pathway and provides an explanation for nocodazole-induced Golgi scattering. *The Journal of Cell Biology* *143*, 1505–1521.
- Stradalova, V., Blazikova, M., Grossmann, G., Opekarová, M., Tanner, W., and Malinsky, J. (2012). Distribution of cortical endoplasmic reticulum determines positioning of endocytic events in yeast plasma membrane. *PLoS One* *7*, e35132.
- Straight, A.F. (2007). Fluorescent protein applications in microscopy. *Methods in Cell Biology* *81*, 93–113.
- Straight, A.F., Field, C.M., and Mitchison, T.J. (2005). Anillin binds nonmuscle myosin II and regulates the contractile ring. *Molecular Biology of the Cell* *16*, 193–201.
- Su, K.-C., Takaki, T., and Petronczki, M. (2011). Targeting of the RhoGEF Ect2 to the equatorial membrane controls cleavage furrow formation during cytokinesis. *Developmental Cell* *21*, 1104–1115.
- Sutton, R.B., Fasshauer, D., Jahn, R., and Brunger, A.T. (1998). Crystal structure of a SNARE complex involved in synaptic exocytosis at 2.4 Å resolution. *Nature* *395*, 347–353.
- Söllner, T., Whiteheart, S.W., Brunner, M., Erdjument-Bromage, H., Geromanos, S., Tempst, P., and Rothman, J.E. (1993). SNAP receptors implicated in vesicle targeting and fusion. *Nature* *362*, 318–324.
- Sütterlin, C., Hsu, P., Mallabiabarrena, A., and Malhotra, V. (2002). Fragmentation and dispersal of the pericentriolar Golgi complex is required for entry into mitosis in mammalian cells. *Cell* *109*, 359–369.
- Taipale, M., Krykbaeva, I., Koeva, M., Kayatekin, C., Westover, K.D., Karras, G.I., and Lindquist, S. (2012). Quantitative analysis of HSP90-client interactions reveals principles of substrate recognition. *Cell* *150*, 987–1001.
- Tanaka, K., Petersen, J., MacIver, F., Mulvihill, D.P., Glover, D.M., and Hagan, I.M. (2001). The role of Plo1 kinase in mitotic commitment and septation in *Schizosaccharomyces pombe*. *The EMBO Journal* *20*, 1259–1270.
- Tang, X., Huang, J., Padmanabhan, A., Bakka, K., Bao, Y., Tan, B.Y., Cande, W.Z., and Balasubramanian, M.K. (2011). Marker reconstitution mutagenesis: a simple and efficient reverse genetic approach. *Yeast (Chichester, England)* *28*, 205–212.
- Tatebe, H., Nakano, K., Maximo, R., and Shiozaki, K. (2008). Pom1 DYRK Regulates Localization of the Rga4 GAP to Ensure Bipolar Activation of Cdc42 in Fission Yeast. *Current Biology* *18*, 322–330.

- Tatebe, H., Shimada, K., Uzawa, S., Morigasaki, S., and Shiozaki, K. (2005). Wsh3/Tea4 Is a Novel Cell-End Factor Essential for Bipolar Distribution of Tea1 and Protects Cell Polarity under Environmental Stress in *S. pombe*. *Current Biology* *15*, 1006–1015.
- TerBush, D.R., Maurice, T., Roth, D., and Novick, P. (1996). The Exocyst is a multiprotein complex required for exocytosis in *Saccharomyces cerevisiae*. *The EMBO Journal* *15*, 6483–6494.
- Terenna, C.R., Makushok, T., Velve-Casquillas, G., Baigl, D., Chen, Y., Bornens, M., Paoletti, A., Piel, M., and Tran, P.T. (2008). Physical mechanisms redirecting cell polarity and cell shape in fission yeast. *Current Biology* : *CB 18*, 1748–1753.
- Thadani, R., Huang, D., and Oliferenko, S. (2011). Robust polarity specification operates above a threshold of microtubule dynamicity. *Cytoskeleton (Hoboken, N.J.)* *68*, 290–299.
- Tiedje, C., Sakwa, I., Just, U., and Ho, T. (2008). The Rho GDI Rdi1 Regulates Rho GTPases by Distinct Mechanisms. *19*, 2885–2896.
- Toda, T., Dhut, S., Superti-Furga, G., Gotoh, Y., Nishida, E., Sugiura, R., and Kuno, T. (1996). The fission yeast *pmk1+* gene encodes a novel mitogen-activated protein kinase homolog which regulates cell integrity and functions coordinately with the protein kinase C pathway. *Molecular and Cellular Biology* *16*, 6752–6764.
- Tolic-Nørrelykke, I.M., Sacconi, L., Stringari, C., Raabe, I., and Pavone, F.S. (2005). Nuclear and division-plane positioning revealed by optical micromanipulation. *Current Biology* : *CB 15*, 1212–1216.
- Toyooka, K., Goto, Y., Asatsuma, S., Koizumi, M., Mitsui, T., and Matsuoka, K. (2009). A mobile secretory vesicle cluster involved in mass transport from the Golgi to the plant cell exterior. *The Plant Cell* *21*, 1212–1229.
- Trucco, A., Polishchuk, R.S., Martella, O., Di Pentima, A., Fusella, A., Di Giandomenico, D., San Pietro, E., Beznoussenko, G. V, Polishchuk, E. V, Baldassarre, M., et al. (2004). Secretory traffic triggers the formation of tubular continuities across Golgi sub-compartments. *Nature Cell Biology* *6*, 1071–1081.
- Tsujita, K., Suetsugu, S., Sasaki, N., Furutani, M., Oikawa, T., and Takenawa, T. (2006). Coordination between the actin cytoskeleton and membrane deformation by a novel membrane tubulation domain of PCH proteins is involved in endocytosis. *The Journal of Cell Biology* *172*, 269–279.
- Tu, L., Tai, W.C.S., Chen, L., and Banfield, D.K. (2008). Signal-mediated dynamic retention of glycosyltransferases in the Golgi. *Science (New York, N.Y.)* *321*, 404–407.
- Ueda, H., Yokota, E., Kutsuna, N., Shimada, T., Tamura, K., Shimmen, T., Hasezawa, S., Dolja, V. V, and Hara-Nishimura, I. (2010). Myosin-dependent endoplasmic reticulum motility and F-actin organization in plant cells. *Proceedings of the National Academy of Sciences of the United States of America* *107*, 6894–6899.

- Uehara, R., Goshima, G., Mabuchi, I., Vale, R.D., Spudich, J.A., and Griffis, E.R. (2010). Determinants of myosin II cortical localization during cytokinesis. *Current Biology* : CB 20, 1080–1085.
- Vale, R.D. (2003). The Molecular Motor Toolbox for Intracellular Transport. *112*, 467–480.
- Vale, R.D., Spudich, J.A., and Griffis, E.R. (2009). Dynamics of myosin, microtubules, and Kinesin-6 at the cortex during cytokinesis in *Drosophila* S2 cells. *The Journal of Cell Biology* 186, 727–738.
- Vasile, E., Perez, T., Nakamura, N., and Krieger, M. (2003). Structural integrity of the Golgi is temperature sensitive in conditional-lethal mutants with no detectable GM130. *Traffic (Copenhagen, Denmark)* 4, 254–272.
- Vavylonis, D., Wu, J.-Q., Hao, S., O’Shaughnessy, B., and Pollard, T.D. (2008). Assembly mechanism of the contractile ring for cytokinesis by fission yeast. *Science (New York, N.Y.)* 319, 97–100.
- Venkatram, S., Tasto, J.J., Feoktistova, A., Jennings, J.L., Link, A.J., and Gould, K.L. (2004). Identification and characterization of two novel proteins affecting fission yeast gamma-tubulin complex function. *Molecular Biology of the Cell* 15, 2287–2301.
- Verde, F., Mata, J., and Nurse, P. (1995). Fission yeast cell morphogenesis: identification of new genes and analysis of their role during the cell cycle. *The Journal of Cell Biology* 131, 1529–1538.
- Verde, F., Wiley, D.J., and Nurse, P. (1998). Fission yeast orb6, a ser/thr protein kinase related to mammalian rho kinase and myotonic dystrophy kinase, is required for maintenance of cell polarity and coordinates cell morphogenesis with the cell cycle. *Proceedings of the National Academy of Sciences of the United States of America* 95, 7526–7531.
- Vergés, E., Colomina, N., Garí, E., Gallego, C., and Aldea, M. (2007). Cyclin Cln3 is retained at the ER and released by the J chaperone Ydj1 in late G1 to trigger cell cycle entry. *Molecular Cell* 26, 649–662.
- Voeltz, G.K., Prinz, W.A., Shibata, Y., Rist, J.M., and Rapoport, T.A. (2006). A class of membrane proteins shaping the tubular endoplasmic reticulum. *Cell* 124, 573–586.
- Volchuk, A., Ravazzola, M., Perrelet, A., Eng, W.S., Di Liberto, M., Varlamov, O., Fukasawa, M., Engel, T., Söllner, T.H., Rothman, J.E., et al. (2004). Countercurrent distribution of two distinct SNARE complexes mediating transport within the Golgi stack. *Molecular Biology of the Cell* 15, 1506–1518.
- Vujanac, M., and Fenaroli, A. (2005). Constitutive Nuclear Import and Stress-Regulated Nucleocytoplasmic Shuttling of Mammalian Heat-Shock Factor 1 Rat12 Tet-Off Phase. 214–229.
- Wachtler, V., Huang, Y., Karagiannis, J., and Balasubramanian, M.K. (2006). Cell cycle-dependent roles for the FCH-domain protein Cdc15p in formation of the actomyosin ring in *Schizosaccharomyces pombe*. *Molecular Biology of the Cell* 17, 3254–3266.

- Wagner, W., Brenowitz, S.D., and Hammer, J.A. (2011). Myosin-Va transports the endoplasmic reticulum into the dendritic spines of Purkinje neurons. *Nature Cell Biology* *13*, 40–48.
- Walker, K.L., Müller, S., Moss, D., Ehrhardt, D.W., and Smith, L.G. (2007). Arabidopsis TANGLED identifies the division plane throughout mitosis and cytokinesis. *Current Biology : CB* *17*, 1827–1836.
- Wang, H., Tang, X., Liu, J., Trautmann, S., Mccollum, D., and Balasubramanian, M.K. (2002). The Multiprotein Exocyst Complex Is Essential for Cell Separation in *Schizosaccharomyces pombe*. *13*, 515–529.
- Wang, L., Kao, R., Ivey, F.D., and Hoffman, C.S. (2004). Strategies for gene disruptions and plasmid constructions in fission yeast. *Methods (San Diego, Calif.)* *33*, 199–205.
- Watanabe, N., Madaule, P., Reid, T., Ishizaki, T., Watanabe, G., Kakizuka, A., Saito, Y., Nakao, K., Jockusch, B.M., and Narumiya, S. (1997). p140mDia, a mammalian homolog of *Drosophila* diaphanous, is a target protein for Rho small GTPase and is a ligand for profilin. *The EMBO Journal* *16*, 3044–3056.
- Watson, P., Townley, A.K., Koka, P., Palmer, K.J., and Stephens, D.J. (2006). Sec16 defines endoplasmic reticulum exit sites and is required for secretory cargo export in mammalian cells. *Traffic (Copenhagen, Denmark)* *7*, 1678–1687.
- Weber, T., Zemelman, B. V., McNew, J.A., Westermann, B., Gmachl, M., Parlati, F., Söllner, T.H., and Rothman, J.E. (1998). SNAREpins: minimal machinery for membrane fusion. *Cell* *92*, 759–772.
- Wedlich-Soldner, R. (2003). Spontaneous Cell Polarization Through Actomyosin-Based Delivery of the Cdc42 GTPase. *Science* *299*, 1231–1235.
- Wedlich-Soldner, R., Wai, S.C., Schmidt, T., and Li, R. (2004). Robust cell polarity is a dynamic state established by coupling transport and GTPase signaling. *The Journal of Cell Biology* *166*, 889–900.
- Welch, W.I., and Suhan, J.P. (1985). Morphological Study of the Mammalian Stress Response " Characterization of Changes in Cytoplasmic Organelles , Cytoskeleton , and Nucleoli , and Appearance of Intranuclear Actin Filaments in Rat Fibroblasts after Heat-Shock Treatment. *101*,.
- Wendeler, M.W., Paccaud, J.-P., and Hauri, H.-P. (2007). Role of Sec24 isoforms in selective export of membrane proteins from the endoplasmic reticulum. *EMBO Reports* *8*, 258–264.
- Werner, M., Munro, E., and Glotzer, M. (2007). Astral signals spatially bias cortical myosin recruitment to break symmetry and promote cytokinesis. *Current Biology : CB* *17*, 1286–1297.
- West, M., Zurek, N., Hoenger, A., and Voeltz, G.K. (2011). A 3D analysis of yeast ER structure reveals how ER domains are organized by membrane curvature. *The Journal of Cell Biology* *193*, 333–346.
- Wheatley, E., and Rittinger, K. (2005). Interactions between Cdc42 and the scaffold protein Scd2: requirement of SH3 domains for GTPase binding. *The Biochemical Journal* *388*, 177–184.

- Wheatley, S.P., Hinchcliffe, E.H., Glotzer, M., Hyman, A.A., Sluder, G., and Wang, Y. I (1997). CDK1 inactivation regulates anaphase spindle dynamics and cytokinesis in vivo. *The Journal of Cell Biology* *138*, 385–393.
- Whittle, J.R.R., and Schwartz, T.U. (2010). Structure of the Sec13-Sec16 edge element, a template for assembly of the COPII vesicle coat. *The Journal of Cell Biology* *190*, 347–361.
- Wickstead, B., and Gull, K. (2011). The evolution of the cytoskeleton. *The Journal of Cell Biology* *194*, 513–525.
- Wiederkehr, A., De Craene, J.-O., Ferro-Novick, S., and Novick, P. (2004). Functional specialization within a vesicle tethering complex: bypass of a subset of exocyst deletion mutants by Sec1p or Sec4p. *The Journal of Cell Biology* *167*, 875–887.
- Win, T.Z., Gachet, Y., Mulvihill, D.P., May, K.M., and Hyams, J.S. (2001). Two type V myosins with non-overlapping functions in the fission yeast *Schizosaccharomyces pombe*: Myo52 is concerned with growth polarity and cytokinesis, Myo51 is a component of the cytokinetic actin ring. *Journal of Cell Science* *114*, 69–79.
- Wong, K.C., Naqvi, N.I., Iino, Y., Yamamoto, M., and Balasubramanian, M.K. (2000). Fission yeast Rng3p: an UCS-domain protein that mediates myosin II assembly during cytokinesis. *Journal of Cell Science* *113* (Pt 1, 2421–2432.
- Wong, K.C.Y., D'souza, V.M., Naqvi, N.I., Motegi, F., Mabuchi, I., and Balasubramanian, M.K. (2002). Importance of a myosin II-containing progenitor for actomyosin ring assembly in fission yeast. *Current Biology* : *CB* *12*, 724–729.
- Wood, S.A., Park, J.E., and Brown, W.J. (1991). Brefeldin A causes a microtubule-mediated fusion of the trans-Golgi network and early endosomes. *Cell* *67*, 591–600.
- Wood, V., Gwilliam, R., Rajandream, M.-A., Lyne, M., Lyne, R., Stewart, A., Sgouros, J., Peat, N., Hayles, J., Baker, S., et al. (2002). The genome sequence of *Schizosaccharomyces pombe*. *Nature* *415*, 871–880.
- Wu, C., Lytvyn, V., Thomas, D.Y., and Leberer, E. (1997). The phosphorylation site for Ste20p-like protein kinases is essential for the function of myosin-I in yeast. *The Journal of Biological Chemistry* *272*, 30623–30626.
- Wu, H., Turner, C., Gardner, J., Temple, B., and Brennwald, P. (2010). The Exo70 subunit of the exocyst is an effector for both Cdc42 and Rho3 function in polarized exocytosis. *Molecular Biology of the Cell* *21*, 430–442.
- Wu, J.-Q., Kuhn, J.R., Kovar, D.R., and Pollard, T.D. (2003). Spatial and temporal pathway for assembly and constriction of the contractile ring in fission yeast cytokinesis. *Developmental Cell* *5*, 723–734.
- Wu, S., Mehta, S.Q., Pichaud, F., Bellen, H.J., and Quioco, F.A. (2005). Sec15 interacts with Rab11 via a novel domain and affects Rab11 localization in vivo. *Nature Structural & Molecular Biology* *12*, 879–885.

- Xiang, Y., and Wang, Y. (2010). GRASP55 and GRASP65 play complementary and essential roles in Golgi cisternal stacking. *The Journal of Cell Biology* 188, 237–251.
- Xu, D., Joglekar, A.P., Williams, A.L., and Hay, J.C. (2000). Subunit structure of a mammalian ER/Golgi SNARE complex. *The Journal of Biological Chemistry* 275, 39631–39639.
- Xu, X.M., Zhao, Q., Rodrigo-Peirís, T., Brkljacic, J., He, C.S., Müller, S., and Meier, I. (2008). RanGAP1 is a continuous marker of the Arabidopsis cell division plane. *Proceedings of the National Academy of Sciences of the United States of America* 105, 18637–18642.
- Xu, Y., Martin, S., James, D.E., and Hong, W. (2002). GS15 forms a SNARE complex with syntaxin 5, GS28, and Ykt6 and is implicated in traffic in the early cisternae of the Golgi apparatus. *Molecular Biology of the Cell* 13, 3493–3507.
- Yamaguchi, Y., Ota, K., and Ito, T. (2007). A novel Cdc42-interacting domain of the yeast polarity establishment protein Bem1. Implications for modulation of mating pheromone signaling. *The Journal of Biological Chemistry* 282, 29–38.
- Yoneda, A., Akatsuka, M., Hoshino, H., Kumagai, F., and Hasezawa, S. (2005). Decision of spindle poles and division plane by double preprophase bands in a BY-2 cell line expressing GFP-tubulin. *Plant & Cell Physiology* 46, 531–538.
- Yorimitsu, T., and Sato, K. (2012). Insights into structural and regulatory roles of Sec16 in COPII vesicle formation at ER exit sites. *Molecular Biology of the Cell* 23, 2930–2942.
- Yu, I.-M., and Hughson, F.M. (2010). Tethering factors as organizers of intracellular vesicular traffic. *Annual Review of Cell and Developmental Biology* 26, 137–156.
- Yumura, S., Ueda, M., Sako, Y., Kitanishi-Yumura, T., and Yanagida, T. (2008). Multiple mechanisms for accumulation of myosin II filaments at the equator during cytokinesis. *Traffic (Copenhagen, Denmark)* 9, 2089–2099.
- Yüce, O., Piekny, A., and Glotzer, M. (2005). An ECT2-centralspindlin complex regulates the localization and function of RhoA. *The Journal of Cell Biology* 170, 571–582.
- Zacharogianni, M., Kondylis, V., Tang, Y., Farhan, H., Xanthakis, D., Fuchs, F., Boutros, M., and Rabouille, C. (2011). ERK7 is a negative regulator of protein secretion in response to amino-acid starvation by modulating Sec16 membrane association. *The EMBO Journal* 30, 3684–3700.
- Zandi, E., Tran, T.N., Chamberlain, W., and Parker, C.S. (1997). Nuclear entry, oligomerization, and DNA binding of the *Drosophila* heat shock transcription factor are regulated by a unique nuclear localization sequence. *Genes & Development* 11, 1299–1314.
- Zhang, D., Vjestica, A., and Oliferenko, S. (2010). The cortical ER network limits the permissive zone for actomyosin ring assembly. *Current Biology : CB* 20, 1029–1034.

- Zhang, D., Vjestica, A., and Oliferenko, S. (2012). Plasma Membrane Tethering of the Cortical ER Necessitates Its Finely Reticulated Architecture. *Current Biology* : CB 22, 2048–2052.
- Zhang, X. (2005). Lethal giant larvae proteins interact with the exocyst complex and are involved in polarized exocytosis. *The Journal of Cell Biology* 170, 273–283.
- Zhang, X., Bi, E., Novick, P., Du, L., Kozminski, K.G., Lipschutz, J.H., and Guo, W. (2001). Cdc42 interacts with the exocyst and regulates polarized secretion. *The Journal of Biological Chemistry* 276, 46745–46750.
- Zhang, X., Orlando, K., He, B., Xi, F., Zhang, J., Zajac, A., and Guo, W. (2008). Membrane association and functional regulation of Sec3 by phospholipids and Cdc42. *The Journal of Cell Biology* 180, 145–158.
- Zhang, Y., Sugiura, R., Lu, Y., Asami, M., Maeda, T., Itoh, T., Takenawa, T., Shuntoh, H., and Kuno, T. (2000). Phosphatidylinositol 4-phosphate 5-kinase Its3 and calcineurin Ppb1 coordinately regulate cytokinesis in fission yeast. *The Journal of Biological Chemistry* 275, 35600–35606.
- Zheng, L., Schwartz, C., Wee, L., and Oliferenko, S. (2006). The fission yeast transforming acidic coiled coil-related protein Mia1p/Alp7p is required for formation and maintenance of persistent microtubule-organizing centers at the nuclear envelope. *Molecular Biology of the Cell* 17, 2212–2222.
- Zheng, Y., Bender, A., and Cerione, R.A. (1995). Interactions among proteins involved in bud-site selection and bud-site assembly in *Saccharomyces cerevisiae*. *The Journal of Biological Chemistry* 270, 626–630.
- Zhou, M., and Wang, Y.-L. (2008). Distinct pathways for the early recruitment of myosin II and actin to the cytokinetic furrow. *Molecular Biology of the Cell* 19, 318–326.
- Ziman, M., O'Brien, J.M., Ouellette, L.A., Church, W.R., and Johnson, D.I. (1991). Mutational analysis of CDC42Sc, a *Saccharomyces cerevisiae* gene that encodes a putative GTP-binding protein involved in the control of cell polarity. *Molecular and Cellular Biology* 11, 3537–3544.
- Zobeck, K.L., Buckley, M.S., Zipfel, W.R., and Lis, J.T. (2010). Recruitment timing and dynamics of transcription factors at the Hsp70 loci in living cells. *Molecular Cell* 40, 965–975.
- Zwaenepoel, I., Naba, A., Da Cunha, M.M.L., Del Maestro, L., Formstecher, E., Louvard, D., and Arpin, M. (2012). Ezrin regulates microvillus morphogenesis by promoting distinct activities of Eps8 proteins. *Molecular Biology of the Cell* 23, 1080–1094.

Appendix I – List of strain used in this study

Strain	Genotype	Source
MBY144	<i>cdc12-112 ura4-D18 leu1-32 h-</i>	Fred Chang
MBY149	<i>sid2-250 ade6-21x ura4-D18 leu1-32 h-</i>	Mohan Balasubramanian
MBY1730	<i>sec63-GFP ura4-D18 leu1-32 h-</i>	This study
MBY286	<i>cdc16-116 leu1-32 ura4-D18 ade6-210 h+</i>	Timothy Mitchison
MBY6656	<i>pAct1:Lifect-GFP::leu+ leu1-32 ura4-D18 h-</i>	Mohan Balasubramanian
MBY671	<i>ost1::GFP-ura4+ ura4-D18 leu1-32 h-</i>	This study
MBY758	<i>cdc15-140 ura4- leu1-32 ade6-210 h-</i>	Paul Nurse
SO1364	<i>sec13-GFP::ura4+ ade6-216 leu1-32 ura4-D18 h+</i>	This study
SO146	<i>tea1-YFP::kanR ura4-D18 leu1-32 ade6-M210 h-</i>	Paul Nurse
SO1509	<i>sec24-GFP::ura4+ ade6-216 ura4-D18 leu1-32 h+</i>	This study
SO1511	<i>anp1-GFP::ura4+ ade6-216 ura4-D18 leu1-32 h+</i>	This study
SO1517	<i>sec72-GFP::ura4+ ade6-216 ura4-D18 leu1-32 h+</i>	This study
SO1626	<i>sec24-GFP::ura4+ ade6-216 leu1-32 ura4-D18 cdc16-116 h?</i>	This study
SO1678	<i>sec72-GFP::ura4+ ade6-216 leu1-32 ura4-D18 cdc16-116 h?</i>	This study
SO1696	<i>anp1-GFP::ura4+ ade6-216 leu1-32 ura4-D18 cdc16-116 h?</i>	This study
SO1833	<i>tea1Δ::ura4+ ura4-D18 leu1? ade? h-</i>	Paul Nurse
SO2412	<i>anp1-mCherry::ura4+ ade6-216 leu1-32 ura4-D18 h+</i>	This study
SO2423	<i>sec24-GFP::ura4+ anp1-mCherry::ura4+ ade6-21x leu1-32 ura4-D18 h?</i>	This study
SO2427	<i>uch2-mCherry::ura4+ ade6-216 leu1-32 ura4-D18 h+</i>	This study
SO2479	<i>sec13-GFP::ura4+ rlc1-RFP::ura4+ ade6-21x leu1-32 ura4-D18 h?</i>	This study
SO2481	<i>sec24-GFP::ura4+ rlc1-RFP::ura4+ ade6-21x leu1-32 ura4-D18 h?</i>	This study
SO2482	<i>anp1-GFP::ura4+ rlc1-RFP::ura4+ ade6-21x leu1-32 ura4-D18 h?</i>	This study
SO2484	<i>sec72-GFP::ura4+ rlc1-RFP::ura4+ ade6-21x leu1-32 ura4-D18 h?</i>	This study
SO2524	<i>sec24-GFP::ura4+ rlc1-RFP::ura4+ cdc15-140 pREP1-mad2 ade6-21x leu1-32 ura4-D18 h?</i>	This study

Strain	Genotype	Source
SO2525	<i>anp1-GFP::ura4+ rlc1-RFP::ura4+ cdc15-140 pREP1-mad2 ade6-21x leu1-32 ura4-D18 h?</i>	This study
SO2526	<i>sec72-GFP::ura4+ rlc1-RFP::ura4+ cdc15-140 pREP1-mad2 ade6-21x leu1-32 ura4-D18 h?</i>	This study
SO2527	<i>sec24-GFP::ura4+ rlc1-RFP::ura4+ cdc25-22 pREP1-cdc15 ade6-21x leu1-32 ura4-D18 h?</i>	This study
SO2800	<i>sec24-GFP::ura4+ uch2-mCherry::ura4+ ade6-21x leu1-32 ura4-D18 h?</i>	This study
SO2801	<i>anp1-GFP::ura4+ uch2-mCherry::ura4+ ade6-21x leu1-32 ura4-D18 h?</i>	This study
SO2802	<i>sec72-GFP::ura4+ uch2-mCherry::ura4+ ade6-21x leu1-32 ura4-D18 h?</i>	This study
SO2803	<i>sec24-GFP::ura4+ uch2-mCherry::ura4+ cdc12-112 ade6-21x leu1-32 ura4-D18 h?</i>	This study
SO2804	<i>anp1-GFP::ura4+ uch2-mCherry::ura4+ cdc12-112 ade6-21x leu1-32 ura4-D18 h?</i>	This study
SO2805	<i>sec72-GFP::ura4+ uch2-mCherry::ura4+ cdc12-112 ade6-21x leu1-32 ura4-D18 h?</i>	This study
SO2806	<i>sec24-GFP::ura4+ uch2-mCherry::ura4+ sid2-250 ade6-21x leu1-32 ura4-D18 h?</i>	This study
SO2807	<i>anp1-GFP::ura4+ uch2-mCherry::ura4+ sid2-250 ade6-21x leu1-32 ura4-D18 h?</i>	This study
SO2808	<i>sec72-GFP::ura4+ uch2-mCherry::ura4+ sid2-250 ade6-21x leu1-32 ura4-D18 h?</i>	This study
SO2865	<i>ade6-210 ura4-D18 leu1-32 h+</i>	Mohan Balasubramanian
SO2866	<i>ade6-216 ura4-D18 leu1-32 h-</i>	Mohan Balasubramanian
SO2942	<i>ost1-GFP::ura4+ rlc1-RFP::ura4+ ura4-D18 leu1-32 h?</i>	This study
SO2943	<i>sec63-GFP::ura4+ rlc1-RFP::ura4+ ura4-D18 leu1-32 h?</i>	This study
SO2997	<i>anp1-mCherry::ura4+ sec72-eGFP::ura4+ ade6-21x leu1-32 ura4-D18 h?</i>	This study
SO3023	<i>ost1-mCherry ade6-210 leu1-32 ura4-D18 h+</i>	This study
SO3026	<i>sec72-GFP::ura4+ anp1-mCherry::ura4+ ade6-216 ura4-D18 leu1-32 h?</i>	This study
SO3041	<i>sec24-GFP::ura4+ uch2-mCherry::ura4+ cdc4-8 ade6-21x leu? ura4-D18 h?</i>	This study
SO3042	<i>anp1-GFP::ura4+ uch2-mCherry::ura4+ cdc4-8 ade6-21x leu? ura4-D18 h?</i>	This study
SO3043	<i>sec72-GFP::ura4+ uch2-mCherry::ura4+ cdc4-8 ade6-21x leu? ura4-D18 h?</i>	This study
SO3045	<i>sec24-GFP ost1-mCherry::ura4+ ade6-21x leu1-32 ura4-D18 h?</i>	This study
SO3046	<i>cdc4-8 ade6-21x leu? ura4-D18 h-</i>	Dan McCollum
SO3047	<i>sec24-GFP::ura4+ rlc1-mCherry::ura4+ ade6-21x leu1-32 ura4-D18 h?</i>	This study

Strain	Genotype	Source
SO3050	<i>sec24-eGFP::ura4+ rlc1-mCherry::ura4+ cdc15-140 ade6-M21x leu1-32 ura4-D18 h?</i>	This study
SO3121	<i>sec24-GFP::ura4+ myo4Δ::ura4+ myo5Δ::ura4+ ade? leu? ura4-D18 h?</i>	This study
SO3288	<i>tts1-linker-GFP::ura4+ uch2-mcherry::ura4+ h?</i>	This study
SO3483	<i>ssa1-3HA::ura4+ ade6-210 ura4-D18 leu1-32 h+</i>	This study
SO3683	<i>tts1-linker-GFP::ura4+ rlc1-mCherry::ura4+</i>	This study
SO3683	<i>tts1-linker-GFP::ura4+ rlc1-mCherry::ura4+</i>	This study
SO3729	<i>cdc15-140 tts1-linker-GFP::ura4+</i>	This study
SO3773	<i>cdc15-140 tts1-linker-GFP::ura4+ rlc1-linker-mCherry::ura4+</i>	This study
SO4281	<i>tea4-GFP::kanMX ade6-M21x leu1-32 ura4-D18 h+</i>	Fred Chang
SO4362	<i>5'UTR^{hsp104}-GFP-3'UTR^{hsp104}::ura4+ @Hsp104 locus ade6-210 ura4-D18 leu1-32 h+</i>	This study
SO4389	<i>mas5Δ::ura4+ ade6-210 ura4-D18 leu1-32 h+</i>	This study
SO4400	<i>hsp104-GFP::ura4+ ade6-210 ura4-D18 leu1-32 h+</i>	This study
SO4435	<i>tts1Δ::ura4+ rtn1Δ::ura4+ yop1Δ::ura4+ sec24-GFP::ura4+</i>	This study
SO4443	<i>cdc12-112 tts1-linker-GFP::ura4+ uch2-mcherry::ura4+</i>	This study
SO4594	<i>pom1-GFP::KanMX+ h-</i>	Jürg Bähler
SO4595	<i>mid1Δ::ura4+ tts1-linker-GFP::ura4+ rlc1-mcherry::ura4+</i>	This study
SO4676	<i>sec24-GFP::ura4+ tts1-mCherry::ura4+</i>	This study
SO4741	<i>sec24-GFP::ura4+ ost1-mCherry::ura4+ rtn1Δ::ura4+</i>	This study
SO4744	<i>sec24-GFP::ura4+ tts1-mCherry::ura4+ rtn1Δ::ura4+</i>	This study
SO4751	<i>sec24-GFP::ura4+ rlc1-mCherry::ura4+ mid1Δ::ura4+</i>	This study
SO4778	<i>vrg4-GFP::ura4+ tts1Δ::ura4+ rtn1Δ::ura4+ yop1Δ::ura4+</i>	This study
SO4875	<i>sec24-GFP::ura4+ mCherry-AHDL::leu+</i>	This study
SO5216	<i>mas5Δ::ura4+ sec6-GFP::ura4+ leu1-32 ade? ura4-D18 h?</i>	This study
SO5217	<i>mas5Δ::ura4+ tea1-YFP::kanR ura4-D18 leu1-32 ade6? h?</i>	This study
SO5274	<i>mas5Δ::ura4+ pom1-GFP::KanMX ura4-D18 leu1-32 ade6? h?</i>	This study

Strain	Genotype	Source
SO5336	<i>GFP-mas5::ura4+ ade6-210 ura4-D18 leu1-32 h+</i>	This study
SO5372	<i>myo52-GFP::kanR ade6-210 leu1-32 ura4-D18 h-</i>	Dan McCollum
SO5374	<i>scd1-GFP::kanR leu-? ura-? h+</i>	Pilar Perez
SO5376	<i>pShk1:CRIB^{S.cerevisiaeGic2}-3GFP:ura4+ ura4-294 leu1-32 h-</i>	Kazuhiro Shiozaki
SO5440	<i>mas5Δ::ura4+ myo52-GFP::kanR ade6? leu1-32 ura4-D18 h?</i>	This study
SO5442	<i>mas5Δ::ura4+ scd1-GFP::kanR leu-?, ura-?</i>	This study
SO5445	<i>mas5Δ::ura4+ pShk1:CRIB^{S.cerevisiaeGic2}-3GFP:ura4+ ade6? ura4-? leu1-32 h?</i>	This study
SO5448	<i>mas5Δ::ura4+ lifeact-GFP::leu1+ h?</i>	This study
SO5451	<i>gef1-3YFP::kanMX ade6-704 leu1-32 ura4D-18 h+</i>	Fulvia Verde
SO5452	<i>rga4-GFP::kanMX ade6-704 leu1-32 ura4D-18 h+</i>	Fulvia Verde
SO5522	<i>mas5Δ::ura4+ hsp104-GFP::ura4+ ade6? ura4-D18 leu1-32 h?</i>	This study
SO5524	<i>mas5Δ::ura4+ rga4-GFP::kanMX ade6-210 ura4-D18 leu1-32 h?</i>	This study
SO5527	<i>mas5Δ::ura4+ 5'UTR^{hsp104}-GFP-3'UTR^{hsp104}::ura4+ @Hsp104 locus ade6-M21x leu1-32 ura4-D18 h+</i>	This study
SO5666	<i>13myc-mas5::ura4+ ade6-210 ura4-D18 leu1-32 h+</i>	This study
SO5672	<i>GFP-hsf1::ura4+ ade6-21x ura4-D18 leu1-32 h-</i>	This study
SO5683	<i>mas5Δ::ura4+ gef1-3YFP::kanMX ade6-? leu1-32 ura4D-18 h?</i>	This study
SO5778	<i>13myc-mas5::ura4+ ade6-21x ura4-D18 leu1-32 h?</i>	This study
SO5873	<i>ssa1Δ::kanR ade6-216 ura4-D18 leu1-32 h-</i>	This study
SO5875	<i>kanR::nmt1-hsf1 ade6-216 ura4-D18 leu1-32 h-</i>	This study
SO5941	<i>swo1-HA6his::ura4+ h?</i>	Paul Russel
SO5942	<i>swo1-HA6his::ura4+ 13myc-mas5::ura4+ ade6? ura4? leu1? h?</i>	This study
SO5946	<i>kanR::nmt1-hsf1 Hsp104-GFP::ura4+ ade6-21x ura4-D18 leu1-32 h?</i>	This study
SO6142	<i>GFP-hsf1::ura4+ swo1-mCherry::ura4+ ade6-21x ura4-D18 leu1-32 h?</i>	This study
SO6143	<i>GFP-hsf1::ura4+ swo1-mCherry::ura4+ mas5Δ::ura4+ ade6-21x ura4-D18 leu1-32 h?</i>	This study

Strain	Genotype	Source
SO6286	<i>cdc15-22::his::ura4+ GFP-cps1::kanR</i>	This study
SO6378	<i>cdc15-22::his5::ura4+ rlc1-mCherry::ura4+ h+</i>	This study
SO6380	<i>cdc15-22::his5::ura4+ cdc7-GFP::ura4+</i>	This study
SO6388	<i>cdc7-GFP::ura4+ h-</i>	This study
SO6393	<i>sec6-GFP::ura4+ ura4-? leu1-32 h-</i>	Mohan Balasubramanian
SO6406	<i>pcp1-mCherry rlc1-mCherry sid2-GFP ade? ura? leu?</i>	This study
SO6409	<i>cdc15-22::his5::ura4+ pcp1-mCherry rlc1-mCherry sid2-GFP ade? ura? leu?</i>	This study
SO6454	<i>pNmt3:GFP-cps1::kanR ade6-21x ura4?leu1? h?</i>	Mohan Balasubramanian
SO6455	<i>pNmt3:GFP-cps1::kanR mas5Δ::ura4+ ade6?ura4?leu1? h?</i>	This study
SO6466	<i>cdc15-22::his5+::ura4+ sid1-GFP::ura4+ pcp1-mCherry::ura4+ rlc1-mCherry::ura4+</i>	This study
SO6467	<i>sid1-GFP::ura4+ pcp1-mCherry::ura4+ rlc1-mCherry::ura4+</i>	This study
SO6549	<i>GFP-hsf1::ura4+ swo1-w1 ura4-D18 leu1-32 h?</i>	This study
SO6550	<i>mas5Δ::ura4+ for3-YFP::kanR ade6? ura4-D18 leu1-32 h+</i>	This study
SO6551	<i>for3-YFP::kanR ade6? ura4-D18 leu1-32 h+</i>	This study
SO6555	<i>gef1Δ::ura4+ pShk1:CRIB^{S.cerevisiaeGic2}-3GFP:ura4+ ade6? ura4? leu1? h? h?</i>	This study
SO6556	<i>rga4Δ::ura4+ pShk1:CRIB^{S.cerevisiaeGic2}-3GFP:ura4+ ade6? ura4? leu1? h?</i>	This study
SO6895	<i>myo5Δ::ura4+ myo4Δ::ura4+ lifeact-linker-mCherry::leu1+ GFP-AHDL::ura4+</i>	This study
SO6965	<i>ssa2Δ::ura4+ ade6-21x ura4-D18 leu1-32 h+</i>	This study
SO6969	<i>GFP-AHDL::ura4+ lifeact-mCherry::leu1+ h+</i>	This study
SO6971	<i>for3Δ::kanR GFP-AHDL::ura4+ lifeact-mCherry::leu1+ h?</i>	This study
SO7020	<i>ssa2Δ::ura4+ hsp104-GFP::ura4+ ade6-21x ura4-D18 leu1-32 h?</i>	This study
SO7021	<i>ssa2Δ::ura4+ 5'UTR^{hsp104}-GFP-3'UTR^{hsp104}::ura4+ @Hsp104 locus ade6-21x ura4-D18 leu1-32 h?</i>	This study
SO7022	<i>ssa2Δ::ura4+ pShk1:CRIB^{S.cerevisiaeGic2}-3GFP:ura4+ ade6? ura4-? leu1-32 h?</i>	This study
SO7025	<i>ssa2Δ::ura4+ GFP-hsf1::ura4+ swo1-mCherry::ura4+ ade6-21x ura4-D18 leu1-32 h?</i>	This study

Strain	Genotype	Source
SO7051	<i>GFP-ssa2::ura4+ ade6-21x ura4-D18 leu1-32 h+</i>	This study
SO7052	<i>ssa1Δ::kanR hsp104-GFP::ura4+ ade6-21x ura4-D18 leu1-32 h?</i>	This study
SO7053	<i>ssa1Δ::kanR 5'UTR^{hsp104}-GFP-3'UTR^{hsp104}::ura4+ @Hsp104 locus ade6-21x ura4-D18 leu1-32 h?</i>	This study
SO7055	<i>ssa1Δ::kanR GFP-hsf1::ura4+ swol-mCherry::ura4+ ade6-21x ura4-D18 leu1-32 h?</i>	This study
SO7108	<i>GFP-ssa2::ura4+ swol-HA6His::ura4+ ade6? ura4? leu1? h?</i>	This study
SO7118	<i>13myc-mas5::ura4+ GFP-ssa2::ura4+ ade6-21x ura4-D18 leu1-32 h?</i>	This study
SO7140	<i>sec24-GFP rlc1-mCherry, pcp1-mCherry</i>	This study
SO7141	<i>cdc15-22 sec24-GFP::ura4+ rlc1-mCherry pcp1-mCherry</i>	This study
SO7346	<i>cdc15-linker-GFP ::ura4+ h+</i>	This study
SO7350	<i>cdc15-22- linker-GFP ::ura4+ h+</i>	This study
SO7357	<i>gef1Δ::ura4+ rga4Δ::ura4+ pShk1:CRIB^{S.cerevisiaeGic2}-3GFP:ura4+ ade6? ura4-? leu1-32 h?</i>	This study
SO7370	<i>pShk1:CRIB^{S.cerevisiaeGic2}-3GFP:ura4+ nmt41:rga4-mCherry::leu1@leu1 locus ura4-294 leu1-32 h-</i>	This study
SO7471	<i>scd1Δ::ura4+ pShk1:CRIB^{S.cerevisiaeGic2}-3GFP:ura4 ade6? ura4? leu1? h?</i>	This study

Appendix II. List of primers used in the qPCR analysis

prSO2601	ATTACTTGCCCCGAGCTTTC	forward qPCR primer for SPBC1711.08 (<i>aha1</i>)
prSO2602	ACTATGCACGGGAAGTCCAC	reverse qPCR primer for SPBC1711.08 (<i>aha1</i>)
prSO2603	TGGATTGTAAAGCCCGAAAG	forward qPCR primer for SPBC1711.12 (<i>dpp5</i>)
prSO2604	GCTTACCACCCAATCAAGA	reverse qPCR primer for SPBC1711.12 (<i>dpp5</i>)
prSO2605	AGTACGCAGTTGCAAGCTCA	forward qPCR primer for SPBC3B9.01 (<i>fes1</i>)
prSO2606	CCGGACTCTCAAGCTGTTTC	reverse qPCR primer for SPBC3B9.01 (<i>fes1</i>)
prSO2607	GCCGACTTTAAGCTCATTGC	forward qPCR primer for SPCC645.14c (<i>sti1</i>)
prSO2608	GGCTTTGTCAGGGTCAATGT	reverse qPCR primer for SPCC645.14c (<i>sti1</i>)
prSO2609	GCTGCTTCTTGGGCAGTTAC	forward qPCR primer for SPACUNK4.16c (<i>tps3</i>)
prSO2610	GCGCACTGAAAACGTAAACA	reverse qPCR primer for SPACUNK4.16c (<i>tps3</i>)
prSO2611	ACCGTAAGGCACATGGAAAG	forward qPCR primer for SPAC22E12.13c (<i>rpl24-3</i>)
prSO2612	GGGGTTCTTGACCTCAGCA	reverse qPCR primer for SPAC22E12.13c (<i>rpl24-3</i>)
prSO2613	CTCAAAAATGCCTGGTGGTT	forward qPCR primer for SPAC4A8.11c (<i>fas2</i>)
prSO2614	AAGAACCGCCTTCAGCAGTA	reverse qPCR primer for SPAC4A8.11c (<i>fas2</i>)
prSO2615	ATTCGACCAGACCGTCAAAC	forward qPCR primer for SPBP8B7.16c (<i>dbp2</i>)
prSO2616	CCAACCATCTTGCTAAGGA	reverse qPCR primer for SPBP8B7.16c (<i>dbp2</i>)
prSO2617	TTCGCTGCCTGTAATTTGTG	forward qPCR primer for SPCC548.06c (<i>ght8</i>)
prSO2618	CACGGCCTTCAGAAGAAGAG	reverse qPCR primer for SPCC548.06c (<i>ght8</i>)
prSO2621	AACCCTCAGCTTTGGGTCTT	forward qPCR primer for SPBC32H8.12c (<i>act1</i>)
prSO2622	ATTTACGCTCAGGAGGAGCA	reverse qPCR primer for SPBC32H8.12c (<i>act1</i>)
prSO2623	CCGATGTTTCCGTTGTTGAC	forward qPCR primer for SPBC354.12 and SPBC32F12.11 (<i>gpd1</i>)
prSO2624	ACGAGCTTGACGAATTGAGG	reverse qPCR primer for SPBC354.12 and SPBC32F12.11 (<i>gpd1</i>)

The Actomyosin Ring Recruits Early Secretory Compartments to the Division Site in Fission Yeast

Aleksandar Vjestica,*[†] Xin-Zi Tang,* and Snezhana Oliferenko*

*Cell Dynamics Group, Temasek Life Sciences Laboratory, 117604 Singapore and [†]Department of Biological Sciences, National University of Singapore, 117543 Singapore

Submitted July 13, 2007; Revised December 17, 2007; Accepted December 27, 2007
Monitoring Editor: Daniel Lew

The ultimate goal of cytokinesis is to establish a membrane barrier between daughter cells. The fission yeast *Schizosaccharomyces pombe* utilizes an actomyosin-based division ring that is thought to provide physical force for the plasma membrane invagination. Ring constriction occurs concomitantly with the assembly of a division septum that is eventually cleaved. Membrane trafficking events such as targeting of secretory vesicles to the division site require a functional actomyosin ring suggesting that it serves as a spatial landmark. However, the extent of polarization of the secretion apparatus to the division site is presently unknown. We performed a survey of dynamics of several fluorophore-tagged proteins that served as markers for various compartments of the secretory pathway. These included markers for the endoplasmic reticulum, the COPII sites, and the early and late Golgi. The secretion machinery exhibited a marked polarization to the division site. Specifically, we observed an enrichment of the transitional endoplasmic reticulum (tER) accompanied by Golgi cisternae biogenesis. These processes required actomyosin ring assembly and the function of the EFC-domain protein Cdc15p. Cdc15p overexpression was sufficient to induce tER polarization in interphase. Thus, fission yeast polarizes its entire secretory machinery to the cell division site by utilizing molecular cues provided by the actomyosin ring.

INTRODUCTION

Cell division is the final event in the cell cycle that results in physical separation of two daughter cells. Despite being studied for more than a hundred years, the underlying molecular mechanisms and the cytological details of the process are still emerging. Various organisms and cell types have established multiple pathways to conduct cell division that are regulated at both signaling and structural levels (for review see Balasubramanian *et al.*, 2004). In recent years, the fission yeast *Schizosaccharomyces pombe* has emerged as an attractive model for the study of cytokinesis because of its fully sequenced genome (Wood *et al.*, 2002), a cell size convenient for cytological studies and the availability of a large set of conditional mutants compromised in various aspects of cell division (Chang *et al.*, 1996; Balasubramanian *et al.*, 1998).

On entry into mitosis, *S. pombe* assembles an actomyosin ring that is thought to drive a binary cell fission through constriction, similar to many other eukaryotes, including nematodes, insects, and vertebrates (for review see Hales *et al.*, 1999). During early mitosis, actin is assembled into a ring structure through the action of several actin nucleating and bundling proteins and molecular motors. These include the formin Cdc12p (Chang *et al.*, 1997), profilin Cdc3p (Balasubramanian *et al.*, 1992), the extended Fer/CIP4 (EFC) domain protein Cdc15p (Fankhauser *et al.*, 1995), and the myosin heavy chain Myo2p (Kitayama *et al.*, 1997) together with its light chains Cdc4p (McCollum *et al.*, 1995; Naqvi *et al.*,

1999) and Rlc1p (Le Goff *et al.*, 2000). It has been proposed that activation of the signaling cascade referred to as the septation initiation network (SIN) triggers actomyosin ring constriction upon nuclear division (for review see Krapp *et al.*, 2004). Concomitantly with ring constriction, membrane material is inserted at the division site and the septum is synthesized (Jochova *et al.*, 1991). Centripetal septum deposition and ring constriction seem to be tightly linked. Indeed, 1,3- β -glucan-synthase loss-of-function mutants that cannot form the septum are also incapable of ring constriction (Liu *et al.*, 2000). As septum biogenesis proceeds, actin reorganizes to clusters of patches on both sides of the septum (Marks and Hyams, 1985). Secondary septa are then formed on either side of the primary one that is eventually dissolved resulting in cell separation (Humbel *et al.*, 2001).

Formation and remodeling of the cell wall depend on action of enzymes such as the (1,3)- β -glucan-synthase and the endo- β -1,3-glucanase that are involved in organizing the (1,3)- β -glucan, the major constituent of the cell wall (Ribas *et al.*, 1991; Martin-Cuadrado *et al.*, 2003). These proteins have been shown to localize to the sites of active growth and their localization depends on secretion (Cortes *et al.*, 2002; Martin-Cuadrado *et al.*, 2003). Application of the drug brefeldin A (BFA), which inhibits the exchange factor for the small GTPase Arf, renders fission yeast cells incapable of localizing the (1,3)- β -glucan-synthase catalytic subunit Cps1p to the division site, presumably because of a block in secretion (Liu *et al.*, 2002). Furthermore, the multiprotein complex involved in the late steps of the exocytic pathway named exocyst is essential for the proper localization of the endo- β -1,3-glucanase, Eng1p (Martin-Cuadrado *et al.*, 2005). In fission yeast, the exocyst-mediated secretion is restricted to the cellular growth regions including cell tips and the cell division site (Wang *et al.*, 2002).

This article was published online ahead of print in *MBC in Press* (<http://www.molbiolcell.org/cgi/doi/10.1091/mbc.E07-07-0663>) on January 9, 2008.

Address correspondence to: Snezhana Oliferenko (snejana@tll.org.sg).

In exocytosis, vesicles originating from the secretory pathway or endosomal recycling (Engstler *et al.*, 2004) fuse with the plasma membrane. The delivery of newly synthesized proteins to the plasma membrane and cell surrounding depends almost exclusively on the function of the secretory pathway (for review see Mellman and Warren, 2000; Nickel, 2003). Proteins to be secreted are processed in the endoplasmic reticulum (ER) and the Golgi apparatus and then are sorted into the post-Golgi vesicles that are delivered to the plasma membrane (Alberts *et al.*, 2002). Most published work on the involvement of protein secretion during polarity establishment has centered on targeting, localization, and delivery of post-Golgi vesicles. For example, it was shown that the early buds of the budding yeast *Saccharomyces cerevisiae* contain numerous secretory vesicles that are rarely observed in the mother cell (Preuss *et al.*, 1992). Such polarized distribution depends on intact actin cables and type V myosins (Johnston *et al.*, 1991; Govindan *et al.*, 1995). However, less is known about the spatial distribution of the early secretory compartments. It was reported that the Golgi apparatus also localized close to the bud site in *S. cerevisiae* (Preuss *et al.*, 1992). Similarly, Bevis *et al.*, 2002 have suggested that the Golgi elements in *Pichia pastoris* might preferentially localize toward the budding site. During hyphal growth in *Candida albicans*, cells assemble the vesicle-rich Spitzenkörper structure at the tips of growing hyphae (Harris *et al.*, 2005). The intimate association between Spitzenkörper behavior and hyphal morphogenesis suggests that the Spitzenkörper might function as a "Vesicle Supply Center," producing the secretory vesicles (Bartnicki-Garcia *et al.*, 1989). In fact, it was recently shown that most of the Golgi apparatus is indeed localized near the growing hyphal tips (Rida *et al.*, 2006).

Considering the functional continuum of the secretory pathway (for review see Guo and Novick, 2004), we were interested in investigating the structural and spatial organization of the tER (transitional ER) and *cis*- and *trans*-Golgi during polarized tip growth and cell division, which represent major aspects of cellular polarity in fission yeast.

In this study we observed an enrichment of tER that was accompanied by the biogenesis of Golgi cisternae at the division site. These processes required assembly of a functional actomyosin ring and, in particular, the function of the EFC domain protein, Cdc15p. Interestingly, overexpression of Cdc15p in interphase was sufficient to induce the equatorial accumulation of the tER. Thus, fission yeast cells polarize the entire secretory machinery to the cell division site by utilizing molecular cues provided by the actomyosin ring.

MATERIALS AND METHODS

S. pombe Strains, Reagents, and Constructs

S. pombe strains used in this study and their genotypes are listed in Supplementary Table 1. Media for vegetative growth (EMM2 or YES) and genetic methods were as described in Moreno *et al.* (1991). Genetic crosses and sporulation were performed on YPD agar plates. The homologous recombination-based method was used to tag endogenous proteins with green fluorescent protein (GFP) or mCherry at their C termini. The candidate proteins were selected based on their homologies to proteins characterized in other yeast systems (accession numbers: SPBC1734.04 [Anp1p], SPAC27F1.07 [Ost1p], SPAC22F8.08 [Sec24p], SPBC36B7.03 [Sec63p], and SPAC30.01c [Sec72p]). Plasmids were constructed using standard molecular biology techniques. Latrunculin A (LatA), a drug that prevents actin polymerization, was purchased from Biomol International LP (Plymouth Meeting, PA). DNA fluorescent stain 4',6-diamidino-2-phenylindole (DAPI) and the microtubule depolymerizing drug methyl-1-(butylcarbamoyl)-2-benzimidazole-carbamate (carbendazime; MBC) were obtained from Sigma-Aldrich (St. Louis, MO). The F-actin stain Alexa Fluor 593 phalloidin was obtained from Invitrogen (Karlsruhe, Germany).

Microscopy

Epifluorescence still images were collected using mercury lamp as an illumination source with appropriate sets of filters on a Zeiss Axiovert 200M (Plan Apochromat NA 1.4 objective, Göttingen, Germany) microscope equipped with CoolSnap camera (Photometrics, Tucson, AZ) and Uniblitz shutter driver (Photonic, Rochester, NY) under the control of Metamorph software package (Universal Imaging, Sunnyvale, CA). Typically, we acquired image stacks that consisted of nine sections of 0.5- μ m spacing. Presented are the z-stack maximum projection images obtained by using Metamorph built-in module (Universal Imaging, West Chester, PA).

Scanning confocal microscopy was performed on a Leica DMI6000B microscope (HCX Plan NA = 1.35 objective) equipped with SP5 confocal system (Leica Microsystems, Mannheim, Germany) controlled by the proprietary software package. Z-stack images were taken with 0.5- μ m spacing and reconstructed in three dimensions using the projection module. Imaging was performed on *S. pombe* cells placed in sealed growth chambers containing 2% agarose YES medium.

Time-lapse fluorescent microscopy images were generated on a Zeiss Axiovert 200M (Plan Apochromat NA 1.4 objective) microscope equipped with UltraView RS-3 confocal system: CSU21 confocal optical scanner, 12 bit digital cooled Hamamatsu Orca-ER camera (OPELCO, Sterling, VA) and krypton-argon triple line laser illumination source (488, 568, and 647 nm) under the control of UltraView software package (PerkinElmer, Boston, MA). Typically, we acquired image stacks that consisted of nine 0.5- μ m-spaced sections. Presented are the z-stack maximum projection images obtained by using ImageJ software package (<http://rsb.info.nih.gov/ij/>; National Institutes of Health, Bethesda, MD). Imaging was performed on *S. pombe* cells placed in sealed growth chambers containing 2% agarose YES medium.

Image Analysis

Single-cell maximum projection images obtained by epifluorescence microscopy were analyzed using customized CellProfiler image analysis software (Carpenter *et al.*, 2006). CellProfiler object processing modules were used to identify *S. pombe* cells. Longitudinal cell axes were approximated by linear regression of cell boundaries. Images were rotated by the angle of inclination of the cell axes to the x-axis, thus orienting cells horizontally. Next, images were cropped to cell boundaries. Using nearest-neighbor interpolation, image width was resized to the nearest multiple of 20 pixels and image height to the nearest multiple of 10 pixels. The average intensity of an image field comprising one-twentieth of the width and one-tenth of the height of this image was represented as a single pixel, thus resulting in a 20 \times 10-pixel image. Intensities were normalized and averaged over 50 images. Furthermore, we calculated intensities along longitudinal cell axes from mean column intensities of the 20 \times 10 images. As above, these were averaged over 50 images and graphed. We determined the statistical significance of differences in fluorescence levels between two axial positions using the Kolmogorov-Smirnov test to calculate the p values. The critical p value (p = 0.05) was adjusted for multiple comparisons using Bonferroni correction.

Three-dimensional reconstructions were performed using Volocity software package (Perkin Elmer-Cetus, Waltham, MA).

Integrated intensity measurements were performed on maximum projection images obtained by time-lapse spinning disk confocal microscopy using the Metamorph built-in module. The measurements were performed over three equal areas corresponding to cell tips and the cell middle. The fluorescence intensities were adjusted for bleaching using interphase cells fluorescence intensities (n = 4 cells), assuming that the marker protein levels did not change during this time. Obtained values are presented as a time sequence of values relative to average intensity at cell tips and the moving average (n = 3) time sequence.

RESULTS

Organization of the Early Secretory Pathway in *S. pombe*

To investigate the organization of the early secretory compartments including the COPII-positive compartments and both *cis*- and *trans*-Golgi, we constructed *S. pombe* strains expressing a number of distinct marker proteins C-terminally tagged with GFP or mCherry at their genomic loci. The candidate proteins were selected based on their homologies to known secretory pathway markers reported in other yeast (see *Materials and Methods*). Tagging of these proteins did not adversely affect their essential functions judging by the normal cell morphology and division patterns.

The general ER markers such as the component of the protein translocation complex Sec63p-GFP (Deshai *et al.*, 1991) and the predicted oligosaccharide transferase Ost1p-GFP (Silberstein *et al.*, 1995) exhibited both cortical and

nuclear envelope (NE) localization (Supplementary Figure 1A), consistent with previously published work (Pidoux and Armstrong, 1993; Broughton *et al.*, 1997). The COPII vesicle coat protein Sec24p-GFP (Barlowe *et al.*, 1994) localized to punctate structures (Figure 1A, left panel) of various sizes. We observed 80 ± 9 such entities in interphase cells and 106 ± 11 of those in dividing cells ($n = 10$ cells; Figure 1C). To explore the organization of COPII structures and *cis*-Golgi with respect to each other, we simultaneously observed the localization of Sec24p-GFP and the component of the Golgi mannosyltransferase complex Anp1p-mCherry (Jungmann and Munro, 1998) that served as a *cis*-Golgi marker protein (Figure 1A, center panel). Because of the large number of the COPII structures, it was difficult to determine the fraction of adjacent COPII-positive membranes and *cis*-Golgi compartments, although we did observe such instances (Figure 1A, right panel).

We further analyzed the relative distribution of the *cis*-Golgi marker Anp1p-mCherry (Figure 1B, center panel) and the Arf GEF Sec72p-GFP (Figure 1B, left panel), a homologue of *S. cerevisiae* Sec7p (Franzusoff *et al.*, 1991) that localizes to the late Golgi compartments in budding yeast. We found that these proteins localized to several punctate structures (18 ± 3 *cis*- and 22 ± 3 *trans*-Golgi compartments during interphase and 23 ± 3 *cis*- and 26 ± 2 *trans*-Golgi compartments in dividing cells, $n = 10$ cells). These two markers often partially overlapped or were found adjacent to each other, consistent with their localization to distinct cisternae within Golgi stacks (Figure 1, B, right panel, and C). We also observed instances of several *cis*-Golgi cisternae adjacent to a single *trans*-Golgi structure. Individual cisternae were present, albeit at a lower frequency ($\sim 10\%$ of early and $\sim 13\%$ of late Golgi compartments, $n = 10$ cells). Thus, the Golgi apparatus in *S. pombe* cells exists as multiple entities comprising mainly stacks of few cisternae and some individual cisternae.

We investigated the dynamics of the early secretory pathway compartments using time-lapse microscopy. By performing epifluorescence microscopy of single planes acquired every 5 s in cells expressing Sec24p-GFP and the nuclear envelope marker Uch2p-mCherry (Li *et al.*, 2000), we found that COPII entities were stable for periods extending 5 min during both cell growth and division (Figure 1D and Supplementary Movie 1). Considering that the protein coat is rapidly disassembled after COPII vesicles have budded (Antonny *et al.*, 2001), we concluded that in fission yeast Sec24p-GFP marks the sites of COPII vesicles production, the tER (for review see Mancias and Goldberg, 2005). We were not able to determine the average tER site lifespan because of technical limitations and the large number of these sites.

Using the spinning disk confocal time-lapse microscopy, we observed instances of early Golgi biogenesis without visible contribution from pre-existing cisternae, as judged by Anp1p-mCherry dynamics (Figure 1, E and F, and Supplementary Movie 2). Moreover, we observed instances of cisternal identity change when Anp1p-mCherry positive structures became predominantly occupied by Sec72p-GFP (Figure 1G and Supplementary Movie 3), in concordance with the Golgi cisternal progression model (for review see Malhotra and Mayor, 2006). The quantification of the fluorescence signals associated with single cisternae maturation (Figure 1H) suggested that this conversion occurred with the fluorescence ratio doubling time of $\sim 30 \pm 7$ s ($n = 12$ maturation events).

Early Secretory Pathway Compartments Accumulate at the Division Site

Although both tER and Golgi compartments exhibited a seemingly random distribution in interphase cells, they were clearly polarized during cell division (Figure 1, A and B). To explore this matter further, we performed epifluorescence microscopy analyses of live fission yeast cells expressing GFP-tagged secretory pathway markers together with the actomyosin ring marker Rlc1p fused to monomeric red fluorescent protein (mRFP) (Le Goff *et al.*, 2000). We confirmed that both tER and Golgi apparatus did not exhibit a clearly polarized distribution of the marker proteins during interphase (Figure 2). However, pronounced recruitment of secretory compartments to the cell division site became noticeable at the time of actomyosin ring formation. Notably, although the tER exhibited the highest levels of accumulation at this time (Figure 2A), the Golgi apparatus appeared only moderately polarized toward the future division site (Figure 2, B and C). As cells progressed through septation, all marker proteins attained maximum polarization levels. It should be noted that tER showed a fairly narrow region of intense accumulation, $\sim 10\%$ of mother cell length, whereas the Golgi marker proteins were enriched in the medial 30% of mother cell length. Thus, for further analyses cells exhibiting such accumulation of both tER and Golgi markers were considered polarized. Because polarization of the tER could be consequential to accumulation of the entire ER in the vicinity of the division site, we investigated the spatial distribution of general ER marker Ost1p-GFP throughout the cell cycle (Supplementary Figure 1A). We did not observe a pronounced accumulation of ER in the central region of dividing cells. We confirmed that the tER polarization did not reflect the general ER localization by performing epifluorescence microscopy on cells simultaneously expressing Sec24p-GFP and Ost1p-mCherry (Supplementary Figure 1B). Quantification of the fluorescence levels of tER and Golgi marker proteins suggested that their accumulation at the site of division was statistically significant (Supplementary Figure 2, $n = 50$ cells per marker per cell cycle stage; see *Materials and Methods* for details).

Actomyosin Ring Assembly Is Required for Secretory Machinery Recruitment to the Division Site

Given that we observed the initial medial accumulation of both tER and Golgi compartments occurring concomitantly with actomyosin ring formation (Figure 2), we hypothesized that the ring itself might serve as a determinant for the early secretory pathway polarization. To explore this question, we introduced the fluorescent markers of the secretory pathway into the *cdc12-112* temperature-sensitive genetic background. The essential *S. pombe* formin Cdc12p plays a crucial role in actomyosin ring formation, and fission yeast cells are incapable of ring assembly when Cdc12p function is compromised (Chang *et al.*, 1997). When grown at the restrictive temperature of 36°C , *cdc12-112* mutant cells are not capable of cytokinesis but undergo the nuclear division (Arai and Mabuchi, 2002). We synchronized exponentially growing cell cultures in early G2 phase of the cell cycle by elutriation. Immediately upon elutriation cells were released into a fresh medium and grown at either permissive or restrictive temperatures. As judged by visualization of the Uch2p-mCherry, anaphase cell population peaked at ~ 75 and 90 min after elutriation for cultures grown at 24 and 36°C , respectively. Samples were taken, fixed, and stained for actin and DNA to confirm that cells were unable to form rings at the restrictive temperature (data not shown). By analyzing the spatial distribution of the

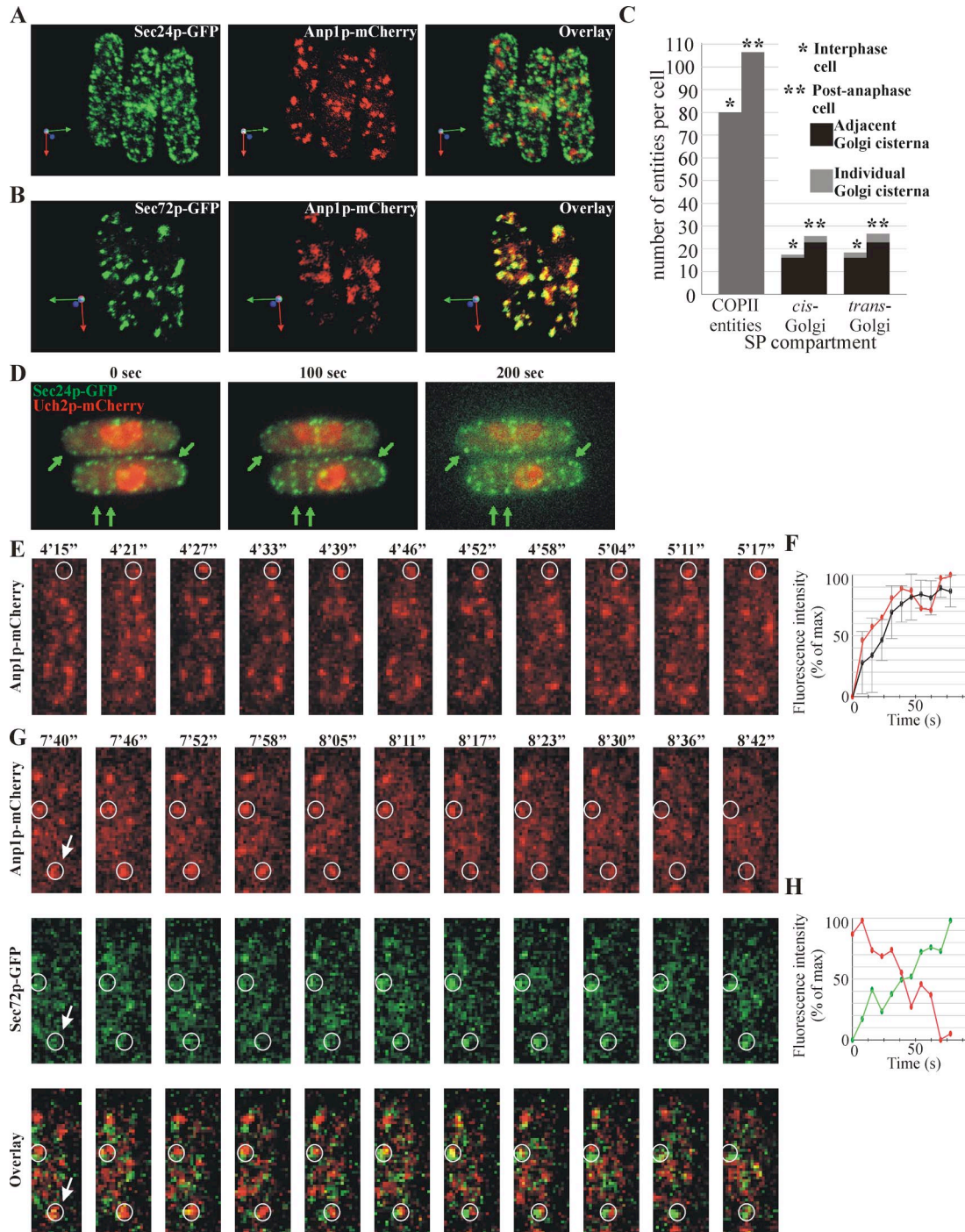


Figure 1. Characterization of the early the secretory pathway in *S. pombe*. (A) 3D reconstruction of scanning confocal microscopy images of *S. pombe* cells expressing COPII vesicle marker Sec24p-GFP (green, left panel) and *cis*-Golgi marker Anp1p-mCherry (red, center panel). Numerous punctate COPII entities and multiple separate *cis*-Golgi cisternae could be visualized, some of which were adjacent or partially overlapping with each other (overlay, right panel). Arrows indicate the spatial orientation of objects in respect to *x*, *y*, and *z*-axis (green, red, and blue, respectively). (B) 3D reconstruction of scanning confocal microscopy images of *S. pombe* cells expressing *cis*-Golgi marker Anp1p-mCherry (red, center panel) and *trans*-Golgi marker Sec72p-GFP (green, left panel). The *trans*-Golgi localized as multiple separate cisternae that were in most cases partially overlapping or adjacent to the *cis*-Golgi cisternae (overlay, right panel). Arrows indicate the spatial orientation of objects in respect to *x*, *y*, and *z*-axis (green, red, and blue, respectively). (C) Quantification of the number of individual COPII entities and individual and adjacent *cis*- and *trans*-Golgi cisternae in fission yeast interphase and post-anaphase cells as visualized by scanning confocal imaging of Sec24p-GFP, Anp1p-mCherry, and Sec72p-GFP, respectively ($n = 10$ cells per compartment). SP, secretory pathway. (D) Representative frames from Supplementary Movie 1. Shown is the single focus plane images obtained by time-lapse epifluorescent microscopy of cells expressing Sec24p-GFP and Uch2p-mCherry. The arrows indicate COPII-positive membranes that persisted throughout the course of the experiment. (E) Representative frames corresponding to Supplementary Movie 2. Shown is the maximum projection image of the *z*-stack obtained by time-lapse spinning disk confocal imaging. Numbers refer to the time, in minutes (') and seconds ("). The encircled area indicates the site of *cis*-Golgi cisterna (Anp1p-mCherry, red) biogenesis as visualized by time-lapse spinning disk confocal imaging.

secretory pathway marker proteins, we noticed a strikingly reduced medial accumulation of tER and Golgi cisternae (Figure 3, A–D). Under permissive conditions ~90 and ~80% of cells exhibited tER and Golgi polarization, whereas only ~10 and ~25% of cells, respectively, polarized these compartments under restrictive conditions. We confirmed that the actomyosin ring structure was important for polarization of the early secretory compartments by examining the spatial distribution of the tER and Golgi compartments in cells with compromised function of the myosin light-chain Cdc4p (McCullum *et al.*, 1995, Supplementary Figure 3). Thus, the establishment of early secretory pathway polarization during mitosis depends on actomyosin ring formation.

Maintenance of a Polarized State of the Early Secretory Pathway Compartments Requires an Intact Actin Cytoskeleton

Our observations indicated that the establishment of the polarized distribution of the early secretory pathway compartments required actomyosin ring assembly. However, the polarized state persisted throughout septation at the time when the ring is disassembled. Thus it was possible that other factors could be used for maintenance of the polarized tER and Golgi distribution. Because actin patches localize at the site of septation after ring constriction, we probed the importance of an intact actin cytoskeleton for this phenomenon. To this end, we analyzed the behavior of the early secretory pathway marker proteins in asynchronously growing cell cultures treated with latrunculin A (LatA), a drug that prevents actin polymerization. LatA at 10 μ M has been shown to cause a rapid depolymerization of the actin cytoskeleton in *S. pombe* (Karagiannis *et al.*, 2005), and we confirmed that both division rings and interphase actin structures were eliminated by staining the fixed cells samples with phalloidin and DAPI (Supplementary Figure 4). We observed that cells treated with LatA for 15 min underwent a significant decrease in polarization of all secretory pathway compartments (Figure 3, E–H). The binucleate mitotic cells treated with LatA did not show any degree of either tER or Golgi accumulation, likely because of their inability to assemble the actomyosin ring. Although some septating cells exhibited polarization 15 min after drug application, 30 min of LatA treatment completely abolished the medial accumulation of the secretory pathway compartments. These data confirmed that the actomyosin ring was essential for the establishment of tER and Golgi compartments polarization and suggested that an intact actin cytoskeleton was required for its maintenance during septation.

Figure 1 (cont). (F) Quantification of Anp1p-mCherry fluorescence intensity (red line) associated with *cis*-Golgi cisternae biogenesis event indicated in E and the fluorescence profile averaged over six biogenesis events (black line). The horizontal axis indicates time in seconds, and the vertical axis indicates fluorescence intensity as percentage of the maximal intensity observed. Error bars, SD. (G) Representative frames corresponding to Supplementary Movie 3. Shown is the single focus plane image sampled from the z-stack obtained by time-lapse spinning disk confocal imaging. Numbers refer to the time, in minutes (') and seconds ("). Encircled areas indicate the single Golgi cisternae maturing from a *cis*-Golgi (Anp1p-mCherry, red) to *trans*-Golgi identity (Sec72p-GFP, green). (H) Quantification of intensity of Anp1p-mCherry (red) and Sec72p-GFP (green) fluorescence associated with a Golgi cisterna maturation event indicated in (G, arrow). Data are graphed as in F.

The Septation Initiation Network Is Required for Maintenance But Not for the Initial Recruitment of the Early Secretory Pathway Compartments at the Division Site

To determine whether accumulation of the secretory compartments to the division site depended on the cell cycle stage, we analyzed the behavior of both the tER and the Golgi apparatus in the *cdc16-116* temperature-sensitive genetic background. Cdc16p is a module of the two-component GTPase-activating protein for the small GTPase Spg1p and thus serves as a negative regulator of the SIN pathway (Furge *et al.*, 1998). Loss-of-function of Cdc16p untimely activates the SIN pathway resulting in successive rounds of septum depositions at any stage of the cell cycle (Minet *et al.*, 1979). Asynchronously growing *cdc16-116* cells expressing GFP fusions with the early secretory pathway markers were shifted to the restrictive temperature of 36°C and imaged 1 h after the temperature shift-up. We found that Sec24p-GFP, Anp1p-GFP, and Sec72p-GFP, which represent tER and early and late Golgi compartments, respectively, accumulated in the vicinity of most ectopic septa (Figure 4, A–C). Considering that some cells simultaneously exhibited more than one ectopic septum, we quantified the number of ectopic septa that recruited the secretory compartments rather than the proportion of cells showing such accumulation (Figure 4D). We concluded that early secretory pathway accumulation spatially and temporally coincided with contractile ring and septum formation independently of the cell cycle.

To explore the possibility that the SIN pathway was directly responsible for the polarization of the early secretory compartments, we observed the spatial distribution of the tER and Golgi marker proteins in the *sid2-250* temperature-sensitive mutant background. Sid2p is the downstream effector kinase of SIN signaling (Balasubramanian *et al.*, 1998; Sparks *et al.*, 1999), and loss of its activity leads to septation failure. Using elutriation, we synchronized cells in the manner described above and observed the localization of Sec24p-GFP, Anp1p-GFP, and Sec72p-GFP in anaphase cells (Figure 4, E, F, and G, respectively) also expressing the nuclear envelope marker, Uch2p-mCherry, at both 24 and 36°C. As indicated by the marker proteins, in mitotic cells all three compartments, including the tER, *cis*-Golgi, and *trans*-Golgi, accumulated medially regardless of whether or not the SIN function was compromised (Figure 4H). It should be noted that medial accumulation of the tER and Golgi compartments did decrease upon longer incubation at the restrictive temperature. This might be attributed to the fact that SIN functions in maintaining the actomyosin ring throughout anaphase and cytokinesis (Balasubramanian *et al.*, 1998; Sparks *et al.*, 1999) and therefore is essential for ensuring the continuous localization of the secretory compartments to the site of septation. To confirm that the SIN pathway activity was not essential for the initial secretory machinery recruitment but was required for the maintenance of its polarization state, we performed the time-lapse imaging of *sid2-250* mutant cells expressing GFP-tagged secretory pathway marker proteins and Uch2p-mCherry, growing either at the permissive temperature of 24°C or after a 1-h shift to the restrictive temperature of 36°C (Supplementary Figure 5). We found that anaphase cells (as indicated by the nuclear envelope marker Uch2p-mCherry) incubated at both 24 and 36°C exhibited initial medial accumulation of the secretory compartments. Although this accumulation persisted in cells grown at 24°C (7/8, 5/6, and 5/5 cells for tER, *cis*-Golgi, and *trans*-Golgi, respectively), it was abolished at

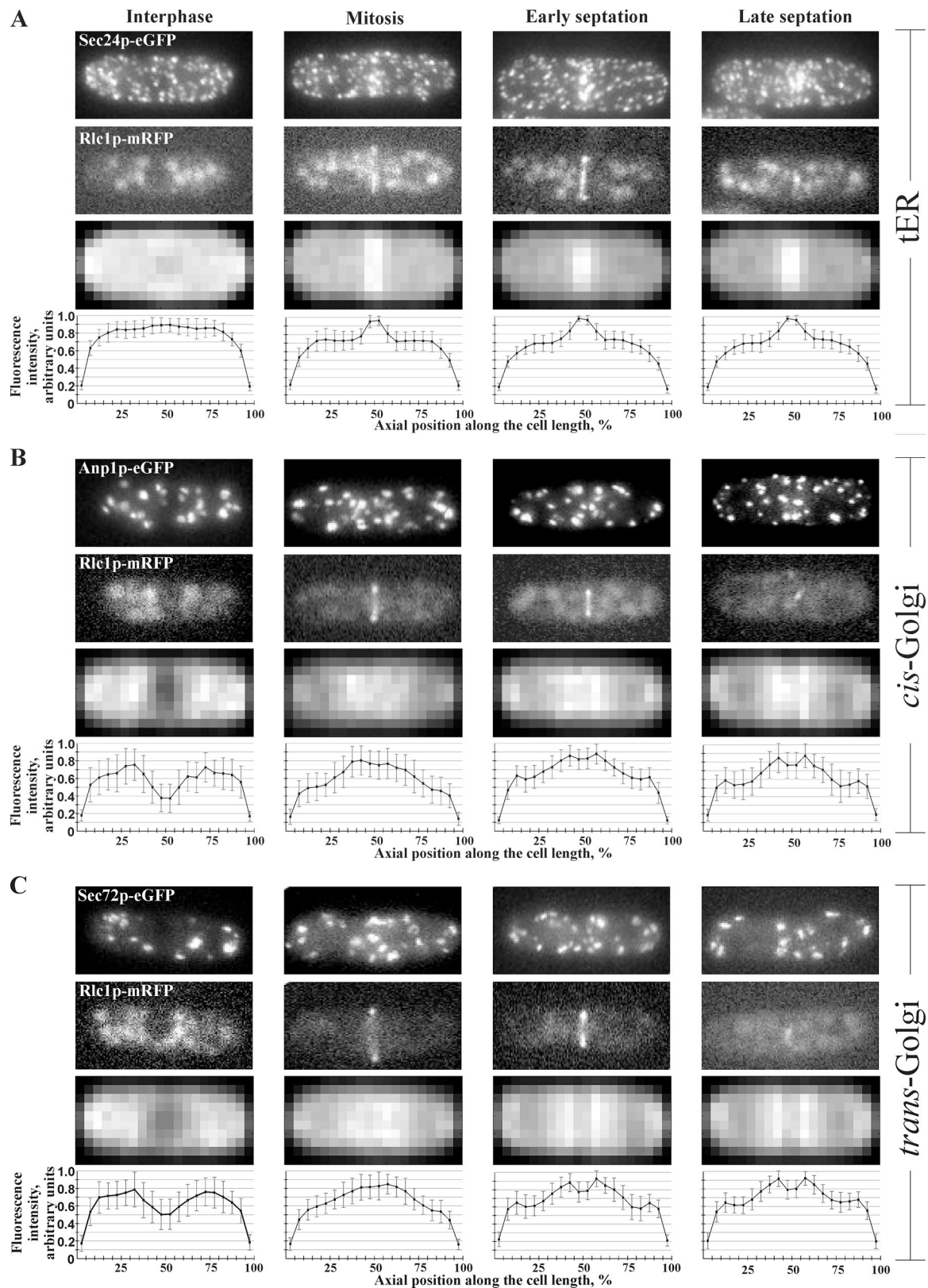


Figure 2. Spatial distribution of the early secretory pathway throughout the cell cycle. (A) tER localization marked by Sec24p-GFP (top row of images) in interphase (first column), mitosis (second column), and early and late septation (third and fourth column). The cell cycle stage was deduced by the morphology of the actomyosin ring marker Rlc1p-mRFP (second row from the top) and the DIC image (not shown). Shown is the maximum projection image of the z-stack obtained by epifluorescence imaging. Epifluorescence maximum projection images of z-stacks of 50 individual cells at the same stage of the cell cycle expressing Sec24p-GFP were standardized and compared with produce an averaged image (third row from the top, for details see *Materials and Methods*). The horizontal axis indicates position along the cell axis

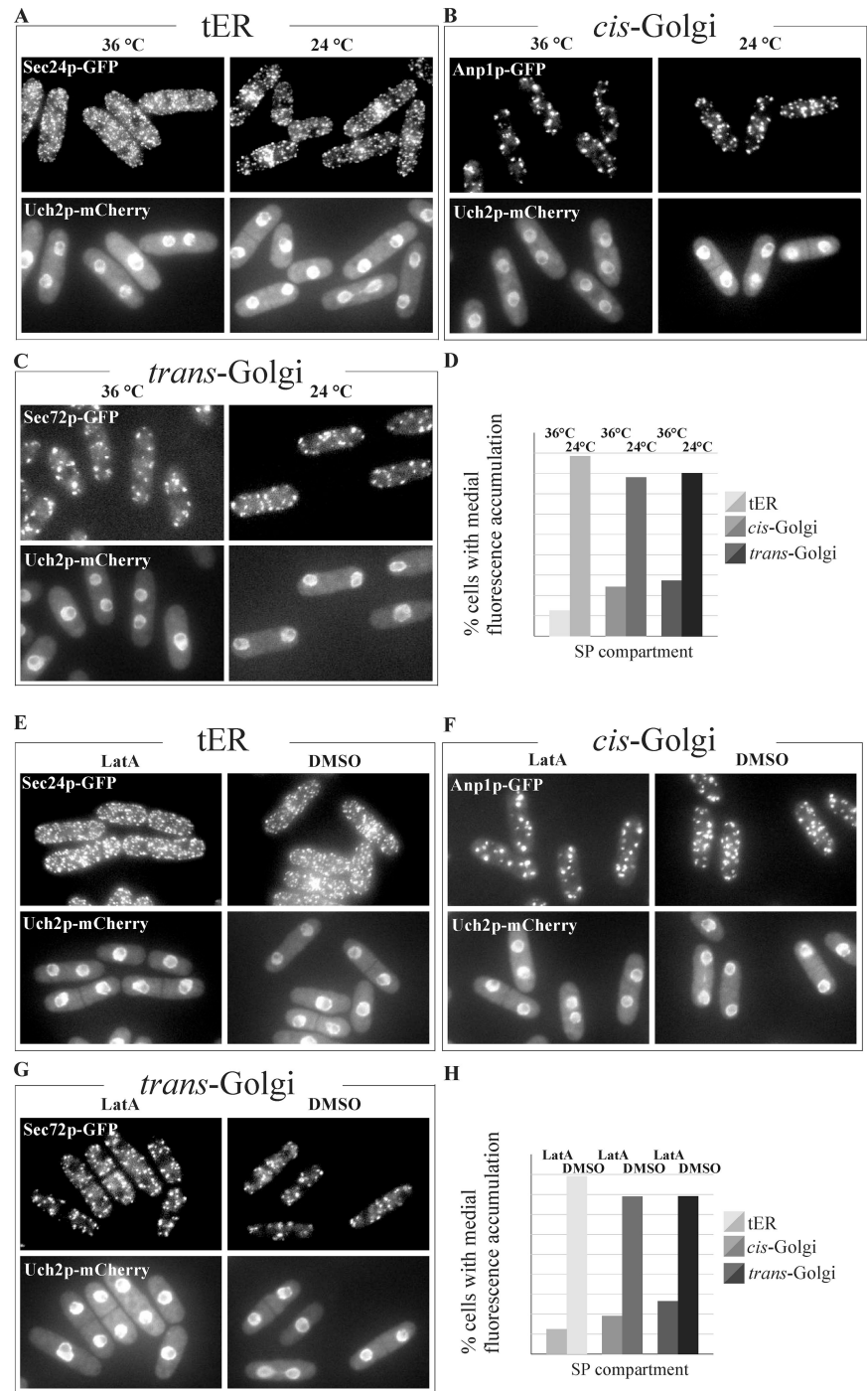


Figure 3. Actomyosin ring assembly is required for secretory pathway recruitment to the division site and maintenance of the polarized state requires an intact actin cytoskeleton. (A) Temperature-sensitive *cdc12-112* mutant cells expressing Sec24p-GFP (top row) and the nuclear marker Uch2p-mCherry (bottom row) were imaged upon entry into anaphase after previously being synchronized in G2 by elutriation, transferred into fresh medium, and allowed to grow at 36°C (left column) and 24°C (right column). Shown is the maximum projection image of the z-stack obtained by epifluorescence imaging. (B) Temperature-sensitive *cdc12-112* mutant cells expressing Anp1p-GFP (top row) and the nuclear marker Uch2p-mCherry (bottom row) were treated as in A. (C) Temperature-sensitive *cdc12-112* mutant cells expressing Sec72p-GFP (top row) and the nuclear marker Uch2p-mCherry (bottom row) were treated as in A. (D) Quantitation of Sec24p-GFP, Anp1p-GFP and Sec72p-GFP polarization under experimental conditions described in A (n = 250 cells per sample). (E) Cells expressing Sec24p-GFP (top row) and Uch2p-mCherry (bottom row) were treated with 10 μ M LatA (left column) or DMSO (right column) for 30 min. Shown is the maximum projection image of the z-stack obtained by epifluorescence imaging. (F) Cells expressing Anp1p-GFP (top row) and Uch2p-mCherry (bottom row) were treated as in E. (G) Cells expressing Sec72p-GFP (top row) and Uch2p-mCherry (bottom row) were treated as in E. (H) Graph quantifying the proportion of cells exhibiting Sec24p-GFP, Anp1p-GFP and Sec72p-GFP polarization under experimental conditions described in E (n = 250 cells per sample).

36°C (only 2/8, 0/4, and 0/4 cells exhibited some residual accumulation in case of tER, *cis*-Golgi, and *trans*-Golgi, respectively). In conclusion, our findings implied that the medial recruitment of the early secretory pathway was SIN

independent, whereas its maintenance did rely on SIN regulated cellular processes.

The EFC Domain Protein Cdc15p Is Required for tER Recruitment to the Division Site

Our results showed that the actomyosin ring is required for the tER and Golgi polarization during mitosis. Cdc15p is a component of the actomyosin ring and is the member of the EFC domain family characterized by an EFC domain at the N-terminus (Tsujita *et al.*, 2006) and an SH3-domain at the C-terminus (Fankhauser *et al.*, 1995). It has been sug-

Figure 2 (cont). in percentages of cell length and the vertical axis indicates fluorescence intensity in arbitrary units. (B) *cis*-Golgi localization marked by Anp1p-GFP; imaging and analysis as in A. (C) *trans*-Golgi localization marked by Sec72p-GFP; imaging and analysis as in A.

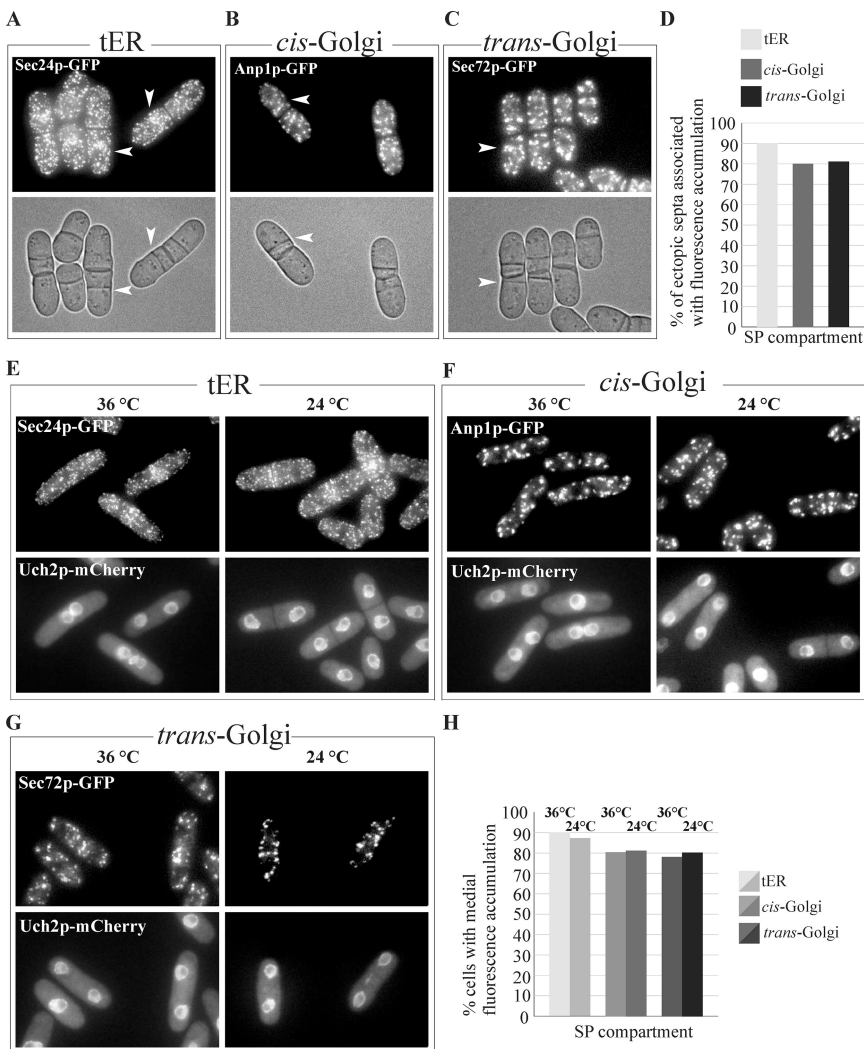


Figure 4. The Septation Initiation Network (SIN) is required for maintenance but not for the initial recruitment of the early secretory pathway compartments at the division site, yet hyperactivation of the SIN pathway results in cell cycle-independent formation of ectopic septa that were accompanied by the tER and *cis*- and *trans*-Golgi recruitment to its vicinity. (A) Epifluorescence and DIC images (top and bottom, respectively) of temperature-sensitive *cdc16-116* mutant cells expressing Sec24p-GFP grown at 36°C. Shown is the maximum projection image of the z-stack obtained by epifluorescence imaging. (B) Epifluorescence and DIC images (top and left column, respectively) of temperature-sensitive *cdc16-116* mutant cells expressing Anp1p-GFP grown at 36°C. (C) Epifluorescence and DIC images (top and left column, respectively) of temperature-sensitive *cdc16-116* mutant cells expressing Sec72p-GFP grown at 36°C. (D) Quantitation of Sec24p-GFP, Anp1p-GFP, and Sec72p-GFP polarization under experimental conditions described in A above ($n = 250$ ectopic septa per sample). (E) Temperature-sensitive *sid2-250* mutant cells expressing Sec24p-GFP (top row) and the nuclear marker Uch2p-mCherry (bottom row) were imaged upon entry into anaphase after previously being synchronized in G2 by elutriation, transferred into fresh medium, and allowed to grow at 36 (left column) and 24°C (right column). Shown is the maximum projection image of the z-stack obtained by epifluorescence imaging. (F) Temperature-sensitive *sid2-250* mutant cells expressing Anp1p-GFP (top row) and the nuclear marker Uch2p-mCherry (bottom row) were treated as in E. (G) Temperature-sensitive *sid2-250* mutant cells expressing Sec72p-GFP (top row) and the nuclear marker Uch2p-mCherry (bottom row) were treated as in E. (H) Graph quantifying the proportion of cells exhibiting Sec24p-GFP, Anp1p-GFP, and Sec72p-GFP polarization under experimental conditions described in E ($n = 250$ cells per sample).

gested that Cdc15p functions downstream of SIN in regulating septum assembly (Marks *et al.*, 1992; Wachtler *et al.*, 2006). Interestingly, the EFC protein family members were shown to couple membrane deformation to the actin cytoskeleton (Tsujita *et al.*, 2006), providing a potential link to COPII vesicle biogenesis (Lee *et al.*, 2005). Thus, we set out to investigate whether Cdc15p functioned during establishment of the polarized state of tER and Golgi during cell division.

Although not essential for actomyosin ring formation in metaphase, Cdc15p is necessary for its maintenance upon SIN activation (Wachtler *et al.*, 2006). Thus, to assess the specific contribution of Cdc15p independently from the actomyosin ring, we observed the spatial distribution of the secretory pathway proteins in wild-type and temperature-sensitive *cdc15-140* mutant cells arrested in metaphase by overexpressing the spindle assembly checkpoint component Mad2p (He *et al.*, 1997) under the *nmt1* promoter (Maundrell, 1990). Briefly, Mad2p overexpression was induced for 20 h at the permissive temperature of 24°C followed by a temperature shift-up for 4 h at 36°C. Samples were taken from cell cultures and stained by phalloidin and DAPI, indicating that under the experimental conditions described ~38% of cells contained actomyosin ring, with ~85% of these appearing arrested in metaphase. We analyzed the

distribution of the early secretory pathway markers in live cells exhibiting Rlc1p-mRFP rings. We observed a marginal difference in the spatial distribution of *cis*- and the *trans*-Golgi compartments between wild-type and *cdc15-140* mutant cells at both 24 and 36°C, with ~50 and 55% cells exhibiting polarization of early and late Golgi elements, respectively (Figure 5, B and C, respectively). On the other hand, the tER marker protein Sec24p-GFP exhibited a more complex distribution (Figure 5A). In wild-type cells, at both 24 and 36°C, ~80% of cells displaying Rlc1p-mRFP ring exhibited a clear recruitment of Sec24p-GFP to the narrow medial band, whereas ~10% of these cells showed some degree of accumulation in a broader, less-defined medial region (Figure 5A, center panel). Sec24p-GFP appeared non-polarized in ~10% of cells. We observed a striking reduction in the number of cells exhibiting clear polarization of the tER in *cdc15-140* cells already at the permissive temperature of 24°C (Figure 5A, bottom panel), suggesting that under these circumstances the mutant Cdc15p protein might be partially inactivated already at 24°C. Among *cdc15-140* cells grown at 24°C and displaying the Rlc1p-mRFP, 40, 40, and 20% exhibited the polarized, marginally polarized, and unpolarized localization of Sec24p-GFP, respectively. On the temperature shift-up to 36°C, the distribution of *cdc15-140* mutant cells with Rlc1p-mRFP rings showing polarized, marginally po-

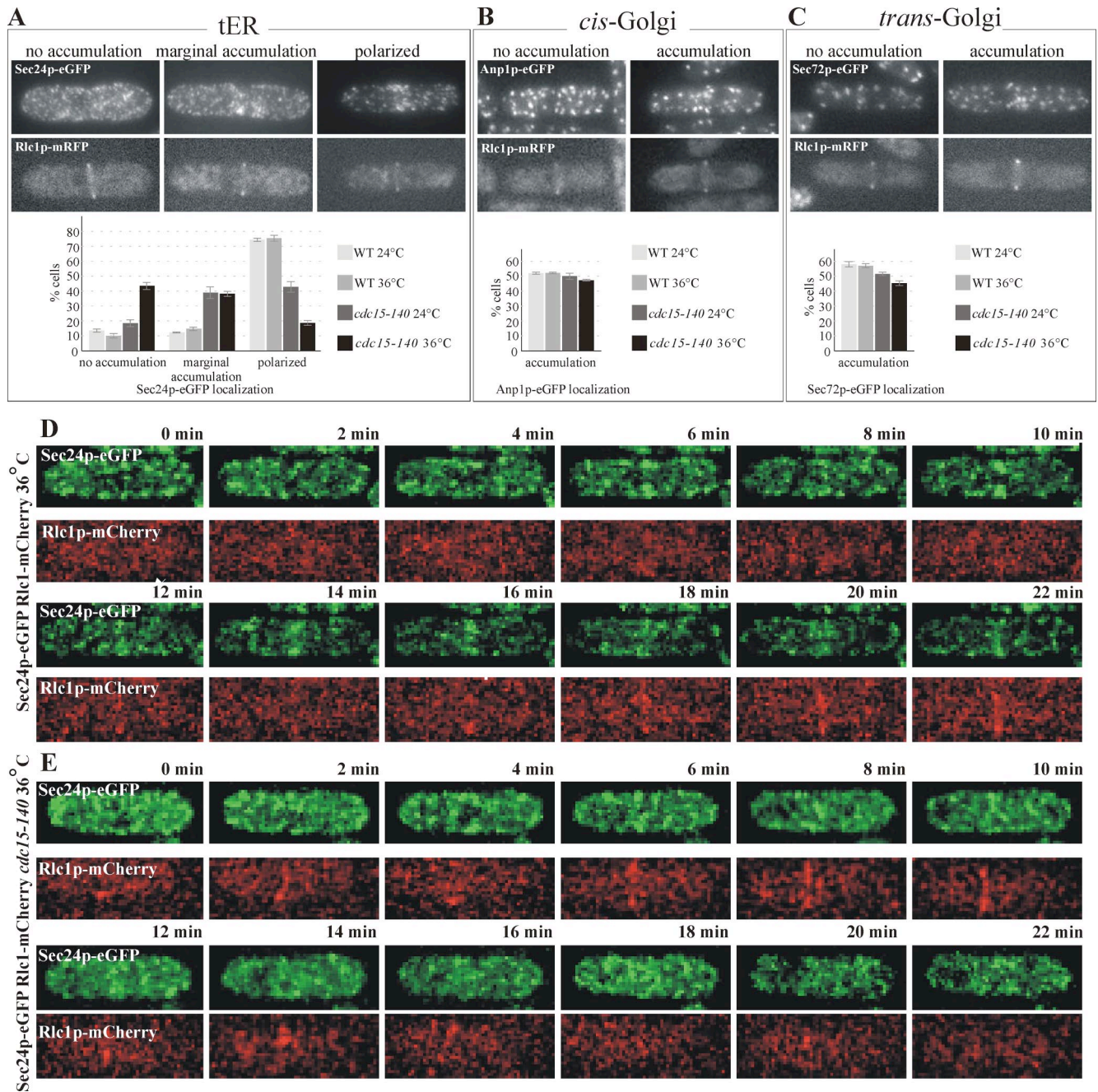


Figure 5. The EFC domain protein Cdc15p was required for the recruitment of the tER to the division site. (A) pREP1-*mad2*⁺ cells coexpressing Sec24p-GFP and Rlc1p-mRFP in wild-type or *cdc15-140* mutant background were grown for 20 h in the absence of thiamine to induce metaphase arrest by overproduction of Mad2p and additionally allowed to grow for 4 h at either 24 or 36°C. In each sample, cells displaying Rlc1p-mRFP rings (second row from the top) exhibited three distinct phenotypes of Sec24p-GFP localization (top row of images). Shown is the maximum projection image of the z-stack obtained by epifluorescence imaging. Quantitation of Sec24p-GFP localization profiles under experimental conditions described is presented in the graph ($n = 250$ cells per sample). (B) pREP1-*mad2*⁺ cells coexpressing Anp1p-GFP and Rlc1p-mRFP in wild-type or *cdc15-140* mutant background were treated as in A. In each sample, cells displaying Rlc1p-mRFP rings (second row from the top) exhibited distinct phenotypes of Anp1p-GFP localization (top row of images). Shown is the maximum projection image of the z-stack obtained by epifluorescence imaging. Quantitation of Anp1p-GFP localization profiles under experimental conditions described are presented in the graph ($n = 250$ cells per sample). (C) pREP1-*mad2*⁺ cells coexpressing Sec72p-GFP and Rlc1p-mRFP in wild-type or *cdc15-140* mutant background were treated as in A. In each sample, cells displaying Rlc1p-mRFP rings (second row from the top) exhibited distinct phenotypes of Sec72p-GFP localization (top row of images). Shown is the maximum projection image of the z-stack obtained by epifluorescence imaging. Quantitation of Sec72p-GFP localization profiles under experimental conditions described are presented in the graph ($n = 250$ cells per sample). (D) Wild-type cells expressing Sec24p-GFP (green) and Rlc1p-mCherry (red) were grown overnight at 24°C and shifted to 36°C for 1 h before imaging. Shown is the maximum projection image of the z-stack obtained by time-lapse spinning disk confocal imaging. (E) *cdc15-140* mutant cells expressing Sec24p-GFP (green) and Rlc1p-mCherry (red) were grown overnight at 24°C and shifted to 36°C for 1 h before imaging. Shown is the maximum projection image of the z-stack obtained by time-lapse spinning disk confocal imaging.

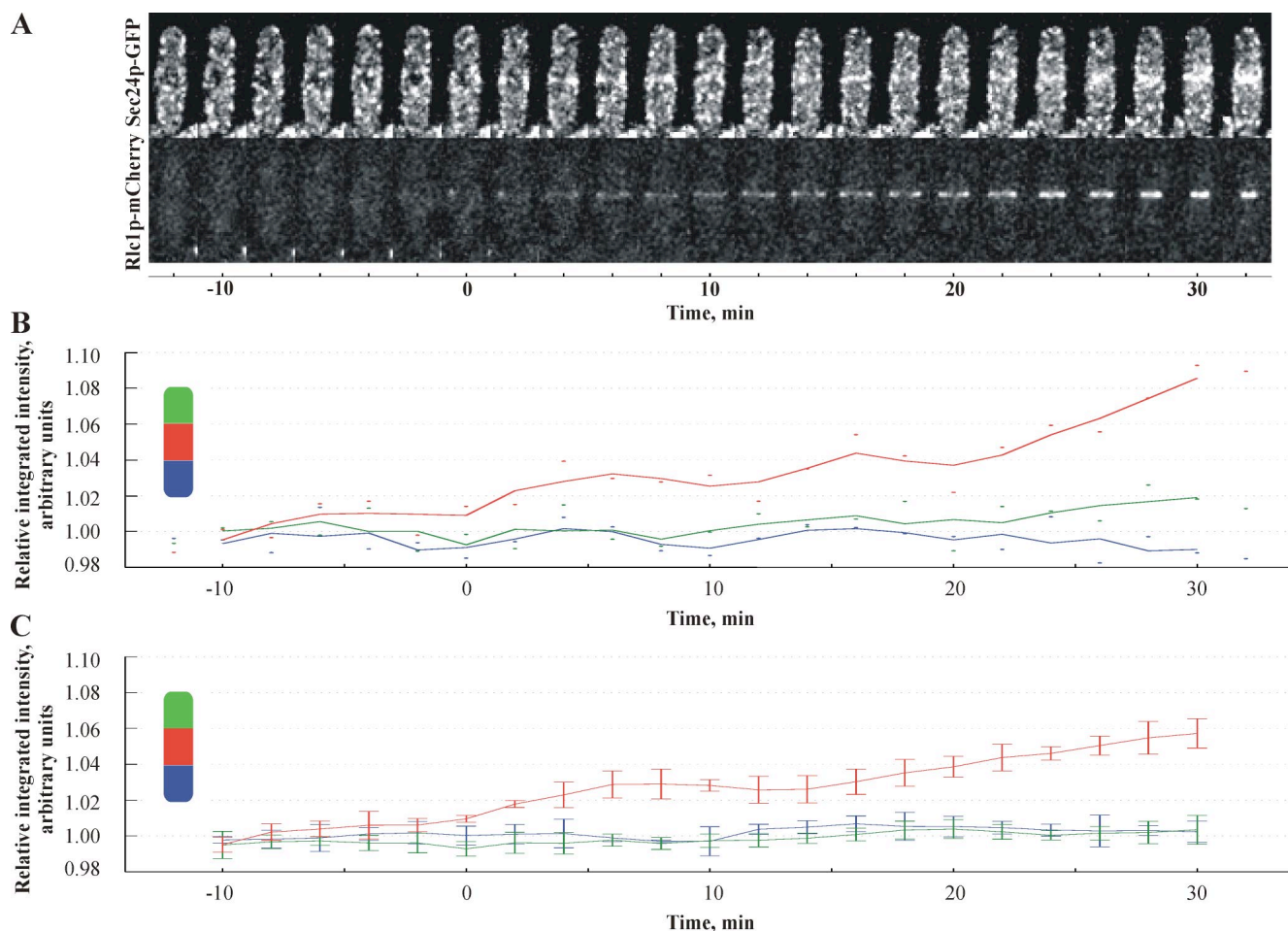


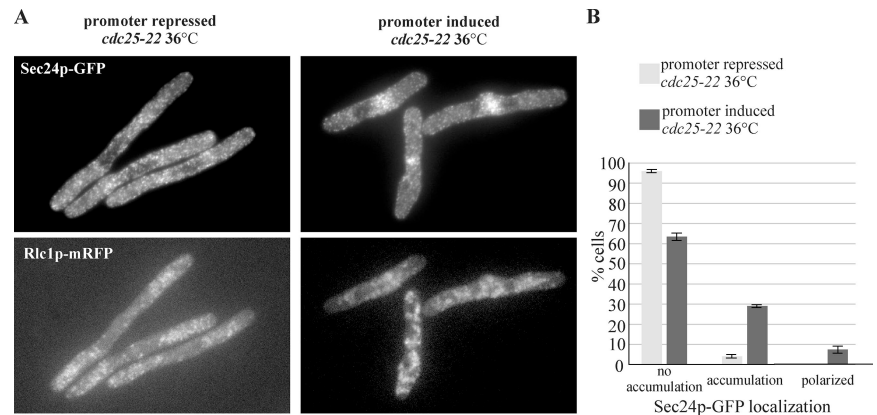
Figure 6. Polarization of tER does not depend on net centripetal movement of pre-existing COPII-positive membranes. (A) Shown is the maximum projection images of the z-stacks obtained by time-lapse spinning disk confocal imaging of cells expressing Sec24p-GFP (top row) and Rlc1p-mCherry (bottom row) grown at 24°C. (B) Quantitation of the relative integrated fluorescence intensities of Sec24p-GFP in tips (green, blue) and the center (red) of the cell presented in A. Dots indicate the measured values at distinct time points, and the graph lines represent the moving average values (for details see *Material and Methods*). (C) Quantitation of the relative integrated fluorescence intensities of Sec24p-GFP in tips (green, blue) and the center (red) of five cells. *y*-axis is scaled relative to average intensity at cell tips. The graph lines represent the moving average values and error bars correspond to the SE (for details see *Material and Methods*).

larized and unpolarized Sec24p-GFP localization changed to ~20, ~40, and ~40%, respectively. We concluded that Sec24p-GFP accumulation at the division site was impaired in metaphase-arrested *cdc15-140* cells despite their ability to assemble actomyosin rings, implicating Cdc15p in tER polarization during cell division.

To further explore the role of Cdc15p in polarization of the tER at the level of individual cells, we performed the time-lapse analyses of either wild-type or *cdc15-140* cells expressing Sec24p-GFP and Rlc1p-mCherry grown overnight at 24°C and shifted to 36°C for 1 h (Figure 5, D and E). The wild-type cells entered mitosis and formed an actomyosin ring that persisted and eventually constricted. We observed a marked and persistent recruitment of tER occurring concomitantly with the actomyosin ring assembly (8/8 cells). The *cdc15-140* cells could form actomyosin rings upon entry into mitosis, but these rings neither persisted nor constricted. Formation of the actomyosin ring in *cdc15-140* cells did not induce pronounced Sec24p-GFP polarization (Figure 5E, 5/8 cells). Incomplete inactivation of Cdc15p temperature-sensitive protein could be a reason for the weak and transient Sec24p-GFP accumulation detected in the remaining cells.

Cdc15p could be involved in targeting the preexisting COPII-positive membranes to the division site. Alternatively, Cdc15p might directly promote tER biogenesis in the vicinity of the actomyosin ring. We assessed whether the COPII structures in dividing cells exhibited the net centripetal movement toward the actomyosin ring by dual color image analyses of Sec24p-GFP and Rlc1p-mCherry (Figure 6A). Measurements of integrated fluorescence intensities of Sec24p-GFP in areas representing both cell tips and cell middle (see *Materials and Methods*) throughout cell division showed that COPII-positive structures accumulated at the division site concurrently with the actomyosin ring formation (Figure 6B, red line). At the same time, the fluorescence intensity of Sec24p-GFP did not change at cell tips (Figure 6B, green and blue lines; see also Figure 6C, *n* = 5 cells). Importantly, Sec24p-GFP accumulated at the division site in cells lacking both type V myosins, Myo4p and Myo5p (Motegi *et al.*, 2004), suggesting that medial accumulation of tER did not require actin cable-directed transport (Supplementary Figure 6, 70% cells exhibited medial accumulation of tER compartments, *n* = 150 cells). Taken together, our data favor the model that Cdc15p could promote tER biogenesis at the division site.

Figure 7. Overexpression of Cdc15p is sufficient to induce medial tER accumulation in interphase. (A) *cdc25-22 pREP1-cdc15⁺* cells expressing Sec24p-GFP (top row) and Rlc1mRFP (bottom row) were grown for 12 h at 24°C and for 4 h at 36° in the absence or presence of thiamine (left and right column, respectively). Shown is the maximum projection image of the z-stack obtained by epifluorescence imaging. (B) Quantitation of Sec24p-GFP polarization under experimental conditions described above (n = 250 cells per sample).



It has been shown that overexpression of Cdc15p causes actin relocalization to the equatorial region in interphase cells (Fankhauser *et al.*, 1995). To assess whether this is sufficient for the early secretory pathway compartments polarization, we overexpressed Cdc15p under the *nmt1* promoter in cells arrested in interphase by the use of *cdc25-22* genetic background (Gould and Nurse, 1989). When we induced Cdc15p overexpression for a total of 16 h (12 h at 24°C and 4 h at 36°C), ~35% of interphase-arrested cells relocalized actin to the cell middle, as judged by DAPI and phalloidin staining, whereas few of these formed an organized ring as judged by localization of Rlc1p-mRFP. We did not observe medial accumulation of either *cis*- and *trans*-Golgi compartments (data not shown). Interestingly, a total of $37 \pm 4\%$ interphase-arrested cells showed a marked accumulation of tER at the medial region, a number that corresponded to the percentage of cells that relocalized actin (Figure 7, A and B). Most cells exhibiting the tER polarization did not assemble the Rlc1p-mRFP-positive actomyosin ring structures (Figure 7A, bottom panel). Taken together, our experiments imply that the EFC domain protein Cdc15p is specifically required for the COP II vesicle polarization at the division site.

DISCUSSION

Here we have shown that in fission yeast the entire early secretory machinery becomes polarized during cell division in an actomyosin ring-dependent manner and relies on the EFC domain protein Cdc15p function.

Organization of the Early Secretory Pathway Compartments in Fission Yeast

As indicated by the tER marker Sec24p-GFP (Figure 1A; and Sec13p-GFP, our unpublished data), the tER of *S. pombe* is not organized as several discrete structures in *P. pastoris* but resemble the delocalized tER of budding yeast (Rossanese *et al.*, 1999). On the other hand, the colocalization studies of two different Golgi compartments, marked by Anp1p and Sec72p (Figure 1, B and C), support the electron microscopy evidence (Johnson *et al.*, 1973; Ayscough *et al.*, 1993) of the Golgi apparatus in fission yeast being predominantly organized as adjacent stacks of few cisternae. In the view of Rossanese and colleagues, the difference in Golgi organization between two budding yeast species could arise from the difference in tER structure. Thus, the stable tER structure of *P. pastoris* would consecutively produce the novel *cis*-Golgi cisternae at a fixed location and maturation of these cisternae will give rise to a stacked Golgi apparatus structure.

Absence of the long-lived, discrete tER sites in *S. cerevisiae* would cause the formation of novel Golgi cisternae at random locations, yielding dispersed Golgi entities. Our results suggest that in fission yeast a relatively disorganized and yet stable tER is present as multiple entities that are accompanied by considerably fewer coherent Golgi stacks (Figure 1, A–C). Such structural organization of the early secretory pathway might reflect the possible involvement of the Golgi matrix (for review see Barr and Short, 2003) or tether (Cai *et al.*, 2007) proteins in maintaining attachment between Golgi cisternae, a function that was lost in *S. cerevisiae* but is present in fission yeast.

Recent advances in high-speed microscopy have allowed the study of Golgi biogenesis and maturation (for review see Hammond and Glick, 2000). Our data provide further evidence supporting the cisternal progression model of Golgi maturation (Figure 1G and Supplementary Movie 3). Time required for Golgi cisternae identity change in fission yeast (Figure 1F) was consistent with maturation dynamics reported previously in *S. cerevisiae* (Losev *et al.*, 2006; Matsuura-Tokita *et al.*, 2006). As judged by the dynamics of the early Golgi marker protein, Anp1p-mCherry, *cis*-Golgi cisternae could also arise de novo (Figure 1, E and F, and Supplementary Movie 2), but the relationship of these biogenesis events to tER was more difficult to establish because of the large number of Sec24p-GFP entities.

Polarization of the Secretory Pathway to the Division Site

The secretory pathway is a major player during cell polarization in many organisms including epithelial polarization in *Drosophila* embryos (Lecuit and Wieschaus, 2000), axon outgrowth in cultured rat embryonic neurons (Bradke and Dotti, 1997) and bud development in *S. cerevisiae* (for review see Finger and Novick, 1998). However, polarized secretion has been mainly studied with respect to the most downstream elements of the secretory pathway, such as the exocytotic machinery and the secretory vesicles. By observing the spatial distribution of the fluorescently tagged proteins specific to distinct early secretory pathway compartments during the cell cycle, we found that the tER and both the *cis*- and *trans*-Golgi established preferential localization to the division site. Surprisingly, although we did not observe the relocalization of the general ER to the site of septation as judged by Ost1p-GFP (Supplementary Figure 1), we found a marked accumulation of tER (Figure 2A). Thus it would be of interest to investigate the manner of tER distribution in other instances where Golgi accumulation at the growth sites was reported (Rida *et al.*, 2006). Interestingly, the Golgi

and the secretory vesicles accumulated at the sites of cell wall formation as judged by three-dimensional (3D) reconstruction of reverting *S. pombe* protoplasts (Osumi *et al.*, 1998). The importance of ER recruitment has been recently reported in a study on the role of the gene *jagunal* in *Drosophila* oocyte development (Lee and Cooley, 2007). This study highlighted the importance of ER reorganization to the subcortical clusters as essential for increased exocytotic membrane traffic that is vital for oocyte development. However, in these cells concordant relocation of the Golgi compartments was not investigated. We propose that although different organisms could undergo polarization of the secretory pathway at various stages of its biogenesis, the common feature of the examples available in the published literature could be a necessity for a rapid increase in cell surface area. It is conceivable that such intense events might require massive trafficking that could be achieved by concentrating the entire secretory machinery to the proximity of the secretion site, rather than relying on a long-range delivery of post-Golgi vesicles. Interestingly, fission yeast cells lacking functional exocyst components still form complete septa, although they are defective in septum cleavage (Wang *et al.*, 2002).

How could such polarization be achieved? One obvious solution is the recruitment of the secretion machinery by cytoskeletal elements. In *S. cerevisiae*, compromised function of actin cytoskeleton components abolishes polarized secretion (for review see Finger and Novick, 1998). In particular, polarized secretion at the bud requires intact actin cables and the type V myosin Myo2 (Govindan *et al.*, 1995). In *S. pombe*, both actin cables (Feierbach and Chang, 2001) and the type V myosin Myo4p (Motegi *et al.*, 2001) are necessary for the establishment of proper cell morphology. Thus, our results on the requirement of the actomyosin ring for the establishment and of an intact actin cytoskeleton for the maintenance of the polarized early secretory pathway are in agreement with the previously reported roles for the actin cytoskeleton in polarized secretion. Again, the tight coupling of ring formation and secretory pathway polarization could be necessary for fission yeast to timely prime the site for intense secretion that is associated with building a septum across the cylindrical cell.

The SIN pathway has been shown to be vital for targeted secretion because its inactivation hinders secretion of the septum material at the division site (Liu *et al.*, 2002). Our data show that the early secretory pathway polarization occurs before SIN activation and does not require its function (Figure 4 and Supplementary Figure 5), therefore suggesting that recruitment of the early secretory machinery and post-Golgi secretion are differentially regulated. Thus it seems that SIN functions in activating most downstream secretion events, such as post-Golgi vesicle trafficking.

Our results are consistent with the possibility that the EFC domain protein Cdc15p might function as the actomyosin ring component recruiting the tER to the site of division. Lee *et al.* (2005) have shown that the COPII coat proteins alone were defective in forming COPII vesicles *in vitro* and required Sar1p function to vesiculate lipid membranes. They suggested that the formation of membrane curvature by components other than COPII vesicle proteins might be vital to the formation of the vesicles. They also suggested that factors such as the microtubule-driven membrane deformation characteristic of mammalian cells could generate curvature that could be subsequently acted upon by the cytosolic coat proteins. Cdc15p possesses an EFC domain that has been shown to induce membrane tubulation in other proteins (Tsujiita *et al.*, 2006). As we neither observed any net

movement of COPII-positive membranes toward the division site (Figure 6) nor involvement of type V myosin (Supplementary Figure 6) in this phenomenon, an exciting possibility is that Cdc15p might be involved in generating membrane curvature and thus promote tER formation in the vicinity of the actomyosin ring. We found that Cdc15p was necessary and sufficient for the medial accumulation of the tER (Figures 5 and 7). Overexpression of the Cdc15p EFC domain alone or of Cdc15p lacking the EFC domain was not sufficient for the induction of tER recruitment to the equatorial region in interphase cells (our unpublished data). Cdc15p was not required for localization of Golgi cisternae, suggesting that the recruitment of tER and Golgi to the division site may occur through different mechanisms. Our experiments together with the published research suggest that actin structures could possibly act as a delivery or anchor system for Golgi apparatus.

In conclusion, our work identifies the fission yeast *S. pombe* as an interesting system for studying the phenomena of secretion and polarity establishment. We propose that the polarization of both tER and Golgi might fulfill the need for massive vesicle trafficking events occurring at the division site. It would be interesting to gain a better understanding of the role of Cdc15p and to identify additional molecular determinants of the process in future.

ACKNOWLEDGMENTS

We are most grateful to M. Balasubramanian and H. Wang (Temasek Life Sciences Laboratory) for sharing *S. pombe* strains and for valuable comments on the manuscript. We thank V. Wachtler and E. Makeyev for critical reading of the manuscript and R. Thadani for valuable discussions. X.-Z.T., a student of Raffles Junior College, Singapore, participated in the Research Attachment Programme (REAP) organized by the Ministry of Education (MOE), National University of Singapore (NUS), and Temasek Life Sciences Laboratory. This work has been supported by intramural funds from the Temasek Life Sciences Laboratory.

REFERENCES

- Alberts, B., Johnson, A., Lewis, J., Raff, M., Roberts, K., and Walter, P. (2002). *Molecular Biology of the Cell*, New York: Garland Science.
- Antonny, B., Madden, D., Hamamoto, S., Orci, L., and Schekman, R. (2001). Dynamics of the COPII coat with GTP and stable analogues. *Nat. Cell Biol.* 3, 531–537.
- Arai, R., and Mabuchi, I. (2002). F-actin ring formation and the role of F-actin cables in the fission yeast *Schizosaccharomyces pombe*. *J. Cell Sci.* 115, 887–898.
- Ayscough, K., Hajibagheri, N. M., Watson, R., and Warren, G. (1993). Stacking of Golgi cisternae in *Schizosaccharomyces pombe* requires intact microtubules. *J. Cell Sci.* 106(Pt 4), 1227–1237.
- Balasubramanian, M. K., Bi, E., and Glotzer, M. (2004). Comparative analysis of cytokinesis in budding yeast, fission yeast and animal cells. *Curr. Biol.* 14, R806–R818.
- Balasubramanian, M. K., Helfman, D. M., and Hemmingsen, S. M. (1992). A new tropomyosin essential for cytokinesis in the fission yeast *S. pombe*. *Nature* 360, 84–87.
- Balasubramanian, M. K., McCollum, D., Chang, L., Wong, K. C., Naqvi, N. I., He, X., Sazer, S., and Gould, K. L. (1998). Isolation and characterization of new fission yeast cytokinesis mutants. *Genetics* 149, 1265–1275.
- Barlowe, C., Orci, L., Yeung, T., Hosobuchi, M., Hamamoto, S., Salama, N., Rexach, M. F., Ravazzola, M., Amherdt, M., and Schekman, R. (1994). COPII: a membrane coat formed by Sec proteins that drive vesicle budding from the endoplasmic reticulum. *Cell* 77, 895–907.
- Barr, F. A., and Short, B. (2003). Golgins in the structure and dynamics of the Golgi apparatus. *Curr. Opin. Cell Biol.* 15, 405–413.
- Bartnicki-Garcia, S., Hergert, F., and Gierz, G. (1989). Computer simulation of fungal morphogenesis and the mathematical basis for hyphal (typ) growth. *Protoplasts* 153, 46–57.

- Bevis, B. J., Hammond, A. T., Reinke, C. A., and Glick, B. S. (2002). *De novo* formation of transitional ER sites and Golgi structures in *Pichia pastoris*. *Nat. Cell Biol.* 4, 750–756.
- Bradke, F., and Dotti, C. G. (1997). Neuronal polarity: vectorial cytoplasmic flow precedes axon formation. *Neuron* 19, 1175–1186.
- Broughton, J., Swennen, D., Wilkinson, B. M., Joyet, P., Gaillardin, C., and Stirling, C. J. (1997). Cloning of SEC61 homologues from *Schizosaccharomyces pombe* and *Yarrowia lipolytica* reveals the extent of functional conservation within this core component of the ER translocation machinery. *J. Cell Sci.* 110(Pt 21), 2715–2727.
- Cai, H., Yu, S., Menon, S., Cai, Y., Lazarova, D., Fu, C., Reinisch, K., Hay, J. C., and Ferro-Novick, S. (2007). TRAPPI tethers COPII vesicles by binding the coat subunit Sec23. *Nature* 445, 941–944.
- Carpenter, A. E. et al. (2006). CellProfiler: image analysis software for identifying and quantifying cell phenotypes. *Genome Biol.* 7, R100.
- Chang, F., Drubin, D., and Nurse, P. (1997). *cdc12p*, a protein required for cytokinesis in fission yeast, is a component of the cell division ring and interacts with profilin. *J. Cell Biol.* 137, 169–182.
- Chang, F., Woollard, A., and Nurse, P. (1996). Isolation and characterization of fission yeast mutants defective in the assembly and placement of the contractile actin ring. *J. Cell Sci.* 109(Pt 1), 131–142.
- Cortes, J. C., Ishiguro, J., Duran, A., and Ribas, J. C. (2002). Localization of the (1,3)-beta-D-glucan synthase catalytic subunit homologue Bgs1p/Cps1p from fission yeast suggests that it is involved in septation, polarized growth, mating, spore wall formation and spore germination. *J. Cell Sci.* 115, 4081–4096.
- Deshaies, R. J., Sanders, S. L., Feldheim, D. A., and Schekman, R. (1991). Assembly of yeast Sec proteins involved in translocation into the endoplasmic reticulum into a membrane-bound multisubunit complex. *Nature* 349, 806–808.
- Engstler, M., Thilo, L., Weise, F., Grunfelder, C. G., Schwarz, H., Boshart, M., and Overath, P. (2004). Kinetics of endocytosis and recycling of the GPI-anchored variant surface glycoprotein in *Trypanosoma brucei*. *J. Cell Sci.* 117, 1105–1115.
- Fankhauser, C., Reymond, A., Cerutti, L., Utzig, S., Hofmann, K., and Simanis, V. (1995). The *S. pombe cdc15* gene is a key element in the reorganization of F-actin at mitosis. *Cell* 82, 435–444.
- Feierbach, B., and Chang, F. (2001). Roles of the fission yeast formin for3p in cell polarity, actin cable formation and symmetric cell division. *Curr. Biol.* 11, 1656–1665.
- Finger, F. P., and Novick, P. (1998). Spatial regulation of exocytosis: lessons from yeast. *J. Cell Biol.* 142, 609–612.
- Franzusoff, A., Redding, K., Crosby, J., Fuller, R. S., and Schekman, R. (1991). Localization of components involved in protein transport and processing through the yeast Golgi apparatus. *J. Cell Biol.* 112, 27–37.
- Furge, K. A., Wong, K., Armstrong, J., Balasubramanian, M., and Albright, C. F. (1998). Byr4 and Cdc16 form a two-component GTPase-activating protein for the Spg1 GTPase that controls septation in fission yeast. *Curr. Biol.* 8, 947–954.
- Gould, K. L., and Nurse, P. (1989). Tyrosine phosphorylation of the fission yeast *cdc2+* protein kinase regulates entry into mitosis. *Nature* 342, 39–45.
- Govindan, B., Bowser, R., and Novick, P. (1995). The role of Myo2, a yeast class V myosin, in vesicular transport. *J. Cell Biol.* 128, 1055–1068.
- Guo, W., and Novick, P. (2004). The exocyst meets the translocon: a regulatory circuit for secretion and protein synthesis? *Trends Cell Biol.* 14, 61–63.
- Hales, K. G., Bi, E., Wu, J. Q., Adam, J. C., Yu, I. C., and Pringle, J. R. (1999). Cytokinesis: an emerging unified theory for eukaryotes? *Curr. Opin. Cell Biol.* 11, 717–725.
- Hammond, A. T., and Glick, B. S. (2000). Raising the speed limits for 4D fluorescence microscopy. *Traffic* 1, 935–940.
- Harris, S. D., Read, N. D., Roberson, R. W., Shaw, B., Seiler, S., Plamann, M., and Momany, M. (2005). Polarosome meets spitzenkorper: microscopy, genetics, and genomics converge. *Eukaryot. Cell* 4, 225–229.
- He, X., Patterson, T. E., and Sazer, S. (1997). The *Schizosaccharomyces pombe* spindle checkpoint protein mad2p blocks anaphase and genetically interacts with the anaphase-promoting complex. *Proc. Natl. Acad. Sci. USA* 94, 7965–7970.
- Humbel, B. M., Konomi, M., Takagi, T., Kamasawa, N., Ishijima, S. A., and Osumi, M. (2001). In situ localization of beta-glucans in the cell wall of *Schizosaccharomyces pombe*. *Yeast* 18, 433–444.
- Jochova, J., Rupes, I., and Streiblova, E. (1991). F-actin contractile rings in protoplasts of the yeast *Schizosaccharomyces*. *Cell Biol. Int. Rep.* 15, 607–610.
- Johnson, B. F., Yoo, B. Y., and Calleja, G. B. (1973). Cell division in yeasts: movement of organelles associated with cell plate growth of *Schizosaccharomyces pombe*. *J. Bacteriol.* 115, 358–366.
- Johnston, G. C., Prendergast, J. A., and Singer, R. A. (1991). The *Saccharomyces cerevisiae* MYO2 gene encodes an essential myosin for vectorial transport of vesicles. *J. Cell Biol.* 113, 539–551.
- Jungmann, J., and Munro, S. (1998). Multi-protein complexes in the cis Golgi of *Saccharomyces cerevisiae* with alpha-1,6-mannosyltransferase activity. *EMBO J.* 17, 423–434.
- Karagiannis, J., Bimbo, A., Rajagopalan, S., Liu, J., and Balasubramanian, M. K. (2005). The nuclear kinase Lsk1p positively regulates the septation initiation network and promotes the successful completion of cytokinesis in response to perturbation of the actomyosin ring in *Schizosaccharomyces pombe*. *Mol. Biol. Cell* 16, 358–371.
- Kitayama, C., Sugimoto, A., and Yamamoto, M. (1997). Type II myosin heavy chain encoded by the *myo2* gene composes the contractile ring during cytokinesis in *Schizosaccharomyces pombe*. *J. Cell Biol.* 137, 1309–1319.
- Krapp, A., Gulli, M. P., and Simanis, V. (2004). SIN and the art of splitting the fission yeast cell. *Curr. Biol.* 14, R722–730.
- Le Goff, X., Motegi, F., Salimova, E., Mabuchi, I., and Simanis, V. (2000). The *S. pombe rlc1* gene encodes a putative myosin regulatory light chain that binds the type II myosins myo3p and myo2p. *J. Cell Sci.* 113(Pt 23), 4157–4163.
- Lecuit, T., and Wieschaus, E. (2000). Polarized insertion of new membrane from a cytoplasmic reservoir during cleavage of the *Drosophila* embryo. *J. Cell Biol.* 150, 849–860.
- Lee, M. C., Orci, L., Hamamoto, S., Futai, E., Ravazzola, M., and Schekman, R. (2005). Sar1p N-terminal helix initiates membrane curvature and completes the fission of a COPII vesicle. *Cell* 122, 605–617.
- Lee, S., and Cooley, L. (2007). Jagunal is required for reorganizing the endoplasmic reticulum during *Drosophila* oogenesis. *J. Cell Biol.* 176, 941–952.
- Li, T., Naqvi, N. I., Yang, H., and Teo, T. S. (2000). Identification of a 26S proteasome-associated UCH in fission yeast. *Biochem. Biophys. Res. Commun.* 272, 270–275.
- Liu, J., Tang, X., Wang, H., Oliferenko, S., and Balasubramanian, M. K. (2002). The localization of the integral membrane protein Cps1p to the cell division site is dependent on the actomyosin ring and the septation-inducing network in *Schizosaccharomyces pombe*. *Mol. Biol. Cell* 13, 989–1000.
- Liu, J., Wang, H., and Balasubramanian, M. K. (2000). A checkpoint that monitors cytokinesis in *Schizosaccharomyces pombe*. *J. Cell Sci.* 113(Pt 7), 1223–1230.
- Losev, E., Reinke, C. A., Jellen, J., Strongin, D. E., Bevis, B. J., and Glick, B. S. (2006). Golgi maturation visualized in living yeast. *Nature* 441, 1002–1006.
- Malhotra, V., and Mayor, S. (2006). Cell biology: the Golgi grows up. *Nature* 441, 939–940.
- Mancias, J. D., and Goldberg, J. (2005). Exiting the endoplasmic reticulum. *Traffic* 6, 278–285.
- Marks, J., Fankhauser, C., and Simanis, V. (1992). Genetic interactions in the control of septation in *Schizosaccharomyces pombe*. *J. Cell Sci.* 101(Pt 4), 801–808.
- Marks, J., and Hyams, J. S. (1985). Localization of F-actin through the cell division cycle of *Schizosaccharomyces pombe*. *Eur. J. Cell Biol.* 39, 27–32.
- Martin-Cuadrado, A. B., Duenas, E., Sipiczki, M., Vazquez de Aldana, C. R., and del Rey, F. (2003). The endo-beta-1,3-glucanase eng1p is required for dissolution of the primary septum during cell separation in *Schizosaccharomyces pombe*. *J. Cell Sci.* 116, 1689–1698.
- Martin-Cuadrado, A. B., Morrell, J. L., Konomi, M., An, H., Petit, C., Osumi, M., Balasubramanian, M., Gould, K. L., Del Rey, F., and de Aldana, C. R. (2005). Role of septins and the exocyst complex in the function of hydrolytic enzymes responsible for fission yeast cell separation. *Mol. Biol. Cell* 16, 4867–4881.
- Matsuura-Tokita, K., Takeuchi, M., Ichihara, A., Mikuriya, K., and Nakano, A. (2006). Live imaging of yeast Golgi distal maturation. *Nature* 441, 1007–1010.
- Maundrell, K. (1990). *nmt1* of fission yeast. A highly transcribed gene completely repressed by thiamine. *J. Biol. Chem.* 265, 10857–10864.
- McCullum, D., Balasubramanian, M. K., Pelcher, L. E., Hemmingsen, S. M., and Gould, K. L. (1995). *Schizosaccharomyces pombe cdc4+* gene encodes a novel EF-hand protein essential for cytokinesis. *J. Cell Biol.* 130, 651–660.
- Mellman, I., and Warren, G. (2000). The road taken: past and future foundations of membrane traffic. *Cell* 100, 99–112.

- Minet, M., Nurse, P., Thuriaux, P., and Mitchison, J. M. (1979). Uncontrolled septation in a cell division cycle mutant of the fission yeast *Schizosaccharomyces pombe*. *J. Bacteriol.* *137*, 440–446.
- Moreno, S., Klar, A., and Nurse, P. (1991). Molecular genetic analysis of fission yeast *Schizosaccharomyces pombe*. *Methods Enzymol.* *194*, 795–823.
- Motegi, F., Arai, R., and Mabuchi, I. (2001). Identification of two type V myosins in fission yeast, one of which functions in polarized cell growth and moves rapidly in the cell. *Mol. Biol. Cell* *12*, 1367–1380.
- Naqvi, N. I., Eng, K., Gould, K. L., and Balasubramanian, M. K. (1999). Evidence for F-actin-dependent and -independent mechanisms involved in assembly and stability of the medial actomyosin ring in fission yeast. *EMBO J.* *18*, 854–862.
- Nickel, W. (2003). The mystery of nonclassical protein secretion. A current view on cargo proteins and potential export routes. *Eur. J. Biochem.* *270*, 2109–2119.
- Osumi, M., Sato, M., Ishijima, S. A., Konomi, M., Takagi, T., and Yaguchi, H. (1998). Dynamics of cell wall formation in fission yeast, *Schizosaccharomyces pombe*. *Fungal. Genet. Biol.* *24*, 178–206.
- Pidoux, A. L., and Armstrong, J. (1993). The BiP protein and the endoplasmic reticulum of *Schizosaccharomyces pombe*: fate of the nuclear envelope during cell division. *J. Cell Sci.* *105*(Pt 4), 1115–1120.
- Preuss, D., Mulholland, J., Franzusoff, A., Segev, N., and Botstein, D. (1992). Characterization of the *Saccharomyces* Golgi complex through the cell cycle by immunoelectron microscopy. *Mol. Biol. Cell* *3*, 789–803.
- Ribas, J. C., Diaz, M., Duran, A., and Perez, P. (1991). Isolation and characterization of *Schizosaccharomyces pombe* mutants defective in cell wall (1-3)beta-D-glucan. *J. Bacteriol.* *173*, 3456–3462.
- Rida, P. C., Nishikawa, A., Won, G. Y., and Dean, N. (2006). Yeast-to-hyphal transition triggers formin-dependent Golgi localization to the growing tip in *Candida albicans*. *Mol. Biol. Cell* *17*, 4364–4378.
- Rossanese, O. W., Soderholm, J., Bevis, B. J., Sears, I. B., O'Connor, J., Williamson, E. K., and Glick, B. S. (1999). Golgi structure correlates with transitional endoplasmic reticulum organization in *Pichia pastoris* and *Saccharomyces cerevisiae*. *J. Cell Biol.* *145*, 69–81.
- Silberstein, S., Collins, P. G., Kelleher, D. J., Rapiejko, P. J., and Gilmore, R. (1995). The alpha subunit of the *Saccharomyces cerevisiae* oligosaccharyltransferase complex is essential for vegetative growth of yeast and is homologous to mammalian ribophorin I. *J. Cell Biol.* *128*, 525–536.
- Sparks, C. A., Morphey, M., and McCollum, D. (1999). Sid2p, a spindle pole body kinase that regulates the onset of cytokinesis. *J. Cell Biol.* *146*, 777–790.
- Tsujita, K., Suetsugu, S., Sasaki, N., Furutani, M., Oikawa, T., and Takenawa, T. (2006). Coordination between the actin cytoskeleton and membrane deformation by a novel membrane tubulation domain of PCH proteins is involved in endocytosis. *J. Cell Biol.* *172*, 269–279.
- Wachtler, V., Huang, Y., Karagiannis, J., and Balasubramanian, M. K. (2006). Cell cycle-dependent roles for the FCH-domain protein Cdc15p in formation of the actomyosin ring in *Schizosaccharomyces pombe*. *Mol. Biol. Cell* *17*, 3254–3266.
- Wang, H., Tang, X., Liu, J., Trautmann, S., Balasundaram, D., McCollum, D., and Balasubramanian, M. K. (2002). The multiprotein exocyst complex is essential for cell separation in *Schizosaccharomyces pombe*. *Mol. Biol. Cell* *13*, 515–529.
- Wood, V. *et al.* (2002). The genome sequence of *Schizosaccharomyces pombe*. *Nature* *415*, 871–880.

Nucleocytoplasmic Shuttling of the TACC Protein Mia1p/Alp7p Is Required for Remodeling of Microtubule Arrays during the Cell Cycle

Yuen Chyao Ling¹, Aleksandar Vjestica¹, Snezhana Oliferenko*

Temasek Life Sciences Laboratory, Singapore, Singapore

Abstract

Microtubule arrays are remodeled as cells proceed through the cell cycle. It is important to understand how remodeling is regulated in time and space. In fission yeast, the conserved microtubule associated TACC/TOG complex plays an important role in organizing microtubules throughout the cell cycle. Here we show that this complex undergoes nucleocytoplasmic shuttling through the nuclear import and export signals located in the TACC protein Mia1p/Alp7p. When the Crm1p-dependent nuclear export signal of Mia1p is disabled, Mia1p accumulates in the nucleus while its partner protein Alp14p/TOG is restricted to the cytoplasm. This leads to defects in assembly of both interphase arrays and the mitotic spindle. Artificial targeting of Alp14p to the nucleus partially rescues the mitotic spindle defects caused by lack of Mia1p nuclear export. Interestingly, the nuclear export sequence of Mia1p appears to overlap with the Alp14p binding site. We propose that intricate regulation of the subcellular distribution of TACC/TOG complexes drives microtubule array remodeling as cells progress through the cell cycle.

Citation: Ling YC, Vjestica A, Oliferenko S (2009) Nucleocytoplasmic Shuttling of the TACC Protein Mia1p/Alp7p Is Required for Remodeling of Microtubule Arrays during the Cell Cycle. PLoS ONE 4(7): e6255. doi:10.1371/journal.pone.0006255

Editor: Kevin G. Hardwick, University of Edinburgh, United Kingdom

Received: March 24, 2009; **Accepted:** June 10, 2009; **Published:** July 16, 2009

Copyright: © 2009 Ling et al. This is an open-access article distributed under the terms of the Creative Commons Attribution License, which permits unrestricted use, distribution, and reproduction in any medium, provided the original author and source are credited.

Funding: This work was carried out with support from the Singapore Millenium Foundation. The funders had no role in study design, data collection and analysis, decision to publish, or preparation of the manuscript.

Competing Interests: The authors have declared that no competing interests exist.

* E-mail: snejana@tll.org.sg

These authors contributed equally to this work.

Introduction

Microtubules are dynamic polymers that often function as higher order arrays of different geometries that form in response to cell cycle and environmental cues. In interphase, cytoplasmic microtubule arrays sustain specific cell morphology and function. As cells enter mitosis, microtubules are reorganized to form a mitotic spindle. In “open” mitosis of higher eukaryotes the nuclear envelope (NE) breaks down enabling microtubules to capture kinetochores. In many organisms, such as fission yeast *Schizosaccharomyces pombe* (*S. pombe*), the NE stays intact so spindles are assembled from tubulin and microtubule-associated proteins (MAPs) that are imported from the cytoplasm through the nuclear pore complexes. Such mitosis is called “closed”. It appears that karyopherins involved in nuclear transport together with the small GTPase Ran play an important role in spindle assembly in both systems. In animal cells, a Ran-GTP mediated release of the microtubule regulators, such as TPX2 [1], NUMA [2,3] and HURP [4,5] from complexes with karyopherins allows spindle assembly. In *S. pombe*, Ran-GTP promotes nuclear accumulation of an evolutionary conserved MAP complex that consists of the transforming acidic coiled coil (TACC) protein Mia1p/Alp7p (which appears to be a direct Ran target) and the TOG protein Alp14p [6]. It is unclear whether nucleocytoplasmic shuttling occurs throughout the cell cycle and why this complex accumulates in the nucleus only at mitotic onset. Here we show that Mia1p/Alp7p shuttles in and out of the nucleus during

interphase by utilizing a nuclear import sequence (NLS) and a nuclear export sequence (NES). When the NES is mutated Mia1p accumulates in the nucleus. This leads to profound microtubule abnormalities at all stages of cell cycle, including mitosis. We link the spindle-related phenotypes to deficient nuclear accumulation of the Mia1p/Alp7p partner, Alp14p. Our results underscore the importance of spatiotemporal regulation of the activity and availability of MAPs for proper microtubule array formation.

Results

Mia1p is exported from the nucleus via a Crm1p-dependent NES

At mitotic entry, Mia1p accumulates in the nucleus, while during interphase it is restricted to the cytoplasm. We wondered what is the mechanism that drives its differential compartmentalization during the cell cycle. The ELM algorithm [7] predicts a putative leucine-rich NES motif at the extreme C-terminus of Mia1p that is recognized by a major cellular exportin Crm1p. Thus, we checked the localization of Mia1p-GFP in cells containing a mutant allele of *crm1*, *crm1-809* [8] and an NE marker, Uch2p-mCherry. At the permissive temperature of 36°C, Mia1p-GFP in interphase cells localized along microtubules in the cytoplasm. However, Mia1p-GFP accumulated in the nuclei of interphase *crm1-809* cells at the restrictive temperature of 18°C (nuclear Mia1p-GFP signal increases ~90%, n = 50 cells, p < 0.01 upon temperature downshift). Its mitotic localization to the spindle

pole bodies (SPBs), kinetochores and along the spindle remained unchanged (Fig. 1A). An obligate partner of Mia1p, Alp14p/TOG colocalized with Mia1p in the nuclei of *crm1-809* cells at 18°C (Fig. S1A), suggesting that the entire TACC/TOG complex shuttles in and out of the nucleus. We confirmed these observations by inhibiting Crm1p function through treatment with leptomycin B (data not shown).

Deletion of the last 17 amino acids (Mia1p-CΔ17) comprising the putative NES led to nuclear accumulation of Mia1p during

interphase (Fig. 1B and C, quantified in Fig. 2B). When fused to GFP, this sequence (LVIAMDQLNL) was sufficient to deplete GFP from the nucleus throughout the cell cycle (Fig. 1D and Fig. S1B). Replacement of last two leucine residues with alanine (LVIAMDQANA) restored the ubiquitous localization of GFP to both nucleus and cytoplasm (Fig. 1D). Thus, we concluded that Mia1p contains a Crm1p-dependent NES and shuttles between the nucleus and cytoplasm, even during interphase.

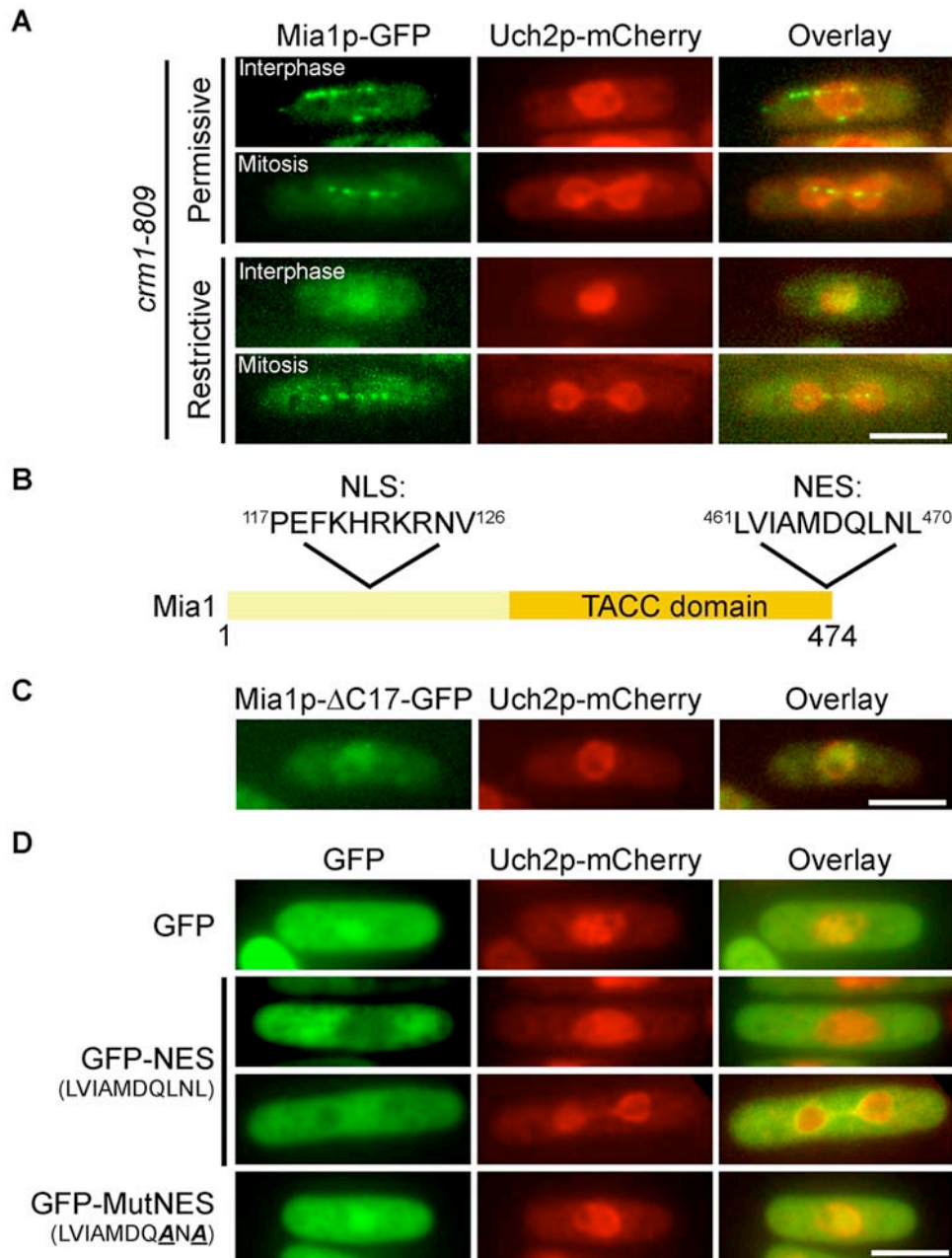


Figure 1. Mia1p is exported from the nucleus via a Crm1p-dependent NES. (A) Mia1p-GFP localized to mitotic spindles and interphase microtubules in *crm1-809* Uch2p-mCherry expressing cells at 36°C but only to the nucleus at 18°C. **(B)** Positions of predicted NLS and NES on Mia1p. **(C)** Mia1p-ΔC17-GFP is enriched in the nucleus in interphase cells. **(D)** GFP-NES but not MutNES is excluded from the nucleus. Shown are single maximum intensity reconstructions of live cells. Scale bars = 5 μm. doi:10.1371/journal.pone.0006255.g001

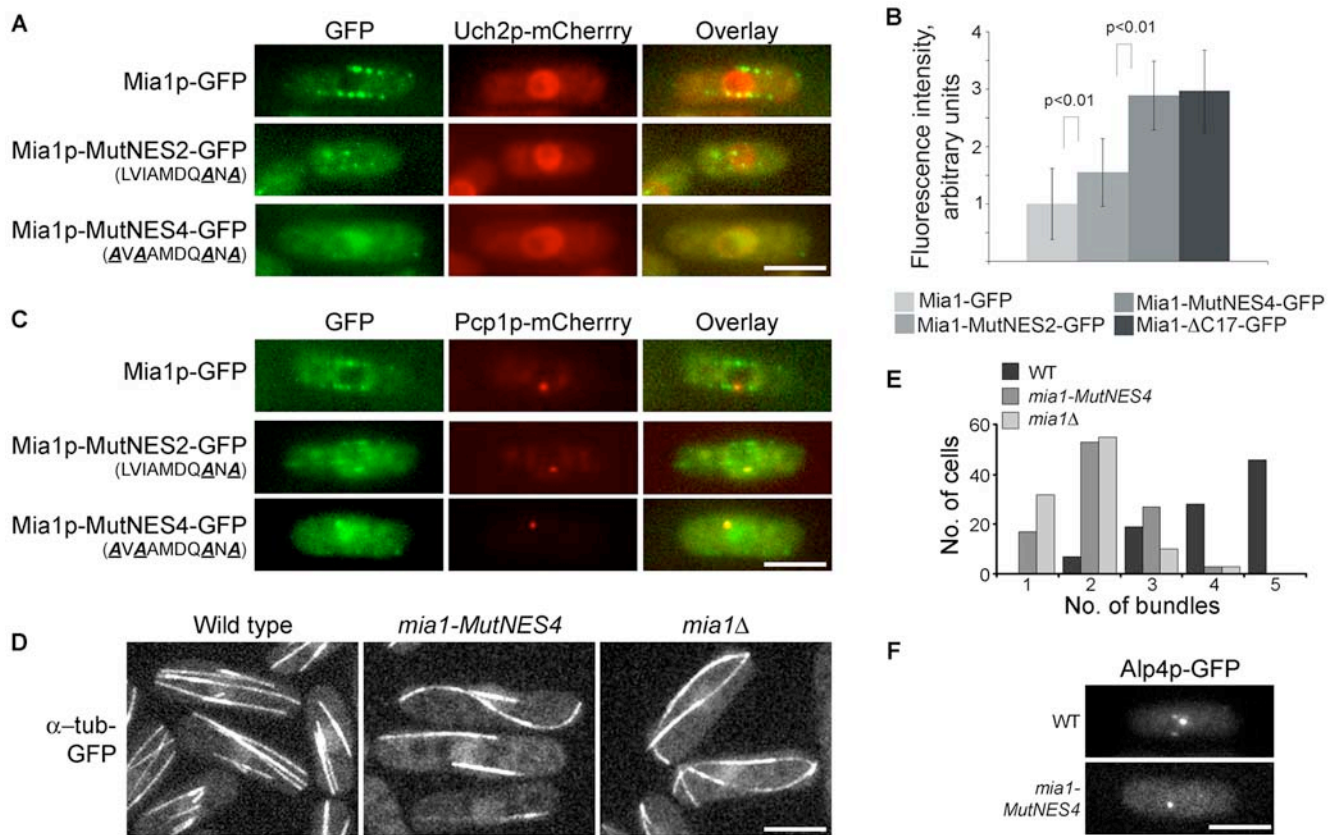


Figure 2. Nuclear retention of Mia1p leads to abnormal organization of interphase microtubule arrays. (A) Localization of Mia1p-GFP in interphase cells, with Uch2p-mCherry as an NE marker. (B) Relative intensities of nuclear Mia1p-GFP fluorescence in interphase cells of various *mia1* mutant backgrounds (n = 100 cells). (C) Localization of Mia1p-GFP in interphase cells, with Pcp1p-mCherry as an SPB marker. (D) *mia1-MutNES4* cells expressing α -tubulin-GFP exhibited fewer interphase microtubule bundles, similar to *mia1Δ* cells. (E) Quantification of the number of interphase microtubule bundles in wild type, *mia1-MutNES4* and *mia1Δ* cells (n = 100 cells). (F) Alp4p-GFP is detected as several distinct dots in wild type but not in *mia1-MutNES4* cells treated with MBC. Shown are single maximum intensity reconstructions of live cells. Scale bars = 5 μ m. doi:10.1371/journal.pone.0006255.g002

Nuclear retention of Mia1p during interphase leads to pronounced defects in assembly of cytoplasmic microtubule arrays

To specifically disrupt NES function we introduced LVIAMDQANA and AVAAMDQANA (denoted Mia1p-MutNES2 and Mia1p-MutNES4, respectively) mutations to the *mia1* open reading frame at its chromosomal locus. Uch2p-mCherry and Pcp1p-mCherry were used as NE and SPB markers. We observed a relative equilibration of Mia1p-MutNES2-GFP fluorescence between the nucleus and cytoplasm of interphase cells and reduced localization of the mutant protein to the linear microtubule arrays. On the other hand, Mia1p-MutNES4-GFP constitutively accumulated in the nucleus and was completely excluded from interphase microtubule arrays (Fig. 2A, B and C), similar to Mia1p-ΔC17-GFP. We concluded that Leu/Ile residues 461, 463, 468 and 470 contributed to NES function *in vivo* and therefore chose the Mia1p-MutNES4 mutant for further characterization.

We then evaluated the functional consequences of Mia1p retention in the nucleus during interphase. First, we expressed α -tubulin-GFP in cells containing untagged Mia1p-MutNES4 mutant protein as the sole source of Mia1p. We observed striking abnormalities in the organization of interphase microtubule arrays (Fig. 2D). Interphase Mia1p-MutNES4 cells contained fewer microtubule bundles and microtubules often curved around cell tips, similar to *mia1Δ* cells (Fig. 2E, Movie S1, compare to the wild type, Movie S2). Upon

addition of the microtubule-depolymerizing drug MBC, interphase microtubule bundles depolymerize to short stubs, usually attached to the NE. These sites are also enriched in the γ -tubulin complex proteins, such as Alp4p and Mto1p [9]. Similar to the *mia1Δ* phenotype, Alp4p-GFP did not exhibit multiple dots around the NE and instead localized only to the SPB in Mia1p-MutNES4 cells (Fig. 2F), indicating that microtubule bundles are not properly organized at the NE. These results suggest a lack of Mia1p function in the cytoplasm and emphasize the necessity for the active nuclear export of Mia1p at the end of mitosis to ensure remodeling of microtubule arrays as cells proceed into the new cell cycle.

Mia1p NES mutation confers abnormalities on mitotic spindle organization

To our surprise, we noticed an increased proportion of mitotic cells in the Mia1p-MutNES4 strain, as well as many instances of mitotic spindle abnormalities including monopolar and broken spindles (Fig. 3A and B). Again, this phenotype was similar to that of *mia1Δ* cells [10]. An abnormally large fraction of Mia1p-MutNES4 cells (~10%) showed the spindle assembly checkpoint (SAC) protein Mad2p present at kinetochores, indicative of faulty microtubule/kinetochore interaction and metaphase delay (Fig. 3C). To compare, Mad2p-GFP was found on kinetochores of ~12% *mia1Δ* cells (Fig. 3C). Disabling of the SAC through deletion of *mad2* was lethal in an *mia1Δ* genetic background

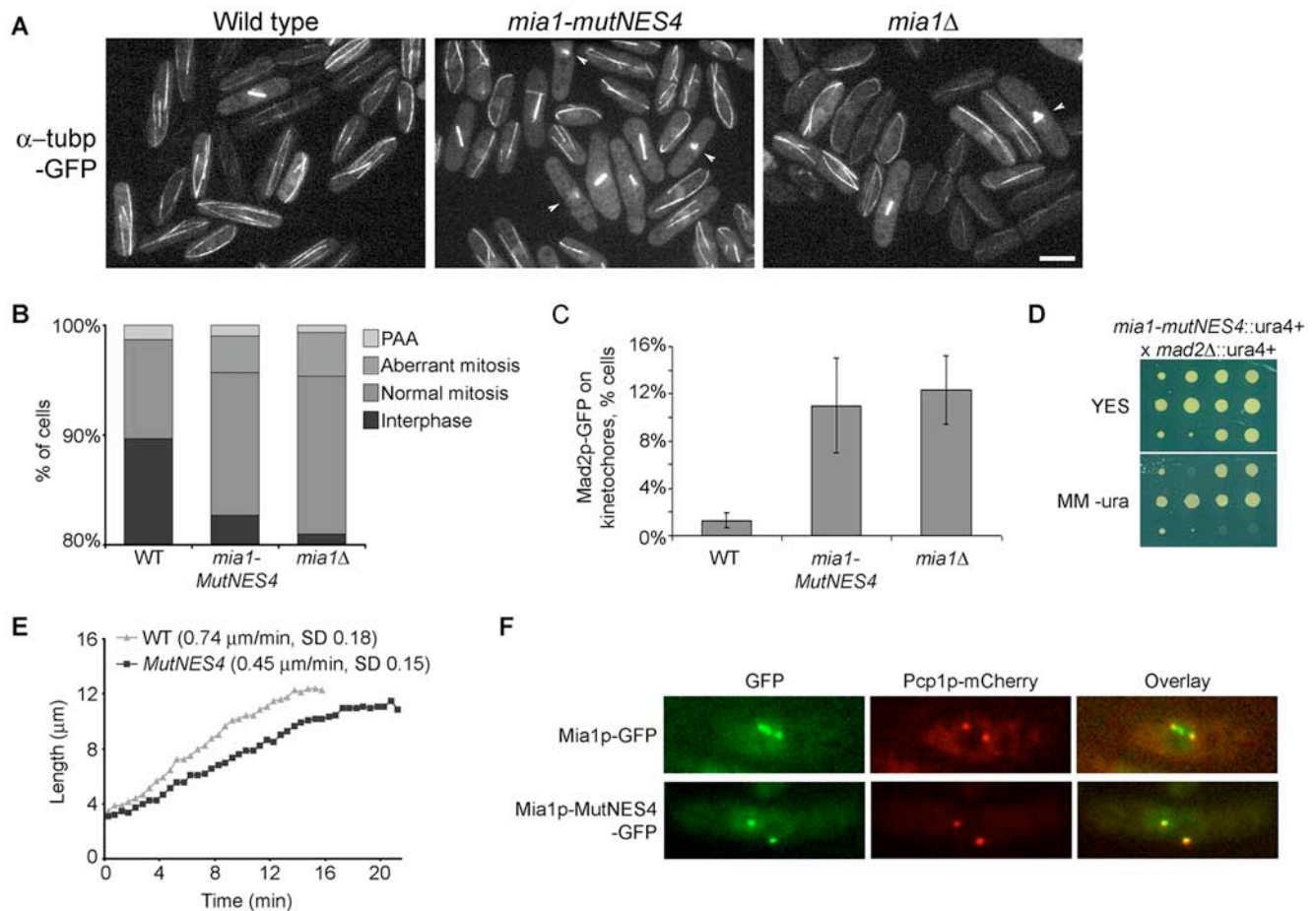


Figure 3. Mutation in the Mia1p NES triggers mitotic spindle abnormalities. (A) *mia1-MutNES4* cells exhibit frequent spindle abnormalities such as monopolar and broken spindles. Shown are representative fields of wild type, *mia1-MutNES4* and *mia1Δ* cells expressing α -tubulin-GFP. Abnormal spindles are indicated by white arrowheads. (B) Percentages of aberrant mitoses in asynchronous cell populations ($n = 300$ cells). PAA, Post-anaphase microtubule arrays. (C) Percentages of cells exhibiting Mad2p-GFP at kinetochores ($n = 300$ cells). (D) *mia1-MutNES4 mad2Δ* cells are severely compromised for growth. Shown are three sets of segregants (from top to bottom: tetratype, parental ditype and non-parental ditype) from tetrads obtained from a cross between *mia1-MutNES4* and *mad2Δ* cells, grown on YES agar (upper panel) and later replicated onto minimal medium lacking uracil (lower panel). Both the *mia1+* and *mad2+* genes were mutated using *ura4+* gene. Note the smaller colony size in double mutants. (E) *mia1-MutNES4* cells exhibit a decreased anaphase elongation rate. (F) Unlike Mia1p-GFP, Mia1p-MutNES4-GFP does not localize to kinetochores during mitosis. Pcp1p-mCherry was used as an SPB marker. Scale bars = 5 μ m. doi:10.1371/journal.pone.0006255.g003

whereas cells carrying both *mad2Δ* and *mia1-mutNES4* mutations were severely compromised for growth (Fig. 3D). Thus, it appears that the SAC functions to correct mitotic abnormalities in an *mia1-mutNES4* background and suggests that a complete absence of Mia1p has more severe functional consequences than an NES mutation. Furthermore, we observed spindle breakage events (Movies S3 and S4) and a decreased anaphase spindle elongation rate as compared to wild type (Fig. 3E).

In mitotic cells, Mia1p normally localizes to the SPBs, kinetochores and along the spindle [10]. Interestingly, while Mia1p-MutNES4-GFP obviously localized to the nucleus during mitosis, it was largely depleted from the kinetochores and instead was restricted to the SPBs (Fig. 3F). Thus, it appears that mutations in the NES compromise localization of Mia1p to kinetochores in mitosis.

Mutations to the NES compromise Mia1p interaction with Alp14p/TOG

Mitotic abnormalities in *mia1Δ* cells are caused largely by the inability of Alp14p to load onto the spindle [6]. In turn, Alp14p

loads Mia1p on kinetochores [10]. We therefore wondered whether Alp14p localization was disrupted in *mia1-mutNES4* cells. We found that Alp14p-GFP was indeed depleted from microtubules in *mia1-mutNES4* cells, not only in the interphase but also during mitosis (Fig. 4A). Instead, Alp14p-GFP exhibited a diffuse cytosolic localization at all stages of the cell cycle, similar to *mia1Δ* cells (Fig. 4A). We verified that Alp14p co-localized with Mia1p but not with Mia1p carrying a mutated NES, by co-expressing Alp14p-TagRFP with either Mia1p-GFP or Mia1p-MutNES4-GFP fusion proteins (Fig. 4B).

Since the C-terminal half of Mia1p has been shown to interact with Alp14p [10], we wondered whether Mia1p NES mutation interfered with Alp14p binding. We investigated this question in the following ways. First, to check for direct protein-protein interaction we assayed whether recombinant MBP-tagged Mia1p or its NES mutant version expressed in bacteria could pull down Alp14p-myc from cellular extracts that were prepared from *mia1Δ* cells to avoid carrying over wild type Mia1p. MBP-Mia1p-MutNES4 could interact with Alp14p, albeit with a diminished efficiency as compared to the wild type Mia1p (Fig. 4C, 0.26:1

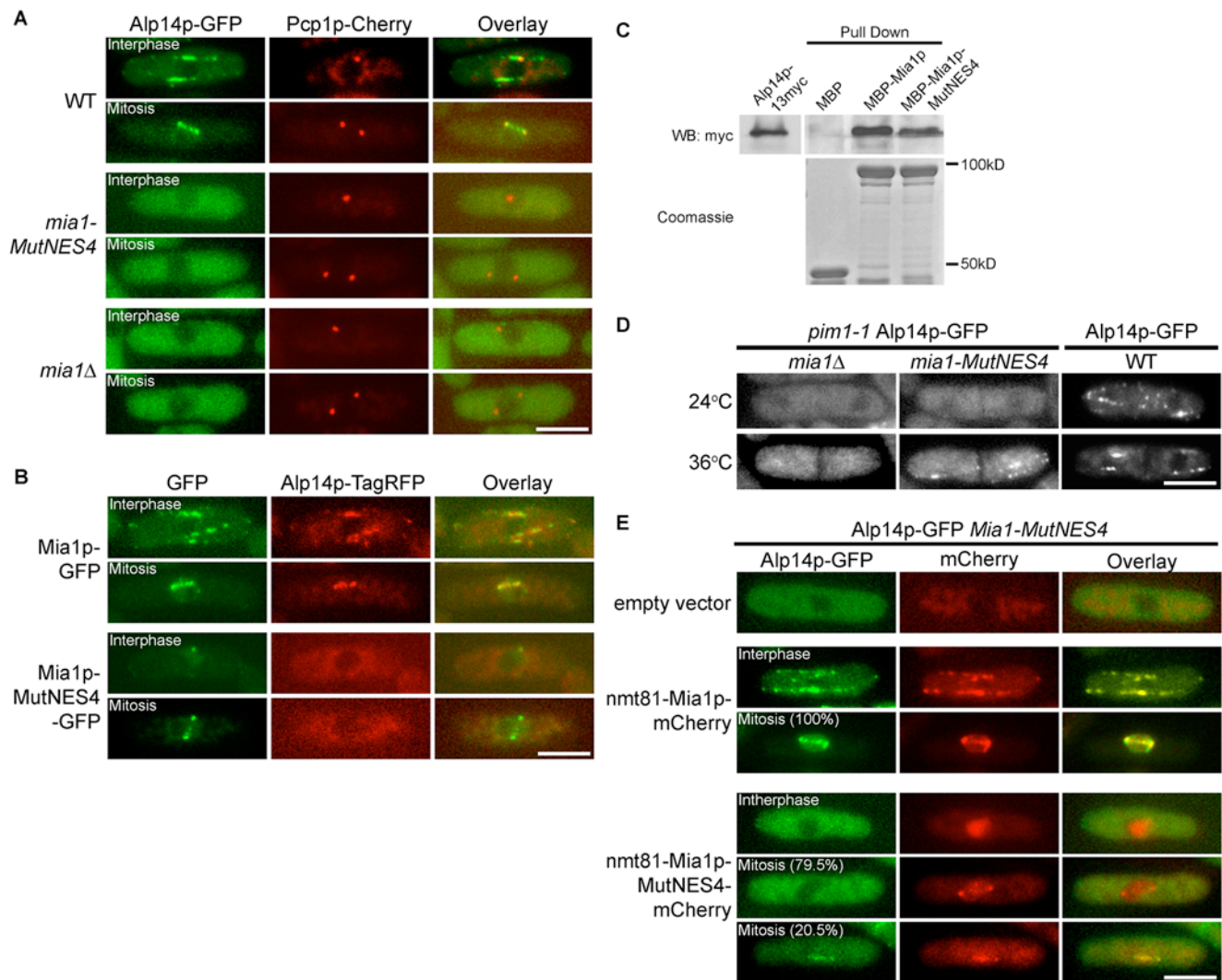


Figure 4. Interaction between Mia1p and Alp14p is affected by mutating the Mia1p NES. (A) Alp14p-GFP does not localize to microtubules in *mia1-MutNES4* and *mia1Δ* cells. Shown are single maximum intensity reconstructions of live cells expressing Alp14p-GFP and Pcp1p-mCherry. (B) Mia1p-GFP and Alp14p-TagRFP are spatially separated in *mia1-MutNES4* cells. (C) MBP-Mia1p-MutNES4 showed weaker interaction with Alp14p-myc in pull-down assays, as compared to MBP-Mia1p. Alp14p-myc yeast lysates were extracted from *mia1Δ* cells and detected with anti-myc antibody. MBP-tagged proteins were detected by Coomassie staining. (D) When released from the nucleus using *pim1-1* mutation at 36°C, Mia1p-MutNES4 is capable of loading Alp14p-GFP on cytoplasmic microtubules. Localization of Alp14p-GFP in wild type septated cells at 24°C and 36°C is included as a control. Shown are single maximum intensity reconstructions of live cells. (E) Overexpression of Mia1p-MutNES4-mCherry partially restores nuclear accumulation and spindle localization of Alp14p-GFP during mitosis. Shown are single maximum intensity reconstructions of live cells. Scale bars = 5 μm.

doi:10.1371/journal.pone.0006255.g004

ratio of Alp14p-myc pulled down by MBP-Mia1p-MutNES4 and MBP-Mia1p respectively). A similar result was obtained when the Alp14p-myc containing cellular extract was prepared from wild type cells (data not shown).

Secondly, to check whether Mia1p-MutNES4 mutant protein could, in principle, interact with Alp14p *in vivo*, we introduced a *pim1-1* temperature-sensitive mutation that abolishes function of the RanGEF, Pim1p, at 36°C [11] into *mia1-mutNES4*, *mia1Δ* and wild type cells expressing Alp14p-GFP. *pim1-1* cells at the restrictive temperature fragment the NE during mitosis but are capable of chromosome segregation: the terminal arrest phenotype presents as septated cells with hyper-condensed chromosomes directly surrounded by cytoplasm. We reasoned that if Mia1p-MutNES4p and Alp14p were capable of interaction, release of Mia1p-MutNES4 from the nucleus would drive recruitment of

Alp14p to microtubules. Indeed, we observed recruitment of Alp14p-GFP to microtubules in *pim1-1 mia1-mutNES4* (93% cells, $n = 72$) but not in *pim1-1 mia1Δ* cells (0% cells, $n = 72$) shifted to 36°C (Fig. 4D), suggesting that while binding between Alp14p and Mia1p-MutNES4 was diminished (Fig. 4C) these proteins could interact when present in the same cellular compartment.

Third, we wondered whether overexpression of Mia1p-MutNES protein that partially retains Alp14p-binding activity could re-establish Alp14p nuclear accumulation during mitosis. For this purpose we expressed either mCherry-tagged Mia1p or Mia1p-MutNES4 under the control of *nmt81* promoter in *mia1-mutNES4 alp14-GFP* cells. As expected, ectopic overexpression of wild type Mia1p in this genetic background efficiently restored nuclear localization of Alp14p in mitotic cells (100%, $n = 44$). It also led to robust loading of Alp14p on interphase microtubules.

Mia1p-mCherry now co-localized with Alp14p throughout the cell cycle (Fig. 4E). When overexpressed, Mia1p-MutNES4-mCherry accumulated in the nucleus at all stages of cell cycle, mimicking localization of this protein expressed under its native promoter (Fig. 4E). Importantly, overexpression of Mia1p-MutNES4-mCherry was able to drive Alp14p to the nucleus in mitosis, albeit with decreased efficiency as compared to the wild type (Fig. 4E, ~20%, n = 44). The lower penetrance is consistent with decreased affinity between the two proteins. We concluded that extra copies of Mia1p-MutNES4 protein could partially alleviate the need for tight Alp14p binding to ensure nuclear localization of Alp14p during mitosis. Thus, mutating the Mia1p NES decreases interaction between Mia1p and Alp14p, indicating that the Alp14p binding site might overlap with the NES.

Artificial accumulation of Alp14p in the nucleus partially rescues mitotic defects caused by mutation of the Mia1p NES

To determine whether mitotic defects in *mia1-mutNES4* cells were indeed due to spatial separation between Alp14p and Mia1p, we attempted to drive Alp14p into the nucleus independently of Mia1p. To this end, we introduced the SV40 T-antigen derived NLS (PKKKRKV) in GFP- or TagRFP-tagged Alp14p and expressed these fusion proteins from the *alp14* chromosomal locus. Although Alp14p-NLS-TagRFP was still found on cytoplasmic microtubules in wild type cells, presence of the exogenous NLS was sufficient to partially accumulate the fusion protein in interphase nuclei (Fig. 5A, upper panel). This in turn appeared to elevate nuclear levels of Mia1p (Fig. 5A, upper panel, compare to control cells in Fig. 4B, upper panel). On the other hand, when the nucleocytoplasmic transport of Mia1p was disabled by NES4 mutation, both Alp14p-NLS-TagRFP and Mia1p-MutNES4-GFP strongly accumulated in the nuclei and were completely depleted from cytoplasmic microtubule arrays (Fig. 5A, lower panel). These data further support the hypothesis that it is the Mia1p NES that is required for the nucleocytoplasmic shuttling of Mia1p and Alp14p.

We then assessed whether nuclear Alp14p could restore Mia1p-MutNES4 localization to the kinetochores in mitosis. Mia1p-MutNES4-GFP was depleted from kinetochores in most cells expressing wild type Alp14p-TagRFP (Fig. 5B, upper panel, and 5C). Alp14p-NLS-TagRFP did not interfere with kinetochore localization of the wild type Mia1p, suggesting that the Alp14p-NLS fusion protein was functional (Fig. 5B, lower panel). Interestingly, presence of Alp14p in the nucleus was sufficient to partially restore recruitment of Mia1p-MutNES4-GFP to the kinetochores (Fig. 5B, middle panel and 5C). Consistently, Alp14p-NLS-TagRFP efficiently localized to the SPBs, along the spindle, and to the kinetochores in wild type cells but only weakly in *mia1-MutNES4* cells (Fig. 5B, middle panel). Partial rescue of Mia1p-MutNES4 localization during mitosis by Alp14p-NLS, together with weak spindle loading of Alp14p-NLS by Mia1p-MutNES4, could indicate that the Mia1p NES mutation does affect Mia1p-Alp14p binding. However, it appears that the residual interaction allows for partial restoration of Mia1p spindle localization.

Next we explored whether nuclear Alp14p could also rescue the spindle defects in *mia1-MutNES4* cells. Indeed, we observed a pronounced diminishing of aberrant mitoses in an *alp14-GFP-NLS mia1-MutNES4* genetic background as compared to *alp14-GFP mia1-MutNES4* cells (Fig. 5D and 5E). As expected, *alp14-GFP-NLS mia1Δ* cells exhibited strong spindle defects, confirming that the rescue by nuclear Alp14p depends on Mia1p function (Fig. 5D and 5E).

Collectively, our results suggest that the mitotic abnormalities caused by Mia1p NES mutation are, in part, due to defective

nucleocytoplasmic shuttling of its partner protein, Alp14p. At steady state, lack of a functional NES in Mia1p sequence likely leads to spatial separation between Mia1p and Alp14p.

Discussion

Microtubule regulators such as the TACC/TOG complex Mia1p/Alp14p [9,10], EB1 protein Mal3p [12], CLASP protein Cls1p [13,14], MAP65 protein Ase1p [15,16] and others function in sustaining dynamics of both the mitotic spindle and cytoplasmic arrays. Therefore, cells have to localize microtubule regulators either to the nucleus or to the cytoplasm, depending on the cell cycle stage. While nuclear localization of large proteins and protein complexes requires specialized NLSs, at least two possibilities may account for the redistribution of MAPs once mitosis is complete. One could involve destruction of the nuclear pool of such protein and its *de novo* synthesis in the cytoplasm. This mechanism could be particularly important for timing spindle disassembly to mitotic exit, as in the case of the budding yeast Ase1p [17]. A delay in spindle disassembly could lead to the shortage of tubulin and MAPs available for cytoplasmic array assembly in organisms with complex cytoplasmic microtubule structures, such as *S. pombe*. Alternatively, the proteins could be actively exported, by Crm1p exportin or other specialized karyopherins. Here we report that a deficiency in Mia1p/TACC nuclear export results in its steady state nuclear accumulation. Consequently, depletion of Mia1p in the cytoplasm leads to manifestation of the *mia1Δ*-like interphase phenotype of abnormal microtubule bundles and often to bent cell shape. Our results underscore the importance of nuclear export of Mia1p/TACC and possibly other MAPs in remodeling microtubule arrays as cells return to growth.

Mia1p carries an NLS [6] and a strong “transferable” Crm1p-dependent NES motif L-X₃-L/I/F/M-X₂-L-X-L. During interphase, a combination of both signals results in a constitutive nucleocytoplasmic shuttling with the bulk of Mia1p located in the cytoplasm at steady state. The balance shifts dramatically during mitosis resulting in strong nuclear enrichment. What could be the mechanism for such regulation? The Mia1p NLS confers only a partial nuclear enrichment when fused to GFP and the nuclear-to-cytoplasmic ratio of GFP-NLS fluorescence intensity does not appear to increase during mitosis (data not shown). NLS activity *in vivo* might therefore depend on the sequence and possibly conformational context. Alternatively, NLS activity might not be subject to regulation and instead, cells could regulate the nuclear export of the protein. In this manner the relative strength of NLS and NES would determine the subcellular distribution of Mia1p. As NES-GFP does not equilibrate between the nucleus and cytoplasm during mitosis, indicating that Crm1p continues to function in nuclear export, we propose that it is the Mia1p NES activity that could be masked, intra- or intermolecularly, by cell cycle dependent post-translational modifications (PTMs) or, possibly, through interactions of the TACC/TOG complex with other proteins. Interestingly, mutating the Mia1p NES caused a reduction in Mia1p binding to Alp14p (Fig. 4 and 5). This could indicate that the NES partially overlaps with the Alp14p binding site. An intriguing possibility could be that under some circumstances (*e.g.* due to mitosis-specific PTMs) Crm1p and Alp14p compete for binding to Mia1p.

The subcellular distribution and possibly microtubule-organizing activity of other TACC proteins could be regulated in a similar manner. Human TACCs partially localize in interphase nuclei [18] suggesting that they could shuttle between the nucleus and cytoplasm. And while animal cells fragment the NE during mitosis

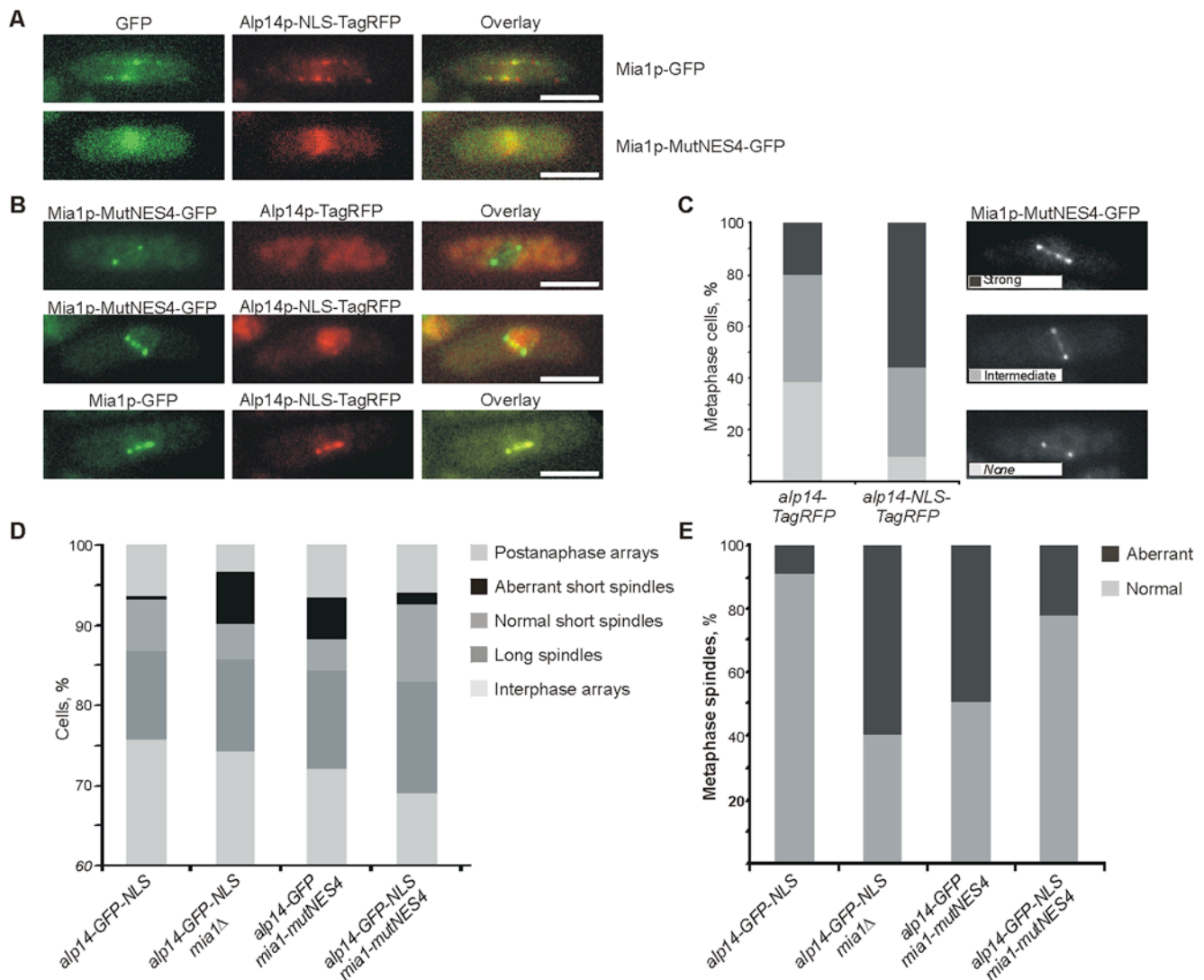


Figure 5. Artificial accumulation of Alp14p in the nucleus partially rescues the mitotic defects observed in Mia1p NES mutant cells. (A) Alp14p-NLS-TagRFP localizes to the nucleus during interphase, partially in *mia1-GFP*, and fully in *mia1-MutNES4-GFP* cells. Shown are single maximum intensity reconstructions of live cells. Scale bars = 5 μ m. (B) Nuclear Alp14p-NLS-TagRFP partially restores localization of Mia1p-MutNES4-GFP to kinetochores during mitosis. Shown are single maximum intensity reconstructions of live cells. Scale bars = 5 μ m. (C) Percentages of cells with various levels of Mia1p-MutNES4-GFP at kinetochores (n = 100 metaphase cells). Cells were binned into three classes based on intensity of GFP signal at kinetochores (strong, intermediate, none). Representative images are shown in the legend. (D) Percentages of aberrant mitoses and other cell cycle stages in asynchronous cell populations (n = 300 cells). Microtubules were immunostained with anti- α -tubulin antibody TAT-1. (E) Percentages of monopolar and broken short spindles (n = 100 spindles). Microtubules were immunostained with anti- α -tubulin antibody TAT-1. doi:10.1371/journal.pone.0006255.g005

it is the TACC activity that could be regulated by interaction with karyopherins [19]. In conclusion, we propose that exquisite regulation of the subcellular distribution of TACC/TOG complexes drives microtubule array remodeling as cells progress through the cell cycle.

Materials and Methods

Schizosaccharomyces pombe strains and constructs

S. pombe strains used in this study and their genotypes are listed in Table S1. We used standard genetic methods and *S. pombe* media for vegetative growth (EMM and YES). Genetic crosses and sporulation were performed on YPD agar plates. NES (LVIAMDQNLN) and MutNES (LVIAMDQANA) sequences were incorporated into the reverse (NES and MutNES) primers

for generating the plasmids pREP81-GFP-NES and pREP81-GFP-MutNES. The expression of these GFP constructs was induced upon thiamine removal from the culture medium. Mia1-MutNES2 or Mia1-MutNES4 were generated using PCR-based targeted-mutagenesis, and were integrated into the original chromosome end of *mia1* for expression under its endogenous promoter. Cold sensitive *cm1-809* strain was a kind gift from Dr. Simon Whitehall.

Fluorescence microscopy and image analysis

Epifluorescence images were collected using a mercury lamp as illumination source with appropriate sets of filters on a Zeiss Axiovert 200 M microscope equipped with a CoolSnap camera (Photometrics) and Uniblitz shutter driver (Photronics, Rochester, NY, USA) under the control of Metamorph software package

(Universal Imaging, Sunnyvale, CA, USA). Presented are the z-stack maximum projection images obtained using Metamorph build-in module.

Sum Z-projection images of z-stacks of 6 sections were used to determine nuclear and cytosolic fluorescence levels. First, the compartments were manually outlined and average fluorescence intensities were determined using in-built functions of ImageJ software (NIH, USA). Next, background signal obtained from non-fluorescent wild type cells for either compartment was subtracted. Statistical analysis was performed in Excel (Microsoft, USA).

Time-lapse fluorescence microscope images were generated on a Zeiss Axiovert 200 M microscope equipped with UltraView RS-3 confocal system: CSU21 confocal optical scanner, 12 bit digital cooled Hamamatsu Orca-ER camera (OPELCO, Sterling, VA, USA) and krypton-argon triple line laser illumination source under the control of Metamorph software package. Typically, we acquired a z-stack of 7 sections, through whole cells, spaced at 0.6 μm , every 30 or 15 seconds. Imaging was performed on *S. pombe* placed in sealed growth chambers containing 2% agarose YES media. Images were processed with Adobe Photoshop 7.0.

Immunofluorescence techniques

Cells were fixed with cold methanol for 8 min and then spheroplasted using lysing enzymes in 1.2 M sorbitol in PBS. Spheroplasts were washed with PBS. PBAL buffer (1 mM sodium azide, 1% BSA, 100 mM Lysin-hydrochloride, 50 $\mu\text{g}/\text{ml}$ Carbenicilin in PBS) was used for blocking and for incubation with anti- α -tubulin primary and secondary antibodies. Imaging was done on a Zeiss Axiovert 200 M microscope with appropriate sets of filters, and images were generated using a CoolSnap camera (Photometrics) and Metamorph software package (Universal Imaging, Sunnyvale, CA).

Protein Expression and pull-down experiments

All reagents were obtained from Sigma unless otherwise stated. ORFs of full length Mia1 (1–474aa) and Mia1-MutNES4 were cloned into pAD2a vector (a kind gift from Andrej Didovik) that contains a maltose binding protein (MBP) gene upstream of the multiple cloning site. The plasmids were transformed into BL21 (DE3) competent cells carrying the pG-KJE8 chaperone plasmid. Overnight bacteria cultures were diluted in fresh medium, and the chaperone plasmid was induced with 0.5 mg/ml L-arabinose and 5 ng/ml tetracycline. Bacteria were grown at 37°C for 2 hours to reach log phase. Expressions of MBP or MBP-fusion proteins were induced by adding 0.5 mM IPTG and incubating at 24°C for another 3 hours. The bacteria were harvested by centrifugation, and the pellets were stored at -80°C or used immediately. The bacteria pellets were resuspended in ice-cold Buffer A (20 mM Tris-HCl pH 7.4, 400 mM NaCl, 1 mM EDTA, 10 mM β -mercaptoethanol) with freshly added protease inhibitors (1.3 mM Benzamidine, 1 mM PMSF, and protease inhibitor cocktail tablet, Roche Applied Science), and disrupted by sonication. Cellular debris was removed by centrifugation (16,000 x g, 10 min). The supernatant was applied to amylose resin (New England Biolabs) pre-equilibrated with buffer A and incubated for 1 h at 4°C. The amylose resin was washed three times in buffer A. For total yeast cell lysate, Alp14p-13myc expressing *mia1 Δ* cells were grown to log phase, harvested and washed once with Buffer A. Cell pellet were

homogenized with glass beads (425–600 μm) using Mini Bead Beater (Biospec) at 4°C. Cell lysates were harvested and centrifuged (16,000 x g, 10 mins) to remove cell debris and insoluble protein. Soluble proteins were incubated with washed amylose resins from above for 1 hour at 4°C before being washed 3 times with Buffer A and resuspended in SDS-loading buffer.

Supporting Information

Figure S1 (A) Mia1p-GFP and Alp14p-TagRFP are retained in the nucleus of interphase *crm1-809* cell at the restrictive temperature of 18°C. (B) NES derived from *mia1* ORF (LVIAMDQLNL) drives exclusion of GFP from the nucleus. Pcp1p-mCherry is used as the SPB marker. Scale bars = 5 μm . Found at: doi:10.1371/journal.pone.0006255.s001 (0.84 MB TIF)

Table S1 Fission yeast strains used in this study Found at: doi:10.1371/journal.pone.0006255.s002 (0.07 MB DOC)

Movie S1 Interphase *mia1-MutNES4* cells expressing Atb2p-GFP. Presented are the maximum intensity projections of 7 planes at 0.6 μm spacing, with time-lapse imaging performed at 30-second intervals.

Found at: doi:10.1371/journal.pone.0006255.s003 (2.49 MB MOV)

Movie S2 Interphase wild type cells expressing Atb2p-GFP. Presented are the maximum intensity projections of 7 planes at 0.6 μm spacing, with time-lapse imaging performed at 30-second intervals.

Found at: doi:10.1371/journal.pone.0006255.s004 (2.52 MB MOV)

Movie S3 Mitotic *mia1-MutNES4* cells expressing Atb2p-GFP. Presented are the maximum intensity projections of 7 planes at 0.6 μm spacing, with time-lapse imaging performed at 30-second intervals.

Found at: doi:10.1371/journal.pone.0006255.s005 (2.63 MB MOV)

Movie S4 Mitotic *mia1-MutNES4* cells expressing Atb2p-GFP. Presented are the maximum intensity projections of 7 planes at 0.6 μm spacing, with time-lapse imaging performed at 30-second intervals.

Found at: doi:10.1371/journal.pone.0006255.s006 (2.98 MB MOV)

Acknowledgments

We are grateful to M. Sato and T. Toda for discussions and to E. Makeyev, P. Rorth and R. Thadani for suggestions on the manuscript and to S. Whitehall and A. Didovik for materials and reagents. Since acceptance of this article, a study by Sato et al., where the authors reached similar conclusions, has been accepted for publication in EMBO Reports. Our work was carried out with support from the Singapore Millenium Foundation.

Author Contributions

Conceived and designed the experiments: YCL AV SO. Performed the experiments: YCL AV. Analyzed the data: YCL AV SO. Wrote the paper: AV SO.

References

- Gruss OJ, Carazo-Salas RE, Schatz CA, Guarguaglini G, Kast J, et al. (2001) Ran induces spindle assembly by reversing the inhibitory effect of importin alpha on TPX2 activity. *Cell* 104: 83–93.
- Wiese C, Wilde A, Moore MS, Adam SA, Merdes A, et al. (2001) Role of importin-beta in coupling Ran to downstream targets in microtubule assembly. *Science* 291: 653–656.

3. Nachury MV, Maresca TJ, Salmon WC, Waterman-Storer CM, Heald R, et al. (2001) Importin beta is a mitotic target of the small GTPase Ran in spindle assembly. *Cell* 104: 95–106.
4. Silje HH, Nagel S, Korner R, Nigg EA (2006) HURP is a Ran-importin beta-regulated protein that stabilizes kinetochore microtubules in the vicinity of chromosomes. *Curr Biol* 16: 731–742.
5. Koffa MD, Casanova CM, Santarella R, Kocher T, Wilm M, et al. (2006) HURP is part of a Ran-dependent complex involved in spindle formation. *Curr Biol* 16: 743–754.
6. Sato M, Toda T (2007) Alp7/TACC is a crucial target in Ran-GTPase-dependent spindle formation in fission yeast. *Nature* 447: 334–337.
7. Puntervoll P, Linding R, Gemund C, Chabanis-Davidson S, Mattingsdal M, et al. (2003) ELM server: A new resource for investigating short functional sites in modular eukaryotic proteins. *Nucleic Acids Research* 31: 3625–3630.
8. Adachi Y, Yanagida M (1989) Higher order chromosome structure is affected by cold-sensitive mutations in a *Schizosaccharomyces pombe* gene *crml+* which encodes a 115-kD protein preferentially localized in the nucleus and its periphery. *The Journal of Cell Biology* 108: 1195–1207.
9. Zheng L, Schwartz C, Wee L, Olfiferenko S (2006) The fission yeast transforming acidic coiled coil-related protein Mia1p/Alp7p is required for formation and maintenance of persistent microtubule-organizing centers at the nuclear envelope. *Molecular Biology of the Cell* 17: 2212–2222.
10. Sato M, Vardy L, Angel Garcia M, Koonruga N, Toda T (2004) Interdependency of fission yeast Alp14/TOG and coiled coil protein Alp7 in microtubule localization and bipolar spindle formation. *Molecular Biology of the Cell* 15: 1609–1622.
11. Sazer S, Nurse P (1994) A fission yeast RCC1-related protein is required for the mitosis to interphase transition. *The EMBO journal* 13: 606–615.
12. Beinhauer JD, Hagan IM, Hegemann JH, Fleig U (1997) Mal3, the fission yeast homologue of the human APC-interacting protein EB-1 is required for microtubule integrity and the maintenance of cell form. *The Journal of Cell Biology* 139: 717–728.
13. Bratman SV, Chang F (2007) Stabilization of overlapping microtubules by fission yeast CLASP. *Developmental Cell* 13: 812–827.
14. Grallert A, Beuter C, Craven RA, Bagley S, Wilks D, et al. (2006) *S. pombe* CLASP needs dynein, not EB1 or CLIP170, to induce microtubule instability and slows polymerization rates at cell tips in a dynein-dependent manner. *Genes & Development* 20: 2421–2436.
15. Loiodice I, Staub J, Setty TG, Nguyen NP, Paoletti A, et al. (2005) Ase1p organizes antiparallel microtubule arrays during interphase and mitosis in fission yeast. *Molecular Biology of the Cell* 16: 1756–1768.
16. Yamashita A, Sato M, Fujita A, Yamamoto M, Toda T (2005) The roles of fission yeast *ase1* in mitotic cell division, meiotic nuclear oscillation, and cytokinesis checkpoint signaling. *Molecular Biology of the Cell* 16: 1378–1395.
17. Juang YL, Huang J, Peters JM, McLaughlin ME, Tai CY, et al. (1997) APC-mediated proteolysis of Ase1 and the morphogenesis of the mitotic spindle. *Science* 275: 1311–1314.
18. Gergely F, Karlsson C, Still I, Cowell J, Kilmartin J, et al. (2000) The TACC domain identifies a family of centrosomal proteins that can interact with microtubules. *Proceedings of the National Academy of Sciences of the United States of America* 97: 14352–14357.
19. Albee AJ, Tao W, Wiese C (2006) Phosphorylation of maskin by Aurora-A is regulated by RanGTP and importin beta. *The Journal of Biological Chemistry* 281: 38293–38301.

Plasma Membrane Tethering of the Cortical ER Necessitates Its Finely Reticulated Architecture

Dan Zhang,^{1,2,3} Aleksandar Vjestica,^{1,2,3} and Snezhana Oliferenko^{1,2,*}

¹Temasek Life Sciences Laboratory, 1 Research Link, Singapore 117604, Singapore

²Department of Biological Sciences, National University of Singapore, 14 Science Drive 4, Singapore 117543, Singapore

Summary

The cortical endoplasmic reticulum (ER) is an intricate network of tubules and cisternae tightly associated with the plasma membrane (PM) in plants, yeast, and the excitable cell types in metazoans [1–5]. How the ER is attached to the cell cortex and what necessitates its highly reticulated architecture remain largely unknown. Here, we identify the integral ER vesicle-associated membrane protein-associated proteins (VAPs), previously shown to control the composition of phosphoinositides at the ER-PM contact sites [6, 7], as major players in sustaining the ER-PM tethering in fission yeast. We show that genetic conversion of the reticulated ER structure to the cisternal morphology shields large areas of the PM, preventing the actomyosin division ring assembly at the equatorial cortex. Using a combination of VAP mutants where the cortical ER is detached from the PM and a set of artificial ER-PM tethers suppressing this phenotype, we demonstrate that the PM footprint of the cortical ER is functionally insulated from the cytosol. In cells with prominent ER-PM contacts, fine reticulation of the ER network may have emerged as a critical adaptation enabling a uniform access of peripheral protein complexes to the inner surface of the plasma membrane.

Results and Discussion

In exponentially growing *Schizosaccharomyces pombe* cells, the endoplasmic reticulum (ER) marked by the artificial luminal ER marker GFP-AHDL [8] underwent extensive remodeling at the growing cell ends but appeared consistently associated with the nongrowing lateral cell periphery (Figure 1A; see also Figure S1A and Movies S1 and S2 available online). The *S. pombe* genome encodes two proteins, Scs2 (SPBC16G5.05c) and Scs22 (SPAC17C9.12), that are homologous to the budding yeast vesicle-associated membrane protein-associated proteins (VAPs) implicated in ER inheritance [9] in addition to their function in phospholipid metabolism [6, 7]. Strikingly, the cortical ER in *S. pombe* cells lacking both VAP proteins was largely dissociated from the cell periphery and accumulated in the cytoplasm, in particular in the vicinity of cell tips (Figure 1B; Movie S3). Of the two proteins, Scs2 appeared to play a more prominent role in maintaining the ER-plasma membrane (PM) attachment (Figure S1B). The GFP-tagged Scs2 localized to the ER and was enriched at the cell sides, the area of stable ER association

with the cellular cortex (Figures 1C and S1C; for details on GFP-tagging strategy, see Experimental Procedures). Consistent with the model that the sites of growth are refractory to forming stable ER-PM contacts, Scs2-GFP was also enriched at nongrowing cell tips but depleted from growing cell tips in monopolar *tea1Δ* cells [10] (Figure S1D).

Accumulation of the detached ER membranes near the tips of *scs2Δscs22Δ* cells suggested that the ER was actively delivered toward the growth sites. Myosin V motors were previously implicated in transporting the ER elements along the actin cables in budding yeast and Purkinje neurons [11, 12]. Similarly, recruitment of the ER to the cell tips in *scs2Δscs22Δ* cells or the wild-type *S. pombe* required myosin type V-based transport (Figures S1E and S1F).

Taking these findings together, we concluded that in fission yeast, the association of the ER with the lateral cortex mostly depends on Scs2 and Scs22. Scs2 appears to play a more decisive role tethering the ER to the cortex either directly (e.g., it has been shown to bind phosphoinositides in vitro [13]) or indirectly, through its PM partners.

To explore biological implications of the cortical ER attachment, we turned to the division-site positioning model. *S. pombe* cells assemble the actomyosin rings at the cell equator and divide perpendicular to the long cell axis. At mitotic entry, the anillin-like protein Mid1 is exported from the centrally positioned nucleus and relocalizes to a narrow band of numerous “nodes” at the medial cortex. A C-terminally located amphiphatic helix plays a critical role in the cortical targeting of Mid1 during mitosis, although additional *cis*-determinants appear to facilitate the process [14]. The Mid1 nodes recruit the downstream actomyosin machinery that eventually compacts into a single ring structure [15–17]. We have previously shown that the *tryΔ* cells, in which the ER structure is converted to a cisternal morphology due to the loss of the tubulating “TRY” proteins Tts1, Rtn1, and Yop1, exhibit mispositioning of the division site due to abnormal spreading of Mid1 along the cell cortex through a poorly understood mechanism [8].

Strikingly, the severe division-site positioning defects in the *tryΔ* genetic background were largely alleviated by the loss of ER-PM tethering (Figures 2A and S2A; 57% *scs2Δscs22ΔtryΔ* cells exhibited straight medial septa as compared to 8.6% in the *tryΔ* mutants, *n* = 500 cells). Removal of Scs2 and Scs22 alone did not cause prominent cytokinesis defects, although we observed a minor fraction of cells with slightly off-center septa (Figures 2A and S2A; *n* = 500 cells). Mid1-GFP was exported in a timely manner from the nucleus and was recruited to a narrow equatorial cortical region in both *scs2Δscs22Δ* cells and *scs2Δscs22ΔtryΔ* cells (Figures 2B, 2C, and S2B).

In fact, in both *scs2Δscs22Δ* and *scs2Δscs22ΔtryΔ* cells, the Mid1-GFP nodes compacted into a single ring significantly faster than in the wild-type, suggesting that the cortical ER elements normally dampen the efficiency of this process (Figure 2C; the compaction took 16 ± 3.1 min in the wild-type, *n* = 30 cells; 9.7 ± 2.5 min in *scs2Δscs22Δ* cells, *n* = 19 cells; 10 ± 3.4 min in *scs2Δscs22ΔtryΔ* cells, *n* = 15 cells). In approximately one quarter of the cases, the Mid1-GFP nodes very rapidly compacted into unusually large clusters at the

³These authors contributed equally to this work

*Correspondence: snejana@tlil.org.sg

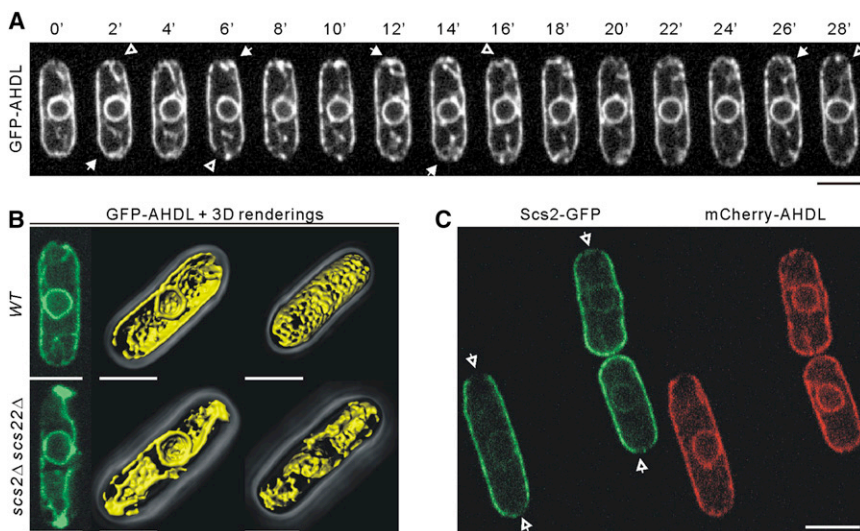


Figure 1. The VAP Proteins Scs2 and Scs22 Link the ER to the Lateral Cortex in *S. pombe*

(A) A time-lapse sequence of a wild-type (WT) cell expressing the artificial ER marker GFP-AHDL, at the central focal plane. Recruitment of the ER elements to the growing cell tips is indicated by solid arrowheads; ER detachment from the tips is denoted by outlined arrowheads. Elapsed time is shown in minutes. See also [Movie S1](#).

(B) Scanning confocal micrographs of WT and *scs2Δscs22Δ* cells expressing GFP-AHDL (left panel) and corresponding 3D-rendered views of the cell center (middle panel) and the cell cortex (right panel). See also [Movie S3](#).

(C) Scanning confocal micrographs at the central focal plane of WT cells coexpressing Scs2-GFP and mCherry-AHDL. Scs2-GFP intensity is diminished at the growing cell tips, as indicated by the outlined arrowheads.

Scale bars represent 5 μm . See also [Figure S1](#).

medial cortex before forming ring structures of irregular fluorescence intensity ([Figure S2B](#); 7 out of 27 cells). Taken together, our data suggested that the ER-PM attachment per se is not required for the division-site placement. Rather, the cortical ER could physically shield the PM, restricting recruitment of Mid1 to ER-free surfaces. Such PM obstruction might become critical in *tryΔ* cells where the large ER sheets could insulate extensive areas of the cellular cortex [8].

To test this hypothesis directly, we designed artificial ER-PM tethers, consisting of an N-terminal transmembrane ER anchor, the fluorescent mCherry protein, and a C-terminal phosphoinositide-binding motif ([Figure 3A](#); see [Experimental Procedures](#) for details). Two alternative lipid-binding motifs were tested including the cortical sorting signal (CSS) of *S. cerevisiae* Ist2 [18] and the pleckstrin homology (PH) domain from the *S. pombe* homolog of the oxysterol-binding protein Osh3 [19]. The ER anchor fused to mCherry served as a control. Expression of these constructs in wild-type cells did not cause obvious growth or polarity defects ([Figure 3A](#)). Importantly, all constructs localized to the ER membrane, and both TM-mCherry-CSS_{Ist2} and TM-mCherry-PH_{Osh3} but not the control TM-mCherry, successfully restored the ER-PM contacts in cells lacking Scs2 and Scs22 ([Figures 3B and S3](#)).

Similarly to *S. cerevisiae* [7], lack of the VAP proteins led to increased phosphatidylinositol-4-phosphate (PI4P) levels at the plasma membrane in both otherwise wild-type and *tryΔ* backgrounds ([Figure 3C](#), upper panel), whereas the levels of its bisphosphorylated derivative phosphatidylinositol-4,5-bisphosphate [PI(4,5)P₂] appeared unchanged ([Figure 3C](#), lower panel). The tether-mediated cortical recruitment of the ER did not rescue the increased PM levels of PI4P in *scs2Δscs22Δ* or *scs2Δscs22ΔtryΔ* cells ([Figure 3D](#)), suggesting that the forced ER-PM interaction could not substitute for the specific function of VAPs in phosphoinositide metabolism.

Remarkably, when we restored the ER-PM association in *scs2Δscs22ΔtryΔ* cells by expressing the artificial tethers, Mid1-GFP spread throughout the cellular cortex and failed to compact into the ring, essentially phenocopying the division-site mispositioning phenotype of *tryΔ* cells ([Figures 4A and S4A](#)). In the *scs2Δscs22ΔtryΔ* genetic background, abnormal Mid1-GFP dispersal was observed in 6 out of 8 cells

expressing TM-mCherry-CSS_{Ist2}, 8 out of 11 cells expressing TM-mCherry-PH_{Osh3}, and only 1 out of 11 cells expressing TM-mCherry. The expression of the ER-PM tethers in the wild-type or *scs2Δscs22Δ* cells did not cause Mid1 mislocalization ([Figures S4B and S4C](#)). Importantly, the timing of Mid1 compaction into a ring in *scs2Δscs22Δ* cells expressing TM-mCherry-CSS_{Ist2} or TM-mCherry-PH_{Osh3} increased to wild-type values (rings fully compacted in 16.1 ± 5.7 and 15 ± 4.4 min, respectively). We concluded that the lateral dispersion of Mid1 in *tryΔ* cells indeed occurs due to a physical blockage of the plasma membrane by the cortically attached ER sheets.

The tight (~ 33 nm on average) ER-PM coupling [20] poses a steric problem in organizing the intracellular cortex. The ER-PM contacts are devoid of ribosomes and appear unfavorable for vesicle targeting, fusion, or membrane invagination [20, 21]. In cells with pronounced cortical ER, many processes are likely restricted to the ER-free PM surfaces. The membrane contacts created by the polygonal ER mesh sustained by several tubulating proteins generate a closely spaced patchwork of plasma membrane sites accessible to the cytosol ([Figure 4B](#)). Transition of the ER to the cisternal morphology in yeast cells lacking the reticulons increases the overall area of contact between the ER and the PM [20] and results in the appearance of large irregularly spaced cortical breaks [8, 20, 22]. Our present work shows that such aberrant spatial organization of the cortex impairs the PM distribution of the cytokinesis regulator Mid1, resulting in failure to properly position the cellular division plane. In addition, occasional emergence of massive Mid1 clusters in cells deficient in ER-PM attachment suggests that the cortical ER network may promote the regular distribution of the Mid1 nodes at the equatorial cortex characteristic of wild-type cells.

The ER-PM contacts likely constrain localization of many other peripheral protein complexes throughout the cellular cortex. For instance, the cell-cycle regulator Cdr2 localized as an equatorial band of regularly spaced nodes in interphase wild-type cells ([Figure S4D](#); [23, 24]) but exhibited a pronounced clustering in cells lacking the ER-tubulating proteins. The irregular pattern of Cdr2 distribution was rescued by the further removal of VAPs ([Figure S4D](#)), suggesting that the architecture of the cortical ER network has a direct bearing

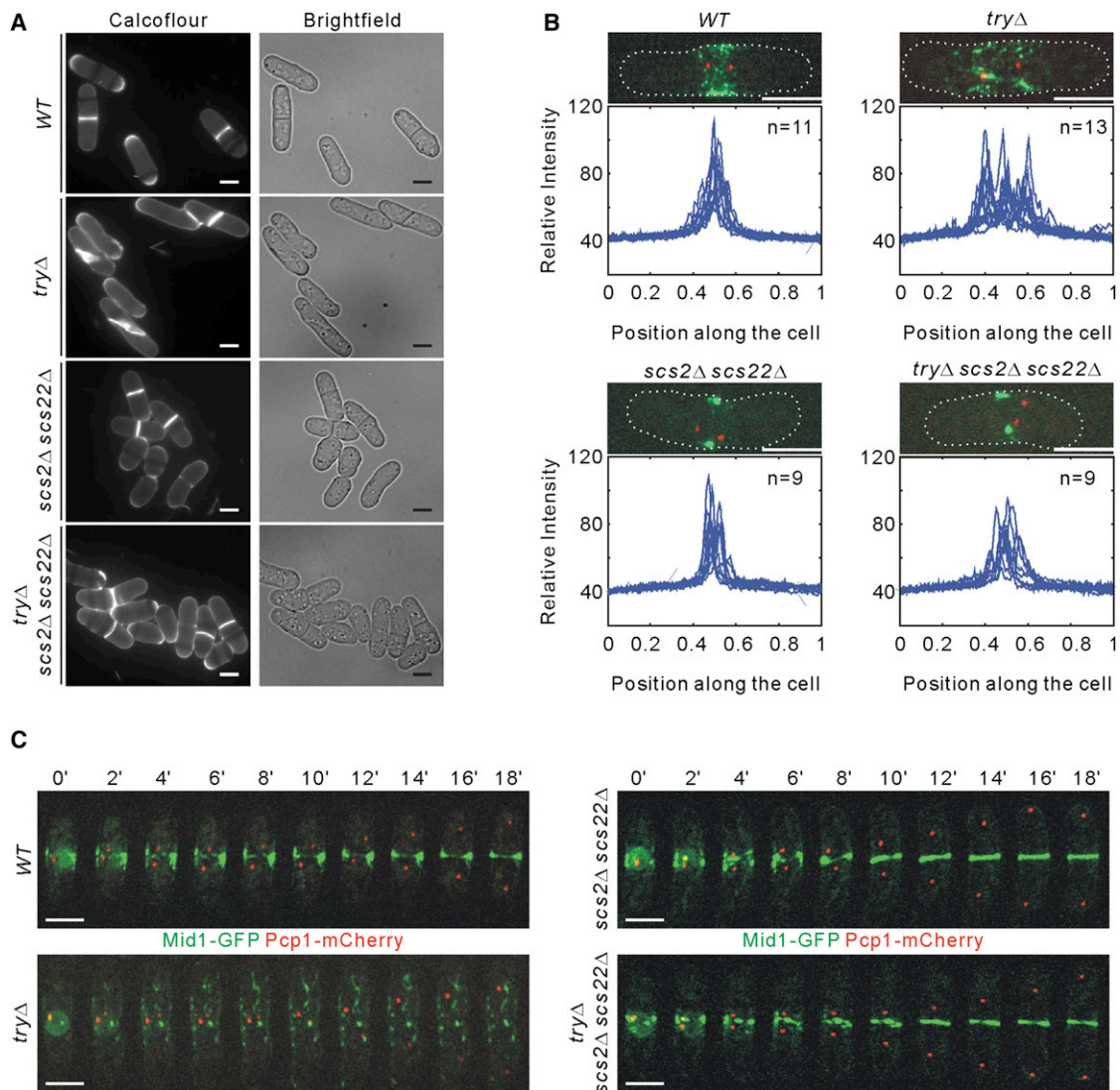


Figure 2. Mid1 Nodes Are Restricted at the Equatorial Cortex When the ER-PM Contacts Are Abolished

(A) Epifluorescence and differential interference contrast images of calcofluor-stained cells of the indicated genotypes. (B) Quantification of Mid1-GFP fluorescence distribution along the long cell axis in early mitotic cells as indicated by the spindle pole body marker Pcp1-mCherry. Maximum-projection images of z stacks obtained by scanning confocal microscopy are shown. Dotted lines indicate cell boundaries. (C) Time-lapse maximum z projection images of spinning-disk confocal stacks of cells of the indicated genetic backgrounds coexpressing Mid1-GFP (green) and Pcp1-mCherry (red). Elapsed time is shown in minutes. Scale bars represent 5 μ m. See also Figure S2.

on the spatial distribution of peripheral Cdr2 complexes within an equatorial domain.

The extensive reticulation of the peripheral ER is thought to increase the surface-to-volume ratio of this organelle to allow efficient execution of surface-dependent functions. We propose that the network organization is also required to provide sufficient access points for the cortex-associated processes and promote unobstructed communication between the cytoplasm and the plasma membrane.

Experimental Procedures

S. pombe Strains, Reagents, and Constructs

S. pombe strains used in this study and their genotypes are listed in Table S1. Growth media and genetic methods were as described in [25]. The in vivo markers for PI4P and PI(4,5)P2 were constructed as described in

[26]. Briefly, the constructs expressing the GFP-fused PH domains from *S. cerevisiae* Osh2 and Num1 under the control of a constitutive *rtn1* promoter were integrated into the *leu1* genomic locus. To construct the artificial ER-PM tethers, the transmembrane anchor consisting of the N-terminal 88 amino acids of the integral ER protein Tts1 was fused to mCherry followed by the phosphoinositide binding motifs. The PH domain was derived from the *S. pombe* Osh3 protein (SPAC23H4.01c, amino acids 150–245) and the CSS originated from the budding yeast Ist2 (amino acids 878–946) [18]. These constructs were integrated into the *leu1* genomic locus under the control of the thiamine-repressible promoter *mtt1*. Expression of these constructs was induced in minimal media lacking thiamine for 20 hr. Scs2-GFP was generated by inserting the GFP between aa 360 and 361 of Scs2 at its endogenous locus under the control of the native promoter. GFP-Scs2 was created by inserting GFP at the N terminus of Scs2 at its native genomic locus. The cell wall dye calcofluor white was obtained from Sigma-Aldrich. Detailed information on microscopy and image analysis can be found in Supplemental Experimental Procedures.

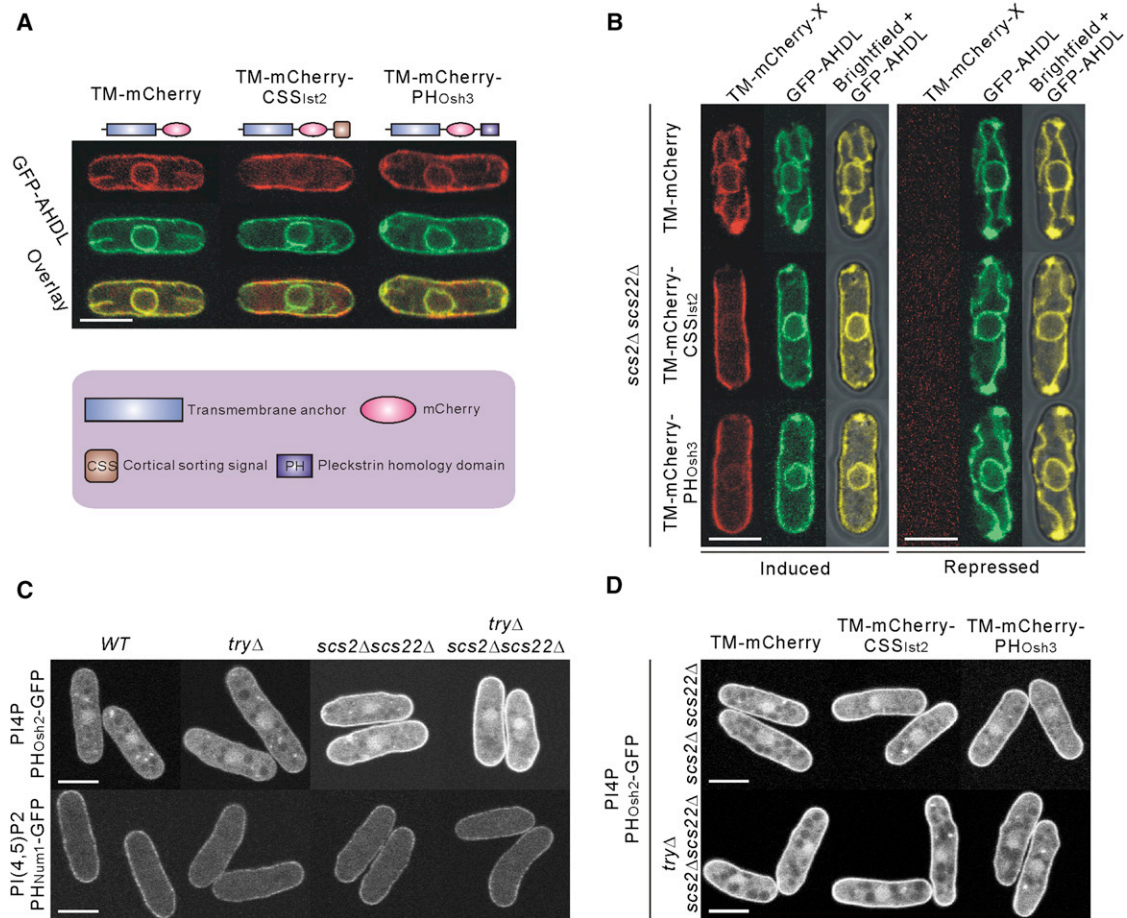


Figure 3. The Artificial ER-PM Tethers Restore the Cortical ER Contacts in Cells Lacking VAPs
(A) Scanning confocal medial plane micrographs of the artificial ER-PM tethers (top) and GFP-AHDL (center) in WT cells, with overlay shown below. Cartoons (key at bottom) illustrate the construct design.
(B) When present, the ER-PM tethers (red) forced cortical ER recruitment in *scs2Δscs22Δ* cells coexpressing GFP-AHDL (green). Scanning confocal medial plane micrographs of cells in which tether expression was induced (left panel) or repressed (right panel) are shown.
(C) Scanning confocal medial plane micrographs of the PI4P marker PH_{Osh2} -GFP (upper panel) and the PI(4,5)P2 marker PH_{Num1} -GFP (lower panel) in the indicated cell types.
(D) Scanning confocal medial plane micrographs of the PI4P marker PH_{Osh2} -GFP in the indicated cell types coexpressing the artificial ER-PM tethers. Scale bars represent 5 μ m. See also Figure S3.

Supplemental Information

Supplemental Information includes four figures, one table, three movies, and Supplemental Experimental Procedures and can be found with this article online at <http://dx.doi.org/10.1016/j.cub.2012.08.047>.

Acknowledgments

We are grateful to M. Balasubramanian and E. Makeyev for discussions and suggestions on the manuscript and to D. Huang for technical assistance. This work was supported by Singapore Millennium Foundation.

Received: May 21, 2012
 Revised: August 2, 2012
 Accepted: August 22, 2012
 Published online: October 4, 2012

References

- Pidoux, A.L., and Armstrong, J. (1993). The BiP protein and the endoplasmic reticulum of *Schizosaccharomyces pombe*: fate of the nuclear envelope during cell division. *J. Cell Sci.* 105, 1115–1120.
- Prinz, W.A., Grzyb, L., Veenhuis, M., Kahana, J.A., Silver, P.A., and Rapoport, T.A. (2000). Mutants affecting the structure of the cortical endoplasmic reticulum in *Saccharomyces cerevisiae*. *J. Cell Biol.* 150, 461–474.
- Schneider, M.F. (1994). Control of calcium release in functioning skeletal muscle fibers. *Annu. Rev. Physiol.* 56, 463–484.
- Wu, M.M., Luik, R.M., and Lewis, R.S. (2007). Some assembly required: constructing the elementary units of store-operated Ca^{2+} entry. *Cell Calcium* 42, 163–172.
- Sparkes, I.A., Frigerio, L., Tolley, N., and Hawes, C. (2009). The plant endoplasmic reticulum: a cell-wide web. *Biochem. J.* 423, 145–155.
- Loewen, C.J., Gaspar, M.L., Jesch, S.A., Delon, C., Ktistakis, N.T., Henry, S.A., and Levine, T.P. (2004). Phospholipid metabolism regulated by a transcription factor sensing phosphatidic acid. *Science* 304, 1644–1647.
- Stefan, C.J., Manford, A.G., Baird, D., Yamada-Hanff, J., Mao, Y., and Emr, S.D. (2011). Osh proteins regulate phosphoinositide metabolism at ER-plasma membrane contact sites. *Cell* 144, 389–401.
- Zhang, D., Vjestica, A., and Olfierenko, S. (2010). The cortical ER network limits the permissive zone for actomyosin ring assembly. *Curr. Biol.* 20, 1029–1034.

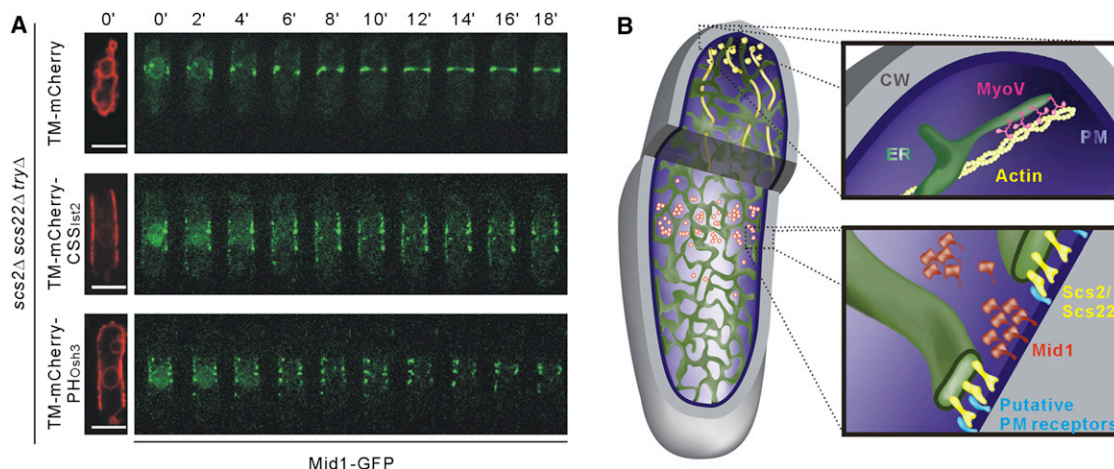


Figure 4. The Cortical ER Obstructs the PM Recruitment of Mid1 Protein Complexes

(A) *scs2Δscs22ΔtryΔ* cells coexpressing the indicated ER-PM tether constructs (red, left panel) and Mid1-GFP (green) were subjected to time-lapse spinning-disk confocal microscopy. Shown are single-plane images for artificial tethers and maximum z projection images for Mid1-GFP. Elapsed time is shown in minutes. Scale bars represent 5 μ m.

(B) A pictorial model for cortical ER arrangement underneath the PM. CW indicates the cell wall.

See also Figure S4.

- Loewen, C.J., Young, B.P., Tavassoli, S., and Levine, T.P. (2007). Inheritance of cortical ER in yeast is required for normal septin organization. *J. Cell Biol.* 179, 467–483.
- Mata, J., and Nurse, P. (1997). *tea1* and the microtubular cytoskeleton are important for generating global spatial order within the fission yeast cell. *Cell* 89, 939–949.
- Estrada, P., Kim, J., Coleman, J., Walker, L., Dunn, B., Takizawa, P., Novick, P., and Ferro-Novick, S. (2003). Myo4p and She3p are required for cortical ER inheritance in *Saccharomyces cerevisiae*. *J. Cell Biol.* 163, 1255–1266.
- Wagner, W., Brenowitz, S.D., and Hammer, J.A., 3rd. (2011). Myosin-Va transports the endoplasmic reticulum into the dendritic spines of Purkinje neurons. *Nat. Cell Biol.* 13, 40–48.
- Kagiwada, S., and Hashimoto, M. (2007). The yeast VAP homolog *Scs2p* has a phosphoinositide-binding ability that is correlated with its activity. *Biochem. Biophys. Res. Commun.* 364, 870–876.
- Celton-Morizur, S., Bordes, N., Fraiser, V., Tran, P.T., and Paoletti, A. (2004). C-terminal anchoring of mid1p to membranes stabilizes cytokinetic ring position in early mitosis in fission yeast. *Mol. Cell. Biol.* 24, 10621–10635.
- Sohrmann, M., Fankhauser, C., Brodbeck, C., and Simanis, V. (1996). The *dmf1/mid1* gene is essential for correct positioning of the division septum in fission yeast. *Genes Dev.* 10, 2707–2719.
- Bähler, J., Steever, A.B., Wheatley, S., Wang, Y., Pringle, J.R., Gould, K.L., and McCollum, D. (1998). Role of polo kinase and Mid1p in determining the site of cell division in fission yeast. *J. Cell Biol.* 143, 1603–1616.
- Paoletti, A., and Chang, F. (2000). Analysis of mid1p, a protein required for placement of the cell division site, reveals a link between the nucleus and the cell surface in fission yeast. *Mol. Biol. Cell* 11, 2757–2773.
- Ercan, E., Momburg, F., Engel, U., Temmerman, K., Nickel, W., and Seedorf, M. (2009). A conserved, lipid-mediated sorting mechanism of yeast *Ist2* and mammalian STIM proteins to the peripheral ER. *Traffic* 10, 1802–1818.
- Levine, T.P., and Munro, S. (2001). Dual targeting of Osh1p, a yeast homologue of oxysterol-binding protein, to both the Golgi and the nucleus-vacuole junction. *Mol. Biol. Cell* 12, 1633–1644.
- West, M., Zurek, N., Hoenger, A., and Voeltz, G.K. (2011). A 3D analysis of yeast ER structure reveals how ER domains are organized by membrane curvature. *J. Cell Biol.* 193, 333–346.
- Stradalova, V., Blazikova, M., Grossmann, G., Opekarová, M., Tanner, W., and Malinsky, J. (2012). Distribution of cortical endoplasmic reticulum determines positioning of endocytic events in yeast plasma membrane. *PLoS ONE* 7, e35132.
- De Craene, J.O., Coleman, J., Estrada de Martin, P., Pypaert, M., Anderson, S., Yates, J.R., 3rd, Ferro-Novick, S., and Novick, P. (2006). Rtn1p is involved in structuring the cortical endoplasmic reticulum. *Mol. Biol. Cell* 17, 3009–3020.
- Moseley, J.B., Mayeux, A., Paoletti, A., and Nurse, P. (2009). A spatial gradient coordinates cell size and mitotic entry in fission yeast. *Nature* 459, 857–860.
- Martin, S.G., and Berthelot-Grosjean, M. (2009). Polar gradients of the DYRK-family kinase Pom1 couple cell length with the cell cycle. *Nature* 459, 852–856.
- Gould, K.L. (2004). Protocols for experimentation with *Schizosaccharomyces pombe*. *Methods* 33, 187–188.
- Yu, J.W., Mendrola, J.M., Audhya, A., Singh, S., Keleti, D., DeWald, D.B., Murray, D., Emr, S.D., and Lemmon, M.A. (2004). Genome-wide analysis of membrane targeting by *S. cerevisiae* pleckstrin homology domains. *Mol. Cell* 13, 677–688.

The Cortical ER Network Limits the Permissive Zone for Actomyosin Ring Assembly

Dan Zhang,^{1,2} Aleksandar Vjestica,^{1,2} and Snezhana Oliferenko^{1,2,*}

¹Temasek Life Sciences Laboratory, 1 Research Link, 117604 Singapore

²Department of Biological Sciences, National University of Singapore, 117543 Singapore

Summary

Precise positioning of the cellular division plane is important for accurate segregation of genetic material and determination of daughter cell fates. Here we report a surprising connection between division site positioning and the organization of the cortical endoplasmic reticulum (ER). The cortical ER is an interconnected network of flat cisternae and highly curved tubules sharing a continuous lumen [1, 2]. Stabilization of high curvature by reticulon and DP1 family proteins contributes to formation of tubules [3–5]. We show that in the fission yeast *Schizosaccharomyces pombe*, the ER network is maintained by a set of three membrane proteins: reticulon/Rtn1p, DP1/Yop1p, and a newly identified evolutionarily conserved protein, Tts1p. Cells lacking the ER domain sustained by these proteins exhibit severe defects in division plane positioning as a result of abnormal dispersion of a key regulator of division site selection, Mid1p, along the cell cortex. This triggers delocalized assembly of actomyosin cables and compromises their compaction into a single medially positioned ring. We propose that the cortical ER network restricts the lateral motion of Mid1p and hence generates a permissive zone for actomyosin ring assembly precisely at the cell equator.

Results and Discussion

The *Schizosaccharomyces pombe* genome encodes one reticulon and one DP1/Yop1 protein, which we term Rtn1p (SPBC31A8.01C) and Yop1p (SPCC830.08C). Rtn1p-GFP predominantly localized to the peripheral (cortical) endoplasmic reticulum (ER) and was largely excluded from the nuclear envelope (NE), consistent with localization in budding yeast [6]. On the other hand, Yop1p-GFP localized to both the peripheral ER and NE (Figure 1A). Interestingly, Rtn1p and Yop1p accumulated at the cell equator during mitosis, following assembly of the actomyosin ring marked by the myosin light chain, Rlc1p (Figure 1A). From a genetic screen for modulators of Cut11p function in spindle pole body anchorage at the NE [7] (unpublished data), we identified an evolutionarily conserved transmembrane protein (SPBC1539.04) with a strikingly similar subcellular distribution. This protein, Tts1p (tetra-spanning protein 1), colocalized with Rtn1p and Yop1p in the peripheral ER and was also found at the NE (Figure 1B). The compartment marked by Tts1p, Rtn1p, and Yop1p was distinct from membranes containing the ER resident protein

oligosaccharide-transferase Ost1p (see Figure S1A available online). Tts1p was enriched at the cell equator during mitosis together with Rtn1p and Yop1p, unlike Ost1p and the translocon subunit Sec63p [8] (Figure 1A; data not shown). Thus, the peripheral ER in fission yeast is organized as an intricately compartmentalized network of high-curvature (tubular) and low-curvature (cisternal) elements.

Mass spectrometry analysis of proteins copurified with the TAP-tagged Tts1p identified Rtn1p as a Tts1p-interacting partner (Figure S1B). We confirmed their interaction by dual coimmunoprecipitation (Figure 1C). Furthermore, Rtn1p interacted with Yop1p (Figure S1C), consistent with reports from budding yeast [3]. We also detected an association between Tts1p and Yop1p by coimmunoprecipitation (Figure S1C). Thus, our data suggest that Rtn1p, Yop1p, and Tts1p colocalize in a subcompartment of the ER and physically associate.

We wondered whether Rtn1p, Yop1p, and Tts1p function together in shaping ER membranes. We examined ER morphology with fluorescent markers for different ER compartments in wild-type and mutant genetic backgrounds. In *rtn1Δ* cells, both Yop1p-GFP- and Tts1p-GFP-marked membranes were significantly depleted from the lateral cortex (Figures 2A and 2B), suggesting diminishment of peripheral tubules. Tts1p and Yop1p in *rtn1Δ* cells were still clearly excluded from the cisternal compartment marked by Ost1p (Figure S2A). Consistent with a conversion to more cisternal ER, Ost1p in *rtn1Δ* cells localized extensively along the lateral cortex, unlike its typical intermittent pattern in wild-type cells (Figure S1A).

Similarly, Rtn1p-GFP showed decreased occupancy at the cell cortex in both *yop1Δ* and *tts1Δ* cells, and its occupancy was further diminished in the double *yop1Δtts1Δ* mutant (Figure 2C). We performed similar analyses for other single and double deletions, with Yop1p-GFP (Figure 2A) or Tts1p-GFP (Figure 2B) as markers for the tubular ER. The reduction in occupancy of tubular ER markers was statistically significant in all cases, with double-deletion strains exhibiting augmented phenotypes. This was not due to compromised marker protein expression (Figure S2B). Of the three proteins, Rtn1p had the largest influence on the distribution of putative tubular ER markers.

As compared to the wild-type, the cortical ER domain visualized by Ost1p-mCherry in the triple *tts1Δrtn1Δyop1Δ* mutant cells (subsequently called *tryΔ*) was more prominent and continuous, with occasional extended breaks (Figure S2C). To address how the deficiency of Rtn1p, Yop1p, and Tts1p affected general ER structure, we constructed artificial luminal ER markers, GFP-AHDL and mCherry-AHDL. Because the ER possesses a continuous intraluminal space, these markers localized to both cisternal and tubular compartments (Figure S2D). In wild-type cells, the cortical ER appeared as an elaborate and regularly distributed membranous network underlying the plasma membrane (Figure 2D, top; n = 50 cells). We observed that this regular network structure was disrupted in *tryΔ* cells: the cortical ER now mostly appeared as continuous sheet-like membranes (Figure 2D, bottom; n = 50 cells). Additionally, we noticed irregular membrane accumulations and occasional breaks at the cortex. Because the geometry

*Correspondence: snejana@tll.org.sg

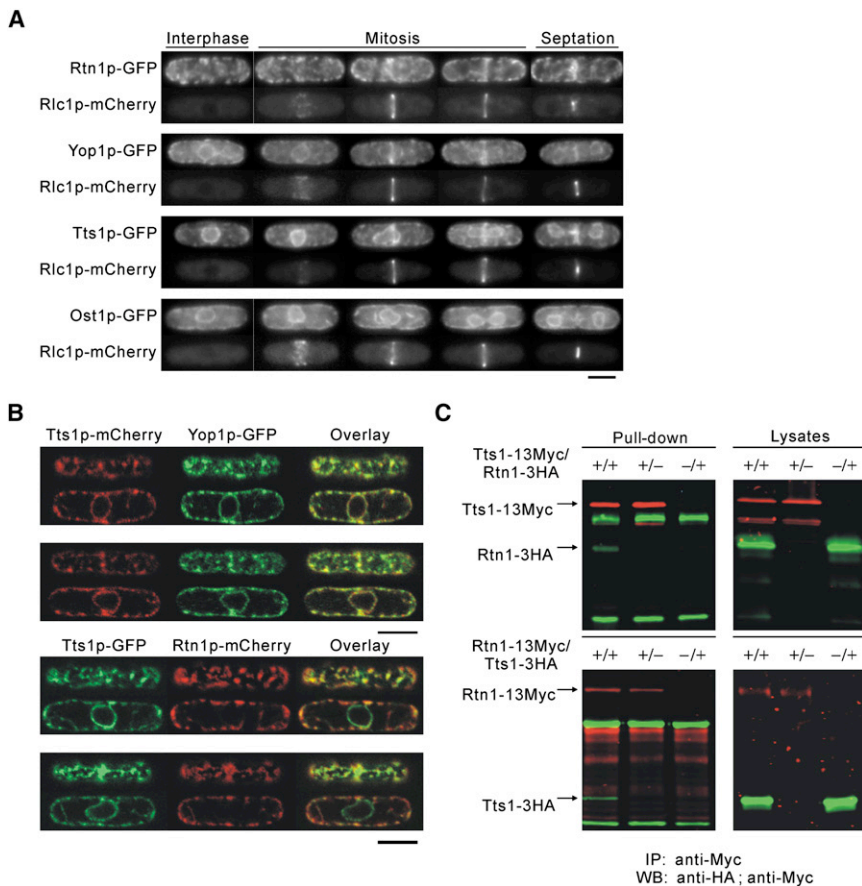


Figure 1. Rtn1p, Yop1p, and Tts1p Colocalize in the Cortical Endoplasmic Reticulum and Accumulate at the Mitotic Cell Equator

(A) Localization of GFP-fused proteins at cell-cycle stages indicated by coexpressed myosin light chain Rlc1p-mCherry as the actomyosin ring marker. Shown are maximum Z projections of epifluorescence micrographs.

(B) Scanning confocal micrographs of cells expressing indicated proteins. Shown are top and middle planes from Z stacks. Scale bars represent 5 μ m.

(C) Coimmunoprecipitation of the indicated proteins from native cell extracts. Samples were probed with the anti-Myc (red) and anti-HA (green) antibodies.

of fission yeast cells impedes the resolution of fine details of cortical ER organization, we visualized GFP-AHDL in spheroplasts where the cell wall was removed and cells assumed a spherical shape. This allowed us to clearly document the transition between the intricate ER network in wild-type cells and continuous sheet-like membranes in a *try* Δ genetic background (Figure 2E). Taken together with work in other systems [3], our results indicate that Rtn1p, Yop1p, and Tts1p collaborate to maintain the tubular ER at the cell periphery.

Surprisingly, we observed a progressive failure in division site positioning as cells lost Tts1p, Yop1p, and Rtn1p. *S. pombe* cells position actomyosin rings in the cell center and divide perpendicular to the long axis of the cell. Single mutants for each *try* gene produced a low incidence of tilted and off-center septa. The proportion increased in double and triple mutant combinations. Interestingly, the deficiency of Rtn1p that individually had the strongest effect on ER structure consistently caused a more prominent cytokinesis defect. The triple mutant *try* Δ cells showed the highest incidence of multiple septa and long-axis septa (Figure 3A). The vast majority of *try* Δ cells (92.3% \pm 1.8%; n = 1500 cells) failed to normally position septa and resembled cells lacking the anillin-like protein Mid1p that determines actomyosin ring positioning [9–12] (Figures 3A and 3B). Deletion of *mid1* in a *try* Δ genetic background did not exacerbate division site mispositioning, suggesting that Mid1p and the TRY proteins function in the same epistasis group (Figures 3A and 3B). The kinase Pom1p functions as a negative regulator of division site selection [13, 14], and cells lacking both Mid1p and Pom1p were reported as inviable [11]. We obtained mutant cells lacking the *try* genes together with *pom1* at a frequency much lower

than expected from tetrad analysis (17% of the expected yield, 88 progeny). The quadruple mutant cells were severely retarded for growth and exhibited extreme septum positioning defects, including frequent tip septa (Figure S3A). This further suggests that the TRY proteins function together with Mid1p in a pathway that is distinct from the Pom1p pathway.

Mid1p shuttles between the nucleus and cell cortex during interphase, but upon entry into mitosis it redistributes to the medial cortex, where it is detectable as distinct nodes [15]. We found that Mid1p-GFP exited normally from

the nucleus in triple mutant cells and was recruited to the cortex (Figure 3C, 20 of 23 wild-type and 8 of 10 *try* Δ cells completed Mid1p export within 4 min following spindle pole body [SPB] separation). The total levels of Mid1p-GFP were comparable in wild-type and *try* Δ cells (Figure S3B). Intriguingly, Mid1p spread along a larger area of the cortex and failed to compact into a tight ring (Figure 3C, see kymographs for Mid1p-GFP time evolution). As a result of this abnormal dispersal, the cortical domain occupied by Mid1p was much broader in early mitotic *try* Δ cells as compared to the wild-type (Figure 3D). Notably, we observed that Mid1p-GFP was now largely present in cortical nodes of lower mean fluorescence intensity (Figure S3C; n = 140, p = 0.0013, Kolmogorov-Smirnov test). Unlike wild-type cells that compacted rings during early mitosis, 10 of 15 *try* Δ cells failed to compact Mid1p into rings, and ring formation was strongly delayed in 5 of 15 *try* Δ cells. We did not observe mislocalization of Pom1p, the negative regulator of Mid1p localization, during interphase (Figure S3D).

Given that cortical Mid1p failed to compact into rings in *try* Δ cells, we examined whether it recruited essential ring components such as myosin II and F-actin by using Rlc1p-mCherry and the GFP-tagged Rng2p calponin homology domain as markers. In *try* Δ cells, Rlc1p-mCherry promptly associated with all cortical Mid1p-GFP nodes, as in the wild-type (Figures 3E and 3F; n = 15 cells). Furthermore, actin filaments appeared around the cortical nodes marked by Rlc1p-mCherry in both wild-type and *try* Δ cells (Figures 3G and 3H; n = 20 cells). The timing of actin recruitment to the cortex was not affected (2.5 \pm 0.9 min after SPB separation in wild-type, n = 9 cells; 2.9 \pm 1.0 min in *try* Δ cells, n = 13 cells; Figure S3E). Thus,

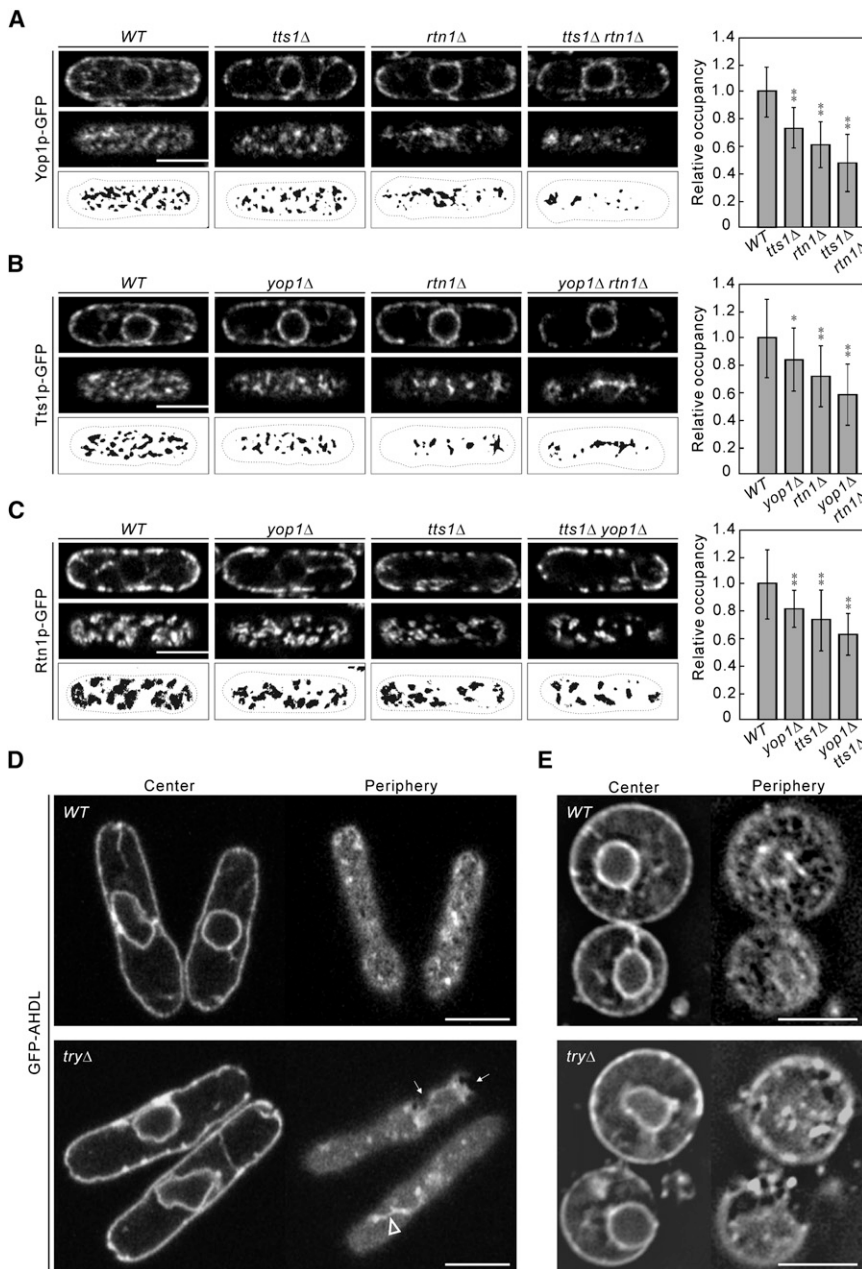


Figure 2. Rtn1p, Yop1p, and Tts1p Maintain the Tubular Structures in the Cortical Endoplasmic Reticulum

(A–C) Scanning confocal micrographs of Yop1p-GFP (A), Tts1p-GFP (B), and Rtn1p-GFP (C) in cells with indicated genetic background. Top: cell center; middle: cell periphery; bottom: thresholded image of cell periphery. Histograms quantify the normalized occupancy of fluorescent regions at the cell periphery (mean \pm standard deviation [SD]; $30 < n < 65$). Error bars represent $2 \times$ SD. $0.001 < *p < 0.005$ and $**p < < 0.001$, in comparison to wild-type (WT) from two-tailed Student's t test.

(D) Scanning confocal micrographs of GFP-AHDL at cell center (left) and cell periphery (right) in wild-type and *tryΔ* cells. Arrows indicate endoplasmic reticulum (ER) breaks at the cortex. Arrowhead indicates an irregular cortical accumulation of ER membranes.

(E) Deconvolved epifluorescence images of wild-type and *tryΔ* spheroplasts expressing GFP-AHDL. Left: cell center; right: cell periphery. Scale bars represent 5 μ m.

that their equatorial accumulation is a consequence of node compaction and should depend on both actomyosin function and Mid1p. Indeed, Tts1p-GFP did not accumulate at the cell equator in cells lacking functional formin Cdc12p [16] (Figure 4E) or the essential myosin II light chain, Cdc4p [17] (data not shown). Furthermore, the Tts1p-positive membranes were not enriched in the vicinity of the abnormal actomyosin structures assembled in *mid1Δ* cells (Figure 4F).

Mid1p is targeted to the cortex through two independent motifs. It further oligomerizes and recruits actomyosin ring components [18, 19]. Thus, Mid1p nodes correspond to higher-order protein assemblies. The cortical drift of Mid1p upon mitotic entry in *tryΔ* cells (Figure 3C) indicates a high rate of diffusion of these peripherally attached complexes along the membrane prior

to cable compaction. Consistent with this proposition, fluorescence recovery after photobleaching (FRAP) analysis of Mid1p-GFP in early mitotic wild-type cells showed only a limited fluorescence recovery (Figure 4G; $28.5\% \pm 10.9\%$ within 2 min, $n = 15$), suggesting that the lateral motion of Mid1p was restricted. On the other hand, Mid1p-GFP fluorescence recovery was significantly higher in early mitotic *tryΔ* cells (Figure 4H; $62.5\% \pm 18.7\%$ within 2 min, $n = 21$, $p < 0.01$). The slanting traces of Mid1p-GFP fluorescence in kymographs of the FRAP experiments in *tryΔ* cells suggest that the observed fluorescence recovery could be due to movement within the plane of the membrane rather than Mid1p turnover (Figure S3F). Thus, it appears that the cortical ER network maintained by the ER tubulating proteins can impede the lateral movement of Mid1p nodes.

Mid1p efficiently recruited the actomyosin ring assembly machinery to the cortex in *tryΔ* cells, but its abnormally broad distribution caused highly delocalized assembly of actomyosin cables. Upon careful examination, we observed that, following efflux from the nucleus, Mid1p-GFP localized to cortical sites that were positioned close to, but did not overlap with, ER tubules marked by Tts1p-mCherry (Figure 4A). The Mid1p-GFP signal was largely excluded from ER cisternae marked by Ost1p-mCherry (Figure 4B), and the general ER was visualized by mCherry-AHDL (Figure 4C). Thus, it appeared that Mid1p concentrated in nodes at the plasma membrane in between the ER elements. Interestingly, as Mid1p-GFP nodes compacted into a ring, the initially uniformly distributed ER tubules gathered at the cell equator (Figure 4D). This phenomenon underlies the specific enrichment of the putative tubular ER domains at the future division site (Figure 1A). This also implies

We do not favor the possibility that tubular ER defects trigger ring mispositioning through vesicular trafficking abnormalities.

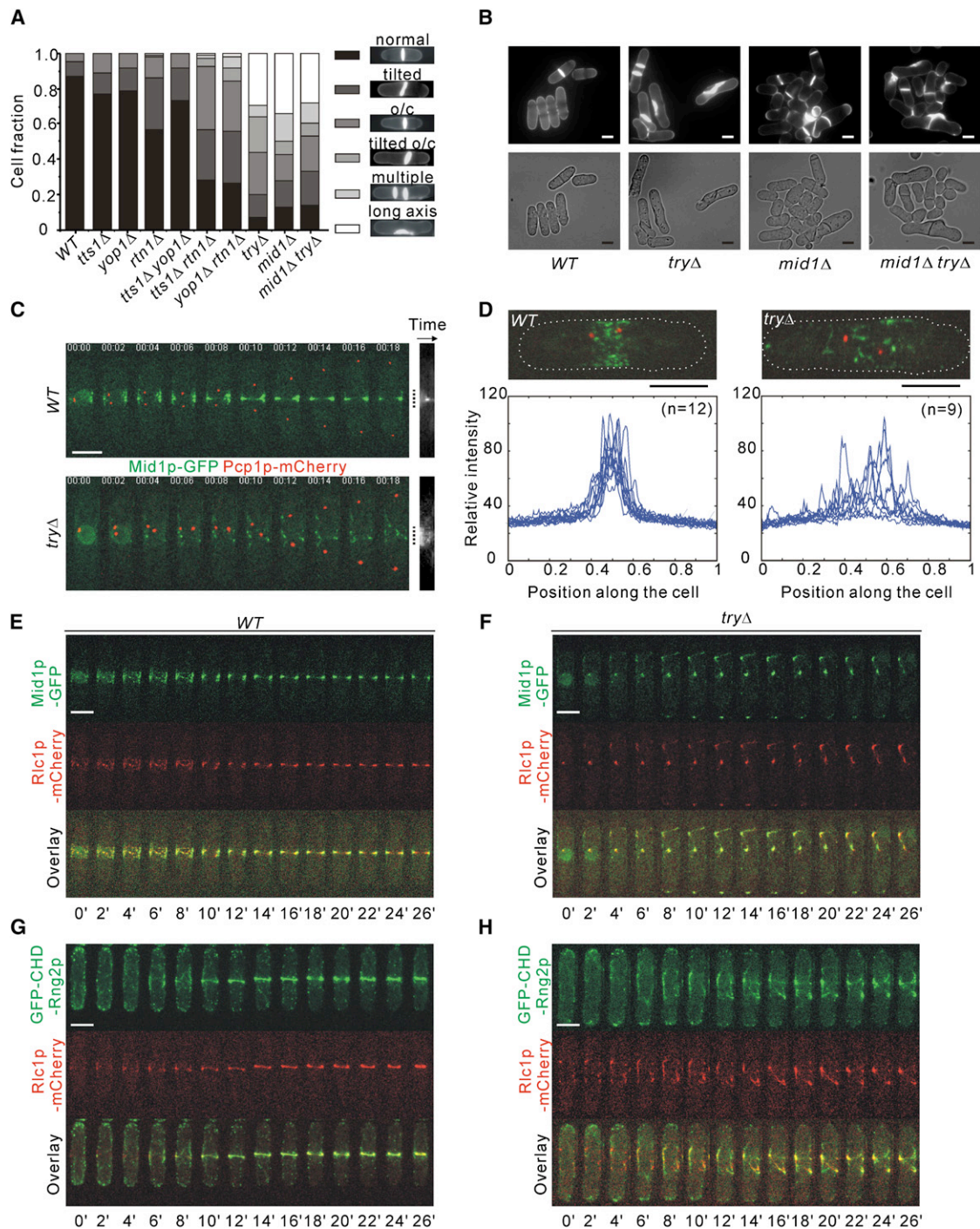


Figure 3. Cells Lacking Rtn1p, Yop1p, and Tts1p Fail to Position and Compact the Actomyosin Ring

(A) Quantification of the septa positioning phenotypes in cells of indicated genotypes ($500 < n < 1500$). o/c indicates off-center. (B) Epifluorescence and differential interference contrast images of Calcofluor-stained cells with indicated genotypes. (C) Time-lapse maximum Z projection images of wild-type and *tryΔ* cells coexpressing Mid1p-GFP and Pcp1p-mCherry (left) and corresponding kymographs (right) of Mid1p-GFP along the long cell axis. Dotted lines indicate positions of the nuclei before Mid1p efflux. (D) Quantification of Mid1p-GFP fluorescence distribution along the long cell axis in wild-type ($n = 12$) and *tryΔ* ($n = 9$) early mitotic cells, as indicated by Pcp1p-mCherry. Shown are the maximum projections of Z stacks obtained from scanning confocal microscopy. (E–H) Time-lapse maximum Z projection images of wild-type (E and G) or *tryΔ* (F and H) cells coexpressing indicated proteins. Scale bars represent 5 μm . The elapsed time is shown in minutes.

We did not observe defects in transitional ER emergence or Golgi biogenesis in *tryΔ* cells (Figure S4). Furthermore, bulk vesicular trafficking deficiencies in *S. pombe* do not lead to

ring assembly or positioning defects [20–22]. Concordantly, the lack of reticulons and Yop1p in budding yeast does not cause major secretion defects [3, 6].

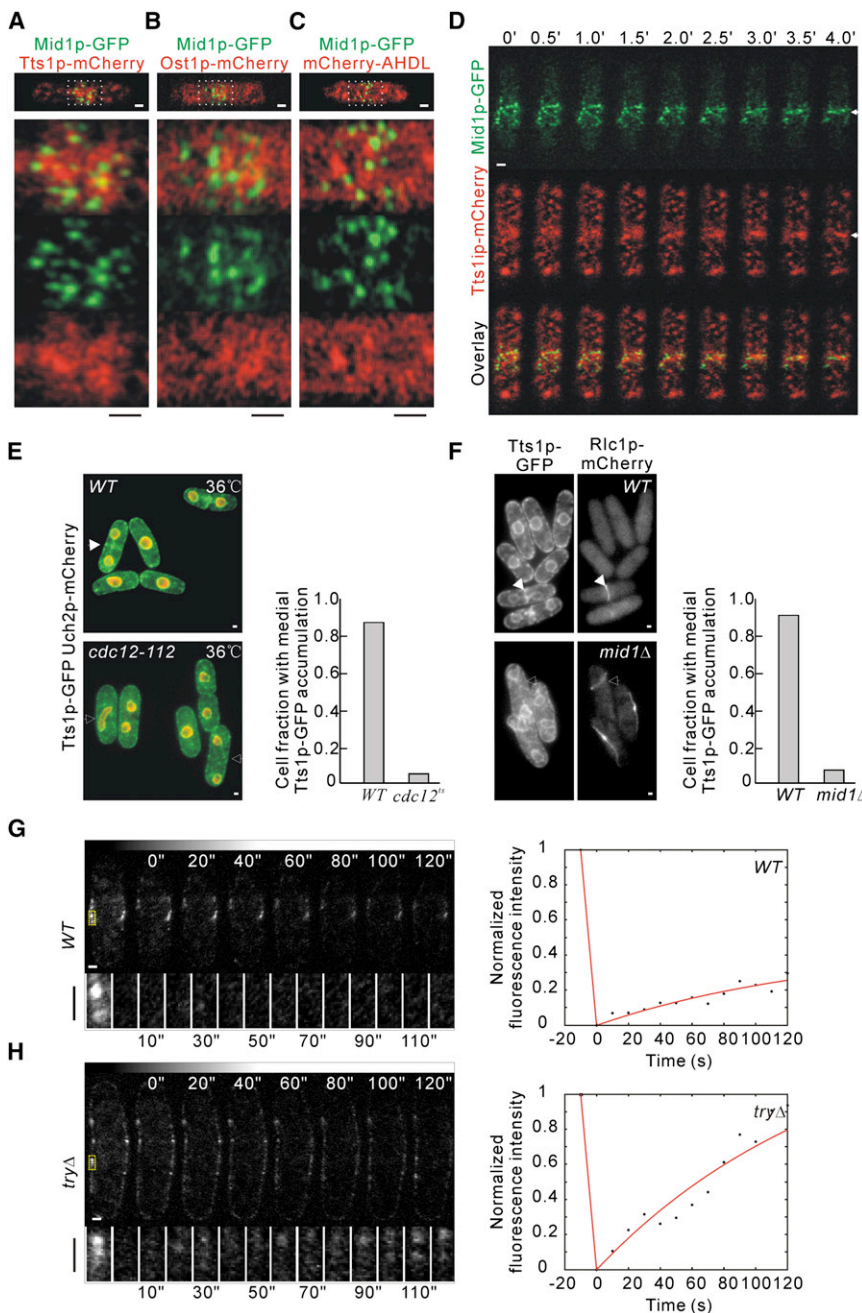


Figure 4. Mid1p Nodes Localize between the Endoplasmic Reticulum Elements during the Actomyosin Ring Compaction

(A–C) Scanning confocal micrographs at peripheral focal plane of wild-type cells coexpressing indicated proteins. Bottom panels show 4× magnification of the framed region.

(D) Time-lapse of early mitotic wild-type cells coexpressing Mid1p-GFP and Tts1p-mCherry imaged by scanning confocal microscopy. Shown is the peripheral focal plane. The arrows indicate the accumulation of Tts1p-mCherry during Mid1p-GFP node compaction. The elapsed time is indicated in minutes.

(E) Localization of Tts1p-GFP (green) in wild-type and *cdc12-112* cells coexpressing Uch2p-mCherry (red) as the nuclear envelope (NE) marker at 36°C. Cells were grown overnight at 24°C and shifted to 36°C for 30 min before imaging. Right: quantification for the medial accumulation of Tts1p-GFP in binucleate cells, *n* = 100. The solid arrow indicates accumulation of Tts1p-GFP; the outlined arrows indicate lack of the medial accumulation.

(F) Localization of Tts1p-GFP in wild-type (top) and *mid1Δ* (bottom) cells during mitosis, as indicated by Rlc1p-mCherry. Right: quantification for the medial accumulation of Tts1p-GFP in binucleate cells, *n* = 100. The solid arrows indicate Tts1p-GFP accumulation at the division site; the outlined arrows indicate the disappearance of this accumulation.

(G and H) Mid1p-GFP fluorescence recovery after photobleaching analyses of early mitotic wild-type (G) and *tryΔ* (H) cells. Shown are representative cells before and after photobleaching at indicated time points and the corresponding fluorescence recovery curves. Gray wedges at the top show the same contrasting. The bleached regions boxed in yellow are magnified in the bottom rows at all acquired time points. Scale bars represent 1 μm.

The cortical ER in various organisms is intimately associated with the plasma membrane through multiple contact sites [23–27]. One possible outcome of an association between the ER and the cortex is the compartmentalization of their membranes, with their contact sites acting as diffusion barriers for peripherally associated protein complexes. In such a manner, the geometry of the ER network could translate into specific patterning of the plasma membrane and therefore affect the efficiency with which the Mid1p nodes are restricted at the medial cortex. An observed change in node size distribution in *tryΔ* cells raises the possibility that, by restricting the spread of Mid1p, the cortical ER network could increase the local concentration of Mid1p and aid its efficient organization into nodes. Furthermore, the ER network could physically hinder the lateral mobility of the nodes, effectively embedding them within the tubular

meshwork. Because the physical proximity between neighboring nodes is essential for efficient formation of tight rings [28], broad node distribution would instead lead to assembly of incomplete and mispositioned actomyosin cables. Interestingly, it was previously suggested that Mid1p could be positioned by “as-yet-undefined structures connecting the nucleus and the cortex” [29]. We propose that the cortical ER network plays an instructive role in delimiting the actomyosin ring assembly at the cell equator.

Similar diffusion-limiting strategies could affect the assembly and function of cortically associated protein networks in other cell types with pronounced ER-plasma membrane attachment sites.

Experimental Procedures

S. pombe Strains, Reagents, and Constructs

S. pombe strains used in this study and their genotypes are listed in Table S1. The promoter and coding sequences for expression of the ER luminal marker GFP-AHDL were introduced at the *leu1* genomic locus with the *S. pombe* integration vector pJK148. GFP-AHDL protein was designed by introducing the signal peptide sequence (25 N-terminal amino

acids) and ER-retention signal (5 C-terminal amino acids) of Bip1p to the N and C termini of the GFP, respectively. Expression of the GFP-AHDL construct was driven by a *bip1* promoter sequence consisting of 1000 bp upstream of the start codon. An identical strategy was used for the mCherry-AHDL construct. Media for vegetative growth and genetic methods were as described in [30]. All experiments were done on cells grown in YES medium. Genetic crosses and sporulation were performed on YPD agar plates. To obtain fission yeast spheroplasts, we grew cells in liquid YES medium overnight to exponential phase and shifted them to a fresh YES medium containing 5 mg/ml Lysing enzyme from Sigma-Aldrich and 3 mg/ml Zymolase (MP Biomedicals) for 90 min to remove the cell wall. The homologous recombination-based method was used to tag endogenous proteins with green fluorescent protein, mCherry, or TAP at their C termini under control of the native promoter. Plasmids were constructed via standard molecular biology techniques. Latrunculin A, a drug that prevents actin polymerization, was purchased from Biomol International LP. DNA fluorescent stain 4',6-diamidino-2-phenylindole (DAPI) and cell wall stain Calcofluor White were obtained from Sigma-Aldrich. The F-actin stain Alexa Fluor 593 phalloidin was obtained from Invitrogen.

Detailed information on microscopy, image analysis, and biochemical techniques can be found in the [Supplemental Experimental Procedures](#).

Supplemental Information

Supplemental Information includes Supplemental Experimental Procedures, four figures, and one table and can be found with this article online at [doi:10.1016/j.cub.2010.04.017](https://doi.org/10.1016/j.cub.2010.04.017).

Acknowledgments

We are grateful to M. Balasubramanian, E. Makeyev, R. Thadani, and S. Cohen for discussions and suggestions on the manuscript. Our work was supported by the Singapore Millennium Foundation.

Received: February 13, 2010

Revised: March 24, 2010

Accepted: April 7, 2010

Published online: April 29, 2010

References

1. Terasaki, M., Jaffe, L.A., Hunnicutt, G.R., and Hammer, J.A., 3rd. (1996). Structural change of the endoplasmic reticulum during fertilization: Evidence for loss of membrane continuity using the green fluorescent protein. *Dev. Biol.* **179**, 320–328.
2. Voeltz, G.K., Rolls, M.M., and Rapoport, T.A. (2002). Structural organization of the endoplasmic reticulum. *EMBO Rep.* **3**, 944–950.
3. Voeltz, G.K., Prinz, W.A., Shibata, Y., Rist, J.M., and Rapoport, T.A. (2006). A class of membrane proteins shaping the tubular endoplasmic reticulum. *Cell* **124**, 573–586.
4. Hu, J., Shibata, Y., Voss, C., Shemesh, T., Li, Z., Coughlin, M., Kozlov, M.M., Rapoport, T.A., and Prinz, W.A. (2008). Membrane proteins of the endoplasmic reticulum induce high-curvature tubules. *Science* **319**, 1247–1250.
5. Shibata, Y., Voss, C., Rist, J.M., Hu, J., Rapoport, T.A., Prinz, W.A., and Voeltz, G.K. (2008). The reticulon and DP1/Yop1p proteins form immobile oligomers in the tubular endoplasmic reticulum. *J. Biol. Chem.* **283**, 18892–18904.
6. De Craene, J.O., Coleman, J., Estrada de Martin, P., Pypaert, M., Anderson, S., Yates, J.R., 3rd, Ferro-Novick, S., and Novick, P. (2006). Rtn1p is involved in structuring the cortical endoplasmic reticulum. *Mol. Biol. Cell* **17**, 3009–3020.
7. West, R.R., Vaisberg, E.V., Ding, R., Nurse, P., and McIntosh, J.R. (1998). cut1(+): A gene required for cell cycle-dependent spindle pole body anchoring in the nuclear envelope and bipolar spindle formation in *Schizosaccharomyces pombe*. *Mol. Biol. Cell* **9**, 2839–2855.
8. Vjestica, A., Tang, X.Z., and Oliferenko, S. (2008). The actomyosin ring recruits early secretory compartments to the division site in fission yeast. *Mol. Biol. Cell* **19**, 1125–1138.
9. Sohrmann, M., Fankhauser, C., Brodbeck, C., and Simanis, V. (1996). The *dmf1/mid1* gene is essential for correct positioning of the division septum in fission yeast. *Genes Dev.* **10**, 2707–2719.
10. Chang, F., Woollard, A., and Nurse, P. (1996). Isolation and characterization of fission yeast mutants defective in the assembly and placement of the contractile actin ring. *J. Cell Sci.* **109**, 131–142.
11. Bähler, J., Steever, A.B., Wheatley, S., Wang, Y., Pringle, J.R., Gould, K.L., and McCollum, D. (1998). Role of polo kinase and Mid1p in determining the site of cell division in fission yeast. *J. Cell Biol.* **143**, 1603–1616.
12. Wu, J.Q., Sirotkin, V., Kovar, D.R., Lord, M., Beltzner, C.C., Kuhn, J.R., and Pollard, T.D. (2006). Assembly of the cytokinetic contractile ring from a broad band of nodes in fission yeast. *J. Cell Biol.* **174**, 391–402.
13. Celton-Morizur, S., Racine, V., Sibarita, J.B., and Paoletti, A. (2006). Pom1 kinase links division plane position to cell polarity by regulating Mid1p cortical distribution. *J. Cell Sci.* **119**, 4710–4718.
14. Padte, N.N., Martin, S.G., Howard, M., and Chang, F. (2006). The cell-end factor pom1p inhibits mid1p in specification of the cell division plane in fission yeast. *Curr. Biol.* **16**, 2480–2487.
15. Paoletti, A., and Chang, F. (2000). Analysis of mid1p, a protein required for placement of the cell division site, reveals a link between the nucleus and the cell surface in fission yeast. *Mol. Biol. Cell* **11**, 2757–2773.
16. Chang, F., Drubin, D., and Nurse, P. (1997). *cdc12p*, a protein required for cytokinesis in fission yeast, is a component of the cell division ring and interacts with profilin. *J. Cell Biol.* **137**, 169–182.
17. McCollum, D., Balasubramanian, M.K., Pelcher, L.E., Hemmingsen, S.M., and Gould, K.L. (1995). *Schizosaccharomyces pombe cdc4+* gene encodes a novel EF-hand protein essential for cytokinesis. *J. Cell Biol.* **130**, 651–660.
18. Celton-Morizur, S., Bordes, N., Fraiser, V., Tran, P.T., and Paoletti, A. (2004). C-terminal anchoring of mid1p to membranes stabilizes cytokinetic ring position in early mitosis in fission yeast. *Mol. Cell. Biol.* **24**, 10621–10635.
19. Almonacid, M., Moseley, J.B., Janvore, J., Mayeux, A., Fraiser, V., Nurse, P., and Paoletti, A. (2009). Spatial control of cytokinesis by Cdr2 kinase and Mid1/anillin nuclear export. *Curr. Biol.* **19**, 961–966.
20. Poloni, D., and Simanis, V. (2002). A DMSO-sensitive conditional mutant of the fission yeast orthologue of the *Saccharomyces cerevisiae* SEC13 gene is defective in septation. *FEBS Lett.* **511**, 85–89.
21. Takegawa, K., Hosomi, A., Iwaki, T., Fujita, Y., Morita, T., and Tanaka, N. (2003). Identification of a SNARE protein required for vacuolar protein transport in *Schizosaccharomyces pombe*. *Biochem. Biophys. Res. Commun.* **311**, 77–82.
22. Wang, H., Tang, X., Liu, J., Trautmann, S., Balasundaram, D., McCollum, D., and Balasubramanian, M.K. (2002). The multiprotein exocyst complex is essential for cell separation in *Schizosaccharomyces pombe*. *Mol. Biol. Cell* **13**, 515–529.
23. Prinz, W.A., Grzyb, L., Veenhuis, M., Kahana, J.A., Silver, P.A., and Rapoport, T.A. (2000). Mutants affecting the structure of the cortical endoplasmic reticulum in *Saccharomyces cerevisiae*. *J. Cell Biol.* **150**, 461–474.
24. Pichler, H., Gaigg, B., Hrastnik, C., Achleitner, G., Kohlwein, S.D., Zellnig, G., Perktold, A., and Daum, G. (2001). A subfraction of the yeast endoplasmic reticulum associates with the plasma membrane and has a high capacity to synthesize lipids. *Eur. J. Biochem.* **268**, 2351–2361.
25. Sparkes, I.A., Ketelaar, T., de Ruijter, N.C., and Hawes, C. (2009). Grab a Golgi: Laser trapping of Golgi bodies reveals in vivo interactions with the endoplasmic reticulum. *Traffic* **10**, 567–571.
26. Schneider, M.F. (1994). Control of calcium release in functioning skeletal muscle fibers. *Annu. Rev. Physiol.* **56**, 463–484.
27. Wu, M.M., Luik, R.M., and Lewis, R.S. (2007). Some assembly required: Constructing the elementary units of store-operated Ca²⁺ entry. *Cell Calcium* **42**, 163–172.
28. Vavylonis, D., Wu, J.Q., Hao, S., O'Shaughnessy, B., and Pollard, T.D. (2008). Assembly mechanism of the contractile ring for cytokinesis by fission yeast. *Science* **319**, 97–100.
29. Daga, R.R., and Chang, F. (2005). Dynamic positioning of the fission yeast cell division plane. *Proc. Natl. Acad. Sci. USA* **102**, 8228–8232.
30. Moreno, S., Klar, A., and Nurse, P. (1991). Molecular genetic analysis of fission yeast *Schizosaccharomyces pombe*. *Methods Enzymol.* **194**, 795–823.

13. Brownfield, L., Hafidh, S., Durbarry, A., Khatab, H., Sidorova, A., Doerner, P., and Twell, D. (2009). Arabidopsis DUO POLLEN3 is a key regulator of male germline development and embryogenesis. *Plant Cell* 21, 1940–1956.
14. Wong, J.L., and Johnson, M.A. (2010). Is HAP2-GCS1 an ancestral gamete fusogen? *Trends Cell Biol.* 20, 134–141.
15. Beale, K.M., Leydon, A.R., and Johnson, M.A. (2012). Gamete fusion is required to block multiple pollen tubes from entering an Arabidopsis ovule. *Curr. Biol.* 22, 1090–1094.
16. Spielman, M., and Scott, R.J. (2008). Polyspermy barriers in plants: from preventing to promoting fertilization. *Sex. Plant Reprod.* 21, 53–65.
17. Prado, A.M., Colaco, R., Moreno, N., Silva, A.C., and Feijo, J.A. (2008). Targeting of pollen tubes to ovules is dependent on nitric oxide (NO) signaling. *Mol. Plant* 1, 703–714.
18. Prado, A.M., Porterfield, D.M., and Feijo, J.A. (2004). Nitric oxide is involved in growth regulation and re-orientation of pollen tubes. *Development* 131, 2707–2714.
19. Völz, R., von Lyncker, L., Baumann, N., Dresselhaus, T., Sprunck, S., and Gross-Hardt, R. (2012). LACHESIS-dependent egg-cell signaling regulates the development of female gametophytic cells. *Development* 139, 498–502.

Cell Biology and Plant Biochemistry,
Biochemie-Zentrum Regensburg, University
of Regensburg, Universitätsstraße 31,
93053 Regensburg, Germany.
*E-mail: thomas.dresselhaus@biologie.uni-r.de

DOI: 10.1016/j.cub.2012.04.048

Nuclear Geometry: Mitotic Nucleus Flares Out When Arrested

Studies of budding yeast arrested in mitosis outline a set of rules for nuclear envelope expansion during closed nuclear division.

Aleksandar Vjestica^{1,2}
and Snezhana Oliferenko^{1,2,*}

A membrane-bound nucleus enclosing the genome and keeping transcription and RNA processing apart from protein synthesis endows eukaryotes with exquisitely sophisticated gene regulation networks and an unparalleled level of control over cellular physiology. The nuclear envelope (NE) serves as a physical boundary of the nucleus. It is composed of two distinct lipid bilayers fused at the nuclear pores, which mediate nucleocytoplasmic transport. The outer nuclear membrane is continuous with the endoplasmic reticulum (ER) while the inner nuclear membrane contains a meshwork of proteins that interact with chromatin and contribute to NE structure and function. Larger cells tend to have larger nuclei [1] and the nuclear size increases as cells grow, maintaining a fixed ratio of nuclear to cell volume (N/C) specific for each cell type [2,3]. Nuclei are often spherical but also come in more complex shapes. The nuclear geometry changes as cells grow, divide and interact with their environment.

The most pronounced changes occur during mitosis when the NE has to be restructured to form two daughter nuclei. In the ‘open’ mitosis widespread across higher eukaryotes, the NE disperses altogether to be reassembled around the segregated daughter genomes. Curiously, many

lower eukaryotes use a so-called ‘closed’ mitosis, where the mother nucleus divides without ever losing the nucleocytoplasmic compartmentalization. Typically, a spherical mother nucleus elongates into a dumbbell shape eventually resolving into two daughters. To enable these transformations, cells must expand the NE in a manner coordinated with intranuclear mitotic spindle elongation and chromosome segregation. The source of membranes for rapid NE growth, the membrane entry point and just how the dividing closed nuclear membrane is shaped remain a mystery. In this issue of *Current Biology*, Witkin *et al.* [4] report that the NE proliferates in the budding yeast *Saccharomyces cerevisiae* arrested in early mitosis, prior to nuclear division. Interestingly, the extra NE folds into a large nuclear extension, a flare, adjacent to the nucleolus. The nucleolus ‘spills’ into the flare and the nucleus assumes a bilobed appearance (Figure 1). When *S. cerevisiae* cells are allowed to resume spindle elongation and chromosome segregation, the flares are absorbed by the divided daughter nuclei that ultimately attain spherical shape [4]. Although describing a peculiar phenomenon induced by mitotic arrest, this report undoubtedly provides insights into nuclear expansion mechanisms during normal cell cycle progression.

In interphase, both nuclear volume and nuclear surface area increase as

cells grow. Importantly, an increase in the NE surface area does not automatically lead to a nucleus of a larger volume. When ER membrane biosynthesis is deregulated, the extra membranes accumulate as membrane protrusions without substantially affecting the N/C ratio [5–7]. The nuclear volume increase could be driven by the nucleocytoplasmic transport machinery [8] coordinated with homeostatic membrane partitioning within the endomembrane system. On the contrary, in closed mitosis the nuclear volume remains fairly constant and the surface area has to expand rapidly to accommodate the formation of daughter nuclei. The source of the extra membrane is most certainly the ER and a body of data suggests a burst of mitotic phospholipid biosynthesis rather than simple redistribution of pre-existing membrane material within the ER–NE system.

A prime candidate for regulating mitotic membrane production is the lipin family protein Pah1. Cells lacking Pah1 or its activator Nem1/Spo7 exhibit constitutive proliferation of the nuclear and ER membranes in interphase. Pah1 is a lipid phosphatase, hydrolyzing phosphatidic acid to diacylglycerol, a key regulatory point for balancing the production of structural versus storage lipids [9]. Pah1 also represses the transcription of key phospholipid biosynthesis genes [10,11], and thus the lack of Pah1 triggers an increase in the levels of structural phospholipids. Pah1 activity is subject to post-translational regulation — two cyclin-dependent kinases, Cdc28/Cdk1 and Pho85–Pho80, were shown to phosphorylate and inactivate Pah1 [12,13]. These modifications are reversed by the membrane-localized

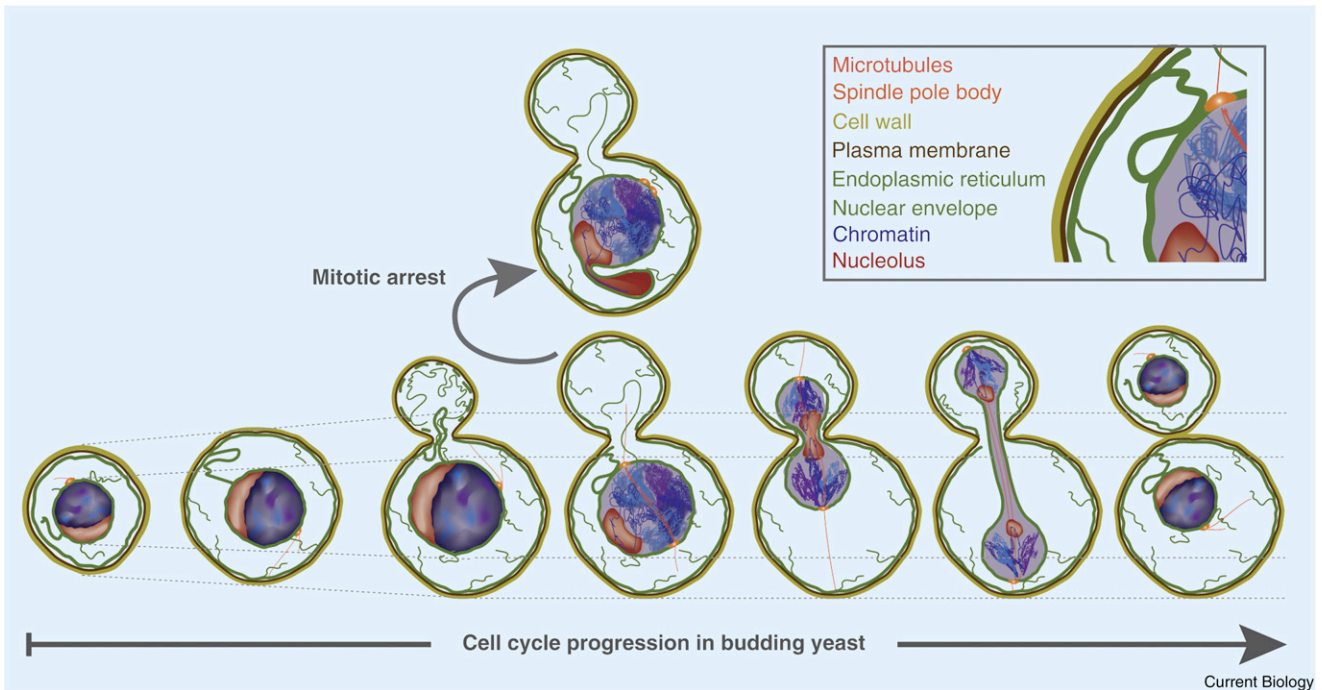


Figure 1. Endomembrane dynamics during cell cycle progression in *S. cerevisiae*.

During interphase, nuclei remain spherical and their growth is balanced with cell growth so that a fixed ratio of nuclear to cell volume is maintained. Upon mitotic entry, the NE expands considerably to accommodate nuclear division through a dumbbell-shaped intermediate. In mitotically arrested cells, the nucleus does not divide and the proliferated NE forms a large flare juxtaposed to the nucleolus.

phosphatase Nem1/Spo7, which dephosphorylates and targets Pah1 to specific sites at the ER [14,15]. Since Cdk1 activity is highest at mitotic entry, inactivation of Pah1 at this point could lead to a spike in the synthesis of structural phospholipids and thus supply the expanding NE with sufficient membrane material. In line with this model, nuclear membrane expansion in mitotically arrested budding yeast is prevented by overexpression of Nem1/Spo7 [4].

A simple explanation for the NE proliferation phenotype observed during prolonged mitosis by Witkin *et al.* [4] is that phospholipid biosynthesis is stuck in high gear due to high Cdk1 activity. As the authors show, these newly synthesized membranes are preferentially partitioning to the NE rather than distributing proportionally throughout the endomembrane system [4]. Furthermore, although the *S. cerevisiae* cells arrested in mitosis continue to grow, the nuclear volume increase does not catch up with the membrane expansion, resulting in formation of NE flares. Thus, it appears that additional, mitosis-specific mechanisms of nuclear growth control must exist, beyond simply the

stimulation of membrane production, e.g. the mitotic restructuring of the endomembrane system to favor preferential growth of NE membrane sheets. Interestingly, the *Schizosaccharomyces pombe* cells that progress through mitosis without the mitotic spindle exhibit membrane proliferation and ruffling, suggesting that massive NE expansion and remodeling is specific to mitosis *per se* rather than to mitotic delay [16].

In pre-anaphase arrested budding yeast, the expanding NE folds into a single flare adjacent to the nucleolus, an intranuclear body involved in ribosome biogenesis. The rest of the NE retains its spherical shape [4]. This type of morphological transformation is not something specific to mitotic arrest — nucleolar-associated flares have been observed in interphase cells with upregulated phospholipid production [6,7,17] and in G1 cells responding to mating pheromone [18]. Direct manipulations of nucleolar size and position suggest that the nucleolus itself is not involved in modulating the NE expansion [17]. Rather, the membrane proximal to the nucleolus is the only large NE domain that is not associated with chromatin. Chromosomal domains are intricately

organized at the NE by a host of tethering factors and this organization is important for many aspects of gene expression and chromatin structure [19]. In principle, the rapid influx of new membranes throughout the entire NE could possibly disrupt the intra-nuclear spatial organization. If that is the case, a membrane 'sink' free of chromatin could act to solve such problems. Investigations of mitotic NE behavior in cells defective for chromatin-NE attachment could test this hypothesis but generating cells where the bulk of chromatin is not tethered to the NE would likely pose a technical challenge [17]. An equally pertinent question (and equally difficult to address) is where the new membranes are added to a normally dividing closed nucleus. During closed mitosis the nucleolus is the last dividing intranuclear structure trailing behind the segregated chromosomes (Figure 1). Whether the membrane influx occurs at the nuclear equator in the vicinity of the nucleolus or the membrane components are added throughout the nuclear membrane remains to be seen. In the absence of methods for tracing the newly synthesized phospholipids, perhaps some answers could be provided

by a careful analysis of the three-dimensional structure of a dividing nucleus and the ER, similar to what was done for interphase *S. cerevisiae* cells [20]. In particular, it would be of interest to explore if any specific architectural features at the mitotic NE–ER interface could serve as a specialized membrane reservoir for the NE expansion.

At present, it would be prudent to conclude that we know very little about the mechanisms underlying NE expansion during mitosis and the field is ripe for major breakthroughs. The flared mitotic nuclei described by Witkin *et al.* [4] should prove a useful experimental setup for dissecting the nuclear growth pathways. While often considered somewhat esoteric, the closed mitosis is in fact a great system for understanding non-scalable nuclear membrane expansion and nuclear shape control in all eukaryotes.

References

1. Cavalier-Smith, T. (2005). Economy, speed and size matter: evolutionary forces driving nuclear genome miniaturization and expansion. *Ann. Bot.* 95, 147–175.
2. Jorgensen, P., Edgington, N.P., Schneider, B.L., Rupes, I., Tyers, M., and Futcher, B. (2007). The size of the nucleus increases as yeast cells grow. *Mol. Biol. Cell* 18, 3523–3532.
3. Neumann, F.R., and Nurse, P. (2007). Nuclear size control in fission yeast. *J. Cell Biol.* 179, 593–600.
4. Witkin, K.L., Chong, Y., Shao, S., Webster, M., Lahiri, S., Walters, A.D., Lee, B., Koh, J.L.Y., Prinz, W.A., Andrews, B.J., *et al.* (2012). The budding yeast nuclear envelope adjacent to the nucleolus serves as a membrane sink during mitotic delay. *Curr. Biol.* 22, 1128–1133.
5. Webster, M.T., McCaffery, J.M., and Cohen-Fix, O. (2010). Vesicle trafficking maintains nuclear shape in *Saccharomyces cerevisiae* during membrane proliferation. *J. Cell Biol.* 191, 1079–1088.
6. Siniosoglou, S., Santos-Rosa, H., Rappsilber, J., Mann, M., and Hurt, E. (1998). A novel complex of membrane proteins required for formation of a spherical nucleus. *EMBO J.* 17, 6449–6464.
7. Santos-Rosa, H., Leung, J., Grimsey, N., Peak-Chew, S., and Siniosoglou, S. (2005). The yeast lipin Smp2 couples phospholipid biosynthesis to nuclear membrane growth. *EMBO J.* 24, 1931–1941.
8. Levy, D.L., and Heald, R. (2010). Nuclear size is regulated by importin alpha and Ntf2 in *Xenopus*. *Cell* 143, 288–298.
9. Carman, G.M., and Han, G.S. (2006). Roles of phosphatidate phosphatase enzymes in lipid metabolism. *Trends Biochem. Sci.* 31, 694–699.
10. O'Hara, L., Han, G.S., Peak-Chew, S., Grimsey, N., Carman, G.M., and Siniosoglou, S. (2006). Control of phospholipid synthesis by phosphorylation of the yeast lipin Pah1p/Smp2p Mg²⁺-dependent phosphatidate phosphatase. *J. Biol. Chem.* 281, 34537–34548.
11. Loewen, C.J., Gaspar, M.L., Jesch, S.A., Delon, C., Ktistakis, N.T., Henry, S.A., and Levine, T.P. (2004). Phospholipid metabolism regulated by a transcription factor sensing phosphatidic acid. *Science* 304, 1644–1647.
12. Choi, H.S., Su, W.M., Morgan, J.M., Han, G.S., Xu, Z., Karanasios, E., Siniosoglou, S., and Carman, G.M. (2011). Phosphorylation of phosphatidate phosphatase regulates its membrane association and physiological functions in *Saccharomyces cerevisiae*: identification of SER(602), THR(723), AND SER(744) as the sites phosphorylated by CDC28 (CDK1)-encoded cyclin-dependent kinase. *J. Biol. Chem.* 286, 1486–1498.
13. Choi, H.S., Su, W.M., Han, G.S., Plote, D., Xu, Z., and Carman, G.M. (2012). Pho85p-Pho80p phosphorylation of yeast Pah1p phosphatidate phosphatase regulates its activity, location, abundance, and function in lipid metabolism. *J. Biol. Chem., In Press.* 10.1074/jbc.M112.346023.
14. Karanasios, E., Han, G.S., Xu, Z., Carman, G.M., and Siniosoglou, S. (2010). A phosphorylation-regulated amphipathic helix controls the membrane translocation and function of the yeast phosphatidate phosphatase. *Proc. Natl. Acad. Sci. USA* 107, 17539–17544.
15. Adeyo, O., Horn, P.J., Lee, S., Binns, D.D., Chandrabhas, A., Chapman, K.D., and Goodman, J.M. (2011). The yeast lipin orthologue Pah1p is important for biogenesis of lipid droplets. *J. Cell Biol.* 192, 1043–1055.
16. Castagnetti, S., Olfiferenko, S., and Nurse, P. (2010). Fission yeast cells undergo nuclear division in the absence of spindle microtubules. *PLoS Biol.* 8, e1000512.
17. Campbell, J.L., Lorenz, A., Witkin, K.L., Hays, T., Loidl, J., and Cohen-Fix, O. (2006). Yeast nuclear envelope subdomains with distinct abilities to resist membrane expansion. *Mol. Biol. Cell* 17, 1768–1778.
18. Stone, E.M., Heun, P., Laroche, T., Pillus, L., and Gasser, S.M. (2000). MAP kinase signaling induces nuclear reorganization in budding yeast. *Curr. Biol.* 10, 373–382.
19. Towbin, B.D., Meister, P., and Gasser, S.M. (2009). The nuclear envelope—a scaffold for silencing? *Curr. Opin. Genet. Dev.* 19, 180–186.
20. West, M., Zurek, N., Hoeng, A., and Voeltz, G.K. (2011). A 3D analysis of yeast ER structure reveals how ER domains are organized by membrane curvature. *J. Cell Biol.* 193, 333–346.

¹Temasek Life Sciences Laboratory, 1 Research Link, 117604 Singapore.
²Department of Biological Sciences National University of Singapore, 117604 Singapore.
*E-mail: snejana@tll.org.sg

DOI: 10.1016/j.cub.2012.04.043

Animal Memory: Rats Can Answer Unexpected Questions about Past Events

A new study has found that rats are able to answer, in a hippocampus-dependent manner, unexpected questions about whether they recently ate food or not. The results highlight potential shared mechanisms for remembering personal events in rats and humans, and offer new insights into the nature of animal memory.

Michael J. Beran

“And where were you last night?” No matter who asks you this question — the inquisitive neighbor, the jealous lover, or the detective interviewing you in the police station — the experience is likely to be similar. You will mentally ‘travel through time’ to the previous evening, remembering the critical ‘who, what,

when, and where’ information relevant to the question being asked. You may even, in some cases, feel as if you were re-living the evening in question. These experiences are routine for humans, and highlight the personal and specific aspects of our memory for events. An important question is whether these experiences are *uniquely* human, or whether other animals have access to the same kinds

of memories for specific events and episodes in their own past. This form of memory, called *episodic memory*, and the question of whether other species experience mental time travel into the future and into the past, as when humans recall personal episodes, is heavily debated in the comparative cognition literature [1,2]. A study reported in this issue of *Current Biology* [3] will certainly add to the debate about episodic memory in animals: Zhou *et al.* [3] report that rats have and use episodic memories that allow them to answer unanticipated questions about their own personal past. These new data are exciting, and will inspire new discussions about the nature of animal memory, and specifically the existence of episodic memory in nonhuman animals.

There have been a number of studies with nonhuman animals that